The Quantum Hall Effect as an Electrical Resistance Standard

CHAPTER · JANUARY 2006

DOI: 10.1007/3-7643-7393-8_3

2 AUTHORS:

Beat Jeckelmann
Federal Institute of Metrology (M…

90 PUBLICATIONS **1,151** CITATIONS

SEE PROFILE

Blaise Jeanneret
Federal Institute of Metrology (M…

116 PUBLICATIONS **1,189** CITATIONS

SEE PROFILE

Progress in Mathematical Physics
Volume 45

The Quantum Hall Effect

Poincaré Seminar 2004

Benoît Douçot
Bertrand Duplantier
Vincent Pasquier
Vincent Rivasseau
Editors

Birkhäuser Verlag
Basel · Boston · Berlin

Editors:

Benoît Douçot
LPTHE
CNRS et Universités Paris 6 et 7
Tour 24-14 5e étage
4 place Jussieu
F-75252 Paris Cedex 05
e-mail: doucot@lpthe.jussieu.fr

Bertrand Duplantier
Service de Physique Théorique
Orme des Merisiers
CEA – Saclay
F-91191 Gif-sur-Yvette Cedex
e-mail: bertrand.duplantier@spht.saclay.cea.fr

Vincent Pasquier
Service de Physique Théorique
Orme des Merisiers
CEA – Saclay
F-91191 Gif sur Yvette Cedex
e-mail: pasquier@spht.saclay.cea.fr

Vincent Rivasseau
Laboratoire de Physique Théorique
Université Paris XI
F-91405 Orsay Cedex
e-mail: Vincent.Rivasseau@th.u-psud.fr

2000 Mathematics Subject Classification 81V70

A CIP catalogue record for this book is available from the Library of Congress, Washington D.C., USA

Bibliographic information published by Die Deutsche Bibliothek
Die Deutsche Bibliothek lists this publication in the Deutsche Nationalbibliografie; detailed bibliographic data is available in the Internet at <http://dnb.ddb.de>.

ISBN 3-7643-7300-8 Birkhäuser Verlag, Basel – Boston – Berlin

ISBN-10: 3-7643-7300-8
ISBN-13: 978-3-7643-7300-9

9 8 7 6 5 4 3 2 1 www.birkhauser.ch

Contents

We thank the Institute of Physics Publishing for its authorization to reproduce the paper by B. Jeckelmann and B. Jeanneret.

Foreword

This book is the third in a series of lectures of the *Séminaire Poincaré*, which is directed towards a large audience of physicists and of mathematicians.

The goal of this seminar is to provide up to date information about general topics of great interest in physics. Both the theoretical and experimental aspects are covered, with some historical background. Inspired by the Bourbaki seminar in mathematics in its organization, hence nicknamed "Bourbaphi", this Poincaré Seminar is held twice a year at the Institut Henri Poincaré in Paris, with contributions prepared in advance. A particular care is devoted to the pedagogical nature of the presentation so as to fulfill the goal of being readable by a large audience of scientists.

This volume contains the sixth such Seminar, held in 2004. It is devoted to the Quantum Hall Effect. After a historical and general presentation by Nobel prize Klaus von Klitzing, discoverer of this effect, the volume proceeds with reviews on the mathematics and physics of both the integer and fractional case, and includes up to date presentations of the tunneling and metrology experiments related to the Quantum Hall Effect.

We hope that the publication of this series will serve the community of physicists and mathematicians at professional or graduate student level.

We thank the Commissariat à l'Énergie Atomique (Division des Sciences de la Matière), the Centre National de la Recherche Scientifique (Sciences Physique et Mathématiques), and the Daniel Iagolnitzer Foundation for sponsoring the Seminar. Special thanks are due to Chantal Delongeas for the preparation of the manuscript.

Benoît Douçot
Bertrand Duplantier
Vincent Pasquier
Vincent Rivasseau

The Quantum Hall Effect, 1 – 21

Poincaré Seminar 2004

25 Years of Quantum Hall Effect (QHE) A Personal View on the Discovery, Physics and Applications of this Quantum Effect

Klaus von Klitzing

1 Historical Aspects

The birthday of the quantum Hall effect (QHE) can be fixed very accurately. It was the night of the 4th to the 5th of February 1980 at around 2 a.m. during an experiment at the High Magnetic Field Laboratory in Grenoble. The research topic included the characterization of the electronic transport of silicon field effect transistors. How can one improve the mobility of these devices? Which scattering processes (surface roughness, interface charges, impurities etc.) dominate the motion of the electrons in the very thin layer of only a few nanometers at the interface between silicon and silicon dioxide? For this research, Dr. Dorda (Siemens AG) and Dr. Pepper (Plessey Company) provided specially designed devices (Hall devices) as shown in Fig.1, which allow direct measurements of the resistivity tensor.

For the experiments, low temperatures (typically 4.2 K) were used in order to suppress disturbing scattering processes originating from electron-phonon interactions. The application of a strong magnetic field was an established method to get more information about microscopic details of the semiconductor. A review article published in 1982 by T. Ando, A. Fowler, and F. Stern about the electronic properties of two-dimensional systems summarizes nicely the knowledge in this field at the time of the discovery of the QHE [1].

Since 1966 it was known, that electrons, accumulated at the surface of a silicon single crystal by a positive voltage at the gate (= metal plate parallel to the surface), form a two-dimensional electron gas [2]. The energy of the electrons for a motion perpendicular to the surface is quantized ("particle in a box") and even the free motion of the electrons in the plane of the two-dimensional system becomes quantized (Landau quantization), if a strong magnetic field is applied perpendicular to the plane. In the ideal case, the energy spectrum of a 2DEG in strong magnetic fields consists of discrete energy levels (normally broadened due to impurities) with energy gaps between these levels. The quantum Hall effect is observed, if the Fermi energy is located in the gap of the electronic spectrum and if the temperature is so low, that excitations across the gap are not possible.

The experimental curve, which led to the discovery of the QHE, is shown in Fig. 2. The blue curve is the electrical resistance of the silicon field effect tran-

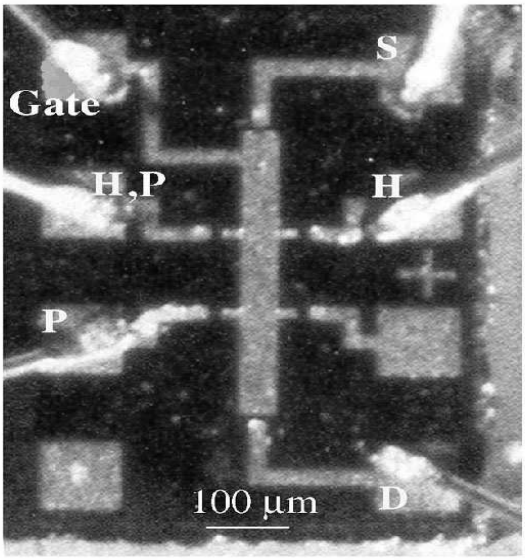

Figure 1: Typical silicon MOSFET device used for measurements of the xx- and xy-components of the resistivity tensor. For a fixed source-drain current between the contacts S and D, the potential drops between the probes $P-P$ and $H-H$ are directly proportional to the resistivities ρ_{xx} and ρ_{xy}. A positive gate voltage increases the carrier density below the gate.

sistor as a function of the gate voltage. Since the electron concentration increases linearly with increasing gate voltage, the electrical resistance becomes monotonically smaller. Also the Hall voltage (if a constant magnetic field of e.g. 19.8 Tesla is applied) decreases with increasing gate voltage, since the Hall voltage is basically inversely proportional to the electron concentration. The black curve shows the Hall resistance, which is the ratio of the Hall voltage divided by the current through the sample. Nice plateaus in the Hall resistance (identical with the transverse resistivity ρ_{xy}) are observed at gate voltages, where the electrical resistance (which is proportional to the longitudinal resistivity ρ_{xx}) becomes zero. These zeros are expected for a vanishing density of state of (mobile) electrons at the Fermi energy. The finite gate voltage regions where the resistivities ρ_{xx} and ρ_{xy} remain unchanged indicate, that the gate voltage induced electrons in these regions do not contribute to the electronic transport- they are localized. The role of localized electrons in Hall effect measurements was not clear. The majority of experimentalists believed, that the Hall effect measures only *delocalized* electrons. This assumption was partly supported by theory [3] and formed the basis of the analysis of QHE data published already in 1977 [4]. These experimental data, available to

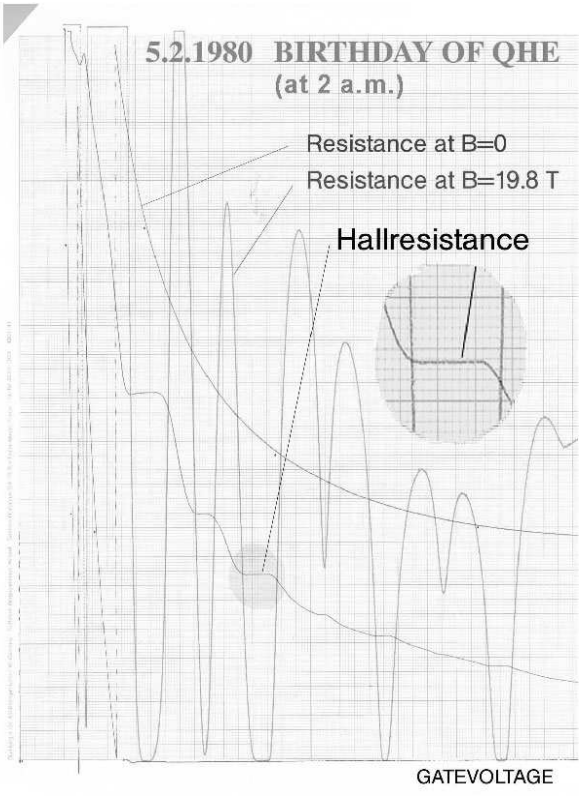

Figure 2: Hall resistance and longitudinal resistance (at zero magnetic field and at $B = 19.8$ Tesla) of a silicon MOSFET at liquid helium temperature as a function of the gate voltage. The quantized Hall plateau for filling factor 4 is enlarged.

the public 3 years before the discovery of the quantum Hall effect, contain already all information of this new quantum effect so that everyone had the chance to make a discovery that led to the Nobel Prize in Physics 1985. The unexpected finding in the night of 4./5.2.1980 was the fact, that the plateau values in the Hall resistance ρ_{xy} are not influenced by the amount of localized electrons and can be expressed with high precision by the equation $\rho_{xy} = h/ie^2$ (h=Planck constant, e=elementary charge and i the number of fully occupied Landau levels). Also it became clear, that the component ρ_{xy} of the resistivity tensor can be measured directly with a volt- and amperemeter (a fact overlooked by many theoreticians) and that for the plateau values no information about the carrier density, the magnetic field, and the geometry of the device is necessary.

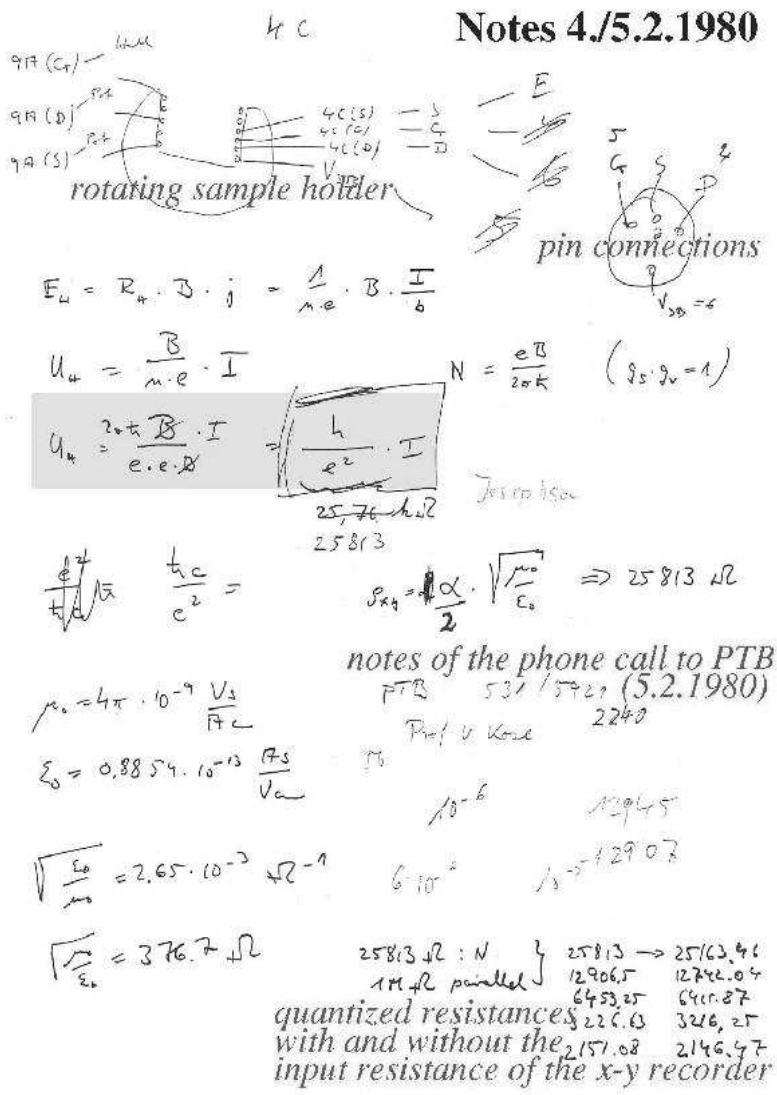

Figure 3: Copy of the original notes, which led to the discovery of the quantum Hall effect. The calculations for the Hall voltage U_H for one fully occupied Landau level show, that the Hall resistance U_H/I depends exclusively on the fundamental constant h/e^2.

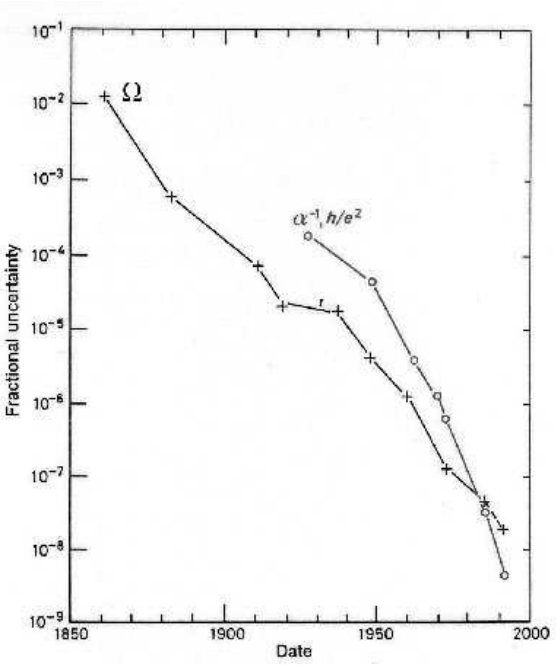

Figure 4: Experimental uncertainties for the realization of the resistance 1 Ohm in SI units and the determination of the fine structure constant α as a function of time.

The most important equation in connection with the quantized Hall resistance, the equation $U_H = h/e^2 \cdot I$, is written down for the first time in my notebook with the date 4.2.1980. A copy of this page is reproduced in Fig. 3. The validity and the experimental confirmation of this fundamental equation was so high that for the experimental determination of the voltage (measured with a $x-y$ recorder) the finite input resistance of 1 $M\Omega$ for the $x-y$ recorder had to be included as a correction. The calculations in the lower part of Fig. 3 show, that instead of the theoretical value of 25813 Ohm for the fundamental constant h/e^2 a value of about 25163 Ohm should be measured with the $x-y$ recorder, which was confirmed with high precision. These first measurements of the quantized Hall resistance showed already, that localized electrons are unimportant and the simple derivation on the basis of an ideal electron system leads to the correct result. It was immediately clear, that an electrical resistance which is independent of the geometry of the sample and insensitive to microscopic details of the material will be important for metrology institutes like NBS in the US (today NIST) or PTB in Germany. So it is not surprising, that discussions with Prof. Kose at the PTB about this new

quantum phenomenon started already one day after the discovery of the quantized Hall resistance (see notes in Fig. 3).

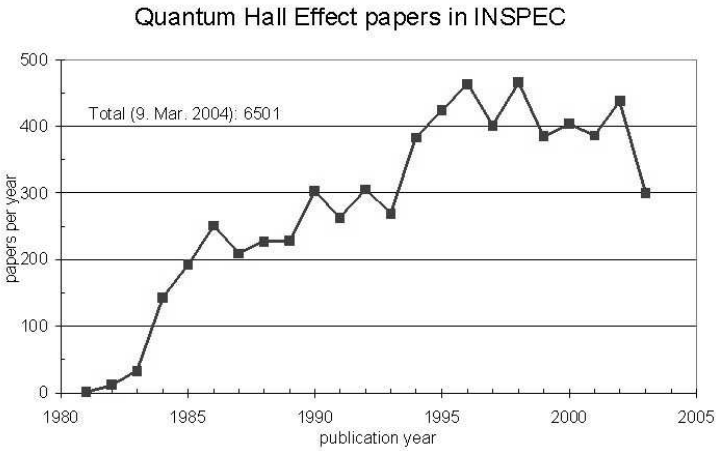

Figure 5: The number of publications related to the quantum Hall effect increased continuously up to a value of about one publication per day since 1995.

The experimental results were submitted to Phys. Rev. Letters with the title: "Realization of a Resistance Standard based on Fundamental Constants" but the referee pointed out, that (at this time) not a more accurate electrical resistor was needed but a better value for the fundamental constant h/e^2. Interestingly, the constant h/e^2 is identical with the inverse fine-structure constant $\alpha^{-1} = (h/e^2)(2/\mu_0 c) = 137.036\cdots$ where the magnetic constant $\mu_0 = 4\pi 10^{-7} N/A^2$ and the velocity of light $c = 299\ 792\ 458\ m/s$ are fixed numbers with no uncertainties. The data in Fig. 4 show indeed, that the uncertainty in the realization of the electrical unit of 1Ω within the International System of Units (SI units) was smaller (until 1985) than the uncertainty for h/e^2 or the inverse fine-structure constant. As a consequence, the title of the first publication about the quantum Hall effect was changed to: "New Method for High-Accuracy Determination of the Fine-Structure Constant Based on Quantized Hall Resistance"[5]. The number of publications with this new topic "quantum Hall effect" in the title or abstract increased drastically in the following years with about one publication per day for the last 10 years as shown in Fig. 5. The publicity of the quantized Hall effect originates from the fact, that not only solid state physics but nearly all other fields in physics have connections to the QHE as exemplarily demonstrated by the following title of publications:

BTZ black hole and quantum Hall effects in the bulk/boundary dynamics [6].
Quantum Hall quarks or short distance physics of quantized Hall fluids [7].
A four-dimensional generalization of the quantum Hall effect [8].

Quantum computation in quantum-Hall systems [9].
Higher-dimensional quantum Hall effect in string theory [10].
Is the quantum Hall effect influenced by the gravitational field? [11].

Up to now, more than 10 books were published about the quantum Hall effect [12–19] and the most interesting aspects are summarized in the Proceedings of the International Symposium "Quantum Hall Effect: Past, Present and Future" [20].

Figure 6: Summary of high precision data for the quantized Hall resistance up to 1988 which led to the fixed value of 25 812.807 Ohm recommended as a reference standard for all resistance calibrations after 1.1.1990 .

2 Quantum Hall Effect and Metrology

The most important aspect of the quantum Hall effect for applications is the fact that the quantized Hall resistance has always a fundamental value of $h/e^2 = 25812.807\cdots$ Ohm. This value is independent of the material, geometry and microscopic details of the semiconductor. After the discovery of this macroscopic quantum effect many metrological institutes repeated the experiment with much higher accuracy than available in a research laboratory and they confirmed, that this effect is extremely stable and reproducible. Fig. 6 summarizes the data (published until 1988) for the fundamental value of the quantized Hall resistance and it is evident that the uncertainty in the measurements is dominated by the uncertainty in the realization of the SI Ohm. From the internationally accepted definitions for the basic SI units "second", "meter", "kilogram", and "Ampere" it is clear, that all mechanical and electrical quantities are well defined. However the overview in Fig. 7 shows also, that the base unit Ampere has a relatively large uncertainty of about 10^{-6} if deduced from the force between current carrying wires.

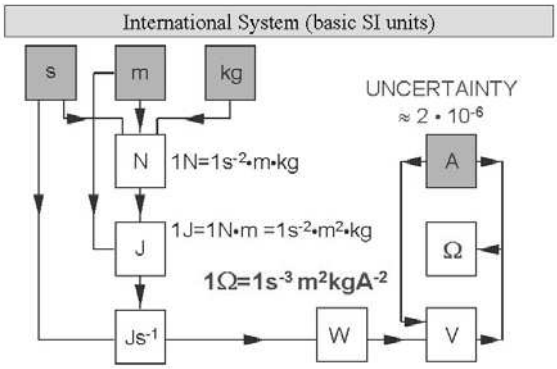

Figure 7: Basic and derived SI units for mechanical and electrical quantities.

Apparently, the derived unit $1\Omega = 1s^{-3}m^2kgA^{-2}$ (which depends in principle on all basic units) should have an even larger uncertainty than 10^{-6}. However, as shown in Fig. 4, the SI Ohm is known with a smaller uncertainty than the basic unit Ampere which originates from the fact, that a resistance can be realized via the a.c. resistance $R = 1/\omega C$ of a capacitor C. Since the capacitance C of a capacitor depends exclusively on the geometry (with vacuum as a dielectric media), one can realize a SI Ohm just by using the basic units time (for the frequency $\omega/2\pi$) and length (for a calculable Thomson-Lampert capacitor [21]), which are known with very small uncertainties. Therefore an uncertainty of about 10^{-7} for the realization of the SI Ohm is possible so that the fine-structure constant can be measured via the QHE directly with the corresponding accuracy. However, the quantized Hall resistance is more stable and more reproducible than any resistor calibrated in SI units so that the Comité Consultatif d'Electricité recommended, "that exactly 25 812.807 Ohm should be adopted as a conventional value, denoted by R_{K-90}, for the von Klitzing constant R_K" and that this value should be used starting on 1.1.1990 to form laboratory reference standards of resistances all over the world [22]. Direct comparisons between these reference standards at different national laboratories (see Fig. 8) have shown, that deviations smaller than $2 \cdot 10^{-9}$ for the reference standards in different countries are found [23] if the published guidelines for reliable measurements of the quantized Hall resistance are obeyed [24]. Unfortunately, this high reproducibility and stability of the quantized Hall resistance cannot be used to determine the fine-structure constant directly with high accuracy since the value of the quantized Hall resistance in SI units is not known. Only the combination with other experiments like high precision measurements (and calculations) of the anomalous magnetic moment of the electron, gyromagnetic ratio of protons or mass of neutrons lead to a least square adjustment of the value of the fine-structure constant with an uncertainty of only $3.3 \cdot 10^{-9}$ resulting

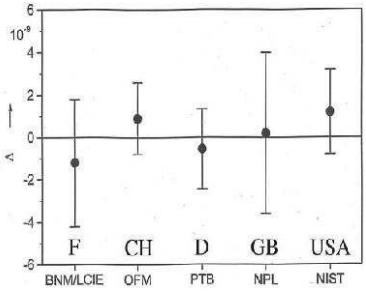

Figure 8: Reproducibility and stability of the quantized Hall resistance deduced from comparisons between different metrological institutes. The observed uncertainties of about 2.10^{-9} is two orders of magnitude smaller than the uncertainty in the realization of a resistance calibrated in SI Ohms.

in a value for the von Klitzing constant of $R_K = 25812.807449 \pm 0.000086$ Ohm (CODATA 2002 [25]). Accurate values for fundamental constants (especially for the fine-structure constant) are important in connection with the speculation that some fundamental constants may vary with time. Publications about the evidence of cosmological evolution of the fine-structure constant are questioned and could not be confirmed. The variation $\partial\alpha/\partial t$ per year is smaller than 10^{-16}.

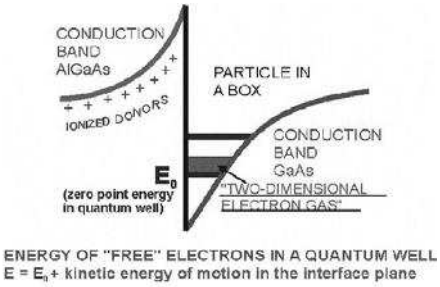

Figure 9: Realization of a two-dimensional electrons gas close to the interface between AlGaAs and GaAs.

The combination of the quantum Hall effect with the Josephson effect (which allows an representation of the electrical voltage in units of h/e) leads to the possibility, to compare electrical power (which depends on the Planck constant h) with mechanical power (which depends on the mass m). The best value for the Planck constant is obtained using such a Watt balance [26]. Alternatively, one may fix the Planck constant (like the fixed value for the velocity of light for the definition of the unit of length) in order to have a new realization of the unit of mass.

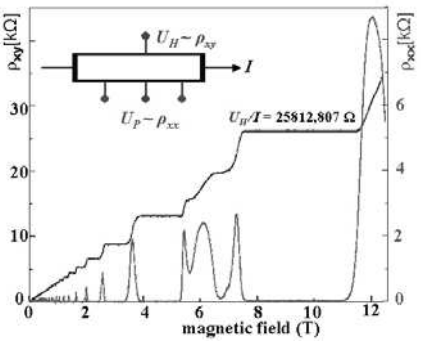

Figure 10: Hall resistance and longitudinal resistivity data as a function of the magnetic field for a GaAs/AlGaAs heterostructures at 1.5 K .

3 Physics of Quantum Hall Effect

The textbook explanation of the QHE is based on the classical Hall effect discovered 125 years ago [27]. A magnetic field perpendicular to the current I in a metallic sample generates a Hall voltage U_H perpendicular to both, the magnetic field and the current direction:

$$U_H = (B \cdot I)/(n \cdot e \cdot d)$$

with the three-dimensional carrier density n and the thickness d of the sample. For a two-dimensional electron gas the product of $n \cdot d$ can be combined as a two-dimensional carrier density n_s. This leads to a Hall resistance

$$R_H = U_H/I = B/(n_s \cdot e)$$

Such a two-dimensional electron gas can be formed at the semiconductor/insulator interface, for example at the $Si-SiO_2$ interface of a $MOSFET$ (Metal Oxid Semiconductor Field Effect Transistor) or at the interface of a $GaAs-AlGaAs\ HEMT$ (High Electron Mobility Transistor) as shown in Fig. 9. In these systems the electrons are confined within a very thin layer of few nanometers so that similar to the problem of "particle in a box" only quantized energies $E_i (i = 1, 2, 3 \cdots)$ for the electron motion perpendicular to the interface exist (electric subbands).

A strong magnetic field perpendicular to the two-dimensional layer leads to Landau quantization and therefore to a discrete energy spectrum:

$$E_{0,N} = E_0 + (N + 1/2)\hbar\omega_c \quad (N = 0, 1, 2, ...)$$

The cyclotron energy $\hbar\omega_c = \hbar eB/m_c$ is proportional to the magnetic field B and inversely proportional to the cyclotron mass m_c and equal to 1.16 meV at 10 Tesla for a free electron mass m_0.

Due to the electron spin an additional Zeeman splitting of each Landau level appears which is not explicitly included in the following discussion. More important is the general result, that a discrete energy spectrum with energy gaps exists for an ideal 2DEG in a strong magnetic field and that the degeneracy of each discrete level corresponds to the number of flux quanta $(F \cdot B)/(h/e)$ within the area F of the sample. This corresponds to a carrier density $n_s = e \cdot B/h$ for each fully occupied spin-split energy level E_0, N and therefore to a Hall resistance $R_H = h/i \cdot e^2$ for i fully occupied Landau levels as observed in the experiment. A typical magnetoresistance measurement on a GaAs/AlGaAs heterostructure under QHE conditions is shown in Fig. 10.

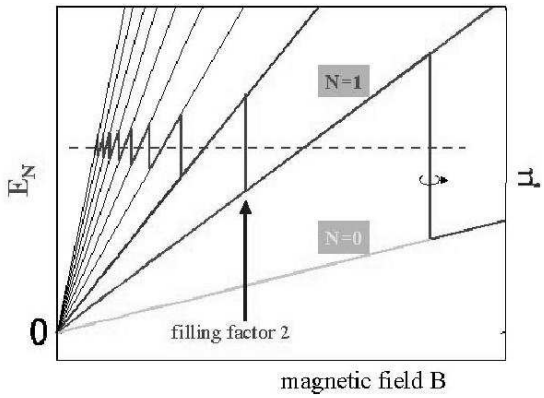

Figure 11: Discrete energy spectrum of a 2DEG in a magnetic field for an ideal system (no spin, no disorder, infinite system, zero temperature). The Fermi energy (full red line) jumps between Landau levels at integer filling factors if the electron concentration is constant.

This simple "explanation" of the quantized Hall resistance leads to the correct result but contains unrealistic assumptions. A real Hall device has always a finite width and length with metallic contacts and even high mobility devices contain impurities and potential fluctuations, which lift the degeneracy of the Landau levels. These two important aspects, the finite size and the disorder, will be discussed in the following chapters.

3.1 Quantum Hall Systems with Disorder

The experimental fact, that the Hall resistance stays constant even if the filling factor is changed (e.g. by varying the magnetic field at fixed density), cannot be explained within the simple single particle picture for an ideal system. A sketch of

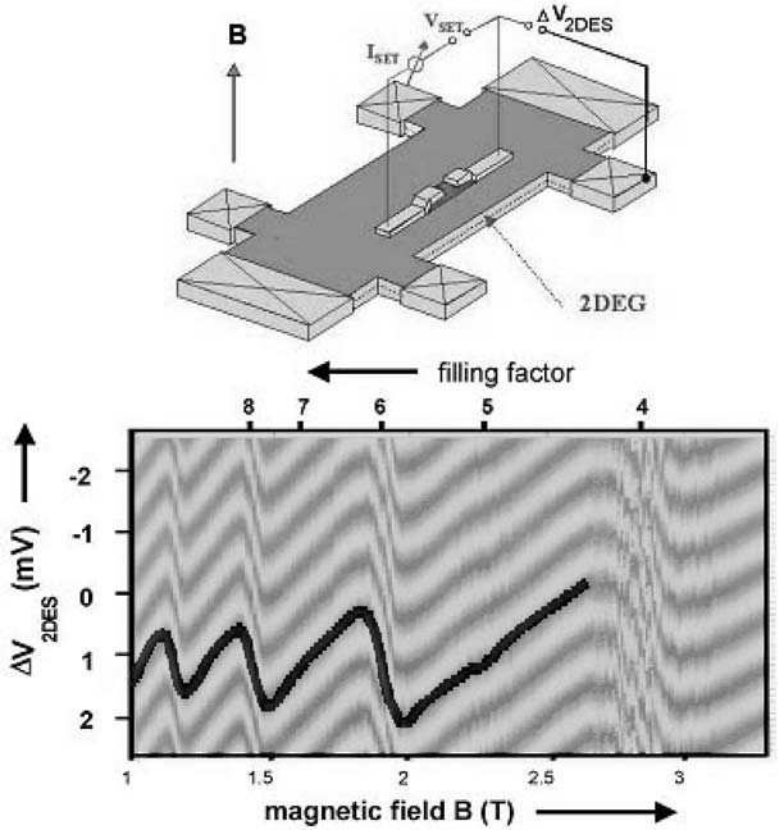

Figure 12: Measured variation of the electrostatic potential of a 2DEG as a function of the magnetic field. The black line marks a maximum in the coulomb oscillations of a metallic single electron on top of the heterostructure, which corresponds to a constant electrostatic potential of the 2DEG relative to the SET.

the energy spectrum and the Fermi energy as a function of the magnetic field is shown in Fig. 11 for such an ideal system at zero temperature. The Fermi energy (full blue line) is located only at very special magnetic field values in energy gaps between Landau levels so that only at these very special magnetic field values and not in a finite magnetic field range the condition for the observation of the QHE is fulfilled. On the other hand, if one assumes, that the Fermi energy remains constant as a function of the magnetic field (dotted line in Fig. 11), wide plateaus for the quantized Hall resistance are expected, since the Fermi energy remains in energy gaps (which correspond to integer filling factors and therefore to quantized Hall resistances) in a wide magnetic field range. However, this picture is unrealistic since

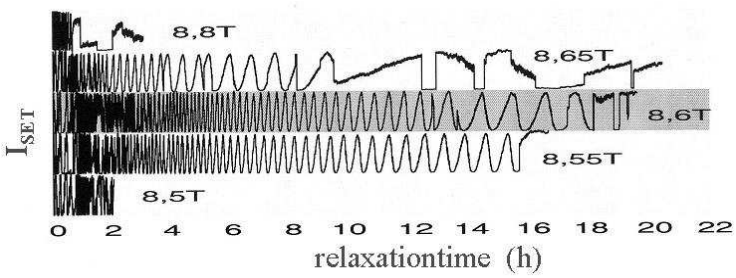

Figure 13: SET current as a function of time for different magnetic fields close to filling factor 1. The oscillations in the current originate from the relaxation of a non-equilibrium electrostatic potential within the 2DEG originating from eddy currents due to the magnetic field sweep in the plateau region. One oscillation in the SET current corresponds to a change in the "gate potential" of about 1 meV.

one has to assume that the electron concentration changes drastically as a function of the magnetic field. If for example the Fermi energy crosses the Landau level $N = 1$, the electron density has to change abruptly by a factor of two from filling factor 2 to filling factor 1. Such a strong redistribution of charges between the 2DEG and an electron reservoir (doping layers, metallic contacts) are in contradiction with electrostatic calculations. The most direct proof, that the Fermi energy jumps across the gap between Landau levels within a relatively small magnetic field range (at least smaller than the plateau width) is given by measurements of the electrostatic potential between a metal (= wire plus sensor connected to the 2DEG) and the two-dimensional electron gas. The *electrochemical* potential within the metal - 2DEG system has to be constant (thermodynamic equilibrium) so that the magnetic field dependent variation in the *chemical* potential (characterized by the Fermi energy) has to be compensated by a change in the *electrostatic* potential difference between the metallic system and the 2DEG (=contact voltage). Such a variation in the electrostatic potential has been measured directly [28] by using a metallic single electron transistor (SET) at the surface of the quantum Hall device as shown in Fig 12. The electrostatic potential of the 2DEG relative to the SET acts as a gate voltage, which influences drastically the current through the SET. (The SET shows Coulomb blockade oscillations with a gate voltage period of about $1mV$). The experimental data shown in Fig. 12 clearly demonstrate, that the contact voltage and therefore the chemical potential of the two-dimensional system changes saw-tooth like as expected. The height of the jumps corresponds directly to the energy gap. The "noise" at 2.8 Tesla (filling factor 4) demonstrates, that the gate potential below the SET detector is fluctuating and not fixed by the applied voltage ΔV_{2DES} since the vanishing conductivity in the quantum Hall regime between the metallic contacts at the boundary of the device and the inner parts of the sample leads to floating potentials within the 2DEG system. Recent

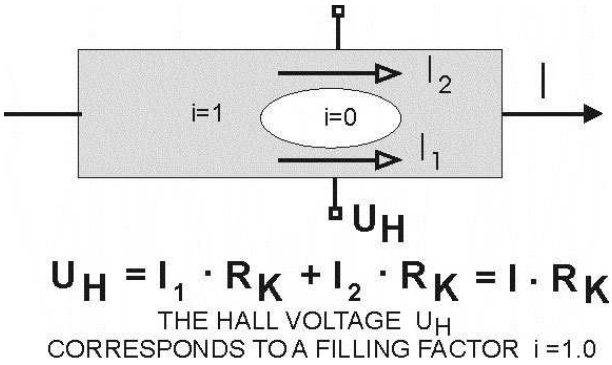

Figure 14: Sketch of a device with a filling factor slightly below 1. Long-range potential fluctuations lead to a finite area within the sample (localized carriers) with vanishing electrons (= filling factor 0) surrounded by an equipotential line. The derivation of the measured Hall voltage U_H show, that closed areas with another filling factor than the main part of the device leads to a Hall effect which is not influenced by localized electrons.

measurements have demonstrated [29], that time constants of many hours are observed for the equilibration of potential differences between the boundary of a QHE device and the inner part of the sample as shown in Fig. 13. The oscillations in the SET current can be directly translated into a variation of the electrostatic potential below the position of the SET since one period corresponds to a "gate voltage change" for the SET of about 1 meV. The non-equilibrium originates from a magnetic field sweep in regions of vanishing energy dissipation, which generates eddy currents around the detector and corresponding Hall potential differences of more than 100 meV perpendicular to these currents. These "Hall voltages" are not measurable at the outer Hall potential probes (at the edge of the sample), since all eddy currents cancel each other. **The current distribution is unimportant for the accuracy of the quantized Hall resistance!**

In order to explain the width of the Hall plateaus, localized electrons in the tails of broadened Landau levels have to be included. A simple thought experiment illustrates, that localized states added or removed from fully occupied Landau levels do not change the Hall resistance (see Fig. 14). For long range potential fluctuations (e.g. due to impurities located close to the 2DEG) the Landau levels follow this potential landscape so that the energies of the Landau levels change with position within the plane of the device. If the energy separation between Landau levels is larger than the peak value of the potential fluctuation, an energy gap still exists and a fully occupied Landau level (e.g. filling factor 1) with the expected quantized Hall resistance R_K can be realized. In this picture, a filling factor 0.9 means, that 10% of the area of the device (= top of the hills in the

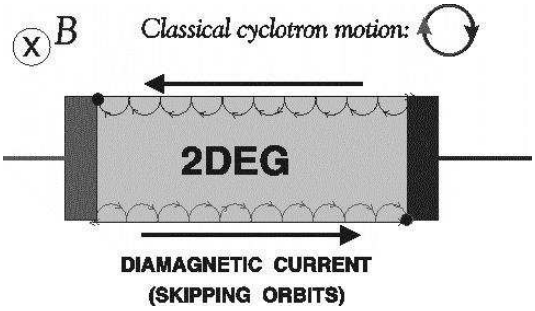

Figure 15: Skipping cyclotron orbits (= diamagnetic current) at the boundaries of a device are equivalent to the edge channels in a 2DEG with finite size.

potential landscape) becomes unoccupied with electrons as sketched in Fig. 14. The boundary of the unoccupied area is an equipotential line (with an unknown potential) but the externally measured Hall voltage U_H, which is the sum of the Hall voltages of the upper part of the sample (current I_2) and the lower part (current I_1), adds up to the ideal value expected for the filling factor 1 (grey regions). Eddy currents around the hole with $i = 0$ will vary the currents I_1 and I_2 but the sum is always identical with the external current I.

The quantized Hall resistance breaks down, if electronic states at the Fermi energy are extended across the whole device. This is the case for a half-filled Landau level if the simple percolation picture is applied. Such a singularity at half-filled Landau levels has been observed experimentally [30].

This simple picture of extended and localized electron states indicates, that extended states *always* exist at the boundary of the devices. This edge phenomenon is extremely important for a discussion of the quantum Hall effect in real devices and will be discussed in more detail in the next chapter. In a classical picture, skipping orbits as a result of reflected cyclotron orbits at the edge lead to diamagnetic currents as sketched in Fig 15. Therefore, even if the QHE is characterized by a vanishing conductivity σ_{xx} (no current in the direction of the electric field), a finite current between source and drain of a Hall device can be established via this diamagnetic current. If the device is connected to source and drain reservoirs with different electrochemical potentials (see Fig. 15), the skipping electrons establish different electrochemical potentials at the upper and lower edge respectively. Energy dissipation appears only at the points (black dots in Fig. 15) where the edge potentials differ from the source/drain potentials.

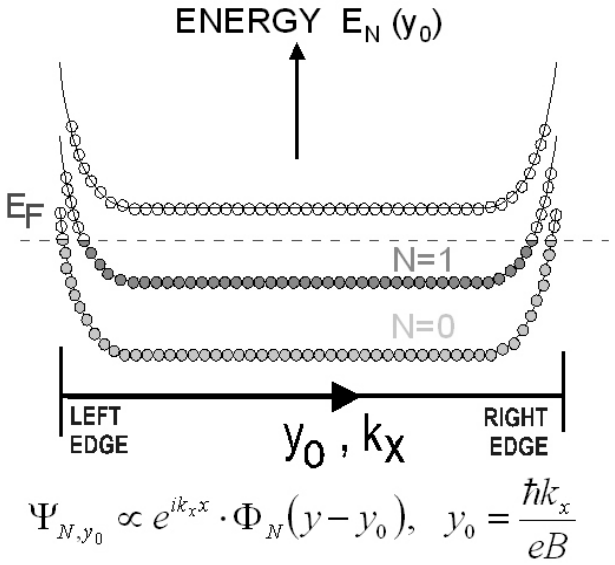

Figure 16: Ideal Landau levels for a device with boundaries. The fully occupied Landau levels in the inner part of the device rise in energy close to the edge forming compressible ("metallic") stripes close to the crossing points of the Landau levels with the Fermi energy E_F.

3.2 Edge Phenomena in QHE Devices

The simple explanation of the quantized Hall resistance as a result of fully occupied Landau levels (with a gap at the Fermi energy) breaks down for real devices with finite size. For such a system *no energy gap* at the Fermi energy exists under quantum Hall condition even if no disorder due to impurities is included. This is illustrated in Fig. 16 where the energy of the Landau levels is plotted across the width of the device. The Fermi energy in the inner part of the sample is assumed to be in the gap for filling factor 2. Close to the edge (within a characteristic depletion length of about $1\mu m$) the carrier density becomes finally zero. This corresponds to an increase in the Landau level energies at the edge so that these levels become unoccupied outside the sample. *All occupied Landau levels inside the sample have to cross the Fermi energy close to the boundary of the device. At these crossing points "half-filled Landau levels" with metallic properties are present.*

Selfconsistent calculations for the occupation of the Landau levels show that not lines but metallic stripes with a finite width are formed parallel to the edge [31]. The number of stripes is identical with the number of fully occupied Landau levels in the inner part of the device. These stripes are characterized by a compressible electron gas where the electron concentration can easily be changed since the Landau levels in these regions are only partly filled with electrons and pinned at the

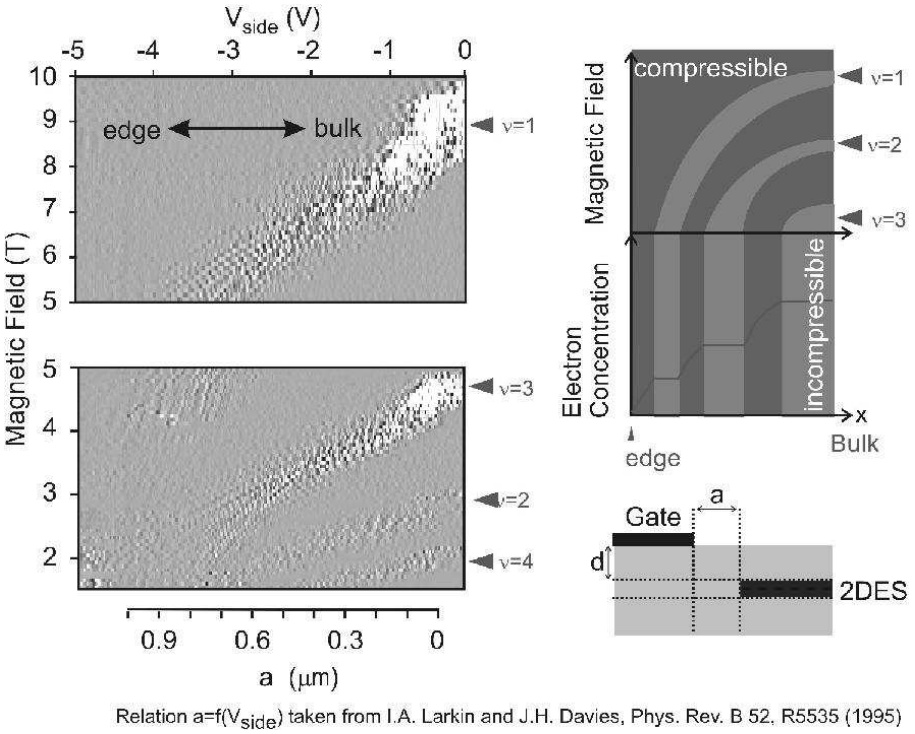

Figure 17: Experimental determination of the position of incompressible (= insulating) stripes close to the edge of the device for the magnetic field range 1.5 - 10 Tesla.

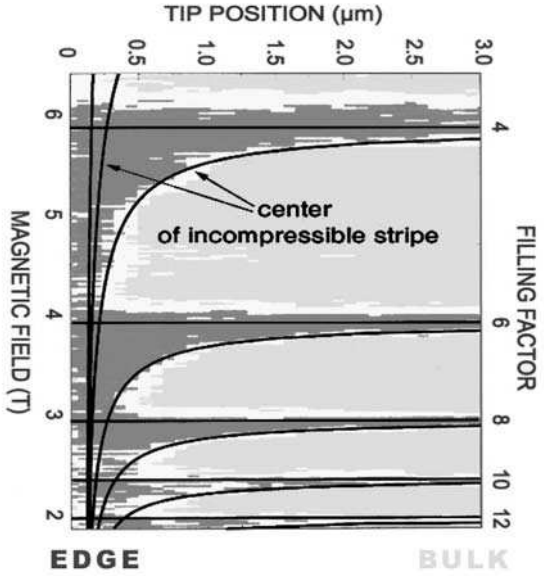

Figure 18: Hall potential distribution of a QHE device measured with an AFM. The innermost incompressible stripe (= black lines) acts as an insulating barrier. The Hall potential is color coded with about half of the total Hall voltage for the dark grey-light grey potential difference.

Fermi energy. In contrast, the incompressible stripes between the compressible regions represent fully occupied Landau levels with the typical isolating behavior of a quantum Hall state. If the single electron transistor shown in Fig. 12 is located above an incompressible region, increased noise is observed in the SET current similar to the noise at 2.8 Tesla in Fig. 12. In order to visualize the position of the stripes close to the edge, not the SET is moved but an artificial edge (= zero carrier density) is formed with a negative voltage at a gate metal located close to the SET. The edge (= position with vanishing carrier density) moves with increasing negative gate voltage closer to the detector and alternatively incompressible (increased SET noise) and compressible strips (no SET noise) are located below the SET detector. The experimental results in Fig. 17 confirm qualitatively the picture of incompressible stripes close to the edge which move away from the edge with increasing magnetic field until the whole inner part of the device becomes an incompressible region at integer filling factor. At slightly higher magnetic fields this "bulk" incompressible region disappears and only incompressible stripes with lower filling factor remain close to the boundary of the device.

The influence of the incompressible stripes on the Hall potential distribution has been measured with an atomic force microscope. The results in Fig. 18 show, that the innermost incompressible stripe has such strong "insulating" properties that about 50% of the Hall potential drops across this stripe. The other 50% of the Hall potential drops close to the opposite boundary of the device across the equivalent incompressible stripe. In principle the incompressible stripes should be able to suppress the backscattering across the width of a Hall device so that even for an ideal device without impurities (= localized states due to potential fluctuations) a finite magnetic field range with vanishing resistivity and quantized Hall plateaus should exist [32]. However, the fact, that the plateau width increases systematically with increasing impurity concentration (and shows the expected different behavior for attractive and repulsive impurities) shows, that localized states due to impurities are the main origin for the stabilization of the quantized Hall resistance within a finite range of filling factors. A vanishing longitudinal resistivity always indicates, that a backscattering is not measurable. Under this condition the quantized Hall resistance is a direct consequence of the transmission of one-dimensional channels [33].

4 Correlated Electron Phenomena in Quantum Hall Systems

Many physical properties of the quantum Hall effect can be discussed in a single electron picture but it is obvious that the majority of modern research and publications in this field include electron correlation phenomena. Even if the fractional quantum Hall effect [34] (which is a manifestation of the strong electron-electron interaction in a two-dimensional system) can be nicely discussed as the integer quantum Hall effect of weakly interacting quasi particles called composite fermions [35], the many-body wave function of the quantum Hall system is the

basis for the discussion of different exciting new phenomena observed in correlated two-dimensional systems in strong magnetic fields. Many of these new phenomena can only be observed in devices with extremely high mobility where the electron-electron interaction is not destroyed by disorder. Experiments on such devices indicate, that phenomena like superfluidity and Bose-Einstein condensation [36], skyrmionic excitations [37], fractional charges [38], a new zero resistance state under microwave radiation [39] or new phases based on a decomposition of a half-integer filling factor into stripes and bubbles with integer filling factors [40] are observable. The two-dimensional electron system in strong magnetic field seems to be the ideal system to study electron correlation phenomena in solids with the possibility to control and vary many parameters so that the quantum Hall effect will remain a modern research field also in the future.

References

[1] T. Ando, A. Fowler, and F. Stern, *Rev. Mod. Phys.* **54**, 437 (1982).

[2] A.B. Fowler, F.F. Fang, W.E. Howard, and P.J. Stiles, *Phys Rev. Lett.* **16**, 901 (1966).

[3] H. Aoki and H. Kamimura, *Solid State Comm.* **21**, 45 (1977).

[4] Th. Englert and K. v. Klitzing, *Surf. Sci.* **73**, 70 (1978).

[5] K. v. Klitzing, G. Dorda and M. Pepper, *Phys. Rev. Lett.* **45**, 494 (1980).

[6] Y.S. Myung, *Phys. Rev.* **D 59**, 044028 (1999).

[7] M. Greiter, *Int. Journal of Modern Physics* **A 13** (8), 1293 (1998).

[8] S.C. Zhang and J. Hu, *Science* **294**, 823 (2001).

[9] V. Privman, I.D. Vagner and G. Kventsel, *Phys. Lett.* **A239**, 141 (1998).

[10] M. Fabinger, *J. High Energy Physics* **5**, 37 (2002).

[11] F.W. Hehl, Y.N. Obukhov, and B. Rosenow, *Phys. Rev. Lett.* **93**, 096804 (2004).

[12] R.E. Prange and S. Girvin (ed.), The Quantum Hall Effect, Springer, New York (1987).

[13] M. Stone (ed.), Quantum Hall Effect, World Scientific, Singapore (1992).

[14] M. Janen, O. Viehweger, U. Fastenrath, and J. Hajdu, Introduction to the Theory of the Integer Quantum Hall Effect, VCH Weinheim (1994).

[15] T. Chakraborty, P. Pietilinen, The Quatnum Hall Effects, 2nd Ed., Springer, Berlin (1995).

[16] S. Das Sarma and A. Pinczuk, Perspectives in Quantum Hall Effects, John Wiley, New York (1997).

[17] O. Heinonen (ed.), Composite Fermions: A Unified View of the Quantum Hall Regime, World Scientific, Singapore (1998).

[18] Z.F. Ezawa, Quantum Hall Effects - Field Theoretical Approach and Related Topics, World Scientific, Singapore (2002).

[19] D. Yoshioka,Quantum Hall Effect, Springer, Berlin (2002).

[20] Proc. Int. Symp. Quantum Hall Effect: Past, Present and Future, Editor R. Haug and D. Weiss, Physica E20 (2003).

[21] A.M. Thompson and D.G. Lampard, *Nature* **177**, 888 (1956).

[22] T.J. Quinn, *Metrologia* **26**, 69 (1989).

[23] F. Delahaye, T.J. Witt, R.E. Elmquist and R.F. Dziuba, *Metrologia* **37**, 173 (2000).

[24] F. Delahaye and B. Jeckelmann, *Metrologia* **40**, 217 (2003).

[25] The most recent values of fundamental constants recommended by CODATA are available at: http://physics.nist.gov/cuu/constants/index.html.

[26] E.R. Williams, R.L. Steiner, D.B. Nevell, and P.T. Olsen, *Phys. Rev. Lett.* **81**, 2404 (1998).

[27] E.H. Hall, *American Journal of Mathematics*, **vol ii**, 287 (1879).

[28] Y.Y. Wei, J. Weis, K. v. Klitzing and K. Eberl, *Appl. Phys. Lett.* **71** (17), 2514 (1997).

[29] J. Hüls, J. Weis, J. Smet, and K. v. Klitzing, *Phys. Rev.* **B69** (8), 05319 (2004).

[30] S. Koch, R.J. Haug, K. v. Klitzing, and K. Ploog, *Phys. Rev* **B43** (8), 6828 (1991).

[31] D.B.Chklovskii, B.I. Shklovskii, and L.I. Glazmann, *Phys. Rev.* **B46**, 4026 (1999).

[32] A. Siddiki and R.R. Gerhardts, *Phys. Rev.* **B70**, (2004).

[33] M. Bttiker, *Phys. Rev.* **B38**, 9375 (1988).

[34] D.C. Tsui, H.L. Stormer, and A.C. Crossard, *Phys. Rev. Lett.* **48**, 1559 (1982).

[35] J.K. Jain, *Phys. Rev. Lett.* **63**, 199 (1989).

[36] M.Kellogg, J.P. Eisenstein, L.N. Pfeiffer, and K.W. West, *Phys. Rev. Lett.* **93**, 036801 (2004).

[37] A.H. MacDonald, H.A. Fertig, and Luis Brey, *Phys. Rev. Lett.* **76**, 2153 (1996).

[38] R. de-Picciotto, M. Reznikov, M. Heiblum, *Nature* **389**, 162 (1997).

[39] R.G. Mani, J.H. Smet, K. V. Klitzing, V. Narayanamurti, W.B. Johnson, and V. Urmanski, *Nature* **420**, 646 (2002).

[40] M.P. Lilly, K.B. Cooper, J.P. Eisenstein, L.N. Pfeiffer, and K.W. West, *Phys. Rev. Lett.* **82**, 394 (1999).

Klaus von Klitzing
Max-Planck-Institut für Festkörperforschung
Heisenbergstr. 1
D-70569 Stuttgart
Germany

email: K.Klitzing@fkf.mpg.de

The Quantum Hall Effect, 23 – 53

Poincaré Seminar 2004

Physics in a Strong Magnetic Field

Benoît Douçot and Vincent Pasquier

1 Introduction

A glance at the behavior of resistance of a two dimensional electron system as a function of the perpendicular magnetic field (Fig.1), reveals immediately why the quantum Hall effect has attracted so much attention in the past years. One usually plots the resistivities along the direction of the current (ρ_{xx}) and in the direction perpendicular to it (ρ_{xy}) as a function of the field B. Very schematically, for certain range of the field ρ_{xx} is nearly equal to zero, and for other ranges it develops a bump. On the average ρ_{xy} grows linearly with the field, but in the regions where ρ_{xx} is equal to zero, ρ_{xy} presents a flat plateau which is a fraction times h/e^2 to an extraordinary accuracy. This is the quantized Hall effect which has led to two Nobel prizes, one in 1985 to Von Klitzing for the discovery of the integer Hall effect, and the other in 1992 to Laughlin, Störmer and Tsui for the fractional Hall effect.

The basic experimental observation is best recast using the conductivities σ_{xx} and σ_{xy} which give the components of the inverse of the resistivity tensor [1]. The quantized Hall regime corresponds to a nearly vanishing dissipation:

$$\sigma_{xx} \to 0 \tag{1}$$

accompanied by the quantization of the Hall conductance:

$$\sigma_{xy} = \nu \frac{e^2}{h} \tag{2}$$

In the integer Hall effect case, ν is an integer with a precision of about 10^{-10}. In the fractional case, ν is a fraction which reveals the bizarre properties of many electron physics. The fractions are universal and independent of the type of semiconductor material, the purity of the sample and so forth. The effect occurs when the electrons are at a particular density encoded in the fraction ν as if the electrons locked their separation at particular values. Changing the electron density by a small amount does not destroy the effect but changing it by a larger amount does, this is the origin of the plateaus.

In this introductory seminar we shall present the basic tools needed to understand these phenomena. We first review briefly the classical motion of an electron

[1] $\sigma_{xx} = \frac{\rho_{xx}}{\sqrt{\rho_{xx}^2+\rho_{xy}^2}},\ \sigma_{xy} = \frac{\rho_{xy}}{\sqrt{\rho_{xx}^2+\rho_{xy}^2}}$

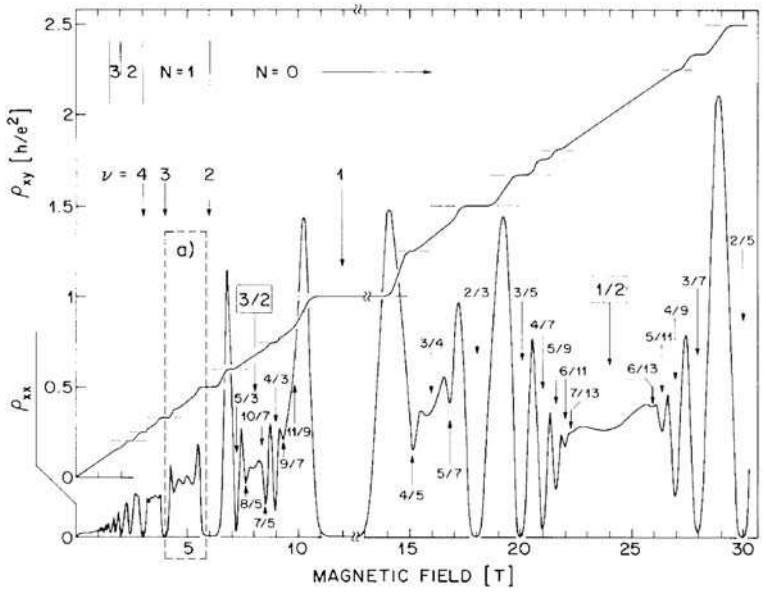

Figure 1: Overview of the diagonal resistivity ρ_{xx} and Hall resistance ρ_{xy} After ref. [4].

in a magnetic field and the classical Hall effect. We then move on to the quantum mechanical description. We introduce the Landau levels and show their relevance to understand the integer Hall effect. Various theoretical ideas to account for the robustness of the plateau values of the Hall conductance are then discussed. Finally, we give some hints of how taking into account electron-electron interactions can explain the occurrence of the fractional Hall effect.

Some classical review papers and references on the quantum Hall effect can be found in ref. [1],[2],[3].

2 Single particle in a magnetic field

2.1 Classical motion in a magnetic field

As a first step we must understand the classical motion of an electron of charge $-e$ confined in a two-dimensional plane (x, y), and subject to a constant magnetic field $B\hat{z}$ perpendicular to this plane. The Newtonian equations of motion due to the Lorentz force are given by:

$$\begin{pmatrix} \ddot{x} \\ \ddot{y} \end{pmatrix} = \frac{eB}{m} \begin{pmatrix} -\dot{y} \\ \dot{x} \end{pmatrix}, \tag{3}$$

where m is the mass of the particle. In complex notation, $z = x + iy$, with ω defined as

$$\omega = eB/m, \tag{4}$$

(3) rewrites

$$\ddot{z} = i\omega\dot{z}. \tag{5}$$

The solution is given by

$$z(t) = z_0 + de^{i\omega t}. \tag{6}$$

The trajectory is a circle of radius $|d|$ run at a constant angular velocity. The frequency ω is independent of the initial conditions and fixed by the magnetic field, the charge and mass of the particle. It is called the cyclotron frequency. The average position of the particle over the time, $z_0 = x_0 + iy_0$, is arbitrary, and is called the guiding center. The radius $|d|$ of the trajectory is proportional to the speed of the particle times its mass. In a Fermi liquid, the speed of the electrons times their mass is frozen and equal to the Fermi momentum. The measurement of the cyclotron radius can thus be used to determine the Fermi momentum [2].

Let us add to the magnetic field an electric field $E\hat{\boldsymbol{y}}$ in the y direction. The equation of motion now becomes,

$$\ddot{z} = i\omega\dot{z} - ieE/m. \tag{7}$$

This equation can be put into the form (5) if we use the variable $z' = z - Et/B$. It results from the fact that the electric field can be eliminated through a Galilean transformation to the frame moving at the speed E/B in the x direction perpendicular to E with respect to the laboratory frame. As a result, in presence of an electric field $\mathbf{E}$, the guiding center moves perpendicularly to the electric field at a speed:

$$\mathbf{v}_0 = \frac{\mathbf{E} \wedge \mathbf{B}}{B^2}. \tag{8}$$

This classical motion is illustrated on Fig. 2.

2.2 Classical Hall effect

Let us study the simple consequences of the classical equation of motion for the resistivity tensor. In a simple model, an electron travels with the Fermi velocity v_f uniformly distributed over all possible directions on a distance given by its mean free path $l_0 = v_f\tau_0$. Here the scattering time τ_0 is the average time between two collisions. This electron is then scattered with the velocity v_f over all possible

[2] Recently, the same experiment has been performed to determine the charge of quasiparticles when the Fermi momentum was known. [32]

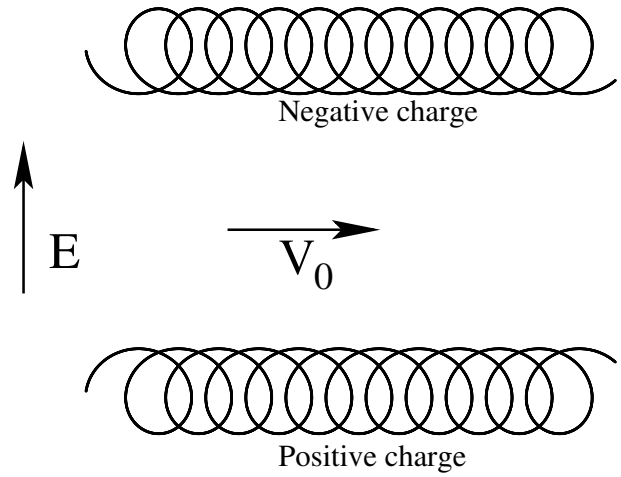

Figure 2: Illustration of cyclotron motion for a classical charged particle in the presence of uniform perpendicular magnetic and electric fields. The magnetic field is perpendicular to the plane of the figure, pointing upwards. The electric field $\mathbf{E}$ lies in the plane as shown. The drift velocity $\mathbf{v}_0 = \frac{\mathbf{E}\wedge\mathbf{B}}{B^2}$ is also represented. We have drawn trajectories for both possible signs of the particle electric charge.

directions. In the presence of an electric field $\mathbf{E}$ it is uniformly accelerated with the acceleration $-e\mathbf{E}/m$ in the direction of the electric field in between two collisions. It thus acquires a mean velocity $\mathbf{v} = -e\mathbf{E}/m\tau_0$ directed parallel to $\mathbf{E}$. In the presence of a uniform magnetic field B, the particles also acquire a uniform speed perpendicular to $\mathbf{E}$. Adding up the contributions of independent electrons with a two dimensional electron number density n, we deduce the resistivity tensor $\boldsymbol{\rho}$ which expresses the linear relation between the current density $\mathbf{j}$ and the electric field $\mathbf{E}$:

$$\begin{pmatrix} E_x \\ E_y \end{pmatrix} = \begin{pmatrix} \rho_{xx} & \rho_{xy} \\ -\rho_{xy} & \rho_{xx} \end{pmatrix} \begin{pmatrix} j_x \\ j_y \end{pmatrix}, \tag{9}$$

where the longitudinal resistivity is:

$$\rho_{xx} = \frac{m}{ne^2\tau_0}, \tag{10}$$

and the transverse (or Hall) resistivity (ρ_{xy}), which relates the current density $j_\perp$ perpendicular to the electric field E to the field itself, has the expression

$$\rho_{xy} = \frac{B}{ne}. \tag{11}$$

This result relies on Galilean invariance only and is not modified by interactions. The simplest way to derive this expression is to assume that the current is known.

To this current, we associate an average electronic velocity $\bar{\boldsymbol{v}}$ so that $\mathbf{j} = -ne\bar{\boldsymbol{v}}$. This velocity generates a Lorentz force $\mathbf{f}_{\mathrm{L}} = -e\bar{\boldsymbol{v}} \wedge \mathbf{B}$, which has to be balanced by a transverse electric field $\mathbf{E}_\perp$ ($\mathbf{E}_\perp.\mathbf{j} = \mathbf{0}$) so that $\mathbf{f}_{\mathrm{L}} - e\mathbf{E}_\perp = \mathbf{0}$, thus giving $\mathbf{E}_\perp = \frac{\mathbf{j}\wedge\mathbf{B}}{ne}$, in agreement with (9) and (11). An alternative viewpoint is that a Galilean transformation to a frame with relative velocity $\bar{\boldsymbol{v}}$ suppresses the transverse electric field $\mathbf{E}_\perp$. If we compare these predictions with the experimental situation mentioned in the introduction, we see that classically the transport is dissipative with a constant longitudinal resistivity, and therefore, the observed vanishing of ρ_{xx} is not predicted by this simple model. However, the average slope of the transverse resistivity with respect to the magnetic field is accurately predicted. At the values for which $\rho_{xx} = 0$, the transverse conductivity is given by the inverse transverse resistivity (11). Comparing the prediction with the experimental result (2) we deduce that the Hall effect occurs when the electron density is close to the value

$$n = \nu \frac{eB}{h}. \tag{12}$$

The quantity h/eB has the dimension of an area and we shall have more to say about it. The fact that Planck's constant appears explicitly in this expression suggests that quantum mechanics plays a crucial role in the formation of those plateaus in ρ_{xy}. But before analyzing the new features induced by quantum mechanics, it is useful to first describe in more detail the Hamiltonian approach to classical motion.

2.3 Hamiltonian formalism

Let us introduce a vector potential $\mathbf{A}(\mathbf{r})$ for the magnetic field:

$$B = \partial_x A_y - \partial_y A_x. \tag{13}$$

The vector potential $\mathbf{A}(\mathbf{r})$ is defined up to a gauge transformation $\mathbf{A}(\mathbf{r}) \to \mathbf{A}(\mathbf{r}) + c\boldsymbol{\nabla}\chi(\mathbf{r})$. The action from which the equations of motion of a mass m and charge $-e$ particle (confined to the plane) in presence of the magnetic field $B\hat{\boldsymbol{z}}$ derive, is given by

$$S = \int_{\mathbf{r}_1}^{\mathbf{r}_2} \left(\frac{m}{2}\dot{\mathbf{r}}^2 - e\mathbf{A}.\dot{\mathbf{r}} \right) dt. \tag{14}$$

Note that the action is not gauge invariant and under a gauge transformation $S \to S - e(\chi(\mathbf{r}_2) - \chi(\mathbf{r}_1))$. Of course, since this change only involves the end points of the electron path, the classical equations of motion are not affected by such a gauge transformation. In presence of a uniform magnetic field, if the particle makes a closed path and returns back to its position, the action accumulated by the potential on the trajectory is eB times the area surrounded by the trajectory.

Using the canonical rules, we obtain a Hamiltonian:

$$H_0 = \frac{1}{2m}\left(\mathbf{p} + e\mathbf{A}\right)^2 = \frac{\boldsymbol{\pi}^2}{2m}, \tag{15}$$

where $\mathbf{p} = m\dot{\mathbf{r}} - e\mathbf{A}$ is the momentum conjugated to $\mathbf{r}$, the quantities $\mathbf{p}$ and $\mathbf{r}$ obey the Poisson brackets:

$$\{p_i, p_j\} = 0, \quad \{r_i, r_j\} = 0, \quad \{p_i, r_j\} = \delta_{ij} \tag{16}$$

and the so-called dynamical momenta:

$$\boldsymbol{\pi} = m\dot{\mathbf{r}} = \mathbf{p} + e\mathbf{A}, \tag{17}$$

obey the Poisson brackets:

$$\{\pi_i, \pi_j\} = \epsilon_{ij} eB, \quad \{r_i, r_j\} = 0, \quad \{\pi_i, r_j\} = \delta_{ij}, \tag{18}$$

where ϵ_{ij} is the antisymmetric tensor $\epsilon_{xy} = -\epsilon_{yx} = 1$.

We can also define new coordinates R_x, R_y which have zero Poisson brackets with the dynamical momenta:

$$R_x = x - \frac{1}{eB}\pi_y, \quad R_y = y + \frac{1}{eB}\pi_x, \tag{19}$$

with the Poisson brackets given by:

$$\{R_i, R_j\} = -\epsilon_{ij}\frac{1}{eB}, \quad \{\pi_i, R_j\} = 0. \tag{20}$$

One can verify that the coordinates so defined coincide with the guiding center defined in (6): $R_x + iR_y = z_0$.

To understand the physical meaning of the guiding center it is instructive to consider the motion of a charged particle in presence of an external potential $V(\mathbf{r})$, which is supposed to vary slowly ($|\partial_i \partial_j V| << m\omega^2$ for all i, j):

$$H = H_0 - eV(\mathbf{r}). \tag{21}$$

The case of the electric field we looked at in the last section, corresponds to $V(\mathbf{r}) = -Ey$. We are interested in the motion of the guiding center in presence of $V(\mathbf{r})$. If the radius of the cyclotron orbital is sufficiently small and the speed of rotation sufficiently fast so that the potential seen during a rotation is approximatively constant, we can average over time; the dynamical momenta acquire a zero expectation value and we can replace the position $\mathbf{r}$ by the guiding center $\mathbf{R}$. In this approximation, the guiding center motion is given by:

$$\dot{\mathbf{R}} = \frac{\mathbf{B} \wedge \boldsymbol{\nabla} V}{B^2}. \tag{22}$$

The motion decomposes into a fast rotation around the cyclotron orbit and a slow motion of the guiding center along the equipotential lines of $V(\mathbf{r})$.

If the potential is smoothly varying, we can divide the equipotential lines into two kinds: Those located near the maxima of V which are closed, and those located near its mean value which can wind a long way through the saddle points of V. We can qualitatively understand why the preceding picture of the transport can be dramatically affected if we take into account the influence of an external potential. In presence of an electric field the potential seen by the electrons becomes $V(\mathbf{R}) - e\mathbf{E}.\mathbf{R}$, and according to whether the equipotential line we consider is closed or extended, the electron traveling along it is localized or not. We shall return to this point later.

A very important consequence of this effective dynamics for guiding centers in the high magnetic field limit is that area is preserved under the time-evolution. This is a special case of Liouville's theorem on the conservation of phase-space volumes for Hamiltonian systems. But here, very remarkably, phase-space has to be identified with the physical plane, since the two coordinates of the guiding center are canonically conjugated according to (20). Physically, this means that if the initial condition is such that the electronic density is constant inside a domain Ω_0, and zero outside, after the system has evolved according to the dynamics (22), it is still constant inside a deformed domain Ω_t of the *same* area as Ω_0 and zero outside. In other words, the electronic fluid is incompressible. As we shall see in section 3.2, this property plays a crucial role in understanding the quantization of σ_{xy}. This can be formalized further if consider the set of Poisson brackets between plane waves $e^{i\mathbf{k}.\mathbf{R}}$ given by:

$$\{e^{i\mathbf{k}.\mathbf{R}}, e^{i\mathbf{k}'.\mathbf{R}}\} = \frac{\mathbf{k} \wedge \mathbf{k}'}{eB} e^{i(\mathbf{k}+\mathbf{k}').\mathbf{R}}. \tag{23}$$

This algebra is known as the algebra of diffeomorphisms which preserve the area.

2.4 Quantum-mechanical description

2.4.1 Quantum formalism

In the Hamiltonian formalism, the quantization of a charged particle in a magnetic field is straightforward. The momenta are operators $p_i = \frac{\hbar}{i}\partial_{r_i}$, where $\hbar = h/2\pi$. The discussion of the preceding section can be repeated with the Poisson brackets replaced by commutators: $\{X, Y\} \to \frac{\hbar}{i}[X, Y]$.

The dynamical momenta and the guiding center define two sets of operators which obey the commutation relations analogous to (18,20):

$$[\pi_i, \pi_j] = -i\hbar\epsilon_{ij}eB, \quad [R_i, R_j] = i\hbar\epsilon_{ij}\frac{1}{eB}, \quad [\pi_i, R_j] = 0. \tag{24}$$

Note that the commutation relations (24) for the dynamical momenta π_i involve the magnetic field at the numerator, whereas those involving the guiding centers

R_i are inversely proportional to the magnetic field. We may therefore expect to recover two different classical limits, when the magnetic field is weak and when it becomes very strong.

To compute the spectrum of H_0 we can define creation and annihilation operators as linear combinations of the two dynamical momenta

$$a = \sqrt{\frac{1}{2\hbar eB}}(\pi_x - i\pi_y), \quad a^+ = \sqrt{\frac{1}{2\hbar eB}}(\pi_x + i\pi_y), \tag{25}$$

obeying the Heisenberg relations:

$$[a, a^+] = 1. \tag{26}$$

In terms of these oscillators the unperturbed Hamiltonian is:

$$H_0 = \hbar\omega(a^+ a + \frac{1}{2}), \tag{27}$$

and its spectrum is that of an oscillator:

$$E_n = \hbar\omega(n + \frac{1}{2}), \tag{28}$$

with $n \geq 0$. Each energy branch is called a Landau level.

The strong magnetic field limit is when the cyclotron radius gets frozen, and the dynamics is fully controlled by the guiding center coordinates. The fact that the guiding center coordinates commute with H_0 implies that its spectrum is extremely degenerate. The two coordinates R_x, R_y do not commute with each other and cannot be fixed simultaneously. There is a quantum uncertainty $\Delta R_x \Delta R_y = \frac{\hbar}{eB}$ to determine the position of the guiding center. It is customary to define the magnetic length l by:

$$l = \sqrt{\frac{\hbar}{eB}}. \tag{29}$$

Due to the uncertainty principle, the physical plane can be thought of as divided into disjoint cells of area $2\pi l^2$ where the guiding center can be localized. This area coincides precisely with the area threaded by one magnetic flux quantum $\Phi_0 = 2\pi\hbar/e$. The degeneracy per energy level and per unit area is $1/2\pi l^2$ so that in an area Ω, the number of degenerate states is:

$$N_\Omega = \frac{\Omega}{2\pi l^2}, \tag{30}$$

so that electrons behave "as if " they acquire some size under a magnetic field, the area being inversely proportional to B.

Imagine now that we continuously fill a bounded region of the plane with noninteracting electrons. Let n be the electron number density. We introduce the so called filling factor as the number of electrons per cell:

$$\nu = n2\pi l^2. \tag{31}$$

Due to the Pauli principle, a cell can be occupied by one electron only per energy level. Therefore, each time the filling factor reaches an integer, an energy level gets filled and the next electron must be added to the next energy level. Thus, the energy per added electron (chemical potential) jumps by a quantity $\hbar\omega$. This is the integer quantum Hall regime, and indeed, comparing (31) with (12) we can identify the filling factors of the Hall effect with the fraction entering the expression of the transverse conductivity (2). Not surprisingly thus, when the filling factor takes integer values, the (integer) Hall effect is observed. This naive approach however, seems to indicate that the integer Hall effect should be observed only at the specific values of the magnetic field for which ν given by (12) or (31) is an integer, instead of some extended regions of B, as seen experimentally. Also, the explanation for the fractional values of ν is out of reach in this approach.

The energy separation between levels must be compared with the other energy scales introduced by the impurities and the interactions which will split the degeneracy. A necessary condition to observe the Hall effect is that the splitting of the energy levels within each Landau level remains small compared to $\hbar\omega$, so that the Landau levels are well separated in energy. This picture however is too naive to account for the width of the plateaus. We must invoke the existence two kinds of energy levels. Extended levels narrowly dispersed around the Landau energy and localized levels which do not carry current but spread in energy. The presence of these localized states is necessary to enable the chemical potential to vary smoothly between two Landau levels instead of jumping abruptly. This seems to ruin the quantization argument made just before, and we shall have more to say to reconcile the quantized picture with the existence of localized states later.

We have just seen that the $\nu = n$ integer Hall effect occurs precisely when the density is such that an integer number of electrons n occupy a magnetic cell. Conversely, we can expect that the $\nu = 1/3$ Hall effect occurs when one electron occupies three cells by himself! This locking of the separation between electrons cannot be accounted for by the Pauli principle. The alternative explanation is that it is due to the interactions between the electrons. This is the starting of Laughlin's theory for the fractional Hall effect, and this aspect is discussed in S. Girvin's lecture.

2.4.2 Landau gauge

Although the bulk properties of a system of electrons must be independent of the gauge choice, it is instructive to carry out the quantization procedure in different gauges. Different gauges can be better suited to different geometries because the shape of the wave functions depends on the gauge choice.

Let us consider the so-called Landau gauge which is well suited to a cylindrical geometry:

$$A_x = -By, \quad A_y = 0. \tag{32}$$

In this gauge the dynamical momenta are:

$$\pi_x = p_x - eBy, \ \pi_y = p_y, \tag{33}$$

and the guiding center coordinates are:

$$R_x = x - \frac{1}{eB}p_y, \quad R_y = \frac{1}{eB}p_x, \tag{34}$$

We can find the simultaneous spectrum of H_0 and R_y, and thus fix the value of the x-momentum $p_x = \hbar k$. We therefore look for eigenfunctions of H_0 in the form:

$$\Psi_k(\mathbf{r}) = e^{ikx} f_k(y). \tag{35}$$

Each value of $R_y = kl^2$ determine an effective one dimensional Hamiltonian for $f_k(y)$:

$$H_k \quad = \quad \frac{1}{2m}p_y^2 + \frac{1}{2}m\omega^2(y - kl^2)^2, \tag{36}$$

where ω is the cyclotron frequency (4). This is the Hamiltonian of a harmonic oscillator centered at a position $y = kl^2$ determined by the momentum in the x direction. The spectrum is independent of k and given by:

$$\epsilon_n = (n + \frac{1}{2})\hbar\omega. \tag{37}$$

Let us for the moment concentrate on the lowest level $n = 0$. The wave functions f_{k0} are Gaussian centered on kl^2 of width l:

$$f_{k0}(y) = \exp\left(-\frac{(y - kl^2)^2}{2l^2}\right). \tag{38}$$

To recover the degeneracy, imagine we impose periodic boundary conditions in the x direction ($x + L_x \equiv x$). This imposes a quantization condition on k which must take the values $k_m = 2\pi m/L_x$ for the wave function (35) to be periodic. For each value of m the Gaussian wave packet $f_{m0}(y)$ is centered on $y_m = 2\pi m l^2/L_x$. The number of allowed values of m in an interval of length L_y is thus $\frac{L_x L_y}{2\pi l^2}$ and we recover the degeneracy (30).

The n^{th} Landau Level wave functions are obtained by acting with the creation operator $(a^+)^n$ on the ground state wave functions $\Psi_k(\mathbf{x})$. One can verify that the wave functions are expressed in terms of Hermite polynomials H_n as:

$$f_{kn}(y) = H_n(\frac{y - kl^2}{l}) \exp\left(-\frac{(y - kl^2)^2}{2l^2}\right). \tag{39}$$

2.4.3 Symmetric gauge

Another useful gauge well suited to study the system on a disc is the so-called symmetric gauge defined by:

$$A_x = -\frac{By}{2}, \quad A_y = \frac{Bx}{2}. \tag{40}$$

In this gauge the guiding center coordinates are:

$$R_x = \frac{x}{2} - \frac{1}{eB}p_y, \quad R_y = \frac{y}{2} + \frac{1}{eB}p_x. \tag{41}$$

We combine them into two oscillators:

$$b = \frac{1}{\sqrt{2}l}(R_x + iR_y), \quad b^+ = \frac{1}{\sqrt{2}l}(R_x - iR_y). \tag{42}$$

The lowest Landau level wave functions are obtained upon acting onto the ground state of (27) with $(b^+)^m$. In this gauge, the angular momentum L is a good quantum number and they carry an angular momentum $L = -m$. Their expression is proportional to [3]:

$$\Psi_{m0}(\bar{z}) = (\bar{z}/l)^m \exp\left(-\frac{z\bar{z}}{4l^2}\right), \tag{43}$$

and they can be visualized as thin circular shells of radius $\sqrt{2m}l$ around the origin. Thus if we quantize the system in a disk of finite radius R, we recover the expected degeneracy (30) by keeping only the wave functions confined into the disk $m \leq m_0 = R^2/2l^2$. By taking linear combinations of wave functions (43) we see that the general wave functions are proportional to polynomials of fixed degree m_0 in z. A useful way to characterize them is through the location of their zeros $\bar{Z}_i$:

$$\Psi_0(\bar{z}) = \prod_{i=1}^{m_0}(\bar{z} - \bar{Z}_i)\exp\left(-\frac{z\bar{z}}{4l^2}\right). \tag{44}$$

3 Hall conductance Quantization: the Integer Effect

3.1 Galilean invariant systems

The first important thing to emphasize is that for a two-dimensional Galilean invariant system, (in the absence of impurities or boundaries) a full quantum-mechanical treatment yields the *same* resistivity tensor as for the pure classical system, namely $\rho_{xx} = 0$ and $\rho_{xy} = B/(ne)$, or equivalently, $\sigma_{xx} = 0$ and $\sigma_{xy} = ne/B$.

[3] This convention is not usual, most people prefer to use conventions for which $\bar{z} \to z$.

To check this, let us consider the following Hamiltonian, for a system of N interacting electrons in the presence of uniform time-independent perpendicular magnetic ($\mathbf{B}$) and electric fields ($\mathbf{E}$):

$$H = \frac{1}{2m}\sum_{j=1}^{N}\left((\mathbf{P}_j + e\mathbf{A}(\mathbf{r}_j))^2 - eV(\mathbf{r}_j)\right) + \frac{1}{2}\sum_{i\neq j} U(\mathbf{r}_i - \mathbf{r}_j) \tag{45}$$

where as usual, $\mathbf{B} = \nabla \wedge \mathbf{A}$, $\mathbf{E} = -\nabla V$, and U is the pair interaction potential. Inspired by the discussion of the classical case, let us now introduce the following transformation on the N-particle wave-function $\Psi(\mathbf{r}_1, \mathbf{r}_2, \ldots, \mathbf{r}_N, t)$:

$$\Psi(\mathbf{r}_1, \mathbf{r}_2, \ldots, \mathbf{r}_N, t) = \exp\left(\frac{i}{\hbar}\sum_{j=1}^{N}\theta(\mathbf{r}_j, t)\right)\tilde{\Psi}(\mathbf{r}'_1, \mathbf{r}'_2, \ldots, \mathbf{r}'_N, t) \tag{46}$$

where $\mathbf{r}_j$ denotes the position of particle j in the laboratory frame and $\mathbf{r}'_j$ its position in the moving frame, with constant velocity $\mathbf{v}_0$ given by:

$$\mathbf{v}_0 = \frac{\mathbf{E} \wedge \mathbf{B}}{B^2}. \tag{47}$$

Therefore, we have the relation: $\mathbf{r}'_j = \mathbf{r}_j - \mathbf{v}_0 t$. It is possible to choose the phase $\theta(\mathbf{r}, t)$ in such a way that $\tilde{\Psi}$ satisfies the time-dependent Schrödinger equation associated to the simplified Hamiltonian $\tilde{H}$ deduced from H by removing the potential term $-e\sum_j V(\mathbf{r}_j)$. So in the inertial frame moving with constant velocity $\mathbf{v}_0$, there is no electrical field, and only the original magnetic field remains. Note that the expression of $\theta(\mathbf{r}, t)$ does depend on the choice of gauge. For instance, in the radial gauge $\mathbf{A} = \frac{1}{2}\mathbf{B} \wedge \mathbf{r}$, we have:

$$\theta(\mathbf{r}, t) = m\mathbf{v}_0.\mathbf{r} - \frac{1}{2}(mv_0^2 + e\mathbf{E}.\mathbf{r})t.$$

The phase-factor does not alter the classical composition rule for currents, and we get

$$\langle\Psi|\mathbf{J}(\mathbf{r})|\Psi\rangle = -ne\mathbf{v}_0 + \langle\tilde{\Psi}|\mathbf{J}(\mathbf{r}')|\tilde{\Psi}\rangle. \tag{48}$$

Now since there is no driving electric field in the moving frame, $\langle\tilde{\Psi}|\mathbf{J}(\mathbf{r}')|\tilde{\Psi}\rangle = \mathbf{0}$, so $\langle\Psi|\mathbf{J}(\mathbf{r})|\Psi\rangle = -ne\mathbf{v}_0$ which is exactly the classical result.

As we have seen, the natural way to measure the electronic density for a two-dimensional quantum system in a magnetic field is the filling factor $\nu = \frac{nh}{eB}$. So we end up with

$$\sigma_{xy} = \nu\frac{e^2}{h}. \tag{49}$$

Although this expression does involve Planck's constant, it is important to note once again that it is *identical* to the classical prediction for a uniform fluid of electrons of areal density n. As illustrated on Fig. 1, this prediction for a Galilean

invariant system coincides with the experimental result for the Hall conductance when the filling factor ν is an integer. The existence of quantized plateaus of the form $\sigma_H = n\frac{e^2}{h}$, with n integer clearly indicates the breakdown of Galilean invariance in real samples, since the two expressions differ when ν is not an integer. This fact is not too surprising, since there is always a random electrostatic potential induced by the impurities which are required to generate charge carriers at the interface between two semi-conductors. The most surprising fact is that despite this random potential (without which there would be no observable Hall quantization!) the measured plateau values are universal with a very high accuracy. Of course, a lot of theoretical work has been dedicated to explain this remarkable phenomenon. To give a simple outline, we may classify most of the existing approaches in the following way:

– the Laughlin argument [5]
– expressing the Hall conductance as a topological invariant [6]
– the Edge-State picture [7].

We shall try here to give a flavor of these important contributions, but let us first begin to present a rather simple and helpful semi-classical analysis [8].

3.2 An intuitive picture

It is indeed very illuminating to consider the limit of an extremely strong magnetic field, so that the magnetic length $l = (\frac{\hbar}{eB})^{1/2}$ is much smaller than the typical length-scales associated to the spacial variations of the impurity potential $U_{\rm imp}(\mathbf{r})$. Classically, we have seen that the guiding center $\mathbf{R}$ of classical orbits for a single electron obeys the following equations of motion:

$$\dot{\mathbf{R}} = \frac{\mathbf{B} \wedge \boldsymbol{\nabla}}{B^2}(V - \frac{U_{\rm imp}}{e})(\mathbf{R}). \tag{50}$$

In particular, this implies that $W(\mathbf{R}) = (V - \frac{U_{\rm imp}}{e})(\mathbf{R})$ is conserved, so the classical trajectories of guiding centers in the infinite B limit coincide with equipotential curves of the function $W(\mathbf{R})$. Using the intuition gained in section **1**, we expect that after quantization, single particle eigenstates are located along narrow strips of width l centered on these equipotential lines. As usual in semi-classical quantization, only a discrete set of classical orbits are allowed. An extension of the Bohr-Sommerfeld principle indicates that for closed classical orbits, only those which enclose an integer number of flux quanta give rise to quantum eigenstates. Let us denote by W_i the potential energies associated to these selected orbits. We get then the following semi-classical spectrum:

$$E_{i,n} = -eW_i + \hbar\omega(n + \frac{1}{2}) \tag{51}$$

where n is any non-negative integer corresponding to quantizing the fast cyclotron motion around the slow moving guiding center. For a fixed value of n, we may

then speak of a generalized n^{th} Landau level, although the degeneracy of this level is lifted by the joint effect of the driving electric field and the impurity potential. When such a level is completely filled, it induces a spacial density of electrons (after coarse-graining on a length-scale of the order of the corresponding cyclotron radius $n^{1/2}l$) equal to $\frac{eB}{h}$, mostly insensitive to the form of the effective potential $W(\mathbf{R})$.

Let us consider now our system to be a horizontal strip defined by $0 \leq y \leq L_y$. We apply an external field along the y direction, in such a way that the edges of the sample $y = 0$ and $y = L_y$ are equipotential lines for V. On average, we expect a global Hall current j_x in the horizontal direction. Each generalized Landau level produces a local current:

$$j_{x,n} = -e\left(\frac{eB}{h}\right)\theta(\mu + eW(\mathbf{R}) - \hbar\omega(n + \frac{1}{2}))v_x(\mathbf{R}) \tag{52}$$

where $v_x(\mathbf{R}) = -\frac{1}{B}\frac{\partial W}{\partial y}(\mathbf{R})$, and μ is the chemical potential of the electronic system. The Heaviside step function $\theta(\mu + eW(\mathbf{R}) - \hbar\omega(n + \frac{1}{2}))$ is the limiting form of the Fermi-Dirac distribution for the semi-classical spectrum (51) at zero temperature. Let us now integrate this local current along a vertical section of the sample, at fixed $x = x_0$. This yields:

$$I_{x,n}(x_0) = \frac{e^2}{h}\int_0^{L_y} dy\, \theta(\mu + eW(x_0, y) - \hbar\omega(n + \frac{1}{2}))\frac{\partial W}{\partial y}(x_0, y). \tag{53}$$

To simplify the discussion, let us assume that the impurity potential vanishes on the edges (for $y = 0$ and $y = L_y$). The above integral is easily computed, and the result distinguishes between four cases:

1)$-eW(x_0, y) + \hbar\omega(n + \frac{1}{2}) \equiv E_n(x_0, y) > \mu$ for both $y = 0$ and $y = L_y$.

This means that the n^{th} generalized Landau level is unoccupied in the presence of the external driving voltage, in the limit where the impurity potential vanishes. In this case, $I_{x,n}(x_0) = 0$. Note that this value is independent of the strength of the local impurity potential. In particular, if $U_{\text{imp}}(\mathbf{R})$ has deep local minima, it may happen that $E_n(\mathbf{R}) < \mu$ in some finite areas, meaning that there are occupied bound states in the n^{th} Landau level localized near impurities. But in this very large field limit, we see that such localized states do not contribute to the global Hall current.

2)$E_n(x_0, y) < \mu$ for both $y = 0$ and $y = L_y$.

In the limit of vanishing impurity potential, the corresponding Landau level is then fully occupied. We obtain:

$$I_{x,n}(x_0) = \frac{e^2}{h}\left(W(x_0, L_y) - W(x_0, 0)\right) = \frac{e^2}{h}\left(V(L_y) - V(0)\right). \tag{54}$$

Again, this result is independent of the strength of the impurity potential. Such a fully occupied level provides therefore a contribution equal to $\frac{e^2}{h}$ to the total Hall conductance.

3)$E_n(x_0, 0) > \mu$ and $E_n(x_0, L_y) < \mu$.

Then

$$I_{x,n}(x_0) = \frac{e^2}{h} \frac{\mu - E_n(x_0, L_y)}{e}. \tag{55}$$

4)$E_n(x_0, 0) < \mu$ and $E_n(x_0, L_y) > \mu$.

Then

$$I_{x,n}(x_0) = \frac{e^2}{h} \frac{E_n(x_0, 0) - \mu}{e}. \tag{56}$$

These last two cases correspond to Landau levels which are partially filled in the absence of impurity potential, but in the presence of the driving field. They destroy the quantization of σ_{xy}. In order to avoid them, one has to fix the chemical potential in a gap of the unperturbed Landau level spectrum, and impose a weak enough driving electric field, typically such that $e|V(x_0, L_y) - V(x_0, 0)| < \hbar\omega$. If these conditions are satisfied, we have an integer number p of filled Landau levels which contribute to the Hall current, so that

$$I_x(x_0) = p\frac{e^2}{h} \left(V(L_y) - V(0)\right) \tag{57}$$

in perfect agreement with:

$$\sigma_{xy} = p\frac{e^2}{h}. \tag{58}$$

When does this simple and appealing picture break down? Clearly, it is problematic when the typical scale of the impurity potential becomes comparable to the magnetic length l. In this case, it is no longer possible to preserve such a simple description of quantum energy eigenstates. Nevertheless, as shown on Fig. 3 illustrating the effect of a strong scatterer modeled as an impenetrable disk of radius a, even when a is small compared to the cyclotron radius, we may expect that such a scatterer does not disturb the shape of a strip-like eigenstate excepted in its immediate vicinity. In particular, the overall direction of propagation of a wave-packet is not modified by the presence of such impurities. These qualitative expectations are confirmed by more detailed perturbative calculations [8].

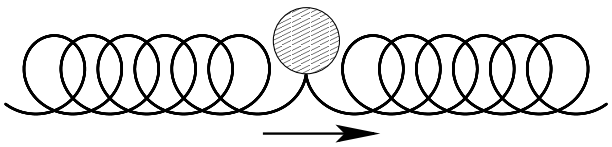

Figure 3: Illustration of cyclotron motion for a classical charged particle in the presence of uniform perpendicular magnetic and electric fields. A hard circular point scatterer is depicted as a dashed-filled circle.

More serious problems arise when strong localized scatterers are densely packed, namely with an average nearest-neighbor spacing of the order of l. In this case, classical trajectories become very complicated. Quantum-mechanically, we expect that such a strong potential induces strong mixing between different Landau levels, and therefore, a perturbative analysis is not very helpful. Fortunately, a very interesting and famous argument has been given by Laughlin [5] which shows that nevertheless a strict quantization of σ_{xy} is still possible.

3.3 The Laughlin argument

Let us consider the same strip as before, defined by $0 \leq y \leq L_y$, but let us fold it into a cylinder by identifying points (x, y) and $(x + L_x, y)$. The magnetic field $\mathbf{B}$ is still normal to this finite domain, and a driving electric field is still applied along the y direction. To evaluate the current $j_x(\mathbf{r})$ in the quantum mechanical ground-state of this system, Laughlin uses the following exact relation:

$$j_x(\mathbf{r}) = -\frac{\partial \langle H \rangle}{\partial A_x(\mathbf{r})} \tag{59}$$

where $\mathbf{A}(\mathbf{r})$ is the external magnetic vector potential. Let us now impose spacial variations $\delta\mathbf{A}(\mathbf{r})$ of the form: $\delta A_x(\mathbf{r}) = \frac{\delta\Phi}{L_x}$ and $\delta A_y(\mathbf{r}) = 0$. Such variations do *not* modify the gauge-invariant electric and magnetic fields, but they introduce an Aharonov-Bohm flux through any closed path winding once around the cylinder in the positive x direction. The corresponding infinitesimal variation of the system average energy is:

$$\delta\langle H \rangle = -\frac{\delta\Phi}{L_x} \int_0^{L_x} dx \int_0^{L_y} dy\, j_x(\mathbf{r}) = -\delta\Phi\, I_x. \tag{60}$$

So the Hall current I_x is simply expressed as:

$$I_x = -\frac{d\langle H \rangle}{d\Phi}. \tag{61}$$

Now Laughlin assumes that as Φ varies, the ground-state wave-function $|\Psi_0(\Phi)\rangle$ undergoes a smooth evolution, Φ being considered as an external parameter of the system Hamiltonian. A sufficient condition for this to occur is when the ground-state is unique, and well separated by a finite energy gap from excited states created in the *bulk* of the system. This happens for instance for non-interacting electrons with an integer filling factor in the limit of a weak impurity potential.

Let us now vary Φ by a *finite* quantity $\Phi_0 = h/e$. Note that the effect of changing Φ is simply the same as changing the periodic boundary condition along the x direction, so its effect on a macroscopic system is expected to be small. One way to see this is to consider single particle eigenstates in the Landau gauge ($A_x = -By$, $A_y = 0$). These states are localized in narrow strips centered around horizontal lines such that $y_m = \frac{2\pi l^2}{L_x}(m + \Phi/\Phi_0)$, m integer. So changing Φ into $\Phi + \Phi_0$ amounts

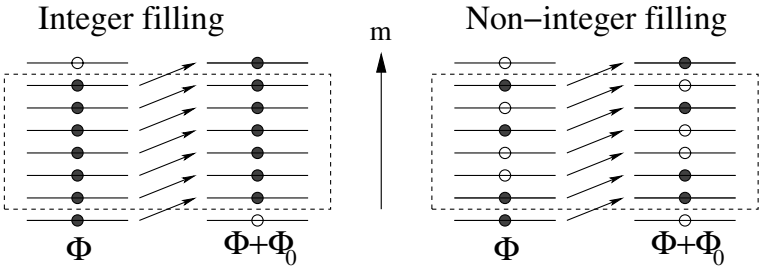

Figure 4: Illustration of the change in the spatial distribution of occupied energy states within a single Landau level, as flux Φ is changed into $\Phi + \Phi_0$. For integer filling, no change occurs in the bulk of the system (depicted by the dashed parallelogram), and the global effect is to transfer one electron from the lower to the upper boundary. For non-integer filling factor, this adiabatic process also implies a change of the level occupancy pattern in the bulk of the system.

simply to changing m into $m+1$ and the single electron spectrum is invariant in this operation. This in fact expresses the gauge-invariance of quantum-mechanics, as first emphasized by Aharonov and Bohm. In particular, this periodicity of the spectrum as a function of Φ with period Φ_0 holds for interacting electron systems such as those described by the Hamiltonian (45). Denoting by $\Delta\langle H\rangle$ the variation of the system energy during such process, Laughlin assumes that we may still write:

$$I_x = -\frac{\Delta\langle H\rangle}{\Phi_0}. \tag{62}$$

Suppose now the chemical potential is such that the ground-state is well separated from excited states by an energy gap, at least when the driving electric field vanishes. Again, this is the case for non-interacting electrons with an integer filling factor in the limit of weak impurity potential. Then upon changing Φ into $\Phi+\Phi_0$, we cannot modify the wave-function in the bulk of the system. However, as the example of non-interacting electrons suggests (see Fig. 4), we may still transfer an integer number p of electrons (since the quantum number m is shifted into $m+1$) from the lower edge to the upper edge. More precisely, for non-interacting electrons with an integer filling factor ν, then $p = \nu$. In this situation, the energy variation $\Delta\langle H\rangle$ during the shift from Φ to $\Phi + \Phi_0$ is of purely electrostatic origin, so that

$$\Delta\langle H\rangle = -pe(V(L_y) - V(0)). \tag{63}$$

From Eq. (62), this yields:

$$I_x = p\frac{e^2}{h}(V(L_y) - V(0)) \tag{64}$$

or equivalently, $\sigma_{xy} = p\frac{e^2}{h}$.

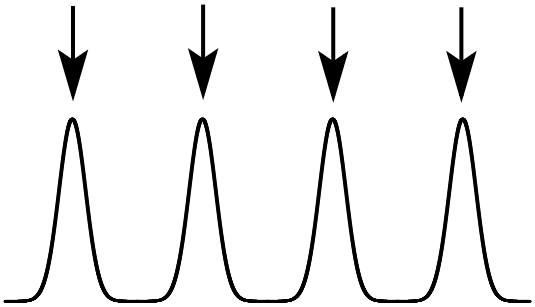

Figure 5: Schematic plot of the density of single particle energy levels, as a function of energy in the presence of a static random impurity potential. The arrows correspond to positions of Landau levels for a pure system, and to extended states in the disordered case. The random potential lifts the huge degeneracy of each Landau level, and most of energy eigenstates become spatially localized.

The strength of this argument is that it is also valid for interacting systems, in the presence of a random potential, as long as the excitation gap present for the pure non-interacting system at integer ν is preserved. To some extent, we may even drop the weak disorder assumption. To see this, let us consider a non-interacting system, but with a possibly large disorder. The density of states has schematically the shape shown on Fig. 5 where the gaps of the Landau level spectrum have been partially filled under the influence of the random impurity potential. In two dimensions, (and in absence of magnetic field), it is very likely that all energy eigenstates are spacially localized [9]. Such localized wave-functions are mostly insensitive to changing boundary conditions, and therefore do not contribute to the adiabatic charge transport process involved in Laughlin's argument. This should yield a vanishing Hall conductance. However, there are theoretical arguments [10, 11] and substantial numerical evidence [12] that in the presence of a uniform magnetic field, some delocalized eigenstates exist for a discrete set of energies, in one to one correspondence with the original Landau levels (see arrows on Fig. 5). Understanding precisely the onset of such extended states as the energy is tuned towards one of these critical values still remains a theoretical challenge [13]. A recent review on these magnetic-field induced delocalization transitions may be found in a paper by Kramer et al. [14]. Combining this picture of the single-particle spectrum (mostly localized states, but isolated energies allowing for extended states) with Laughlin's argument shows that the quantized Hall conductance $\sigma_{xy} = p\frac{e^2}{h}$ may still exist in a relatively strong disorder regime.

Finally, let us mention briefly the case of arbitrary filling factors ν. We may still use Eq. (62) to evaluate the Hall conductance. In the case of non-interacting electron for a pure system, we have a partially filled Landau level crossing the

Fermi energy. Therefore, the process of adding one flux quantum Φ_0 in the system translates the pattern of occupied and empty horizontal strip-like single particle states by the amount $\Delta y = \frac{2\pi l^2}{L_x}$, as shown on Fig. 4. Another way to say this is that this adiabatic process induces particle-hole excitations inside the partially occupied Landau level, which affect now the bulk of the system, and not only its boundaries. The corresponding change in electrostatic energy is then proportional to the total number of electrons, and this implementation of the Laughlin argument yields the *classical, unquantized* value $\sigma_{xy} = \nu \frac{e^2}{h}$. The situation changes dramatically in the presence of electron-electron interactions, and indeed plateau values of the form $\sigma_{xy} = \frac{p}{q}\frac{e^2}{h}$ have been observed, where p is an integer and q an odd integer [15]. In a pioneering insight [16], Laughlin explained the appearance of these fractional values as a consequence of two remarkable properties of the system:
i)Interactions are lifting completely the degeneracy of the partially filled Landau level, at least for filling factors $\nu = 1/q$, q odd. The corresponding ground-state is liquid-like, isotropic and translationally-invariant.
ii)The elementary locally charged excitations correspond to collective reorganizations of the electron fluid producing a fractional charge $e^* = 1/q$.
These two surprising properties of the energy spectrum and of elementary excitations have been incorporated by Laughlin in his 1981 argument to account for the existence of quantized plateaus in σ_{xy} with a fractional value. Since the theory of this fractional effect is the subject of S. Girvin's contribution to this seminar, we shall not discuss it further here.

3.4 The Hall conductivity as a topological invariant

Let us further modify the geometry used for the Laughlin argument by gluing together the lower ($y = 0$) and upper ($y = L_y$) edges of the cylinder, thus forming a torus. The small external driving field is still uniform, directed along $\hat{\boldsymbol{y}}$, and we shall still measure the current density $\langle j_x \rangle$ along the $\hat{\boldsymbol{x}}$ direction. As we wish to apply linear response theory, it is convenient to work with a time-dependent electric field:

$$E_y(t) = \int \frac{d\omega}{2\pi} e^{-i\omega t} \tilde{E}_y(\omega). \tag{65}$$

The frequency-dependent Hall conductivity $\sigma_{xy}(\omega)$ is defined by:

$$\tilde{j}_x(\omega) = \sigma_{xy}(\omega)\tilde{E}_y(\omega). \tag{66}$$

Quantum-mechanically, the simplest way to introduce an electric field is through a time-dependent vector-potential $\delta\mathbf{A}(t)$ such that $E_y(t) = -\frac{\partial \delta A_y(t)}{\partial t}$, or equivalently: $\tilde{E}_y(\omega) = i\omega\delta\tilde{A}_y(\omega)$. If we define $K_{xy}(\omega)$ to be such that $\tilde{j}_x(\omega) = K_{xy}(\omega)$ $\delta\tilde{A}_y(\omega)$, then: $\sigma_{xy}(\omega) = \frac{K_{xy}(\omega)}{i\omega}$. For a uniform electric field, δA_y is also spatially uniform. In real space and time, the response kernel K_{xy} is given by the standard

Kubo linear response formula:

$$K_{xy}(\mathbf{r},t;t') = \frac{i}{\hbar}\langle[\frac{\delta H}{\delta A_x(\mathbf{r})}, \int \frac{\delta H}{\delta A_y(\mathbf{r}')} d^2\mathbf{r}']\rangle, \tag{67}$$

where we have used again $j_x(\mathbf{r}) = -\frac{\delta H}{\delta A_x(\mathbf{r})}$, and the fact that δA_y is uniform. The quantum-mechanical expectation values are taken in the ground state of the system, since we are assuming a very low temperature. In the absence of impurities, we expect a uniform current, but if impurities are present, only the total current $I_x(x) = \int_0^{L_y} dy\, j_x(x,y)$ is independent of x (because of current conservation) in the static limit. It is therefore natural to average the above response function over the "probe" position $\mathbf{r}$. Introducing fluxes Φ_x and Φ_y as in the previous section, but now along the two main directions of the torus, we may write this space-averaged response function as:

$$K_{xy}(\mathbf{r},t;t') = \frac{i}{\hbar}\frac{1}{L_x L_y}\langle[\int \frac{\delta H}{\delta A_x(\mathbf{r})} d^2\mathbf{r}, \int \frac{\delta H}{\delta A_y(\mathbf{r}')} d^2\mathbf{r}']\rangle = \frac{i}{\hbar}\langle[\frac{\partial H}{\partial \Phi_x}, \frac{\partial H}{\partial \Phi_y}]\rangle. \tag{68}$$

Transforming to Fourier-space, we now obtain:

$$\sigma_{xy}(\omega) = \frac{i}{\hbar\omega}\sum_\alpha \left\{ \frac{\langle 0|\partial_x H|\alpha\rangle\langle\alpha|\partial_y H|0\rangle}{\omega - \omega_{\alpha 0}} - \frac{\langle 0|\partial_y H|\alpha\rangle\langle\alpha|\partial_x H|0\rangle}{\omega + \omega_{\alpha 0}} \right\} \tag{69}$$

where $|0\rangle$ is the ground-state and $|\alpha\rangle$ denotes a complete orthonormal basis of energy eigenstates of H, with energies E_α. The Bohr frequencies $\omega_{\alpha 0}$ are equal to $(E_\alpha - E_0)/\hbar$. In this expression, H is the *full* Hamiltonian of the system in the absence of driving electric field. It may therefore include both impurity potentials and interaction effects. To simplify notations, $\partial_x H$ and $\partial_x H$ stand respectively for $\frac{\partial H}{\partial \Phi_x}$ and $\frac{\partial H}{\partial \Phi_y}$. Gauge-invariance requires that the current vanishes when a static uniform vector potential is applied. This enables us to replace the above expression by:

$$\sigma_{xy}(\omega) = \frac{i}{\hbar}\sum_\alpha \left\{ \frac{\langle 0|\partial_x H|\alpha\rangle\langle\alpha|\partial_y H|0\rangle}{\omega_{\alpha 0}(\omega - \omega_{\alpha 0})} + \frac{\langle 0|\partial_y H|\alpha\rangle\langle\alpha|\partial_x H|0\rangle}{\omega_{\alpha 0}(\omega + \omega_{\alpha 0})} \right\} \tag{70}$$

which has a well-defined static limit $\omega \to 0$ provided the system has a finite energy gap, so that denominators are not vanishing in this limit. We may then write the static Hall conductance as:

$$\sigma_{xy} = \frac{\hbar}{i}\sum_\alpha \left\{ \frac{\langle 0|\partial_x H|\alpha\rangle\langle\alpha|\partial_y H|0\rangle}{(E_0 - E_\alpha)^2} - \frac{\langle 0|\partial_y H|\alpha\rangle\langle\alpha|\partial_x H|0\rangle}{(E_0 - E_\alpha)^2} \right\}. \tag{71}$$

It is now convenient to view the Aharonov-Bohm fluxes Φ_x and Φ_y as external parameters. The ground-state $|0\rangle$ becomes a function of $(\Phi_x, \Phi_y) \equiv \mathbf{\Phi}$ and we shall denote it by $|\mathbf{\Phi}\rangle$. This allows us to recast the previous equation as:

$$\sigma_{xy}(\mathbf{\Phi}) = \frac{\hbar}{i}\left(\frac{\partial\langle\mathbf{\Phi}|}{\partial\Phi_x}\frac{\partial|\mathbf{\Phi}\rangle}{\partial\Phi_y} - \frac{\partial\langle\mathbf{\Phi}|}{\partial\Phi_y}\frac{\partial|\mathbf{\Phi}\rangle}{\partial\Phi_x} \right). \tag{72}$$

This may be regarded as the curl of a two-dimensional vector:

$$\frac{1}{i}\left(\langle\mathbf{\Phi}|\frac{\partial|\mathbf{\Phi}\rangle}{\partial\Phi_x},\langle\mathbf{\Phi}|\frac{\partial|\mathbf{\Phi}\rangle}{\partial\Phi_y}\right). \tag{73}$$

Since $\langle\mathbf{\Phi}|\mathbf{\Phi}\rangle = 1$, this vector has purely real components. The above expression depends on a choice of two Aharonov-Bohm fluxes (Φ_x, Φ_y), which by gauge transformations is equivalent to choosing the following boundary conditions for the wave-functions (for simplicity of notation, we consider just one electron here, since generalization to N electrons is obvious):

$$\Psi(x+L_x,y) = e^{i2\pi\frac{\Phi_x}{\Phi_0}}\Psi(x,y) \tag{74}$$

$$\Psi(x,y+L_y) = e^{i2\pi\frac{\Phi_y}{\Phi_0}}\Psi(x,y). \tag{75}$$

This is of course connected to the idea that all physical quantities, like $\sigma_{xy}(\mathbf{\Phi})$ are periodic functions of both Φ_x and Φ_y with period Φ_0. So the $\mathbf{\Phi}$-plane may be folded onto a two-dimensional torus.

Let us now make the assumption that $\sigma_{xy}(\mathbf{\Phi})$ is only very weakly modified upon changing these boundary conditions. In the case where the ground-state is well separated from excited states by a finite energy gap, arguments have been given to show that $\sigma_{xy}(\mathbf{\Phi})$ becomes constant for a large system, up to corrections of order l/L_x, l/L_y [6]. We may therefore replace $\sigma_{xy}(\mathbf{\Phi})$ by its average over the $\mathbf{\Phi}$-torus and then transform the two-dimensional integral of a curl into a line-integral along the boundary of the square $[0,\Phi_0]\times[0,\Phi_0]$:

$$\sigma_{xy} = \frac{e^2}{h}\frac{1}{2\pi i}\int_{\square}\langle\mathbf{\Phi}|d|\mathbf{\Phi}\rangle. \tag{76}$$

But as shown in Appendix, the quantity $\frac{1}{2\pi i}\int_{\square}\langle\mathbf{\Phi}|d|\mathbf{\Phi}\rangle$ is equal to $2\pi n_{\mathrm{C}}$ where n_{C} is an integer called a Chern number. Finally, we get [17, 6]:

$$\sigma_{xy} = n_{\mathrm{C}}\frac{e^2}{h}. \tag{77}$$

Note that this formula seems to be valid in great generality, so we may wonder how we might explain fractional values for the Hall conductance. In fact, the above derivation requires the ground-state to be *unique* for all values of $\mathbf{\Phi}$. For fractional filling factors of the form $\nu = p/q$, Tao and Haldane have shown that the ground-state is q-fold degenerate on a torus in the absence of impurities [18]. Furthermore, since these degeneracies are associated only to the center of motion of the electron fluid, the effect of impurities on the energy spectrum is rather small whenever there is an energy gap for internal excitations. These authors have shown how such degeneracies induce values of the form p/q in unity of e^2/h for the Hall conductivity.

We have not covered here all the aspects related to this description of the Hall conductivity as a topological invariant. A recent very accessible review may

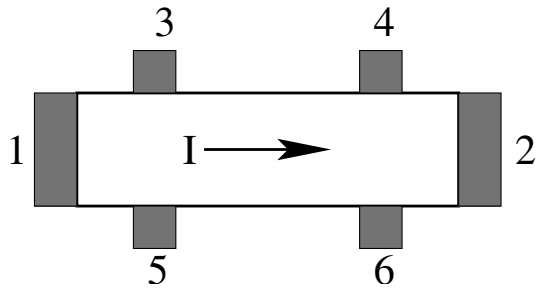

Figure 6: Typical geometry of a Hall bar. The current I is injected in the sample through contacts labelled 1 and 2. Lateral contacts labelled from 3 to 6 are used to measure the longitudinal voltage as for instance $V_3 - V_4$ or the Hall voltage as for instance $V_3 - V_5$.

be found in [19]. We also mention briefly that such topological ideas have generated a rigorous proof of the integer Hall conductance quantization for an infinite disordered system of non-interacting electrons [20]. This work uses a rather elaborate mathematical apparatus (K-theory for C^* algebras) which we will not try to describe here, so the interested reader is invited to consult the original paper [20].

3.5 Edge-state picture of the Quantum Hall effect

Starting from an influential paper by Halperin [21], this viewpoint has been emphasized by Büttiker [7], and plays a crucial role in experiments aimed at showing the existence of fractionally charged quasi-particles in the fractional regime. These experiments will be discussed in detail by C. Glattli. Here, we shall just present a brief introduction to this approach.

Usually, experiments and metrological applications of the quantum Hall effect involve
rectangular-shaped samples schematized on Fig. 6. Current is injected along the long axis of the Hall bar, and voltage probes located on the sides of the sample are used to measure longitudinal and Hall resistivities. In such systems, there is a strong but smooth lateral confining potential for electron approaching outer boundaries. The corresponding semi-classical spectrum for non-interacting electron has the shape shown on Fig. 7(a) inspired from [21]. From our description of the dynamics in a large magnetic field, we expect that even in the absence of external electric field, the strong confining potential gradients will induce static currents along boundaries. With a positive magnetic field along the $\hat{\boldsymbol{z}}$ direction, electrons acquire a positive group velocity along the upper boundary ($y \simeq L_y$) and a negative group velocity along the lower one ($y \simeq 0$). The same reasoning as in section 3.2 applies here showing that the total current across a section of the system vanishes, so there is no global current along the sample in equilibrium.

What happens when the system is driven out of equilibrium by a non-zero average longitudinal current injected in the sample by external contacts (labeled 1 and 2 on Fig. 6)? This simply means that the population of edge states will be increased (resp. decreased) with respect to their equilibrium values when edge currents move in the same (resp. opposite) direction as the injected current. In other words, the chemical potentials $\mu(L_y)$ and $\mu(0)$ on both edges are now different. The difference $\mu(L_y) - \mu(0)$ is precisely equal to $-e(V(L_y) - V(0))$ which is the energy cost to transfer an electron from the Fermi level at $y = 0$ to the Fermi level at $y = L_y$. Adapting Eq. (53), we now have:

$$I_{x,n}(x_0) = \frac{e^2}{h} \int_{-\infty}^{\infty} dy\, \theta(\mu(y) + eW(x_0, y) - \hbar\omega(n + \frac{1}{2})) \frac{\partial W}{\partial y}(x_0, y). \tag{78}$$

Here, $W(x, y)$ is the sum of random impurity and confining electrostatic potentials. By contrast to the discussion in section 3.2, it does not include an external driving field, since the current is viewed here as the result of imposing an out of equilibrium distribution of single-particle states along edges. The integral has now been extended to $[-\infty, \infty]$ since the precise locations of the sample edges do depend on the populations of edges states as illustrated on Fig. 7(b). Each filled Landau level produces now an integrated current:

$$I_{x,n}(x_0) = \frac{e^2}{h}(W(L_y) - W(0)). \tag{79}$$

But we have

$$-e(W(L_y) - W(0)) = \mu(L_y) - \mu(0) = -e(V(L_y) - V(0)). \tag{80}$$

So finally:

$$I_{x,n}(x_0) = \frac{e^2}{h}(V(L_y) - V(0)) \tag{81}$$

for each filled Landau level.

These edge states have been the subject of intense research during the last fifteen years. Many directions have been explored, including the precise modeling of electron transport through mesoscopic coherent samples [22, 23, 24], the theoretical and experimental investigation of interaction effects [25, 26], the generalization of edge states to the fractional quantum Hall regime [27], and possible applications of edge channels to quantum information processing [28, 29], ...

4 Interactions, a preview

This section has no ambition to be exhaustive, it reflects the author's understanding of the role of interactions in the Hall effect. We have seen earlier that the main feature of electrons in a strong magnetic field is the large degeneracy of the Landau levels. It is therefore natural to expect that in this regime, the physics can

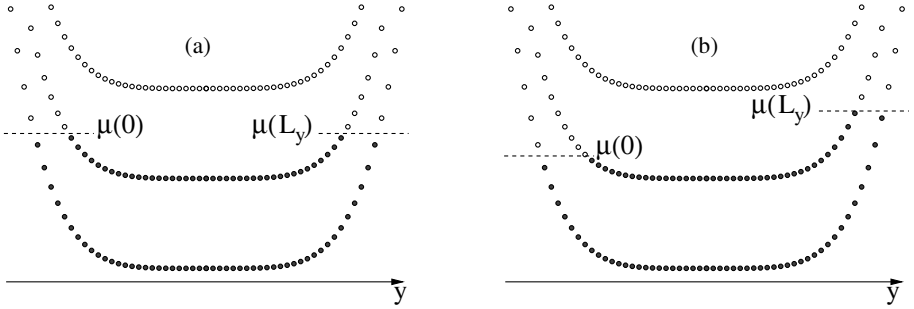

Figure 7: Semi-classical energy spectrum for three Landau levels, as a function of the position y across a Hall bar. In (a), an equilibrium situation is depicted, where the chemical potential is uniform. Filled (resp. empty) circles represent occupied (resp. empty) single-particle states. Currents flow along the x direction in regions where these levels depend strongly on y, that is near the edges. In (b), a non-equilibrium state is depicted, with a smaller chemical for $y = 0$ than for $y = L_y$. As a result, the sum of currents flowing along both edges is non-zero.

be understood through degenerate perturbation theory. In all phenomena where the filling factor is less than one, the projection on the lowest Landau level should therefore give an accurate description of the physics. Here, we indicate how the projection mechanism results in rigid properties of the interacting electron system, which are fairly independent of interactions involved. Also, the properties of the quasiparticles which emerge, such as their charge, are completely different from those of the original electrons.

It is instructive to consider the dynamics of two particles within the lowest Landau level. The two particles interact through a potential $V(\mathbf{r_1} - \mathbf{r_2})$ which is supposed to be both translation and rotation invariant. In a physical situation the potential is the Coulomb interaction between the electrons, but it can in principle be any potential. For reasons that will become clear in the text we consider particles with a charge respectively equal to q_1 and q_2 times the charge of the electron. Our aim is to show that, to a large extent, the properties of the dynamics are independent of the detailed shape of the potential. More precisely, the potential interaction is a two body operator which can be projected into the lowest Landau level. Up to normal ordering ambiguities, the projection consists in replacing the coordinates, $\mathbf{r_1}$, $\mathbf{r_2}$, with the guiding center coordinates, $\mathbf{R_1}$, $\mathbf{R_2}$. After the projection is taken, the potential becomes an operator which is the effective Hamiltonian for the lowest Landau level dynamics. By choosing conveniently a basis, we can see that the eigenstates of the potential do not depend on it, as long as it is invariant under the isometries of the plane. In other words, the two body wave functions of the Hall effect are independent of the interactions. By extension, we are led to

expect that the many body wave functions have some universality properties, and do not depend on the details of the potential.

In this section, we use the symmetric gauge, and l denotes the magnetic length (29). The guiding center coordinates for a particle of charge $q > 0$ times the charge of the electron have the expression

$$b = \sqrt{2}(l\partial_{\bar{z}} + q\frac{z}{4l}), \quad b^+ = \sqrt{2}(-l\partial_z + q\frac{\bar{z}}{4l}). \tag{82}$$

Together with the angular momentum, L, they generate a central extension of the algebra of the isometries of the plane:

$$[b, b^+] = q, \quad [L, b^+] = -b^+, \quad [L, b] = b. \tag{83}$$

This algebra commutes with the Hamiltonian H, and therefore acts within the lowest Landau level. It plays a role similar to the angular momentum in quantum mechanics, and the operators b, b^+, L are the analogous of the angular momentum operators J^-, J^+, J^z . The Landau level index n plays the same role as the representation index j in the rotation group, and it can be recovered as the eigenvalue of a Casimir operator: $C = 2b^+b/q + L$. The states within each Landau level can be labeled by their angular momentum $m \leq n$.

When two particles of positive charge q_1 and q_2 are restricted to their respective lowest Landau level, we can form the operators $b^+ = b_1^+ + b_2^+$, $b = b_1 + b_2$ and the total angular momentum $L = L_1 + L_2$. These operators obey the commutation relations of the algebra (83) with the charge $q = q_1 + q_2$. Thus, as for the angular momentum, a product of two representations decomposes into representations of the isometry of the plane (83). The physically interesting case is when the two charges are equal to the electron charge ($q_1 = q_2 = 1$). It is easy to verify that each representation is constructed from a generating state annihilated by b: $(b_1^+ - b_2^+)^n|0\rangle$, and the value of the Casimir operator is $C = -n$. The corresponding wave functions are:

$$\Psi_n(\bar{z}_1, \bar{z}_2) = (\bar{z}_1 - \bar{z}_2)^n \exp\left(-(\bar{z}_1 z_1 + \bar{z}_2 z_2)/4l^2\right), \tag{84}$$

an expression that plays an important role in the theory of the fractional Hall effect. The potential being invariant under the displacements, it is a number V_n in each representation. Conversely, the information about the V_n is all the information about the potential that is retained by the lowest Landau level physics. The numbers V_n are called pseudopotentials, and turn out to be extremely useful to characterize the different phases of the fractional Hall effect [30].

A case of even more interest is when the two particles have charges of opposite sign, $q_1 > 0$ and $q_2 < 0$, $|q_2| < q_1$. Because of the sign of the second charge, b_2^+ and b_2 become respectively annihilation and creation operators and the lowest Landau level wave functions are polynomials in z_2 instead of $\bar{z}_2$. The same analysis can be repeated, but now the Casimir operator has a positive value n exactly as for the Landau levels. The physical interpretation is that a couple of charges with

opposite sign behaves exactly like a bound state of charge $q^* = q_1 - |q_2|$. The states annihilated by b have a wave function independent of the precise expression of the potential, given by:

$$\Psi_n(\bar{z}_1, z_2) = z_2^n \exp\left(-q_1 \bar{z}_1 z_1/4l^2 - |q_2|\bar{z}_2 z_2/4l^2 + |q_2|\bar{z}_1 z_2/2l^2\right), \tag{85}$$

and they are the n^{th} Landau level's wave functions with the largest possible angular momentum $L = n$.

Heuristically, let us indicate how a scenario involving these composite particles enables to apprehend the region of magnetic field between 21 and 27 Tesla on Fig.1. For this, we use the well established theoretical fact that a quantized Hall effect (for bosons) develops at the filling factor $\nu_0 = 1/2$. We assume that the ground state is the $\nu_0 = 1/2$ quantum Hall liquid made of particles of charge $-q_1 e$. The physical motivation to start from this bosonic ground-state is that it exhibits a rather low Coulomb energy, since the probability for two particles to come close from each other is small in this state. More details on these correlated ground-states are presented in S. Girvin's contribution to which we direct the reader. To recover fermionic statistics, we add on top of this ground state a sea of quasiparticles which are the bound-states introduced above, made of an electron of charge $-e$ and a hole (of charge $q_1 e$) in the $\nu_0 = 1/2$ ground state . The charge of the quasiparticles is thus $-q^* e$, with:

$$q^* = 1 - q_1. \tag{86}$$

To obtain the values of the filling factor that give rise to a Hall effect, using (29) and (31) generalized to particles of an arbitrary charge, we see that for a fixed magnetic field and a fixed density, the following proportionality relation between the charge and the filling factor holds:

$$\text{charge} \propto \frac{1}{\text{filling factor}}, \tag{87}$$

When the magnetic field is varied, the charge $q_1 e$ adjusts itself so that the filling factor of the ground-state is always equal to $1/2$. Thus, $q_1 e \propto 2$. Then, an integer quantum Hall effect will develop when the filling factor of the quasiparticles is an integer p. So, when $q^* e \propto 1/p$. Finally, we can recover the normalization coefficient through the relation between the filling factor of the electrons and their charge: $e \propto 1/\nu$. Substituting these relations in (86) we obtain the following expression for the filling factors giving rise to a Hall effect:

$$\frac{1}{\nu} = 2 + \frac{1}{p}. \tag{88}$$

These filling factors are those predicted by Jain [31], and fit well with the Hall effect observed at $\nu = 3/7, 4/9, 5/11, 6/13$ in Fig.1. The fractions on the other side of $1/2$ are the complement to one of the previous ones, and the corresponding

states can be obtained through a particle hole transformation. In the region, close to $\nu = 1/2$, the quasiparticles have practically zero charge, and therefore see a weak magnetic field. They should therefore behave very much like a neutral Fermi liquid. This has been confirmed by several experiments. One of them measures directly the charge q^* of the quasiparticles through the cyclotron radius of their trajectory [32] (see the footnote of section 2.1).

At $\nu = 1/2$ exactly, let us introduce a simple model to grasp the physics of these composite particles. At this value of the magnetic field, the particle and the hole have exactly opposite charge so that the quasiparticle has exactly zero charge (86). Let us assume for simplicity that the particle and the hole are linked by a spring of strength K. In a strong magnetic field, we disregard the kinetic energy term in the action (14). Thus, after we include the interaction term, the action becomes:

$$S = \int \left(-e\mathbf{A}(\mathbf{r_1}).\dot{\mathbf{r}}_1 + e\mathbf{A}(\mathbf{r}_2).\dot{\mathbf{r}}_2 - \frac{K}{2}\left(\mathbf{r}_1 - \mathbf{r}_2\right)^2 \right) dt. \tag{89}$$

If we denote by $\mathbf{P} = \mathbf{p_1} + \mathbf{p_2}$ the total momentum of the system, straightforward quantization leads to:

$$\mathbf{P} = \hbar\hat{\mathbf{z}} \wedge \frac{\mathbf{r}_1 - \mathbf{r}_2}{l^2}, \tag{90}$$

and

$$H = \frac{\mathbf{P}^2}{2m^*}, \tag{91}$$

where the quasiparticle mass is $m^* = (Be)^2/4K$. Thus, these neutral quasiparticles behave like free particles, and do not feel the external magnetic field. Note that their effective mass m^* is independent of the true electron mass, and reflects the properties of the interactions. Eq. (90) tells us that the quasiparticles are dipoles oriented perpendicularly to $\mathbf{P}$, with a dipole size proportional to the momentum. At this moment, no experimental evidence of their dipolar structure has yet been given.

Finally, let us say a few words about the second quantized formalism in the lowest Landau level. If $V(\mathbf{r})$ denotes the interacting potential, the dynamics is governed by the Hamiltonian:

$$H = \int \tilde{V}(\mathbf{q})\rho_{\mathbf{q}}\rho_{-\mathbf{q}}d^2\mathbf{q}, \tag{92}$$

where $\tilde{V}(\mathbf{q})$ are the Fourier modes of the potential multiplied by the short distance cut-off factor $e^{-\mathbf{q}^2 l^2/2}$, and $\rho_{\mathbf{q}}$ are the Fourier modes of the density. Again, due to the projection to the lowest Landau level, the density Fourier modes do not commute as in the usual case. Instead, they obey the commutation relations

analogous to (23) ($\rho_{\mathbf{q}} \equiv \sum_{i=1}^{N_e} e^{i\mathbf{q}.\mathbf{R_i}}$):

$$[\rho_{\mathbf{q}}, \rho_{\mathbf{q}'}] = \frac{1}{i} \sin \frac{l\mathbf{q} \wedge l\mathbf{q}'}{2} \rho_{\mathbf{q}+\mathbf{q}'}. \tag{93}$$

It can be verified that for a finite size system, $\mathbf{q}$ can take only N^2 values where $N = \text{area}/2\pi l^2$ is the degeneracy of the lowest Landau level, and the algebra (93) is the Lie algebra of the group $U(N)$. In the limit of strong magnetic field, $l \to 0$, and one recovers the algebra of area preserving diffeomorphisms (23) as the classical limit of (93).

Appendix: Chern number for a two-dimensional torus

In section 3.4, we have introduced the ground-states $|\mathbf{\Phi}\rangle$, where $\mathbf{\Phi} \equiv (\Phi_x, \Phi_y)$ denotes two Aharonov-Bohm fluxes associated to the two main topologically non-trivial closed loops winding around the real-space torus defining our electron system. These states are periodic functions of $\mathbf{\Phi}$, up to possible phase-factors, so we may write:

$$|\Phi_0, \Phi_y\rangle = e^{i\lambda(\Phi_y)} |0, \Phi_y\rangle \tag{94}$$

$$|\Phi_x, \Phi_0\rangle = e^{i\mu(\Phi_x)} |\Phi_x, 0\rangle. \tag{95}$$

$$\tag{96}$$

In particular, we get

$$|\Phi_0, \Phi_0\rangle = e^{i(\lambda(0)+\mu(\Phi_0))} |0,0\rangle = e^{i(\mu(0)+\lambda(\Phi_0))} |0,0\rangle. \tag{97}$$

Consequently:

$$\lambda(\Phi_0) - \lambda(0) - \mu(\Phi_0) + \mu(0) = 2\pi\, n \tag{98}$$

where n is an integer. Now:

$$\begin{aligned}
\frac{1}{2\pi i} \int_{\square} \langle \mathbf{\Phi} | d | \mathbf{\Phi} \rangle &= \frac{1}{2\pi i} \int_0^{\Phi_0} d\Phi_x \left(\langle \mathbf{\Phi} | \frac{\partial}{\partial \Phi_x} | \mathbf{\Phi} \rangle (\Phi_x, 0) - \langle \mathbf{\Phi} | \frac{\partial}{\partial \Phi_x} | \mathbf{\Phi} \rangle (\Phi_x, \Phi_0) \right) \\
&+ \frac{1}{2\pi i} \int_0^{\Phi_0} d\Phi_y \left(\langle \mathbf{\Phi} | \frac{\partial}{\partial \Phi_y} | \mathbf{\Phi} \rangle (\Phi_0, \Phi_y) - \langle \mathbf{\Phi} | \frac{\partial}{\partial \Phi_y} | \mathbf{\Phi} \rangle (0, \Phi_y) \right) && (99) \\
&= \frac{1}{2\pi i} \int_0^{\Phi_0} d\Phi_x \left(-i \frac{\partial \mu}{\partial \Phi_x} (\Phi_x) \right) + \frac{1}{2\pi i} \int_0^{\Phi_0} d\Phi_y \left(i \frac{\partial \lambda}{\partial \Phi_y} (\Phi_y) \right) && (100) \\
&= \frac{1}{2\pi} (\lambda(\Phi_0) - \lambda(0) - \mu(\Phi_0) + \mu(0)) && (101) \\
&= n. && (102)
\end{aligned}$$

References

[1] The Quantum Hall Effect, Edited by R.E. Prange and S. Girvin, Springer-Verlag, New York, (1990).

[2] S.M. Girvin, "The Quantum Hall Effect: Novel Excitations and broken Symmetries", Les Houches Lecture Notes, in Topological Aspects of Low Dimensional Systems, Springer-Verlag, Berlin and Les Editions de Physique, Les Ulis, (1998).

[3] Perspectives in Quantum Hall Effects, Edited by S. Das Sarma and A. Pinczuk, Wiley, New-York, (1997).

[4] R.L. Willet, H.L. Stormer, D.C. Tsui, A.C. Gossard and J.H. English, *Phys. Rev. Lett.* **59**, 1776 (1987).

[5] R.B. Laughlin, *Phys. Rev.* **B 23**, 5632 (1981)

[6] Q. Niu, D.J. Thouless, and Y.-S. Wu, *Phys. Rev.* **B 31**, 3372 (1985).

[7] M. Büttiker, *Phys. Rev.* **B 38**, 9375 (1988).

[8] R.E. Prange and R. Joynt, *Phys. Rev.* **B 25**, 2943 (1982).

[9] E. Abrahams, P.W. Anderson, D.C. Licciardello, and T.V. Ramakrishnan, *Phys. Rev. Lett.* **42** , 673 (1979).

[10] D.E. Khmelnitskii, *Pis'ma Zh. Eksp. Teor. Fiz.* **38**, 454 (1983), translated as *JETP. Lett.* **38**, 552 (1983).

[11] H. Levine, S.B. Libby, and A.M.M. Pruisken, *Phys. Rev. Lett.* **51**, 1915 (1983).

[12] B. Huckestein, *Rev. Mod. Phys.* **67**, 357 (1995).

[13] M.R. Zirnbauer, e-preprint, hep-th/9905054.

[14] B. Kramer, S. Kettemann, T. Ohtsuki, *Physica* **E 20**, 172 (2003).

[15] D.C. Tsui, H.L. Stromer, and A.C. Gossard, *Phys. Rev. Lett.* **48**, 1559 (1982).

[16] R.B. Laughlin, *Phys. Rev. Lett.* **50**, 1395 (1983).

[17] J.E. Avron, and R. Seiler, *Phys. Rev. Lett.* **54**, 259 (1985).

[18] R. Tao, and F.D.M. Haldane, *Phys. Rev.* **B 33**, 3844 (1986).

[19] J.E. Avron, D. Osadchy, and R. Seiler, Physics Today, August 2003, page 38.

[20] J. Bellissard, in Proceedings of the Harald Bohr Centenary workshop, Copenhagen April 87, Edited by C. Berg and B. Flugede, The Royal Danish Academy of Sciences and Letters, Copenhagen 1989.

[21] B.I. Halperin, *Phys. Reb.* **B 25**, 2185 (1982).

[22] C.J.B. Ford, S. Washburn, M. Büttiker, C.M. Knoedler, and J.M. Hong, *Phys. Rev. Lett.* **62**, 2724 (1989).

[23] H.U. Baranger, and A.D. Stone, *Phys. Rev. Lett.* **63**, 414 (1989).

[24] C.W.J. Beenakker, and H. van Houten, *Phys. Rev. Lett.* **63**, 1857 (1989).

[25] D.B. Chklovskii, B.I. Shklovskii, and L.I. Glazman, *Phys. Rev.* **B 46**, 4026 (1992).

[26] E. Ahlswede, P. Weitz, J. Weis, K. von Klitzing, and K. Eberl, *Physica* **B 298**, 562 (2001).

[27] X.-G. Wen, *Int. Journ. Mod. Phys.* **B 6**, 1711 (1992).

[28] D.V. Averin, and J.J. Goldman, e-preprint, cond-mat/0110193.

[29] M. Büttiker, P. Samuelsson, and E.V. Sukhorukov, e-preprint, cond-mat/0404123.

[30] F.D.M. Haldane, Chap. 8 in ref.[1].

[31] For a review, see Chapters by B.I. Halperin and J.K. Jain in ref. [3].

[32] V.J. Goldman, B. Su and J.K. Jain, *Phys. Rev. Lett.* **72**, 2065 (1994).

Benoît Douçot
LPTHE
CNRS et Universités Paris 6 et 7
Tour 24-14 5e étage
4 place Jussieu
75252 Paris Cedex 05
France

email: `doucot@lpthe.jussieu.fr`

Vincent Pasquier
Service de Physique Théorique
CEA Saclay
91191 Gif sur Yvette Cedex
France
email: pasquier@spht.saclay.cea.fr

The Quantum Hall Effect, 55 – 131

Poincaré Seminar 2004

The Quantum Hall Effect as an Electrical Resistance Standard

Beat Jeckelmann and Blaise Jeanneret

Abstract. The quantum Hall effect (QHE) provides an invariant reference for resistance linked to natural constants. It is used worldwide to maintain and compare the unit of resistance. The reproducibility reached today is almost two orders of magnitude better than the uncertainty of the determination of the ohm in the International System of Units SI.

In this article, mainly the aspects of the QHE relevant for its metrological application are reviewed. After a short introduction of the theoretical models describing the integer QHE, the properties of the devices used in metrology and the measurement techniques are described. A detailed summary is given on the measurements carried out to demonstrate the universality of the quantized Hall resistance and to assess all the effects leading to deviations of the Hall resistance from the quantized value. In addition, the present and future role of the QHE in the SI and the field of natural constants is discussed.

1 Introduction

Parallel to the progress made in the physical sciences and in technology, the International System of Units SI has evolved from an artefact based system to a system mainly based on fundamental constants and atomic processes during the last century. For example, the unit of time, the second, is now defined as the duration of a fixed number of periods of the radiation corresponding to an atomic transition in Cs. The unit of length, the metre, is the path traveled by light in vacuum in a fixed fraction of a second. This definition assigns a fixed value to the speed of light which is one of the most fundamental constant in physics. The modern units have major advantages over their artefact counterparts: they do not depend on any external parameters like the ambient conditions and, most important, they do not drift with time. In addition they can be simultaneously realized in laboratories all over the world which strongly simplifies and improves the traceability of any measurements to the primary standards.

With the discovery of the Josephson and the quantum Hall effects, two electrical quantum standards became available. As a first consequence, the worldwide consistency in the realization and maintenance of the electrical units and the electrical measurements based on them has improved hundredfold in the last decade. The two quantum effects will certainly also play a major role in the next modernization of the SI when the last remaining base unit in the SI still based on an artefact, the kilogram, will be linked to fundamental constants.

The aim of the present review is to highlight the role of the quantum Hall effect (QHE) in metrology and to recall the theoretical and experimental background which is necessary for its understanding. Earlier review articles focusing on similar aspects may be found in references [1, 2, 3].

The QHE was discovered in the night to February 5 1980, when Klaus von Klitzing was investigating the transport properties of a Si-MOSFET device at very low temperature and high magnetic field in Grenoble [4]. The discovery, which was totally unanticipated by the physics community, relied on the existence of a two-dimensional electron gas (2DEG) in a semiconducting device. The great technological progress that followed the invention of the transistor lead to the realization of the first 2DEG in semiconducting devices in the middle of the sixties. The first measurements performed with Si-MOSFETs at low temperature and high magnetic field were done by Fowler *et al*[5] in 1966. Later on, due to improvements in device fabrication, Kawaji *et al*[6] observed the dissipationless state in a Si-MOSFET. In 1978, Hall resistance plateaus were observed in such inversion layers by Englert and von Klitzing [7]. However, the idea of analyzing the Hall plateaus in terms of the fundamental value h/e^2 emerged that particular night for the first time. Further measurements [8] confirmed that the fundamental quantization relation for the Hall resistance $R_{\mathrm{H}} = h/ie^2$ was accurate to 10 parts in 10^6. Von Klitzing was awarded the Nobel prize for his discovery in 1985 [9].

In 1982, using GaAs/AlGaAs heterostructures, the 2DEG mobility was increased to a level where the fractional quantum Hall effect (FQHE) could be discovered by Tsui, Störmer and Gossard [10]. In 1998, Tsui, Störmer and Laughlin were awarded the Nobel prize for their discovery [11, 12, 13]. The FHQE opens the way to the study of a large spectrum of interesting physical phenomena (see e.g. [14] for a recent review). Unfortunately the current at which the FHQE breaks down is so low that an application in metrology is not conceivable.

This review is organized as follows: Section 2 presents the basics of the quantum Hall effect. The localization and the edge state model of the QHE are shortly reviewed. Section 3 describes the devices needed to observe the QHE whereby emphasis is put on the two types of systems that are mostly used in metrology, the Si-MOSFET and the GaAs/AlGaAs heterostructure. A short paragraph describes the role of electrical contacts to the 2DEG. Section 4 describes in detail the precision measurement techniques used to compare the quantized Hall resistance (QHR) to traditional resistance standards. Section 5 reviews the most important physical properties of the QHE and their influence on high precision measurements of the QHR. In section 6, it is shown that the QHR has a universal character: it does not depend on the device type (Si-MOSFET or GaAS heterostructures), on the plateau index, on the mobility, nor on the device width at the level of the relative measurement uncertainty of 3×10^{-10}. Section 7 discusses the QHE in the framework of the SI, including the role of the QHR in the metrological triangle and in the replacement of the kilogram. Section 8 presents the progress made in ac measurements of the QHR in view of its implementation as a primary ac resistance standard.

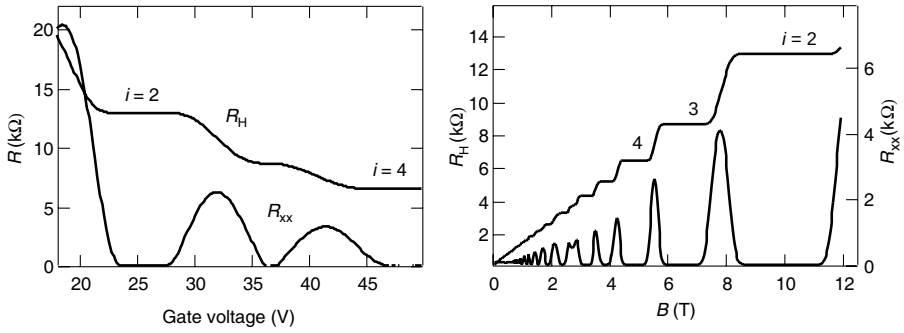

Figure 1: Experimental measurements of the Hall resistance $R_{\rm H}$ and of the longitudinal resistance R_{xx} for a Si-MOSFET (B = 13.8 T) and a GaAs/AlGaAs heterostructure at a temperature of 0.3 K.

2 Basic Principles

2.1 The Integer Quantum Hall Effect

The QHE is observed in a two-dimensional electron gas at low temperature and high magnetic field. In figure 1, typical resistance measurements made on a Si-MOSFET and a GaAs/AlGaAs sample are shown. A current I flows in the 2DEG of width w, and a longitudinal voltage V_x is measured between two contacts separated by a distance L. At the same time, the transverse voltage V_y is recorded. The voltages and currents are related by

$$V_x = R_{xx}I_x + R_{xy}I_y \quad (1)$$
$$V_y = -R_{xy}I_x + R_{xx}I_y, \quad (2)$$

where R_{xx} is the longitudinal resistance and $R_{xy} = R_{\rm H}$ is the Hall resistance. In figure 1 broad steps can be observed in the Hall resistance. Simultaneously, the longitudinal resistance vanishes. In a two-dimensional system, the Hall resistance is equal to the Hall resistivity $\rho_{xy} = R_{\rm H}$. The longitudinal resistance is related to the longitudinal resistivity by $\rho_{xx} = (w/L)R_{xx}$. However, in the quantum Hall regime, $R_{xx} = \rho_{xx} = 0$. Therefore, the resistances are as fundamental as the resistivities in contrast to the three-dimensional case, where geometrical corrections are required. On a plateau, the Hall sample is a perfect conductor with $\rho_{xx} = 0$. However, due to the tensorial nature of the resistance in two dimensions, it is a perfect insulator as well: $\sigma_{xx} = 0$. This can be seen from the relation between the resistivities and

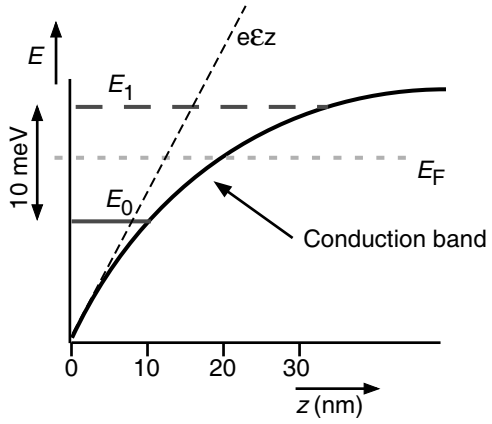

Figure 2: Schematic energy diagram showing the potential well and the first two electrical subbands E_0 and E_1. E_F is the Fermi energy. The potential $e\mathcal{E}z$ generated by the electric field $\mathcal{E}$ is represented as a dashed line. Only the first subband is filled.

the conductivities

$$\rho_{xx} = \frac{\sigma_{xx}}{\left(\sigma_{xx}^2 + \sigma_{xy}^2\right)} \qquad \rho_{xy} = \frac{-\sigma_{xy}}{\left(\sigma_{xx}^2 + \sigma_{xy}^2\right)} \tag{3}$$

$$\sigma_{xx} = \frac{\rho_{xx}}{\left(\rho_{xx}^2 + \rho_{xy}^2\right)} \qquad \sigma_{xy} = \frac{-\rho_{xy}}{\left(\rho_{xx}^2 + \rho_{xy}^2\right)}. \tag{4}$$

Following this succinct preview, the rest of this chapter will briefly cover the physical ingredients necessary to understand the integer QHE. A large number of books [15, 16, 17, 18] and review articles [9, 19, 20, 21, 22, 23] is available, which can more deeply introduce the interested readers to the physics of the QHE.

2.2 The two-dimensional electron gas

The 2DEG needed to observe the QHE can be realized in various types of semiconducting heterostructure devices (see section 3 for the device details). The electrons are confined by a potential well (see figure 2) due to the infinite barrier of the interface (left side of the well) and the electric field that confines the electrons to the interface (right side of the well). The motion of the electrons is therefore limited to the xy plane. In the independent electron approximation, the electronic wave function can be written as $\Psi(x, y, z) = \psi(x, y)\zeta(z)$. Solving the Schrödinger equation along the z axis with the potential as depicted in figure 2, the following energy spectrum is obtained:

$$E_l = \left(\frac{\hbar^2}{2m_z}\right)^{1/3} \left[\frac{3\pi\mathcal{E}}{2}\left(l + \frac{3}{4}\right)\right]^{2/3}, \tag{5}$$

where $\mathcal{E}$ is the average electric field, m_z the transverse effective electron mass and l the subband index. The electric field can be calculated from the number of 2D electrons per unit area [19]. The energy levels of the 2DEG form many subbands, each having the energy E_l. The total energy of the electrons can be written as

$$E = E_l + E_\perp = E_l + \frac{\hbar^2 k_\perp^2}{2m}, \tag{6}$$

where the second term is the energy associated with the motion in the xy plane. This enregy contribution will be analyzed in the next paragraph.

In the following we will only consider systems where the first electrical subband is filled. The energy difference between the first two subbands is on the order of 10 meV (100 K), much larger then the energy corresponding to the temperature where the QHE is observed.

The spatial extension of the first subband wave function ζ_0 is on the order of 3 to 5 nm, shorter than the de Broglie wave length, therefore the electron gas can be considered as two-dimensional.

2.3 Landau quantization

In this section we will consider a perfect 2DEG of non interacting spinless electrons placed in a perpendicular magnetic flux density B parallel to the z axis at zero temperature. The solution of this problem is obtained by solving the Schrödinger equation with the following Hamiltonian:

$$H_0 = \frac{1}{2m} \left[\mathbf{p} + e\mathbf{A}\right]^2. \tag{7}$$

The effective mass in the xy plane is denoted by m, $\mathbf{A}$ is the vector potential associated to $\mathbf{B}$ by the relation $\mathbf{B} = curl\mathbf{A}$. In the Landau gauge, $\mathbf{A} = (0, Bx, 0)$, the problem is reduced to a shifted harmonic oscillator equation. The eigenenergies, called Landau levels, are given by

$$E_n = \hbar\omega_c \left(n + \frac{1}{2}\right) \qquad n = 0, 1, 2, 3 \ldots, \tag{8}$$

where $\omega_c = \frac{eB}{m}$ is the cyclotron energy which is on the order of 10 meV at a magnetic flux density of 10 T. Thus the energy of the 2DEG becomes quantized as shown in figure 3.

In the case where the spin of the electrons is not neglected, the cyclotron energy has an additional term, the Zeeman splitting, of the form $sg^*\mu_b B$, where $s = \pm 1/2$ is the spin of the electron, $\mu_b = \frac{e\hbar}{2m_e}$ is the Bohr magneton and g^* is the effective Landé g-factor. The effective electron mass m is much smaller than the bare electron mass m_e (for example, $m = 0.07\ m_e$ in GaAs and $m = 0.2\ m_e$ in Si), therefore the Zeeman splitting is much smaller than the Landau splitting.

The effective g-factor is enhanced with respect to its bulk value ($g = 2$ in Si and $g = 0.5$ in GaAs resp.). Typical values are around $g^* = 3$ to 6, depending on the electron density [24, 25, 26, 27, 28].

The wave function of the electrons consists of a plane wave in the y direction and the eigenstates of a harmonic oscillator in the x direction [15, 16]. The harmonic oscillator wave function is characterized by the magnetic length l which is basically the size of the cyclotron orbit in a classical model (cyclotron radius)

$$l = \sqrt{\frac{\hbar}{eB}}. \tag{9}$$

Comparable to other typical lengths of the system, the magnetic length is in the range 5 to 10 nm, and is independent of material parameters. The number of states in a filled Landau level N is the size of the system divided by the surface of a cyclotron orbit, thus the number of states per unit area n_B is given by:

$$n_B = \frac{1}{2\pi l^2} = \frac{eB}{h}. \tag{10}$$

The filling factor is defined as $\nu = n_s/n_B$. When a Landau level is full, the filling factor is an integer number i and the number of electrons per unit area is $n_s = in_B$. The substitution of the previous relation in the expression for the classical Hall effect [29] $R_\mathrm{H} = B/en_s$ gives the following relation:

$$R_\mathrm{H} = \frac{h}{ie^2} = \frac{R_\mathrm{K}}{i}, i = 1, 2, 3 \ldots. \tag{11}$$

According to this simple model, an ideal 2DEG shows a quantized Hall resistance when the magnetic flux density is adjusted in such a way that the filling factor ν is an integer. Under these conditions, the Fermi level lies in a gap and the electronic scattering rate vanishes [15]. Without scattering, the electrons cannot move along the electric field but move along a direction perpendicular to both the electric field and the magnetic field with a velocity $v_y = E_x/B$. Hence the conductivity σ_{xx} of the 2DEG is zero and the Hall conductivity is given by $\sigma_{xy} = -e \cdot n_s/B = -ie^2/h$. Thus the resistivity ρ_{xx} is zero and the Hall resistance is given by $R_\mathrm{H} = \rho_{xy} = h/ie^2$, as observed in experiment. This simple model gives a quantized Hall resistance for certain values of B, however it does not explain the presence of plateaus in the Hall resistance. Those plateaus are a consequence of disorder in the system as explained in the next section.

2.4 Disorder and localization

In real Hall samples, the electrons move in a lattice of positive charges. Despite the technological progress achieved in crystal growth, this lattice is far from being perfect when inspected at a microscopic level. Every point defect or impurity acts like a scattering centre for the electrons. This scattering adds up to the phonon

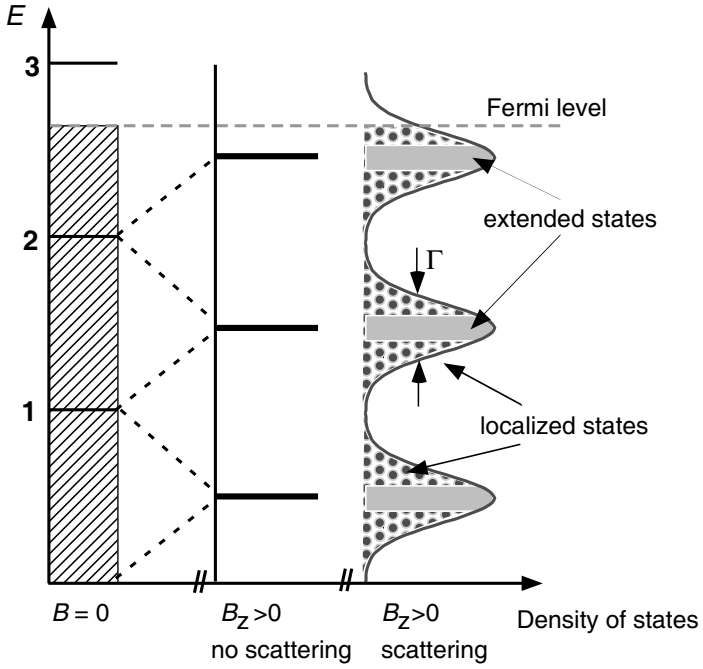

Figure 3: Landau quantization of a spinless 2DEG. The continuum of states that exists in zero field (left side) becomes quantized in Landau levels when the magnetic flux density is turned on (central part). When disorder is added to the system, the Landau levels are broadened in localized and extended states (right side). The region of the localized states is called the mobility gap.

scattering. However, given the temperature at which the QHE is observed, the impurity scattering largely dominates. These impurities, located at position $\mathbf{r}_j$ in the vicinity of the 2DEG, give rise to a random potential $V(\mathbf{r})$ which is the sum of all individual impurity potentials $v_j(\mathbf{r})$, i.e.

$$V(\mathbf{r}) = \sum_j v_j(\mathbf{r} - \mathbf{r}_j). \tag{12}$$

Solving the Schrödinger equation with the above potential in a high magnetic flux density is a formidable task and a subject on its own. Among the many books and review articles dealing with this subject, e.g. the following have a link to the QHE: [19, 16, 30, 22, 17].

The first implication of the presence of these impurities is to completely lift the degeneracy of the Landau levels. Therefore, the levels are broadened into Landau subbands (see figure 3). In the self-consistent Born approximation [19], the Landau subbands have an elliptic profile of width Γ. This elliptic profile gives a

satisfactory approximation of real systems. Experimentally, the width of a Landau subband was found to be well approximated by [31]

$$\Gamma = p\sqrt{\frac{B}{\mu}}, \tag{13}$$

where μ is the mobility of the sample and $p = 2.3 \pm 0.3$ meV/T. It is important to note that for good quality samples, $\Gamma \ll \hbar\omega_c$.

The second fundamental consequence of the impurity potential is to create two different kinds of electronic states: localized and extended states (see figure 3). The most simple, though very instructive model to show the existence of such states is the single δ-function impurity potential introduced shortly after the discovery of the QHE by Prange [32]. This model also includes an external electric field $\mathbf{E}$ in the plane of the 2DEG, therefore the total potential is given by:

$$V(\mathbf{r}) = \lambda\delta(\mathbf{r} - \mathbf{r_0}) + e\mathbf{E}\mathbf{r}. \tag{14}$$

Two kinds of solutions emerge from the Schrödinger equation. The first yields a completely localized state whose energy is shifted by $\pm\lambda$ from the Landau level depending whether the potential is attractive or repulsive. At zero temperature, this state cannot carry any current, therefore the current does not depend on whether localized states are occupied by electrons or not. The second solution is composed of $N - 1$ extended states located close to the unperturbed Landau level $n\hbar\omega_c$. These extended states will carry the current. As mentioned above, the presence of an impurity reduces the number of states that are able to carry the current. However, it can be shown [32] that the electrons passing by an impurity will speed up to increase the current to compensate exactly the deficit of current due to the presence of the localized state. This model is of course an oversimplification of the physics of a 2DEG. However, it provides a qualitatively correct description of the density of states.

By increasing the electron density n_s, the various electronics states are gradually filled up. This is equivalent to shifting the Fermi energy E_F through the density of states. When E_F moves in a mobility gap (region where electronic states are localized), the occupation of the extended states does not change and, since only these states carry the current, the Hall resistance will not change either, giving rise to a Hall plateau. It is crucial that the energy of the extended states in the middle of this plateaus is well away from E_F. In this way, inelastic processes like phonon absorption do not change the occupation of the extended states. Simultaneously to the occurrence of the Hall plateau, the longitudinal resistance vanishes since only localized states are in the vicinity of E_F. As soon as E_F approaches the next Landau level, dissipation appears in the system and the Hall resistance makes a transition to the next plateau. Therefore, the QHE can be understood as a succession of localization-delocalization transitions when the Fermi energy E_F moves across the density of states, as depicted in figure 3.

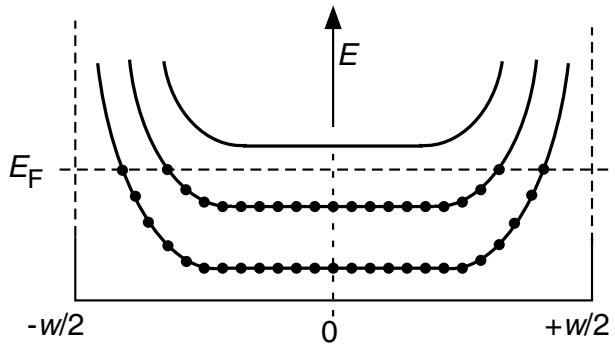

Figure 4: Energy spectrum of a 2DEG in a magnetic field with an infinite confining potential at the edges of the sample. States below the Fermi energy are occupied (solid dots). The edge channels are located at the intersection of the Landau levels with the Fermi energy.

There have been many alternative approaches to describe the physics of the QHE. A broad review can be found in [17]. Most of these models describe ideal systems at zero temperature. Real experiments, however, are carried out with samples of finite size at non-zero temperatures. For the current injection, source and drain contacts are needed which short out the Hall voltage at both ends of a device. Therefore, electrons enter and exit at diagonally opposite corners of the device and the source drain resistance equals the Hall resistance. As a consequence, an electrical power of $R_{\mathrm{H}}I^2$ is dissipated in the contacts. All these non-ideal features are difficult to model. Therefore, a complete quantitative theory which predicts e.g. deviations from the exact quantization under non-ideal conditions is still missing.

2.5 The edge-state model

Most of the theoretical models put forward to explain the QHE, including the localization theory presented above and the elegant topological argument of Laughlin [33], are considering ideal systems with specific boundary conditions. Although these models provide clear and detailed insight in the physics of the 2DEG, resistance measurements performed in real samples rely on finite size devices with imperfect electrical contacts to the 2DEG. Therefore, the question of whether these models properly describe the experimental situation, especially in high precision measurements, was quite open in the early days of the QHE.

At the edges of a real sample the confining potential produces an upward bending of the Landau levels (see figure 4). For each Landau level intercepting the Fermi energy a one-dimensional edge channel is formed. Classically this corresponds to the trajectories of an electron moving along the edge of the device in a

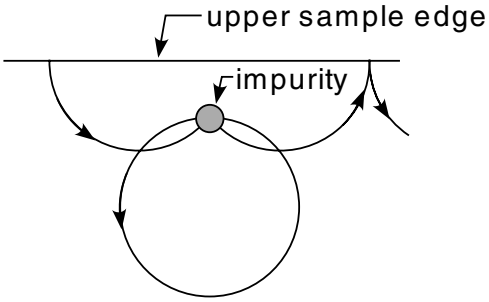

Figure 5: Quasiclassical skipping orbits along the upper edge of the sample in presence of a localized impurity. In a high magnetic field, back-scattering over distances large compared to the cyclotron radius is suppressed. (After [43]).

magnetic field (skipping orbit). As a consequence, there exist extended states at the Fermi energy near the sample boundaries.

Soon after the discovery of the QHE, Halperin recognized [34] the importance of theses edge channels in the transport properties of the 2DEG. Several edge related theories were then developed, based on different approaches [35, 36, 37, 38] and some experimental evidence was also given that the current in a Hall bar is flowing close to the edges [39]. The need to develop theories that describe geometries closer to the experimental arrangement was also pointed out [40].

However, it was in combination with the Landauer formalism [41, 42] for transport that the edge state approach proved to be really very efficient to understand electrical transport at high field. In the following, we will very briefly summarize the approach adopted by Büttiker [43], although some pioneering work was done by Středa *et al*[44] and by Jain *et al*[45]. For additional information, excellent review papers have been published on the subject [30, 46].

In the Landauer formalism of transport, the current is taken as the driving force and the electric field can be obtained by calculating the charge distribution due to the current flow. Using transmission and reflection probabilities, the current is given as a function of the electrochemical potential at the contacts. For a single edge state k located between two electron reservoirs at electrochemical potential μ_1 and μ_2, the current fed by the contact in the absence of scattering is

$$I = ev_k D(E)(\mu_1 - \mu_2) = \frac{e}{h}\Delta\mu, \tag{15}$$

where v_k is the drift velocity of the electron which is proportional to the slope of the Landau level and therefore has an opposite sign on each side of the device. The density of states $D(E)$ is given by $D(E) = 2\pi\hbar v_k$ in a one-dimensional channel [43]. The voltage drop V between the reservoirs is $eV = \Delta\mu$ and the two-terminal

resistance of the edge state is $R = h/e^2$. For N channels, one obtains

$$R = \frac{h}{e^2}\frac{1}{N}. \tag{16}$$

When elastic scattering takes place along the edge channels with a transmission probability T across the disordered region, the two-terminal resistance becomes

$$R = \frac{h}{e^2}\frac{1}{NT}. \tag{17}$$

The situation of a localized impurity scattering in an edge channel is schematically depicted in figure 5. In a very intuitive way, the figure shows that the magnetic field suppresses back-scattering of the electrons over a distance larger then the cyclotron orbit. This suppression of back-scattering, which allows dissipationless current to flow along the edges, is the fundamental property responsible for the occurrence of the quantum Hall effect. As a consequence, $T = 1$ and the resistance is again given by equation 16.

The power of the edge channel approach lies in the possibility of studying the role of the contacts which are fundamental in precision measurements as already noticed in 1992 by Büttiker [46]: "...It is likely, therefore, that in the future, contacts will play an essential role in assessing the accuracy of the quantum Hall effect." In case the two contacts are non-ideal, they will selectively populate the edge channels, i.e., $T_{1,2} \neq 1, R_{1,2} \neq 0$. In this case the current can be written as

$$I = \frac{NT_1T_2}{N^2 - R_1R_2}\Delta\mu, \tag{18}$$

giving a two-terminal resistance of

$$R = \frac{h}{e^2}\frac{N^2 - R_1R_2}{NT_1T_2}. \tag{19}$$

The two-terminal resistance shows a deviation from perfect quantization. However, inelastic scattering will equilibrate the population between the edge states on the same side of the sample (back-scattering is still suppressed). One inelastic scattering length away from the contact, the Hall voltage V_{H} is calculated to be

$$eV_{\mathrm{H}} = \frac{NT_1T_2}{N^2 - R_1R_2}\Delta\mu, \tag{20}$$

leading to a perfectly quantized resistance $R_{\mathrm{H}} = (h/e^2)(1/N)$. This brief discussion shows the robustness of the quantum Hall effect with regard to the quality of the contact. It stresses the importance of inelastic scattering, which equilibrates the edge states, in establishing exact quantization. A deeper discussion on the role of the contacts in metrological measurements will be presented in section 5.4.

The situation of a real Hall bar is depicted in figure 6. The contacts are characterized by transmission T_i and reflection R_i coefficients. As the contacts are

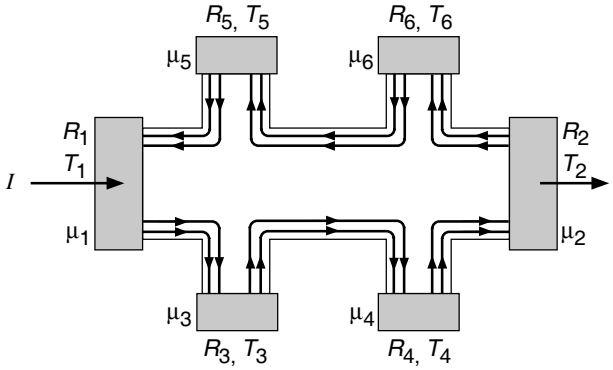

Figure 6: Schematic picture of a Hall bar with six Ohmic contacts separated by a distance larger then the inelastic scattering length. The filling factor corresponds to the second Hall plateau. The contacts are characterized by reflection R_i and transmission T_i coefficients. Each contact is at an electrochemical potential μ_i. The dc transport current I flows between contact 1 (source) and 2 (drain). (After [43])

separated by a distance larger than the inelastic scattering length, $T_i = 1$ and $R_i = 0$ for all the contacts whether they are ideal or not. The electrochemical potentials are related by $\mu_1 = \mu_3 = \mu_4$ and $\mu_2 = \mu_5 = \mu_6$. These conditions lead to $I = Ne(\mu_2 - \mu_1)$ and $V_{\rm H} = V_{56} = V_{34} = \Delta\mu$, yielding $R_{\rm H} = h/Ne^2$ and $R_{xx} = 0$, as expected.

This edge state model allows a realistic description of the electronic transport in high magnetic field as long as the difference in electrochemical potentials $\Delta\mu$ is small compared to the cyclotron energy $\hbar\omega_c$. For high current densities, however, the current flows mainly in the bulk of the 2DEG and an extension of the edge state model is needed to explain the QHE in this regime.

The edge state picture has been successfully used to explain many experimental results. In [47, 48], a gate located above the 2DEG was used to selectively induce reflection of edge channels. As a function of the gate voltage, the Hall plateaus appearing at non integer value of $R_{\rm K}$ were well explained with the edge state model. In [49, 50], it was shown that inter-Landau-level scattering was suppressed over macroscopic distances as large as 200 μm and the role of contacts was also investigated. In [51], the equilibration length was found to be around 80 μm. The non local behaviour of the four-terminal Hall resistance was demonstrated in [52]. These studies were the first to rely on the edge state model. They were followed by numerous additional experiments which have been carefully reviewed in [53].

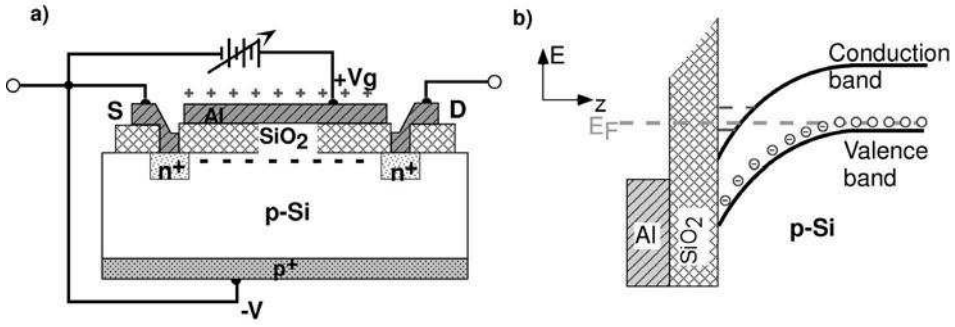

Figure 7: Silicon MOSFET. (a) cross section, (b) schematic energy diagram

In the one-electron picture adopted above, the edge channels formed at the intersection of the Landau levels with the Fermi energy are like metallic wires running along the sample boundary and their spatial extension is comparable to the magnetic length (about 10 nm at 10 T). However, this description does not include the screening that takes place near the sample boundary. This screening at high magnetic fields forces the channels into compressible strips separated by incompressible regions [54]. In a quantitative study, Chklovskii *et al*[55] calculated the width of the edge channels to be on the order of 1 μm on the second Hall plateau. This width is two orders of magnitude larger than in the one-electron picture and agrees fairly well with experimental measurements [56, 57, 58].

3 The devices

In real samples, the two-dimensional electron gas is located in the inversion layer found in various semiconductor devices. Inversion layers are formed at the interface between a semiconductor and an insulator (like the Si-MOSFET) or at the interface between two semiconductors, one of them acting as the insulator (like the AlGaAs/GaAs heterostructures). The quantum Hall effect was discovered in a Si-MOSFET. However, particularly in metrology, mostly AlGaAs/GaAs heterostructures are used.

In the following, we will not describe the processing involved to grow the devices (MOCVD, MBE ...). The interested readers can find a good review in [59]. In addition, a deeper and broader description of the physics and technology of semiconductor devices can be found in [60, 61].

3.1 Si-MOSFET

A schematic representation of a Si-MOSFET is depicted in figure 7 (a). The Si substrate, lightly p doped, is coated with 500 nm of SiO_2 which isolates the Al gate. The contact area (source S and drain D) is heavily $n+$ doped to favour the

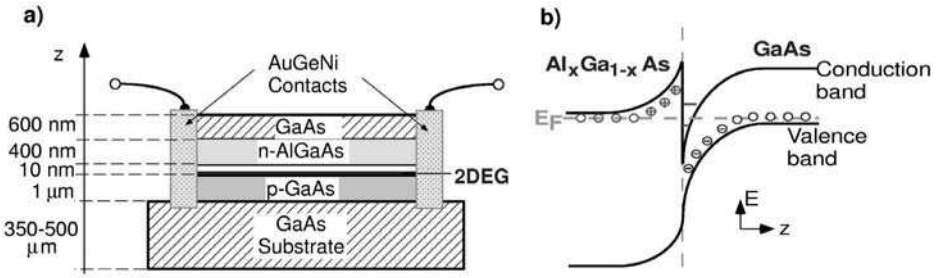

Figure 8: GaAs heterostructure. (a) cross section, (b) schematic energy diagram.

formation of an Ohmic contact to the 2DEG. The 2DEG realization is represented in the band diagram of figure 7 (b). The gate held at a potential $+V_g$ creates an electric field which attracts the electrons to the Si-SiO_2 interface. In addition, this field induces a bending of the valence and conduction bands. As the substrate is p doped, electrons of the valence band will populate the level of the acceptors and leave holes in the valence band. The electrons attracted to the interface fill these holes first. However, if the gate voltage is high enough, the bottom of the conduction band can be shifted below the Fermi level E_F, allowing the electrons to fill the bottom of the conduction band. This is the inversion layer: the bottom of the conduction band is below the top of the valence band, reversing the usual order. The 2DEG is located within this inversion layer which is around 3 to 5 nm wide. This width is smaller than the de Broglie wave length, hence the electron gas can be considered as two-dimensional: the motion along the z axis is fully quantized (see section 2.2). The region where all the acceptor levels are filled is called the depletion length. This region which is on the order of 500 nm in Si has no free charge carriers and is insulating. Impurities trapped in the oxide layer and lattice discontinuities at the interface limit the mobility of the 2DEG to $\approx 1\ \mathrm{T}^{-1}$. The density of the charge carriers in the 2DEG can be tuned by the gate voltage $+V_g$.

3.2 GaAs-AlGaAs heterostructures

The AlGaAs system shown in figure 8 has strong similarities with the Si-MOSFET. In this case, GaAs is the semiconductor (energy gap $E_g = 1.5$ eV) and $\mathrm{Al_xGa_{1-x}As}$ ($x \approx 0.3$), which has a higher gap ($E_g = 2.2$ eV), plays the role of the insulator. Using the molecular beam epitaxy technique (MBE see [59]), it is possible to fabricate interfaces with an atomic regularity given the close lattice match between the two materials. The $\mathrm{Al_xGa_{1-x}As}$ material is deliberately n doped to populate the bottom of its conduction band. From there electrons will migrate and populate the holes located at the top of the valence band of the GaAs (which is lightly p doped). Most of them, however, will fill the bottom of the conduction band of

the GaAs. The positive charge left on the donors gives rise to an electric field which attracts the electrons towards the interface and, in a similar way to the Si-MOSFET, bends the valence and conduction bands. The transfer of electrons continues until the dipolar layer composed of the positive donors and the negative inversion layer is strong enough. This dipolar layer produces a discontinuity of the potential and finally aligns the Fermi energy of the two materials. The electronic density in the inversions layer is determined by the density of the dopant which is fixed for each sample, in contrast to the Si-MOSFET where it can be varied with the gate voltage.

A technique called modulation doping [62] consists in growing an additional layer of ≈ 10 nm of undoped $Al_xGa_{1-x}As$ at the interface. The idea is to separate the charge carriers from the ionized impurities so that carriers can attain a mobility not affected by impurity scattering. At present, the mobility of the 2DEG can reach values as high as 200 T^{-1}.

3.3 The Ohmic contacts to the 2DEG

In precision measurements, the quality of the electrical contacts to the 2DEG is a critical issue. First, this quality must be such that the measurements are not affected by the contact resistance and second, the contacts have to be reliable because the quantum Hall resistors which are routinely used over periods of years must withstand numerous thermal cycles between room and cryogenic temperatures.

The contact technology for the Si-MOSFET which has been well established since the seventies, provides reliable low resistance contacts (see [60] and references therein) that work down to cryogenic temperatures. The region of the contact is heavily $n+$ doped ($N_d \geq 10^{19}\text{cm}^{-3}$) to favour the contact with a metal having a low barrier height ϕ_B (e.g. $\phi_B = 0.25$ eV for the Al/Si system). Such contacts can have specific resistances as low as $\rho_c = 10^{-6}\ \Omega\text{cm}^2$.

The situation for the GaAs/AlGaAs system is somewhat different. In the beginning, the contacts were made by alloying In or Sn through the heterostructures. This method provided low contact resistance. However, its reliability was not suitable for metrology since the contacts deteriorate with time due to diffusion processes. Therefore, the technique used in optoelectronics devices to contact bulk GaAs was modified to take into account the presence of the AlGaAs layer and the modulation doping technique. The result is to sequentially evaporate an alloy of AuGeNi [63]. First, a layer of AuGe eutectic alloy is evaporated, then a layer of Ni, and finally a layer of Au. The wafer stays at room temperature during this process. This metallization is alloyed in an oven containing an atmosphere of N_2/H_2. The sample is heated at 430 °C for 15 s and then cooled down to room temperature in 10 min. During the alloying process, the Ge atoms diffuse into the GaAs and substitute for Ga atoms in the crystal to create an $n+$ doped zone in the semiconductor. The Ni atoms, which also diffuse into the GaAs, enhance the diffusion of the Ge, but act as a barrier to avoid interdiffusion between the AuGe

layer and the Au top layer. In addition to these effects, the Ni reduces the surface tension of the AuGe liquid during the alloying which improves the homogeneity of the contact. The atomic ratio of Ge to Ni was found to be an important parameter in view of achieving the lowest possible contact resistance. Various investigations result in an optimum Ge/Ni atomic ratio of 0.8 to 1.0.

Contacts produced in this way regularly have a contact resistance below $R_c = 100$ mΩ. This contact resistance does not depend on the current (as long as the current stays below its breakdown value) and does not depend on the plateau index, as long as $\rho_{xx} \approx 0$. In addition, samples with such contacts have been very intensely used as resistance standards without showing any time deterioration over a period of 10 years.

4 Measurement techniques

For the accurate measurement of resistance, mainly two techniques are in use today: the potentiometric method and the current comparator bridge technique.

4.1 The potentiometric method

The principle of the potentiometric set-up is shown in figure 9. The two resistances $R_{\rm H}$ and R_s to be compared are connected is series and driven by the same dc current source. The voltage drop $V_{\rm H}$ across $R_{\rm H}$ is compared against a closely adjusted voltage V_p generated by a potentiometer using a high impedance voltage detector. After this first measurement, V_p and the detector are switched to R_s using a low thermal switch and the second voltage difference $V_s - V_p$ is measured. The difference measurements are repeated for the reversed current polarity. The sequence of current reversals and change of measurement positions is chosen such that linear drifts of the current sources and the thermal voltages are eliminated. The detector D should have a high input impedance and the linearity of the potentiometer has to be checked to allow for a reasonable deviation of the resistance standards from nominal.

Several laboratories have developed resistance comparators of this type to compare the quantized Hall resistance to a conventional resistance standard of the same nominal value. Since in this case, the ratio $V_{\rm H}/V_s$ is close to 1, the linearity requirements on the potentiometer are not critical. At $R_{\rm H} = R_s$ =12.9 kΩ and a current level of 50 μA, a measurement time of 15 min is required to reach a relative type-A uncertainty of 10^{-8} [64, 65]. After this step, the problem of the scaling from the level of the QHR to decadic resistance levels, e.g. 10 kΩ or 100 Ω, still remains. The method adopted by several laboratories is the use of a series-parallel resistor network of the Hamon type [66].

A significant improvement of the 1:1 potentiometric bridge is possible by using a Josephson array voltage standard (JAVS) [67] to realize the auxiliary voltage V_p. Modern JAVSs allow the generation of any voltage between 0 V and 10 V. It becomes thus possible to compare e.g. $R_{\rm H}(2)$ against a 10 kΩ standard. The

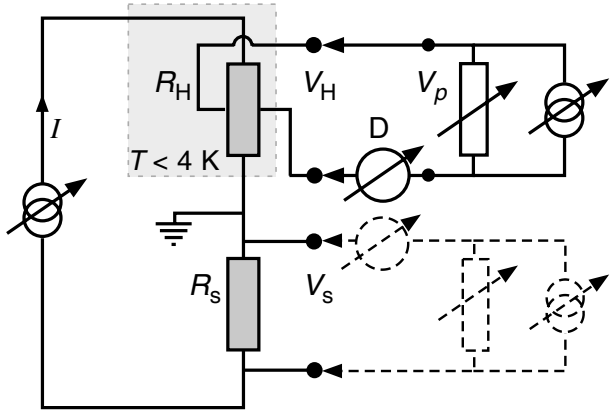

Figure 9: Schematic circuit diagram for a potentiometric resistance bridge. The voltage across the resistors to be compared is closely adjusted against the voltage V_p generated by the potentiometer. The remaining voltage difference is sensed by a high impedance voltage detector.

Josephson voltage $V_J = nf \cdot h/(2e)$ (n = step number, f = Josephson frequency) can be adjusted very closely to V_H and V_s, respectively ($\Delta V_H \simeq \Delta V_s \simeq 0$). The resistance ratio is then given by

$$\frac{R_H}{R_s} = \frac{\Delta V_H + V_{J1}}{\Delta V_s + V_{J2}} \simeq \frac{n_1 f_1}{n_2 f_2}\left(1 + \frac{\Delta V_H}{V_H} - \frac{\Delta V_s}{V_s}\right), \tag{21}$$

where n_1, f_1 and n_2, f_2 are the step number and frequency in the R_H and R_s position, respectively. Such measurement systems were first described in [68, 69]. The relative uncertainty reported by the authors was a few parts in 10^8.

4.2 Current comparator bridges

Because of the sequential measurements, the potentiometric method is mainly limited by the short term stability of the source. This disadvantage can be eliminated when the two resistance standards to be compared are in two separate current loops which track one another. The set-up of the current comparator bridge is schematically shown in figure 10. The ratio of the two currents is controlled by a dc comparator first realized by Kusters [70, 71]. The two windings N_p and N_s are wound on a high permeability toroidal core. The difference of the magnetomotive forces ($N_p I_p - N_s I_s$) can be measured using a second-harmonic flux-gate magnetometer. If an ac modulation is applied to the magnetic core, harmonic components of the modulation are generated if a dc flux is present in the core. A zero-flux condition ($N_p I_p = N_s I_s$) is achieved by means of a servo circuit operating from the output of the magnetometer. Now N_p is adjusted such that the voltage drops

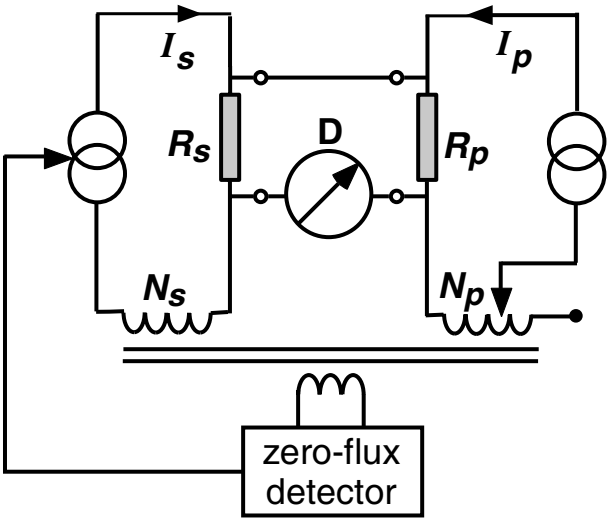

Figure 10: Schematic circuit diagram for a dc current comparator bridge. A servo circuit operating from the output of the magnetometer establishes the zero-flux condition in the magnetic core and accurately sets the current ratio I_p/I_s to the winding ratio N_s/N_p.

across the two resistors R_p and R_s are the same (detector D balanced). Finally, if the flux and voltage balance are met simultaneously, then $R_p/R_s = N_p/N_s$. An accuracy of a few parts in 10^8 can be achieved for the measured ratio. The resolution of the bridge is limited by the noise of the magnetic modulation. Commercial systems are available today [72] where a binary step-up of the windings in the current comparator allows a self-calibration of the current ratios.

The best ratio accuracy and the lowest random uncertainty are attained with the cryogenic current comparator (CCC) proposed and first realized by Harvey in 1972 [73]. The principle of the method is shown in figure 11 (a). If a current carrying wire is passed through a superconducting tube, a shielding current is induced on the surface of the tube such that a zero magnetic flux density is maintained in the interior of the superconductor (Meissner effect). The shielding current runs in the same direction as the initial current on the outside of the tube. The current density is uniform over the hole surface and thus independent on the geometrical position of the wire inside the tube. This principle is put in practice in a CCC as illustrated in figure 11 (b). In an arrangement called type I and introduced in [74], the superconducting tube is bent to a torus with overlapping ends like a snake swallowing its tail. The overlapping ends are electrically insulated, the length of the overlap has to be > 2 turns to keep the end effects on an acceptable level. Several windings, e.g. N_p and N_s with currents I_p and I_s, respectively, are placed inside the torus. The magnetic flux created by the shielding current on the

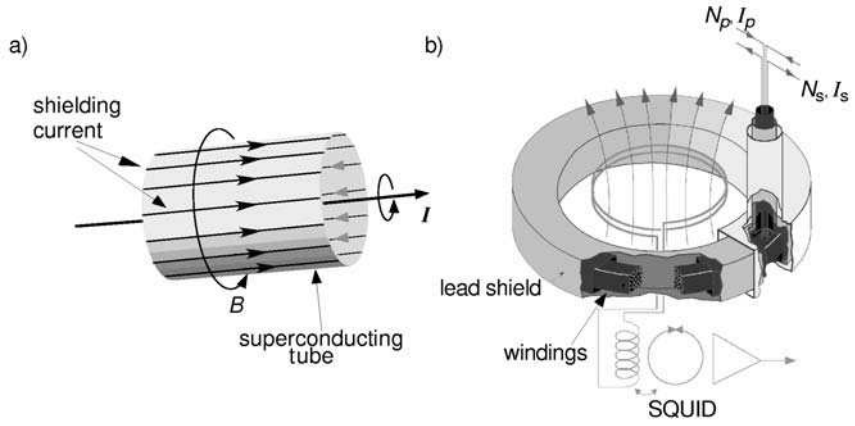

Figure 11: The cryogenic current comparator. (a) Illustration of the principle: a shielding current equal to I is induced on the external surface of the superconducting tube. (b) Set-up of the ratio coils: The windings of the current comparator form a toroidal coil which is enclosed in a superconducting shield. The shield overlaps itself like a snake swallowing its tail. The ampere-turns balance is sensed by measuring the magnetic flux in the pick-up coil using a SQUID.

torus is proportional to $N_pI_p + N_sI_s$. This flux is sensed by a superconducting quantum interference device (SQUID) through a pick-up coil placed in the flux. In an alternative type II arrangement which is topologically equivalent to the type I [75], the pick-up winding is surrounded by the superconducting shield.

With a CCC, current ratios $I_s/I_p = N_p/N_s$ with a relative accuracy of 10^{-12} can be realized. Theoretical estimations of the ratio accuracy for type I [76] and type II [77] agree well with measurements. An experimental check of the ratio accuracy is accomplished if the windings have a binary build-up. By measuring the SQUID signal of two windings with an equal number of turns put in an anti-series configuration, the error of the 1:1 ratio can be determined. In a binary build up, every winding with $2j$ turns can be compared directly with the combination

$$1 + \sum_{i=0}^{j-1} 2^i, \quad j = 1, 2, 3, \ldots \tag{22}$$

of windings already tested.

The superconducting flux transformer used to couple the SQUID to the shielding current flowing on the overlapping toroidal shield is illustrated in figure 12. A simple circuit analysis shows that the current resolution of the CCC is optimal when the inductance of the pick-up coil L_{pu} equals the inductance of the

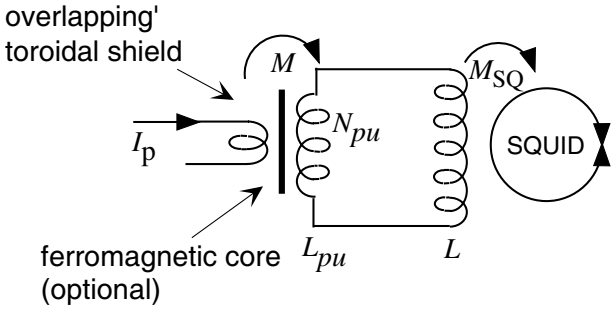

Figure 12: Input circuit of the SQUID sensor in a CCC with a superconducting flux transformer. N_{pu} is the number of turns in the pick-up coil and L_{pu} denotes its inductance. L is the inductance of the input coil of the SQUID. M and M_{SQ} are the mutual inductances.

input coil L of the SQUID. It can be shown [78, 79] that under this condition the best current resolution or minimum noise current is given by

$$\frac{\langle i_p^2 \rangle}{\Delta f} = \frac{8E_{SQ}}{A_L}. \tag{23}$$

In this expression $\langle i_p^2 \rangle = N_p^2 \langle I_p^2 \rangle$ is the mean square value of the noise current per single turn of the primary winding. N_p is the total number of turns in the primary ratio winding. E_{SQ} is the energy resolution of the SQUID and $A_L = L_{pu}/N_{pu}^2$ the magnetic conductance of the transformer. Because the sensitivity varies inversely as the number of turns in the pick-up coil, $N_{pu} = 1$ would be ideal. On the other hand, L_{pu} should be designed to be close to the inductance of the input coil L of the SQUID which is typically 2 μH. With $N_{pu} = 1$, a very large sensor volume would result, which increases the noise due to stray fields. Another way to get close to the ideal situation is to introduce a ferromagnetic core around which the pick-up coil and the windings of the CCC are wound. The relative permeability of the core can be adjusted such that $N_s \leq 1$ is achieved with a reasonably sized sensor volume [78, 79, 80]. The drawback of this method, however, is an additional noise component from the ferromagnetic core.

In practice [79], the rms-value of the current noise per turn in a dc SQUID based CCC is around 10^{-10} A in a bandwidth of 0.01 Hz to 1 Hz ($1/f$ corner of the SQUID at 0.3 Hz). This is about a factor of ten above the optimum value.

The CCC bridge arrangement is schematically shown in figure 13. A stabilized voltage source steers the primary and the secondary current sources. The ratio N_p/N_s of the windings is set as close as possible to the nominal ratio of the two resistors R_p/R_s to be measured. The output voltage of the SQUID system regulates the secondary current source in a closed feedback loop. The feedback assures that $N_p I_p = N_s I_s$. The detector, usually a battery operated nanovoltmeter, indicates

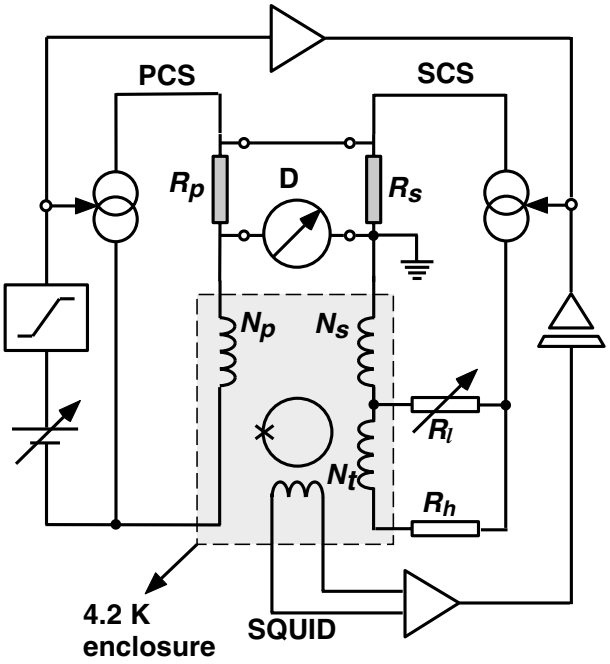

Figure 13: Schematic circuit diagram for a cryogenic current comparator bridge. The feedback signal from the SQUID accurately adjusts the current ratio between primary (left) and secondary (right) circuit to the ratio given by the windings N_p and N_s. The divider circuit composed of the trim coil, the adjustable resistor R_l and R_h is used to balance the detector D.

the difference between the resistance ratio and the winding ratio. The detector can be balanced with the help of an additional divider circuit composed of the trim coil N_t, a variable resistance R_l and a fixed high value resistor R_h. The ratio to be measured is then given by

$$\frac{R_p}{R_s} = \frac{N_p}{N_s}\frac{1}{(1+d)}\frac{1}{\left(1+\frac{V_m}{V}\right)};\; d = \frac{N_t}{N_s}\frac{R_l}{(R_l+R_h)}, \tag{24}$$

where V_m is the detector reading ($\simeq$0) and V the voltage drop across the resistors. The resolution of the bridge is mainly given by three factors: The SQUID noise, the thermal noise of the resistors and the detector noise.

The current noise of the SQUID detection system, as given above, transforms through the resistance R_s to a voltage noise seen by the detector (typically 0.5 nV/$\sqrt{\text{Hz}}$ for $R_s = 100\ \Omega$ and $N_s = 16$). The white thermal noise of a resistance R at a temperature T in a frequency bandwidth b is given by the Nyquist formula

$$V_{n-th} = \sqrt{4k_B T\ R\ b}, \tag{25}$$

where k_B is the Boltzmann constant. The thermal noise is often the limiting factor for resistance measurements above 10 kΩ. The third important noise component originating form the detector itself is often the dominating part for resistances below 100 Ω. Above this value, the best nanovoltmeters usually stay below the corresponding thermal noise of the source resistance at room temperature.

Typical parameters for a comparison of the QHR for $i = 2$ ($R_{\mathrm{H}}(2) = 12.9\,\mathrm{k\Omega}$) against a 100 Ω standard are: $N_p = 2065$, $N_s = 16$ and $I_p = 50\ \mu$A. For this configuration, the total rms voltage noise amounts to 7 $\mathrm{nV}/\sqrt{\mathrm{Hz}}$. It is dominated by the detector noise because R_p is at 1 K. According to this figure, a type-A relative uncertainty of 1 nΩ/Ω is expected within a measurement time of 2 min. In reality, slightly worse performance is achieved because of $1/f$ noise components (fluctuations of thermal voltages, detector and SQUID).

Today, the lowest uncertainties in resistance comparisons for $1\ \Omega \leq R \leq 100\ \mathrm{k\Omega}$ are obtained using CCC bridges (see e.g. [81, 82, 83, 84]).

Cryogenic current comparators working at dc are limited to a great extent by very low frequency noise of the $1/f$ type (null detector, SQUID) and by thermal effects (slowly varying thermal voltages, Peltier effect). To overcome these problems, ac CCCs working at a frequency close to 1 Hz were developed [85, 86]. As it turns out, the CCC coil has not to be specially designed to work at low frequency. However, quite some complexity is added to the bridge set-up to allow in-phase and quadrature current ratio matching and to avoid errors caused by stray capacitive effects.

5 Physical properties of the QHE devices

5.1 Temperature effect

In the previous paragraphs, the effect of the temperature on the transport properties of the 2DEG was neglected. In the quantum Hall regime at zero temperature, the longitudinal conductivity is so small [88, 89] that it is very difficult to measure. In fact, to the best of our knowledge, the dissipation measured in a QHR at very low temperature is the smallest measured in any non superconducting systems. Values of resistivities of $\rho_{xx} = 10^{-10}\Omega/\square$ were measured, which corresponds to a bulk resistivity of $\rho_{xx} = 10^{-16}$ Ωcm [89]. However, the situation at finite temperatures is different and various transport processes can be distinguished depending on the temperature range.

5.1.1 Thermal activation

In an intermediate temperature range ($\simeq 1\ \mathrm{K} \ldots 10\ \mathrm{K}$), the conductivity in the quantum Hall regime is predominately determined by electrons excited in the nearest Landau level and the longitudinal conductivity is given by

$$\sigma_{xx}(T) = \sigma_{xx}^{0} e^{-\Delta/kT}, \tag{26}$$

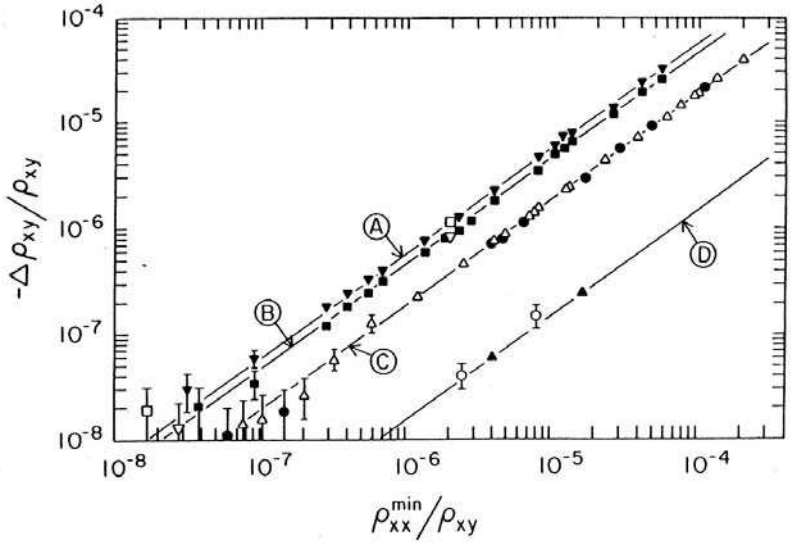

Figure 14: Log-log plot of the relative deviation $\delta\rho_{xy}(T)$ as a function of the normalized longitudinal resistivity $\rho_{xx}(T)$ for temperatures ranging between 1.2 K and 4.2 K. The measurements were performed with two different GaAs heterostructures in the middle of the $i = 4$ plateau with both magnetic field polarities and two different voltage probe pairs. The linear relation between $\delta\rho_{xy}$ and ρ_{xx} is observed over four orders of magnitude in ρ_{xx}. (Reproduced after [87]).

where Δ is the energy difference between the Fermi energy E_F and the next Landau level. The thermally activated conductivity has been studied in great detail in the integer and in the fractional QHE, both theoretically [90, 91, 92, 93, 94] and experimentally [95, 96, 97, 98, 99, 100, 101, 102, 103]. The question of the universality of the prefactor σ_{xx}^0 was also addressed [104]. An activated temperature behaviour is also expected for the deviation of the Hall conductivity from its quantized value

$$\delta\sigma_{xy}(T) = \sigma_{xy}(T) - \frac{e^2\nu_0}{h}, \tag{27}$$

where ν_0 is the filling factor at the plateau centre. Such a temperature behaviour leads to a linear dependence between the deviation $\delta\sigma_{xy}(T)$ and the longitudinal conductivity $\sigma_{xx}(T)$.

In early measurements, such linear dependencies were observed [87, 105, 106] in the resistivities according to

$$\delta\rho_{xy}(T) = s\rho_{xx}(T). \tag{28}$$

In figure 14 (reproduced after [87]) the relative deviation of the Hall resistivity is plotted as a function of the longitudinal resistivity. The measurements were carried out close to the $i = 4$ plateau centre of two GaAs heterostructures. The linear dependence was observed over four orders of magnitude in ρ_{xx}, for two different samples and various cool downs. The proportionality factor varied between $s = -0.01$ and $s = -0.51$, depending on the device, the Hall probe used and the magnetic field direction. Other experiments [2, 107] reported different values for s, including positive values. It should be emphasized that all the measurements reported above were performed at the plateau centre.

In another study [108], the slope of the plateau was measured as a function of ρ_{xx} for GaAs heterostructures and Si-MOSFET samples at temperatures between 1.5 K and 4.2 K. In the GaAs samples, the slope was found to be activated over the whole range of temperatures, including at temperatures where ρ_{xx} was no longer in the activated regime. In the MOSFET devices, where ρ_{xx} was always activated, the slope remained linear over three orders of magnitude in ρ_{xx}.

More recently, a systematic study of the temperature dependence of the 2DEG resistivity was performed on large heterostructure Hall bars [102, 103]. Data were taken at temperatures ranging between 0.3 K and 20 K over the entire plateau region for $i = 2, 3$ and 4 plateaus at very low current level to rule out any current heating effect. The longitudinal resistivity shows an activated behaviour over three decade in ρ_{xx} in the temperature range from 1 K to 10 K. The prefactor was found to be $\sigma^0_{xx} = 2e^2/h$ at the plateau centre, in agreement with [104].

The investigation of the activated transverse resistivity showed a linear relation according to equation 28 over 3 decades of ρ_{xx} as long as $\rho_{xx} < 10\ \Omega$. This result is in agreement with the early experiment reported previously [87, 105]. However, at higher dissipation, a crossover to a quadratic dependence was observed in agreement with the finite size scaling theories [23], the semicircle rule [109] and the gauge theory [33]. In figure 15, the slopes $s = \delta\rho_{xy}/\rho_{xx}$ observed in the linear response are plotted as a function of the filling factor for plateaus $i = 2, 3$ and 4 (solid symbol). On the high B side (low ν), the values can be explained by a geometrical effect [110]. Due to the finite width w_p of the voltage probes, a small component of the longitudinal voltage is mixed into the Hall voltage and accordingly, the measured Hall resistivity becomes

$$\rho^{meas}_{xy}(T) = \rho_{xy}(T) - \frac{w_p}{w}\rho_{xx}(T), \tag{29}$$

where w is the sample width. However on the low B side (high ν), slope values as large as $s = -1.1$ have been measured. Geometrical effects cannot account for such large deviations which have to be explained by a percolation model incorporating different transport regimes depending on the position of the Fermi energy in the Landau level tail [103]. The strong asymmetry observed in the middle of the odd plateaus can very well explain the scattering of the values reported for s in the earlier studies performed at the plateau centre.

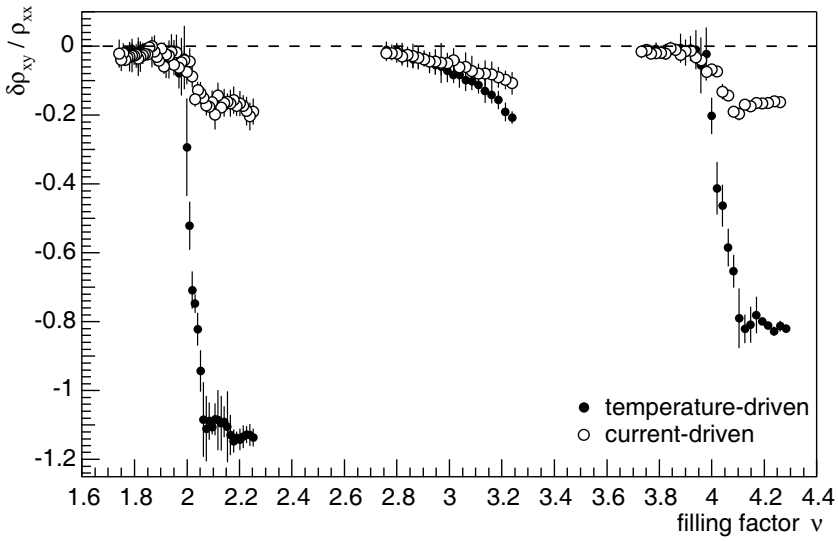

Figure 15: The slope $s = \delta\rho_{xy}/\rho_{xx}$ are plotted as a function of the filling factor ν for the plateaus $i = 2, 3$ and 4. Solid symbol: temperature driven data from experiments performed at constant low current in the thermally activated regime. Open symbol: current driven data performed at low temperatures ($T = 0.3$K) in the variable range hopping regime. (Reproduced after [103]).

Finally, for metrological applications, it is crucial to note that in all measurements reported so far the transverse resistivity always extrapolates to h/ie^2 at zero dissipation ($\rho_{xx} \to 0, T \to 0$).

5.1.2 Variable-range hopping

At the lowest temperatures ($T < 1$ K), so called variable-range hopping (VRH) [111] dominates the behaviour of the conductivity. The VRH consists of electrons tunnelling between localized states within an energy range on the order of kT around the Fermi energy by the emission or absorption of phonons. In this case the longitudinal conductivity is given by

$$\sigma_{xx} = \sigma_{xx}^{T} e^{-(T_1/T)^{\alpha}}. \tag{30}$$

While equation 30 with $\alpha = \frac{1}{3}$ describes the Mott hopping [112] in two-dimensional systems, it was not found to be appropriate for the 2DEG at high magnetic fields where a soft coulomb gap exists at the Fermi energy [113]. In this case, an exponent of $\alpha = \frac{1}{2}$ was derived [111, 113, 114, 115, 116, 117]. The evaluation of the prefactor σ_{xx}^{T} and the coefficient T_1 was a very disputed question

and no consensus does exist at the moment. Experimentally, an exponent of $\alpha = \frac{1}{2}$ and a prefactor $\sigma_{xx}^{T} \propto 1/T$ are usually observed [103, 118, 119, 120, 121, 122].

The behaviour of the Hall resistance in the VRH has only attracted a limited amount of interest. In [103], it was found that the deviation $\delta\rho_{xy}$ measured in the VRH regime can be explained by the geometrical effect described by equation 29 over the entire plateau range, for plateaus $i = 2, 3$ and 4. This is in agreement with a theoretical prediction [115] of a negligibly small VRH contribution to $\delta\rho_{xy}$ compared to ρ_{xx}.

In the VRH regime, a non-Ohmic conductivity appears under strong electric field $\mathcal{E}$ and the longitudinal conductivity is then expected to follow [117]

$$\sigma_{xx}(I) = \sigma_{xx}^{I} e^{-\sqrt{\mathcal{E}_1/\mathcal{E}_{\mathrm{H}}}}, \tag{31}$$

where $\mathcal{E}_{\mathrm{H}}$ is the Hall electric field and $\mathcal{E}_1$ is a characteristic value related to the hopping temperature T_1 [117].

The non-Ohmic regime was experimentally studied by Furlan [103]. The longitudinal and Hall resistivities were measured as a function of the current ($1\ \mu\mathrm{A} < I < 100\ \mu\mathrm{A}$) at a constant bath temperature of $T = 0.3$ K. As in the temperature experiment, $\delta\rho_{xy}$ was found to be linearly related to ρ_{xx} over three decade in ρ_{xx}. In figure 15, the slopes are reported as a function of the filling factor (open symbols). Similarly to the temperature driven resistivities, asymmetries are also observed, however, with a much smaller amplitude. On the low ν side, both experiments can be explained by the geometrical effect. On the high ν side, the slope values are a factor of 4 to 6 smaller than for the temperature driven resistivities. This is attributed [103] to the different prefactors involved in the relations 26 and 31.

Based on a field dependent hopping model [117] in the VRH regime due to the presence of the Hall electric field $\mathcal{E}_{\mathrm{H}}$, we can adopt the picture of the existence of a quasi-Fermi level tilted by $\mathcal{E}_{\mathrm{H}}$. As a consequence, formation of the local Fermi distribution corresponds to an effective electron temperature $T_{\mathrm{eff}} \propto \mathcal{E}_{\mathrm{H}}$. This dependence can be tested by comparison of measured conductivities $\sigma_{\mathrm{xx}}(T)$ and $\sigma_{\mathrm{xx}}(I)$ at fixed filling factor ν, which relates the current I to an effective temperature like

$$k_{\mathrm{B}} T_{\mathrm{eff}}(I) = e\xi \frac{\rho_{\mathrm{xy}} I}{2w}, \tag{32}$$

where ξ is the localization length and w the sample width. Besides the direct determination of the fundamental length scale ξ as suggested from equation 32, the linear dependence of T_{eff} on the current I was experimentally confirmed [103]. Therefore, electron heating effects may play a role and have to be taken into account in precision measurements irrespective of the further possibility of QHE breakdown (see section 5.3). It is important to note that other measurements [123, 124] which reported a square root dependence $T_{\mathrm{eff}} \propto \sqrt{I}$ were based on a different experimental approach: the ρ_{xx} peak width or the maximum slope $(\mathrm{d}\rho_{\mathrm{xy}}(B)/\mathrm{d}B)_{\max}$ may also yield an effective temperature [117]. However, the assumption of the model of

a constant dielectric function $\epsilon_r(\nu)$ is not justified for varying ν [103], and neglect of this fact can lead to confusion and inappropriate interpretations.

In conclusion, the temperature has a significant effect on the transport properties of the 2DEG. However, as long as the transport is in the variable-range hopping regime and the longitudinal resistance is exponentially small, the Hall resistance is quantized to a value which is expected to be h/ie^2.

5.2 Current distribution

For a homogeneous 2DEG in the QHE regime, the electric Hall field is perpendicular to the current flow direction. Thus, no power is dissipated in the interior of the sample. In a Hall bar, the Hall voltage is shunted out at both ends of the device by the current contacts forcing the electrons to enter and exit the 2DEG at diagonally opposite corners of the device. The total power dissipation is $R_H I^2$ and occurs exclusively at the contacts. This was experimentally observed by Klass *et al*[125] utilizing the fountain pressure effect of superfluid helium.

The way the current is distributed across the Hall bar has been discussed continuously since the discovery of the QHE. According to the underlying theoretical models, two pictures for the current distribution are proposed: In the edge current picture (see section 2.5), the current flows in narrow channels located near the edges of the device, i.e. the Hall voltage drops entirely in these regions. Experiments carried out in mesoscopic devices at low current levels ($\Delta\mu < \hbar\omega_c$) measuring the equilibrium rate between the current carrying edge states [51] or the non-local conductivity [52] can be well described by the pure edge-state picture. Because the Hall current is caused by the drift of electrons in crossed electric and magnetic fields, the bulk current picture also has to be considered. In this view, the Hall electric field is essential and the current is carried by the extended states near the centre of the broadened bulk Landau levels. The Hall current is proportional to local changes in the potential, it does not depend upon sample geometry or the existence of edges. This picture implies that, at least for a homogeneous sample, the Hall voltage should gradually drop across the width of the device. Results on Corbino disks [126], where edge states do not contribute to the electronic transport for topological reasons, show that the QHE as a consequence of pure bulk transport is possible.

The crossover between the edge state and bulk transport depends on the experimental situation and is not understood in all details yet. Various theoretical studies and numerical simulations [127, 128, 129, 130, 131, 132, 133, 134] suggest that in wide Hall bars at high current levels, a substantial amount of the current is carried by the bulk states.

The first experimental method used to measure the current distribution was the direct electrical measurement of the potential distribution by placing a series of metallic contacts in the interior of a Hall bar device [135, 136, 137]. Outside the plateau regions, it was found that the current distribution varies more or less linearly across the device. In the QHE regime, however, a strongly inhomogeneous

current distribution and bunching of the current as a function of the applied magnetic field was observed. This behaviour was attributed to the presence of gradients in the electron density. The objections raised against these results are that the interior contacts themselves may strongly alter the potential distribution and, in addition, they tend to decouple from the 2DEG in the QHE regime due to the Corbino effect.

To overcome such difficulties, contactless methods were applied to measure the current distribution. One approach was the application of the linear electro-optical effect (Pockels effect) in GaAs. An applied electric field influences the birefringence property of the crystal and, therefore, the polarization direction of light changes as a function of the local potential while passing through the 2DEG. Using this method, Fontein *et al*[138] found in a 2 mm wide sample at a current of 5 μA that approximately 80 % of the Hall voltage drop near the sample edges. Applying the same technique in a 200 μm wide strip, Knott *et al*[139] observed a concentration of the Hall potential in the middle of the channel. The shape of the profile varied as a function of the magnetic field and the current along the plateau. In subsequent measurements of Dietsche *et al*[140], using wider samples, a potential drop along one side of the device over a width of about 100 μm was found.

In a different approach Yahel *et al*[141] measured the current distribution by means of an inductive coupling technique. The authors showed that gates placed below or above the sample strongly influence the electrostatic potential profile of the 2DEG and, as a result, distort the Hall current distribution. This may explain the current bunching effect observed in earlier experiments. For samples without any gate, the current distribution in the QHE regime remained almost uniform like in the dissipative regime.

Recently, McCormick *et al*[142] used an atomic force microscope to measure the Hall voltage profile in a 2DEG. On the QHE plateaus, the Hall currents were located primarily in the bulk and showed complex spatial variations.

The edge channel picture (see section 2.5) implies that a sequence of compressible strips with metal-like screening properties and incompressible strips with insulator-like behaviour exists near the edges of a 2DEG in the QHE regime. New experimental techniques using a single-electron tunnelling (SET) transistor as a detecting device allow the mapping of these strips. Wei *et al*[143] have fabricated a GaAs/AlGaAs device with a metal SET transistor mounted on top. Yacoby *et al*[144] use a SET transistor mounted on the tip of tapered glass fiber which can be scanned 100 to 200 nm above the surface of a QHE device. The current through the SET transistor is modulated by the potential changes underneath. Using this technique, both groups were able to resolve the edge strips. The number of the strips was found to be consistent with the value of the bulk Landau level filling factor.

In conclusion, for higher currents the experiments do not give a conclusive picture on the relative importance of edge and bulk transport. Some results seem to be in contradiction with others. Comparisons, however, should be made with

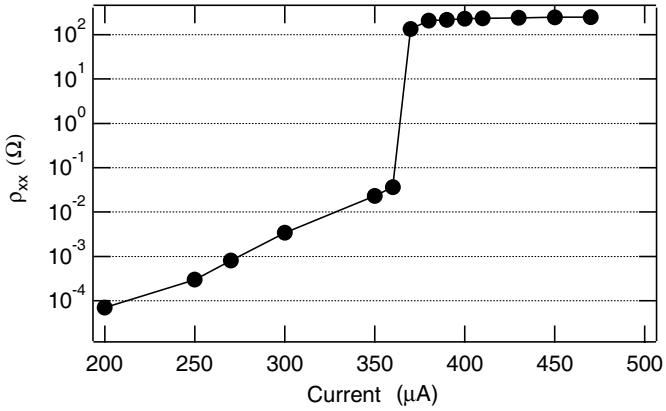

Figure 16: Current dependence of the longitudinal resistivity for the $i = 2$ plateau of a GaAs device (width = 400 μm).

care because the experimental conditions (sample geometry, current level, gate arrangements, spatial resolution) vary a lot from one experiment to the other.

5.3 Breakdown of the QHE

As shown in section 5.1, the longitudinal resistivity ρ_{xx} in the QHE regime and the deviation $\Delta\rho_{xy}$ from the QHR gradually increase with increasing temperature or current. When the current exceeds a certain critical value I_c , ρ_{xx} suddenly increases by several orders of magnitude and the QHE breaks down. This behaviour is illustrated in figure 16. The critical current decreases linearly as B departs from the plateau centre as shown in figure 17.

The breakdown of the QHE due to high current densities was and still remains a subject of much theoretical and experimental work (see also [146] for a further review). On one hand the phenomenon attracts attention because of its importance for the understanding of the QHE. On the other hand, knowledge of the breakdown is crucial for the resistance standard based on the QHE where a critical current as high as possible is aimed at for maximum resolution.

The first experimental study devoted to current breakdown of the QHE was published by Ebert *et al*[147]. The authors measured the critical current in a series of low mobility GaAs Hall bar devices with different carrier concentrations. A subset of the results is shown in figure 18 where the critical Hall field calculated from the average current density at breakdown is plotted against the plateau centre. E_c is found to be roughly proportional to $B^{3/2}$. Other early experiments [148, 149, 150] reported similar values for the critical current density using Hall bar devices with mobilities below 30 T^{-1}. In contrast to these reports Bliek *et al*[151] found critical current densities up to 32 A/m when measuring the longitudinal

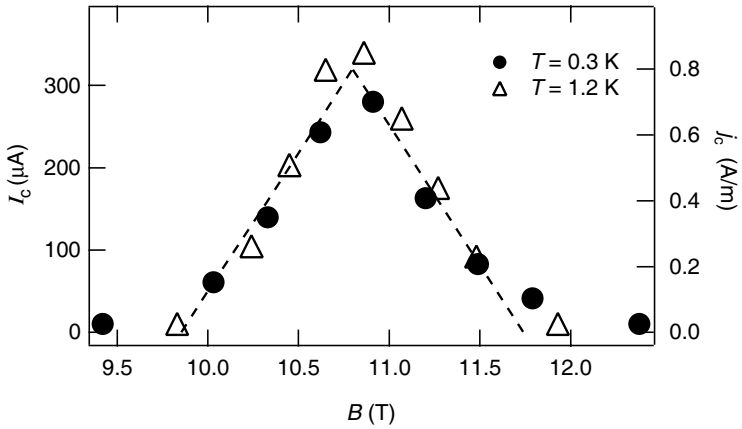

Figure 17: Critical current $I_c = j_c w$ (sample width $w = 400$ μm) as a function of the magnetic flux density for the $i = 2$ plateau. The dashed line is a guide to the eye. Data from Jeckelmann *et al*([145]).

voltage across a short constriction (10 μm long and up to 66 μm wide) in a Hall bar.

The B dependence of E_c was also studied by Kawaji *et al*[152] in butterfly-type devices and Jeckelmann *et al*[145] in 400 μm wide Hall bars. As shown in figure 18, these results confirm the $B^{3/2}$ dependence found earlier.

Several groups studied the width dependence of the critical current $I_c = j_c w$ [145, 152, 153, 154, 155] and found a linear increase with the sample width w. The results are summarized in figure 19 and strongly support the picture of a homogeneous current distribution in samples wider than 10 μm and at a current around I_c. In addition, no dependence of j_c on the mobility up to a value of 130 T^{-1} was seen in [145, 152]. In contrast to these results, Balaban *et al*[154] claimed a sublinear w dependence of I_c in high mobility samples ($\mu = 70$ to 90 T^{-1}). In a low mobility sample, a linear width dependence changed to sublinear behaviour after illumination. According to Nachtwei [146], the length scale of the inhomogeneities of the carrier density and their distribution could be the key to the observed differences. In case of short range fluctuations (typical length scale smaller than w), a linear dependence is expected whereas long-range fluctuations are consistent with the sublinear increase of I_c. It is conceivable that in the narrow devices ($w < 40$ μm) used by Balaban *et al*, the long-range inhomogeneities were dominant after illumination or at high mobility.

Many different theoretical models were put forward to explain the typical signatures of the QHE breakdown. Soon after the first measurements, Streda and von Klitzing [156] proposed a mechanism of abrupt phonon emission (Cerenkov like) triggering the breakdown. This model and the electron heating process described

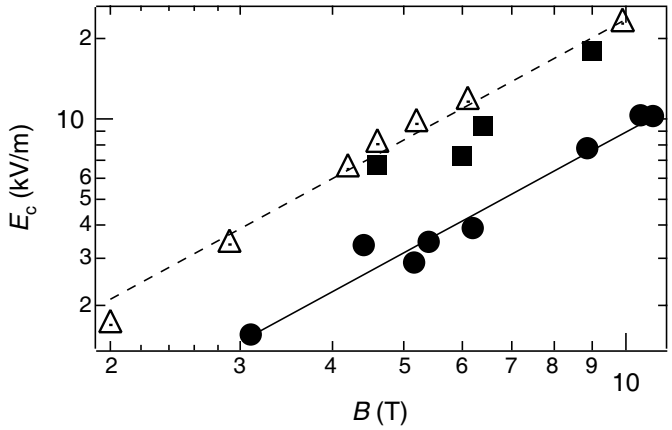

Figure 18: B dependence of the critical Hall field reported by different authors. ●: Jeckelmann *et al*[145], normal 400 μm wide Hall bars. ■: Ebert *et al*[118], normal 380 μm wide Hall bars. △: Kawaji *et al*[152], Hall bars with a 600 μm long constriction in the middle (butterfly-type). The straight lines on the log-log plot have a slope of 3/2.

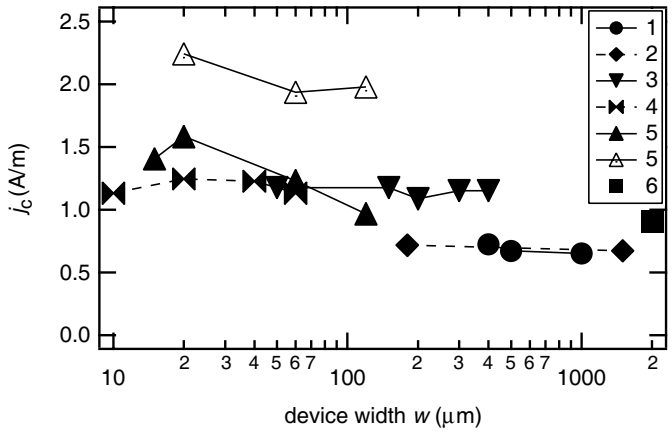

Figure 19: Critical current density as a function of the device width reported by different authors. Full symbols: standard Hall bars; open symbols: Hall bar with a constriction in the middle (butterfly-type). 1: [145], 2: [155], 3: [153], 4: [154], 5: [152], 6: [150]

by Komiyama *et al* [149] shortly afterwards predict a linear dependence of the critical field E_c on B which is not observed in experiments. In a model by Eaves and Sheard [157] based on the quasieleastic inter-Landau level scattering (QUILLS) the breakdown is induced by transitions of electrons in the highest populated Landau level into the lowest unpopulated level due to the high Hall electric field. This model predicts the observed $B^{3/2}$ dependence of E_c. However, the value for the critical field is one order of magnitude larger than experimentally observed and the dependence on the plateau number is not correctly reproduced.

Recently, Komiyama and Kawaguchi [158] have developed a theoretical model to explain the breakdown of the QHE based on thermodynamical arguments. They propose an avalanche type electron-hole pair multiplication process, referred to as bootstrap-type electron heating (BSEH). The process starts when the local electric fields exceeds a critical level and needs a minimal distance L_B for the cascading generation of electron-hole pairs to significantly develop. In high mobility GaAs devices, L_B is on the order of 100 μm. The avalanche normally starts near the electron injection point in the source contact where the electric field is generally larger than the average Hall electric field in the main 2DEG channel. The further evolution towards breakdown in the entire 2DEG channel, can be distinguished in two cases:

- If w is larger than the minimal length L_B, the breakdown of the QHE in the entire Hall bar is preceded by a local breakdown around the source contact. Its signature is a finite voltage drop in the vicinity of the source contact which emerges once the nonequilibrium distribution of electrons is extended along the whole boundary between contact and 2DEG and starts to affect the edge state population. This was experimentally observed by measuring the spatial distribution of the cyclotron radiation emitted from nonequilibrium electrons [155].

- If w is smaller than L_B, the cascadelike electron-hole pair excitation takes place as the electrons traverse the Hall bar along its length. The evolution of the breakdown starts at the source contact and develops towards the drain contact. Such a spatial evolution has recently been confirmed experimentally [146]. In addition, the critical field E_c expected from the BSEH model is close to the experimental results [158] and the reported $B^{3/2}$ dependence is reproduced. Because of the role of the length L_B in the breakdown, the model is also consistent with the high critical current observed in short constrictions (see above).

Another feature reported in some breakdown experiments is the observation of time dependent fluctuations between the low dissipative QHE condition and one or several resistive states. When measuring the longitudinal voltage between two voltage contacts in a standard Hall bar, Cage *et al*[159] observed a series of discrete voltage steps quantized in units of the cyclotron energy. Pronounced steps in the longitudinal voltage with a rich time-dependent structure were also

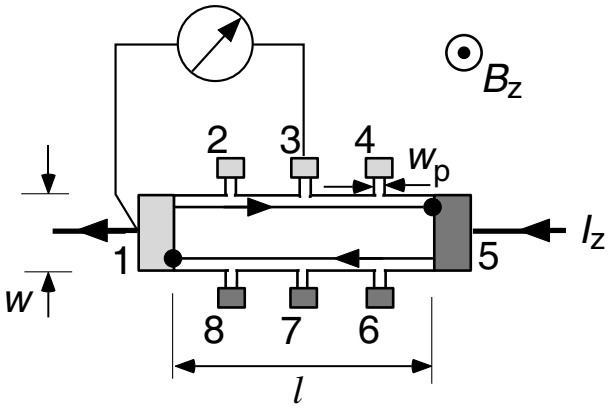

Figure 20: Hall bar configuration and schematic diagram for the measurement of the contact resistance R_c of the current contact 1. The black dots indicate the regions where the electrons enter or leave the device. The contacts 1, 2, 3 and 4 are at potential 0 and contacts 5 ,6, 7, 8 at potential $R_{\mathrm{H}}I$.

observed in [160]. Ahlers *et al*[161] measured the longitudinal voltage across a narrow constriction in a Hall bar near breakdown and found switching behaviour between different dissipative states. In contrast to Cage *et al*, the voltage steps were not correlated with $\hbar\omega_c$. Ahlers *et al*explained their results with time-dependent fluctuations of macroscopic hot-electron domains.

In summary, the breakdown of the QHE is difficult to model because its characteristics depend on the microscopic details of the 2DEG. Although much progress was made so far, a complete understanding of the phenomenon is still missing.

5.4 Contact effects

In the edge state picture (see section 2.5), the contacts to the 2DEG influence the four-terminal Hall resistance in an essential manner. This was first shown by Büttiker [43] and subsequently in a quantitative model by Komiyama and Hirai [162]. The basic idea is that a non-ideal current contact populates different Landau levels to different degrees. This unequal population leads to different electrochemical potentials at different edge states. If this nonequilibrium distribution travels over macroscopic distances and is selectively probed by a non-ideal voltage contact, the Hall resistance deviates from the quantized value. These effects have been observed experimentally [50, 51, 163] and they are, at least qualitatively, in agreement with the edge state picture. It was also shown that the non-equilibrium distribution in the edge channels can travel over macroscopic distances ($> 100\ \mu$m) [163]. It should be noted, however, that the majority of experiments investigating

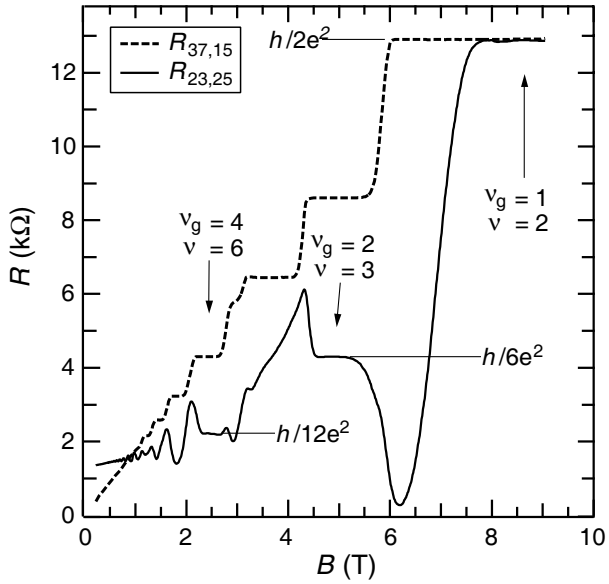

Figure 21: Resistance measured across a partially depleted region in a voltage probe as a function of the magnetic flux density. Plateaus appear when the filling factors for the depleted region ν_g and for the rest of the device are integers [165]. The sample configuration is shown in figure 20. For the resistance $R_{kl,mn}$, m, n and k, l are the current and potential contacts respectively.

the edge transport are carried out in the linear regime where the chemical potential difference $\Delta\mu$ between the boundaries of the device is smaller than the Landau level spacing $\hbar\omega_c$. In the metrological application of the QHE much higher currents are passed through a device of macroscopic dimensions and $\Delta\mu \gg \hbar\omega_c$. As a consequence, the pure edge-state description is no longer appropriate and the influence of bad contacts is less clear.

The quality of the contacts is characterized by their resistance R_c which is measured in the QHE using a method first proposed by Rikken *et al*[164]. The voltage drop across the contact j to be characterized and the next contact situated at the same Hall potential is measured while passing a current through contact j and one of the current contacts (see figure 20). If the sample is well quantized, ρ_{xx} can be neglected and R_{cj} is obtained directly. The resistance of a good AuGeNi contact is usually well below 1 Ω, provided the device is cooled slowly from room temperature down to the working temperature of <2 K.

The resistance of the contact region can also be varied in a controlled way by using a gate placed over the probe, i.e. the narrow arm which links the contact pad to the main channel of the device in the usual Hall bar geometry. Applying a voltage to the gate partially depletes the 2DEG under the gate. In metrological

applications of the QHE with ungated standard Hall bar devices, a similar local reduction of the carrier concentration in the narrow voltage probes can be generated accidentally by cooling a device too fast, by passing a current above the critical current through the potential probe or even by leaving the device in the cold for several days. The effect of depletion of the carrier concentration in a probe is illustrated in figure 21 where the contact resistance is plotted as a function of the magnetic flux density B. Plateaus appear in the regions where the filling factors both of the Hall bar ν and of the partially depleted voltage probe ν_g are integers (see e.g. [53] for an explanation). The original contact properties are restored by cycling the device through room temperature or by illuminating the device at low temperature with infrared radiation [166].

The influence of non-ideal voltage contacts on the QHR was extensively studied by Jeckelmann *et al*[165, 167]. It was shown that deviations $\Delta R_{\mathrm{H}}/R_{\mathrm{H}}$ of up to 1 part in 10^6 can occur as a consequence of R_c values in the kΩ range. At the same time, a corresponding positive or negative longitudinal voltage V_{xx} is measured along the side of the device where the bad contacts are connected to. A zero V_{xx} is measured on the opposite side if the corresponding contacts have a low resistance. There is no simple relation between ΔR_{H} and R_c. The data show, however, that the maximum deviation ΔR_{H} at a given R_c is proportional to R_c/R_{H}. The deviations become more pronounced when going to higher filling factors. In addition they are inversely proportional to the current and they decay exponentially with increasing temperature (see. figure 22). The data finally demonstrate that deviations in the QHR above the experimental resolution of 0.5 nΩ/Ω are to be expected if the resistance of the potential contacts exceeds 100 Ω when measuring on the $i = 2$ plateau and 10 Ω in the case of $i = 4$. These limits apply for a temperature of 0.3 K and a current above 10 μA and it is assumed that the resistance of the current contacts is in the mΩ range.

A model based on the Büttiker formalism for contacts [168] allows an estimate to be made on the upper limit for the deviation of the four-terminal resistance as a function of the contact resistance. The magnitude of the effects is similar to the experimental findings of [167]. On the other hand the model, as it only considers pure edge state transport in a uniform device, does not explain the detailed pattern of the observations.

5.5 QHE devices with multiple connections

For the practical application of the QHE as a resistance standard it is desirable to have quantized resistance values covering a wide range of quantum numbers. In reality, however, it turns out that the device characteristics are usually such that only the plateaus two and four are well quantized under normal operational conditions. The question thus arises whether a combination of several QHE devices in a series or parallel configuration may yield the practical resistance value needed in a specific application.

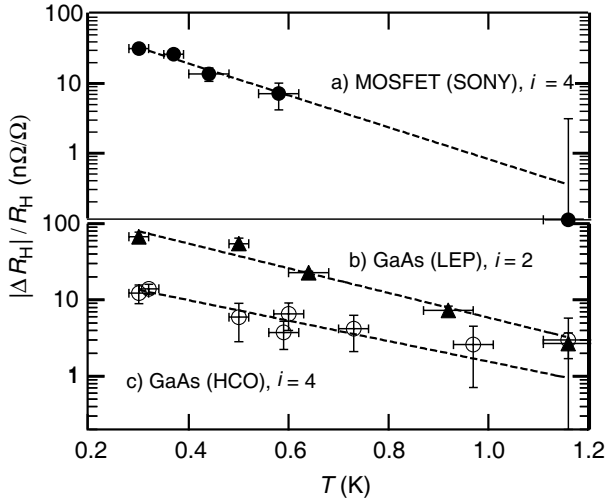

Figure 22: Temperature dependence of the QHR deviations caused by non-ideal voltage contacts [165]. For all three devices, one of the QHR measuring voltage contacts has a high resistance. The QHR deviations decrease exponentially with increasing temperature.

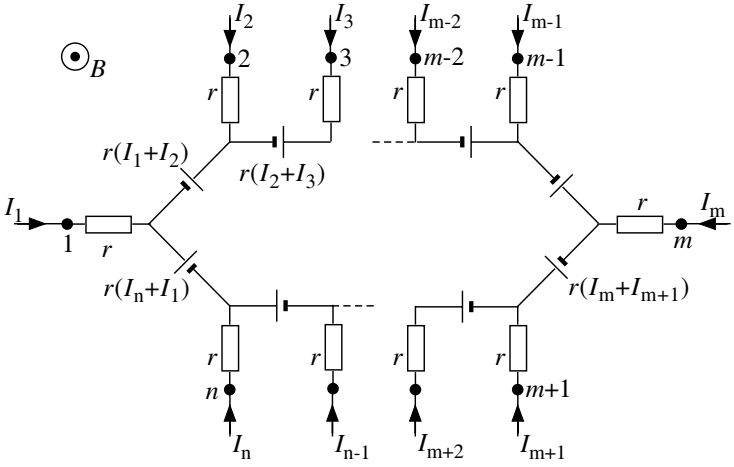

Figure 23: Equivalent circuit of an ideal multi-terminal quantum Hall device (after [169]). Each arm of the Hall bar ends at a resistance $r = R_{\mathrm{R}}/2$.

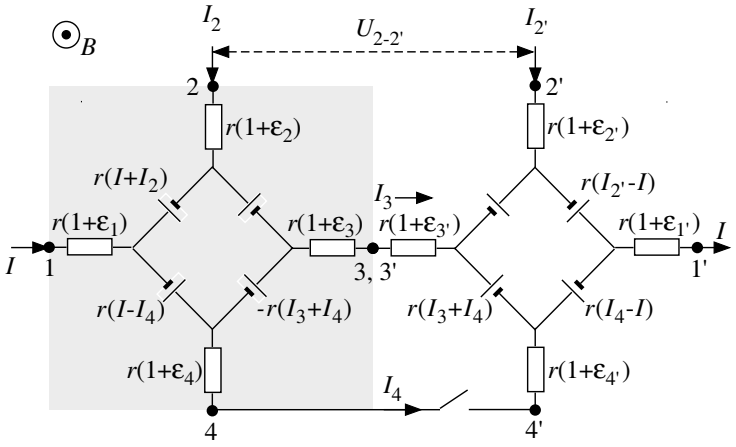

Figure 24: Equivalent circuit of a double-series connection of two four-terminal quantum Hall devices.

Ricketts and Kemeny [169] first described the electrical behaviour of a QHE device in terms of an equivalent circuit (see figure 23). In a fully quantized multiterminal device, each arm ends at a resistance $R_{\mathrm{H}}/2 + R_c = r(1+\varepsilon)$, where R_c is the resistance of the contact to the 2DEG and of the connecting wires ($\varepsilon = 2R_c/R_{\mathrm{H}} \ll 1$). Between each pair of arms k, l there is a voltage generator $V_{kl} = r(I_k + I_l)$ where I_k and I_l are the currents flowing into the device through the contacts k and l respectively. It is easily shown that in this model, the two-terminal resistance between any pair of contacts k, l is given by $R_{\mathrm{H}} + R_{ck} + R_{cl}$, and the four-terminal Hall resistance $R_{kl,mn}$ is equal to R_{H}, where m, n and k, l are the current and potential contacts respectively.

If several QHE devices are put in series or parallel in a network, the resistances of the contacts and the connecting wires have to be taken into account when the overall resistance of the network is determined. In the case of multiterminal devices, however, Delahaye [170] has shown that the contact effects can be drastically reduced if the number of links between neighbouring devices is increased. To illustrate this interesting property let us consider the simple case where two four-terminal QHE devices are put in series (see figure 24). If the two devices are linked together using contacts 3 and 3' only, a voltage drop $I(R_{c3} + R_{c3'})$ develops between contacts 4 and 4' and as a consequence a deviation in the Hall voltage $U_{2,2'}$ from the quantized value $2R_{\mathrm{H}}I$ is observed. Now, let us introduce an additional connection between the contacts 4 and 4'. Applying Kirchhoff's laws yields:

$$I_3(\varepsilon_3 + \varepsilon_{3'}) = I_4(4 + \varepsilon_4 + \varepsilon_{4'}), I_4 + I_3 = I. \tag{33}$$

The Hall voltage between contacts 2 and 2' is given by

$$U_{2,2'} = 4rI + r(\varepsilon_4 + \varepsilon_{4'})I_4. \tag{34}$$

Combining the three equations and neglecting the higher order terms in ε gives a Hall resistance deviation from the nominal value of

$$\frac{R_{22',11'}}{2R_{\mathrm{H}}} \simeq 1 + \frac{1}{16}((\varepsilon_3 + \varepsilon_{3'})(\varepsilon_4 + \varepsilon_{4'})). \tag{35}$$

The terminal effects thus decrease to a term of order ε^2 when the two devices are connected by two links.

Applying the same analysis to n links, it can been shown that the series resistance will differ from its nominal value by a term of the order ε^n. Similar results are obtained for multiple parallel connections.

A series array of 10 QHE devices with triple series connections ($n = 3$) integrated on one chip was recently investigated [171]. The series resistance for $i = 2$ was found to be equal to $10 \cdot R_{\mathrm{H}}(2)$ within the experimental uncertainty of 14 nΩ/Ω.

Multiple connections can also be made between the terminals of a single device. Fang and Stiles [172] have shown that with appropriate connections two-terminal resistances which are multiples or fractions of R_{H} can be obtained. As in the case of the combination of several samples, the effects of the contacts and connections can be reduced if additional connections between unused terminals are made [170].

The technique of multiple series connections in a single device allows a reduction in the difference between the two-terminal resistance between the current contacts of a standard Hall bar device and the quantized Hall resistance to a negligible level. This is achieved [170] by connecting together several voltage contacts and the current contact at the same potential. In figure 25, a triple series connection scheme is illustrated. Applying the analysis procedure described above, it can be shown that in the quantum Hall regime, the resistance between the junction points A and B differs from the QHR by a term of the order $(r_c/r)^3$ where r_c is the resistance of the links. The main link connecting to the current terminal carries the major part of the device current I. The current I_2 is of the order $Ir_c/(2r)$ and I_3 is further reduced to order $I(r_c/(2r))^2$. The multiple series arrangement thus allows a reduction of the influence of link resistances to very small levels. This makes the scheme very useful if QHE devices are, for example, used as elements in ac bridges (see section 8.3).

The dc equivalent circuits with multiple series connections have been experimentally verified [170, 173]. The results demonstrate that the model calculations are correct within the relative experimental uncertainty of a few parts in 10^9.

6 Universality of the QHR

As was shown in the previous section, an incomplete quantization of a plateau due to high current through the device or due to increased temperature leads to a finite ρ_{xx}. A linear relationship exists between the deviation in the measured Hall

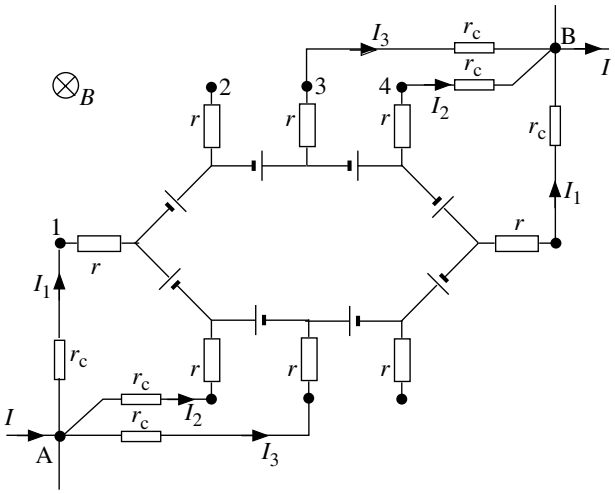

Figure 25: Equivalent circuit of a triple-series connection in an eight-terminal quantum Hall device. r_c is the resistance in the links (resistance of the connecting cable and the contact to the 2DEG). The two-terminal Hall resistance measured between A and B differs from the QHR by a term of the order $(r_c/r)^3$.

resistance from the expected value and ρ_{xx} (see section 5.1). Finite longitudinal voltages can also be measured as a result of non-ideal contacts. The question is whether the extrapolated value $R_{\mathrm{H}}\,(i, \rho_{xx} \to 0)$ is the same irrespective of the device geometry, material and fabrication process, the carrier mobility and density, the plateau number or other factors. Due to absence of quantitative theoretical models, this question has essentially been approached experimentally.

6.1 Device, material and step independence

Already in 1987 an experimental study [174] has shown that the QHRs observed in four different GaAs devices were in agreement at the level of 5×10^{-9}. The search for possible differences between the QHR realized in a GaAs heterostructure and a Si-MOSFET, respectively, was of special interest. In a direct comparison Hartland *et al*[175] found that the difference between the QHR in the two device types was smaller than 3.5 parts in 10^{10}. However, at about the same time several other groups [176, 177, 178] reported anomalous values of the QHR measured in a particular Si-MOSFET device. The authors claimed to see differences in R_{H} up to several parts in 10^7 despite the absence of any measured dissipation within the experimental resolution. Subsequently, a theoretical model [179] was presented which explains such deviations by the presence of short-range elastic scatterers located at the edges.

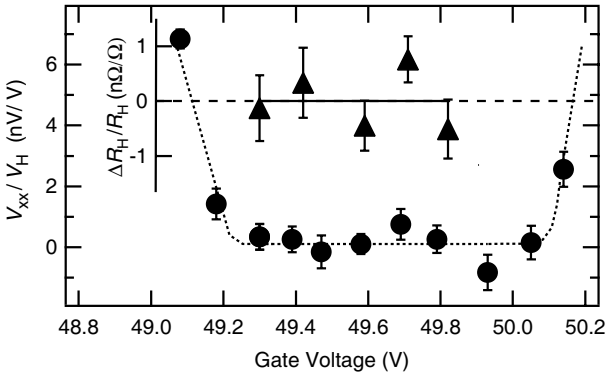

Figure 26: Variation of both the Hall resistance $R_{\rm H}(4)$ and the longitudinal voltage V_{xx} as a function of gate voltage for a Si-MOSFET measured at $T = 0.3$ K, $I = 30$ μA and $B = 13.8$ T [165].

More recently, a comprehensive study on the universality of the QHR was carried out by Jeckelmann *et al*[165]. The metrological characteristics of 7 different GaAs and 2 different kinds of MOSFET devices were determined. One of the MOSFET devices was the one which had shown the reported anomalies. The results can be summarized as follows:

An agreement between Si-MOSFET and GaAs was found at the level of the experimental uncertainty of 2.3 parts in 10^{10}. This result was realized with MOSFET devices grown and configured at Southampton University. They feature a 800-nm-thick gate oxide and consequently wide Hall plateaus as a function of gate voltage. A subset of the results is shown in figure 26.

The MOSFET devices with the reported anomalous results were made from Sony wafers. They operate at considerably smaller gate voltage and have a small critical current which makes precision measurements difficult. The main finding was that V_{xx} measured as a function of gate voltage was usually not flat along the plateau (see figure 27). In addition V_{xx} critically depended on the device side measured and on the pair of contacts chosen. It was possible to obtain $V_{xx} = 0$ on one side and at the same time non-zero values on the other side of the device. It is obvious that under such circumstances deviations in the Hall resistance from the expected values have to occur. By measuring the two longitudinal and two Hall voltages around a rectangle defined by two adjacent pairs of contacts it was clearly demonstrated that deviations of $R_{\rm H}$ always and only occur when V_{xx} for at least one of the sides of the rectangle is nonzero. The results of these measurements show the signature of effects caused by non-ideal contacts. This interpretation is also supported by the fact that the observed structure in V_{xx} and as a consequence the QHR deviations decrease with increasing temperature, as illustrated in figure 27.

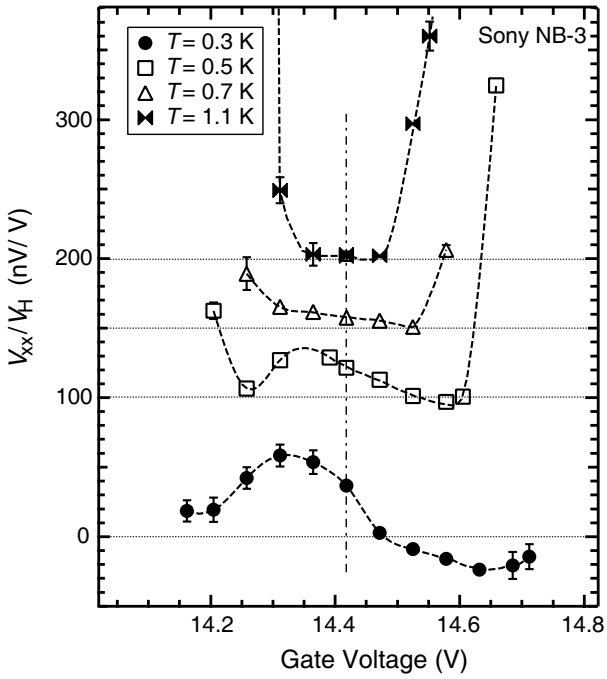

Figure 27: Temperature variation of V_{xx} vs gate voltage for a Sony MOSFET device on plateau $i = 4$. The curves are offset in y direction for clarity. The dotted lines indicate the respective zero positions [165].

In the same work [165], it was also shown that the extrapolated Hall resistance value R_{H} ($i = 2, 4, \rho_{xx} \to 0$) does not depend on the device mobility ($13\ \mathrm{T}^{-1} \leq \mu \leq 135\ \mathrm{T}^{-1}$) and the fabrication process (MBE or MOVCD) within 3 parts in 10^{10}.

As for the plateau number i, the results confirm that in GaAs devices no dependence on this quantum number can be seen:

$$\frac{\overline{i \cdot R_H\,(i)}}{2 \cdot R_H\,(2)} = 1 - (1.2 \pm 2.9) \cdot 10^{-10},\ i = 1, 3, 4, 6, 8. \tag{36}$$

6.2 Sample width dependence

Among the large number of theoretical papers, a few [36, 180, 181, 182, 183, 184] address the question of size effects in the QHE, including the question of the device width dependence of the quantized Hall resistance $R_{\mathrm{H}}(i)$, i being the plateau index. A majority of these papers [36, 180, 181, 182], based on different approaches to the problem, found that the relative variation of $R_{\mathrm{H}}(i)$ should scale like the inverse

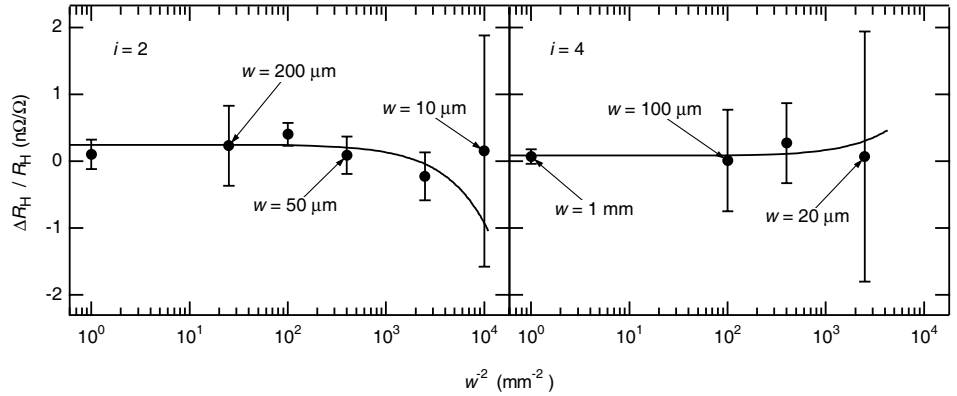

Figure 28: $\Delta R_H(i)/R_H(i)$ as a function of the inverse square of the device width w^{-2} for plateaus $i = 2$ and $i = 4$. The linear fits to the data (note the semi-log scaling) yield $\alpha_2 = (1.8 \pm 1.8)10^{-3}$ and $\alpha_4 = (0.70 \pm 5)10^{-3}$ for plateaus $i = 2$ and $i = 4$ respectively. See text for the definition of α.

square of the device width w, i.e.

$$\frac{\Delta R_{\mathrm{H}}(i)}{R_{\mathrm{H}}(i)} = \alpha \left(\frac{l}{w}\right)^2, \tag{37}$$

where $\Delta R_{\mathrm{H}}(i) = R_{\mathrm{H}}(i, w) - R_{\mathrm{H}}(i, w = \infty)$, l is the magnetic length and α is a parameter reflecting the strength of size effects. It is worth noting that none of the mentioned papers gives a numerical estimate of α. On the other hand, models leading to first order corrections in w^{-1} [183, 184] or an exponential correction $e^{(-w/l)}$ [40] as well as a model predicting no size effect [185] were also proposed.

Considering the difficulties to model a real sample, the problem whether the size effects really occur and can be described by the proposed theoretical models require an experimental approach. A few experimental papers marginally address the question of the width dependence of R_{H} [31, 186, 187]. In [31], a difference of (20 ± 15) nΩ/Ω is reported between a 10 μm and a 100 μm wide GaAs/AlGaAs sample. From [186], a measured difference of (-0.22 ± 3.5) nΩ/Ω between a 330 μm wide MOSFET and a 400 μm wide GaAs/AlGaAs sample allows a limit to be set on the first order corrections in w^{-1}, despite the small difference in width. A direct comparison [187] between a 150 μm wide and a 250 μm wide GaAs/AlGaAs heterostructure sets the upper limit for $\alpha \leq 0.13$.

More recently, a systematic study addressed the width dependence of the QHR in more detail [188]. In order to rule out any device specific effect, the samples involved in this experiment were patterned out of the same GaAs/AlGaAs heterostructure wafer. At a temperature of 4 K, the mobility μ and charge density n of the 2DEG are $\mu = 42$ T^{-1} and $n = 4.8 \times 10^{15}$m^{-2}. Each sample contains

four devices with a constriction of width w_c in the central part. The constriction's widths are $w_c = 100\ \mu\text{m}, 50\ \mu\text{m}, 20\ \mu\text{m}, 10\ \mu\text{m}$. These narrow samples were compared with a reference sample of width $w = 1$ mm using a cryogenic current comparator (see section 4.2).

Before and after any precision measurements, the longitudinal voltage V_{xx} was measured to check that dissipation was at an acceptable level (typically $\rho_{xx} < 100\ \mu\Omega$). The voltage was measured on both sides and along the full length of the sample. Measurements were made in both forward and reversed magnetic field, using several pairs of voltage contacts to measure the Hall voltage V_{H}.

The main results are summarized in figure 28, where $\Delta R_{\text{H}}(i)/R_{\text{H}}(i)$ is plotted as a function of the inverse square of the device width w^{-2} for plateau $i = 2$ and $i = 4$. The uncertainties on the single data point are well below 1 nΩ/Ω except for the narrowest devices, both on plateau $i = 2$ and $i = 4$. A linear fit to the data allows α to be calculated. On plateau $i = 2$ and $i = 4$, it was found $\alpha_2 = (1.8 \pm 1.8)10^{-3}$ and $\alpha_4 = (0.70 \pm 5)10^{-3}$ respectively. The small values obtained for α are not significant within their experimental uncertainties, showing that size effects are not observed. Moreover, the values of α would be even smaller if the current was not homogeneously distributed across the device width.

The fit of figure 28 and its related uncertainties allow to set an upper limit for the deviation that could be observed in a typical 500 μm-wide metrological sample due to size effects, under the assumption they really exist. It was found that $\Delta R_{\text{H}}(i)/R_{\text{H}}(i)$ would be smaller than 0.001 nΩ/Ω on plateau $i = 2$ and smaller than 0.003 nΩ/Ω on plateau $i = 4$. These values are three orders of magnitude below the resolution of the best cryogenic current comparators available today.

A similar analysis can be performed in the framework of a model where $\Delta R_{\text{H}}(i)/R_{\text{H}}(i)$ is assumed to be proportional to w^{-1} instead of w^{-2}. In this case the values obtained for the proportionality constant are also negligible within the experimental uncertainties, and the limits for the deviation observed in a typical 500 μm-wide metrological sample are smaller than 0.03 nΩ/Ω on plateau $i = 2$ and smaller than 0.06 nΩ/Ω on plateau $i = 4$. Although one order of magnitude larger than in the previous model, they are still well below the present measurement capabilities.

These results clearly show that possible size effects are totally negligible for the sample sizes presently used in metrology.

7 The QHE, fundamental constants and the SI

In the last section we have seen that there is convincing experimental evidence that $i \cdot R_{\text{H}}(i)$ observed in the fully quantized regime (vanishing longitudinal voltage) is a universal quantity. This is, however, not sufficient to prove that the relation $i \cdot R_{\text{H}}(i) = h/e^2$ is correct. There may still exist some unforeseeable corrections and, therefore, independent realizations of the von Klitzing constant $R_{\text{K}} \equiv h/e^2$ are required to establish the final proof.

7.1 Expressing the QHR in terms of the ohm

As we have shown, the QHE can be used to realize very reproducible resistance values which, to our knowledge, depend only on natural constants. To be used as a practical standard, the value of the QHR has to be known in SI units. In the SI, the electrical units are defined in terms of the SI mechanical base units metre, kilogram and second through the definition of the ampere and the assumption that electrical power and mechanical power are equivalent. The ampere is defined as the constant current which, if maintained in two straight parallel conductors of infinite length and negligible circular cross-section and placed one metre apart in vacuum, would produce a force of 2×10^{-7} newton per metre of length. This definition assigns the value of $4\pi 10^{-7}$ N/A^2 to the magnetic permeability of free space μ_0. To put the concept of the electrical units in the SI in practice, it is sufficient to realize two electrical units in terms of the m, kg and s. At present, the ohm and the watt are the two chosen units, since they are the most accurately determined.

The realization of the ohm is based on an electrostatics theorem discovered in 1956 by Thompson and Lampard [189]. If we assume an infinitely long conducting pipe of constant cross section in vacuum and divide it into four segments as shown in figure 29, the theorem states that the cross capacitance per unit length C_1' and C_2' between two opposite segments is given by

$$\exp\left(\frac{-\pi C_1'}{\varepsilon_0}\right) + \exp\left(\frac{-\pi C_2'}{\varepsilon_0}\right) = 1. \tag{38}$$

In a real experiment, the electrodes consist of four cylinders made as symmetrical as possible to make the two cross capacitances C_1' and C_2' agree as closely as possible. For $C_1' = C_2' = C'$ and $\varepsilon_0 = 1/\left(\mu_0 c^2\right)$, the expression simplifies to

$$C' = \frac{\ln(2)}{\mu_0 c^2 \pi} \simeq 1.95 \text{ pF/m}. \tag{39}$$

To eliminate the end effects in a practical set-up of finite dimensions, the change of capacitance ΔC due to change in the position of a movable, centrally inserted guard tube is measured (see figure 30). ΔC is on the order of 0.1 to 1 pF. It can be measured with a relative uncertainty of <10 nF/F. Using ac bridge techniques [190], the capacitance of the calculable capacitor is scaled to a value which can be compared to the resistance of an ac resistor using a quadrature bridge. After proper scaling, this ac resistor is compared to another AC resistor which has a small and calculable ac/dc difference. Dc techniques are finally applied to link the calculable resistor to the QHR.

Despite the long and complicated measurement chain, an accuracy of a few parts in 10^8 is reached using this method [191, 192, 193].

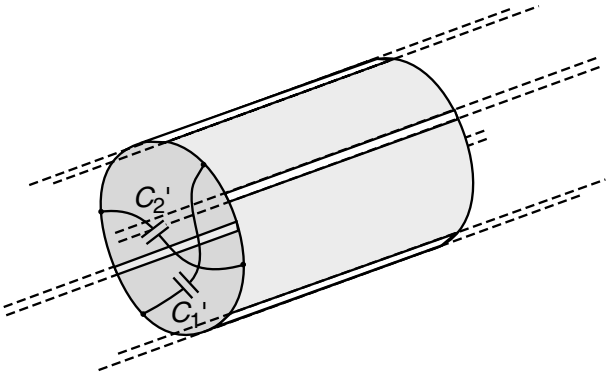

Figure 29: Illustration of the Thompson-Lampard theorem.

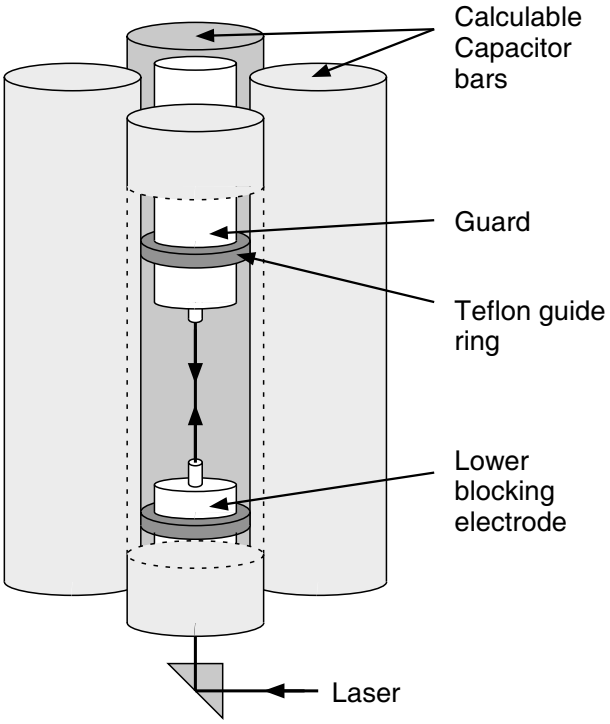

Figure 30: Arrangement of the four electrodes in a calculable capacitor. The displacement of the guard electrode is measured by a laser interferometer.

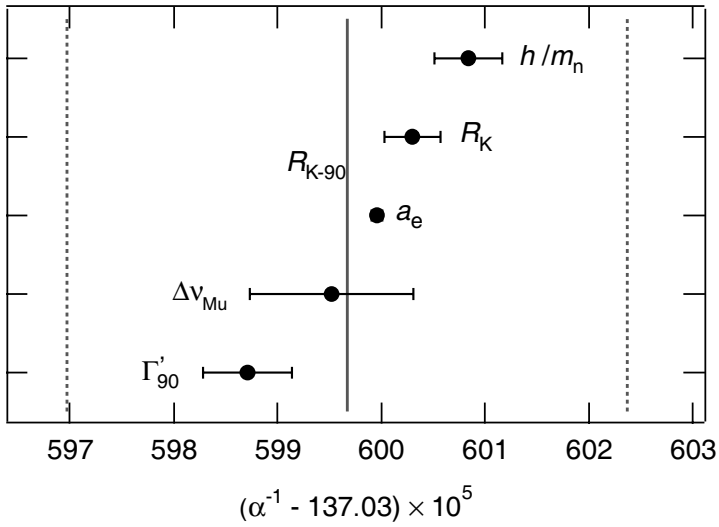

Figure 31: Values for the fine structure constant taken into account in the 1998 adjustment of fundamental constants [194]. The vertical lines indicate the value corresponding to $R_{\text{K-90}}$ and its uncertainty. Γ'_{90} is the value from the measurement of the gyromagnetic ratio of the shielded proton; $\Delta\nu_{\text{Mu}}$ is related to the muonium ground-state hyperfine splitting, a_e to the anomalous magnetic moment of the electron and h/m_n to the ratio of the Planck constant and the neutron mass.

7.2 The fine structure constant

The von Klitzing constant R_{K} is related with the fine structure constant through the simple relation

$$R_{\text{K}} \equiv \frac{h}{e^2} = \frac{\mu_0 c}{2\alpha}. \tag{40}$$

In the SI, the permeability of vacuum μ_0 and the speed of light c are fixed quantities with $\mu_0 = 4\pi \times 10^{-7}$ NA^{-2} and $c = 299\ 792\ 458$ m s^{-1}. The fine structure constant can thus be used to determine R_{K} and test possible corrections to the QHR. Conversely, if R_{K} is assumed to be identical to $i \cdot R_{\text{H}}(i)$, the QHE opens up an additional route to the determination of α which does not depend on QED calculations. In figure 31 all the results are shown which contributed to the least square adjustment of α, as given in the 1998 set of fundamental physical constants recommended by the CODATA task group [194].

At present, the most accurate value for α is derived from the anomalous magnetic moment a_e of the electron measured using single electrons or positrons stored in a Penning trap at 4.2 K and exposed to a magnetic flux [195]. A relative experimental uncertainty of 3.7×10^{-9} has been reached so far [194]. A value for the fine structure constant can be obtained from the experimental value of a_e

by comparing it to the theoretical value which can be, up to some insignificant correction terms due to electroweak and hadronic interactions, expressed in the framework of quantum electrodynamics as a power series in α. The most important terms in the series can be calculated analytically, but for some of the higher order terms extensive numerical calculations are necessary [196]. The uncertainty of the theoretical calculation of a_e is estimated to be 1 part in 10^9 [194].

The second most important result taken into account in the calculation of the actual value for α comes from the realization of R_{K} through the calculable capacitor assuming $R_{\mathrm{H}}(i = 1) = R_{\mathrm{K}}$. As the comparison shows, there is no disagreement between the R_{K} and the a_e derived value for α within the experimental uncertainty.

7.3 A conventional value for R_{K}

As we have seen in section 7.1, the best realization of the ohm in the SI is about two orders of magnitude less accurate than the reproducibility of the QHR. A similar situation is found in the case of the volt where the Josephson effect represents a voltage standard which is far more reproducible than the realization of the SI voltage unit. Two electrical units realized in terms of the non-electrical SI units metre, kilogram and second are needed to make the other electrical units measurable in the SI. With the QHE and the Josephson effect, two fundamentally stable standards are available and thus it was realized the world-wide consistency of electrical measurements could be improved by defining conventional values for R_{K} and for the Josephson frequency to voltage coefficient $K_{\mathrm{J}} \equiv 2e/h$. It was the task of the Comité Consultatif d'Électricité (CCE) to recommend such values based on the data available. All the values for R_{K} and K_{J} available by June 1988 in units of the SI were analyzed and the following conventional values were proposed [197]:

$$\begin{aligned} R_{\mathrm{K\text{-}90}} &= 25812.807\ \Omega \\ K_{\mathrm{J\text{-}90}} &= 483597.9\ \mathrm{GHz/V}. \end{aligned}$$

Relative uncertainties with respect to the SI of 2×10^{-7} and 4×10^{-7} respectively were assigned to the two values. The conventional values were accepted by all member states of the Metre Convention and came into effect as of January 1, 1990.

In the case of $R_{\mathrm{K\text{-}90}}$, the chosen value is essentially the mean of the most accurate direct measurements of R_{K} based on the calculable capacitor and the value from the calculation of the fine-structure constant based on the anomalous magnetic moment of the electron [197]. In the most recent least-square adjustment of fundamental constants carried out by the CODATA Task Group on Fundamental Constants [194], $R_{\mathrm{K}} = 25812.807572\ \Omega$ with a relative uncertainty of 3.7 parts in 10^9 was evaluated. This new value is in good agreement with the conventional value, $R_{\mathrm{K\text{-}90}}$. Figure 31 shows the results that were taken into account in the

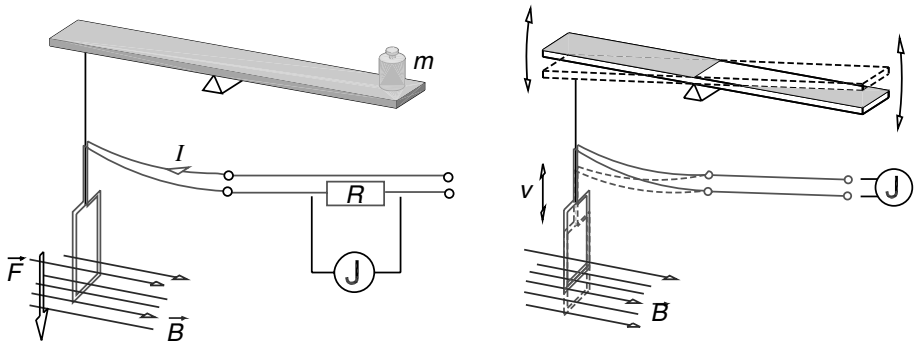

Figure 32: Principle of the moving coil watt balance

calculation of the new R_K value and consequently the new recommended value for α.

7.4 The possible role of R_K in the redefinition of the kg

With the definition of $R_{K\text{-}90}$ and $K_{J\text{-}90}$, the electrical units profit from the stability and reproducibility of the quantum standards based on the QHE and the Josephson effect. This situation is, nevertheless, unsatisfactory as the consistency of the SI system as a whole still depends on the difficult experiments which link mechanical and electrical units. In addition, the unit of mass, which is one of the base mechanical units, is the last remaining artefact in the SI. The kilogram is defined as the mass of the international prototype of the kilogram, made of platinum-iridium and kept at the Bureau International des Poids et Mesures (BIPM) under special conditions. One of the major disadvantages of this definition is the fact that the kilogram is subject to possible changes in time. As a consequence, the electrical units which all depend on the kilogram may drift also with time. Metrologists worldwide are trying hard to find a proper replacement of the kg which should be based on fundamental constants. Among the different experimental ideas pursued at present (see eg. [198]), the most promising approach seems to be the concept of the moving coil watt balance proposed by Kibble [199] from the National Physical Laboratory (NPL), UK, in 1976.

The experiment is performed in two parts (see figure 32). Consider a coil carrying a constant current I. The straight part with length l is immersed in a uniform magnetic flux density B perpendicular to l. The force on the conductor is balanced against the weight of test mass m and we have $F = m \cdot g = (B \cdot l) \cdot I$, where g is the local acceleration due to gravity. In the second part of the experiment, the coil is moved with constant velocity v in vertical direction through the flux and the voltage U induced across the coil is measured, being $U = (B \cdot l) \cdot v$ at the location of the weighing. The elimination of the product $(B \cdot l)$ from the two

expressions then leads to

$$U \cdot I = m \cdot g \cdot v. \tag{41}$$

The experiment thus allows the comparison of the watt realized electrically (left hand side of the equation) to the watt realized mechanically. If the electrical quantities are measured using the Josephson and quantum Hall effects, the test mass can be expressed in terms of the metre, the second and the Planck constant h:

$$m = \frac{h}{4}\frac{1}{g \cdot v} K_{\text{J-90}}^2 R_{\text{K-90}} \{U\}_{V90} \{I\}_{A90}, \tag{42}$$

where the notation $\{U\}_{V90}$ and $\{I\}_{A90}$ implies that the numerical values of these quantities are expressed in the units $R_{\text{K-90}}$ and $K_{\text{J-90}}$.

Experiments of this type are currently pursued at the NPL [200] in the UK, the National Institute of Standards and Technology(NIST) in the U.S.A. [201] and the Swiss Federal Office of Metrology and Accreditation (METAS) [202]. A relative accuracy of 2×10^{-7} in the determination of h was obtained in the first set-up at NPL [200]. Recently the NIST group has published a value with an uncertainty of 8.7×10^{-8}[203]. Presently, NPL and NIST, using an improved version of their experiment, and the METAS group, which has only started recently, are aiming at a relative uncertainty of 10^{-8}. Once such an accuracy level is reached by different independent experiments, serious consideration to redefining the unit of mass in the SI should be given. As the Planck constant plays a unique role among the fundamental constants, both as quantum of action and as a factor of proportionality in many equations, it would be a natural choice to fix the value of h and to link the kilogram to this value using experiments like the watt balance. To assure the continuity to the old SI, the conventionally fixed value of h would be the generally accepted experimental value at the time of the new definition. According to a proposition of Taylor [204], the new definition of the kg could be as follows: *"The kilogram is the mass of a body at rest whose equivalent energy equals the energy of a collection of photons whose frequencies sum to* 135639274×10^{42} Hz*."* The definition is based on the well-known Einstein relation $E = mc^2$ and the relation $E = h\nu$ valid for the energy of photons.

7.5 The use of the QHR as a standard of resistance

Since January 1, 1990, most major national metrology institutes are using the QHE to realize a representation of the SI-unit ohm on the basis of the conventional value $R_{\text{K-90}}$. As we have seen in previous sections of this paper, the value of R_{K} is independent of the experimental conditions as long as the QHE device is fully quantized. Temperature, current or contact effects may cause deviations from the correct value. Most important, however, test measurements can reveal whether the device is in a proper state or not. This means that the value of the QHR can be made as reproducible as today's measurement techniques allow without making reference to an external standard. These are the criteria a standard has to fulfil to be accepted as primary standard.

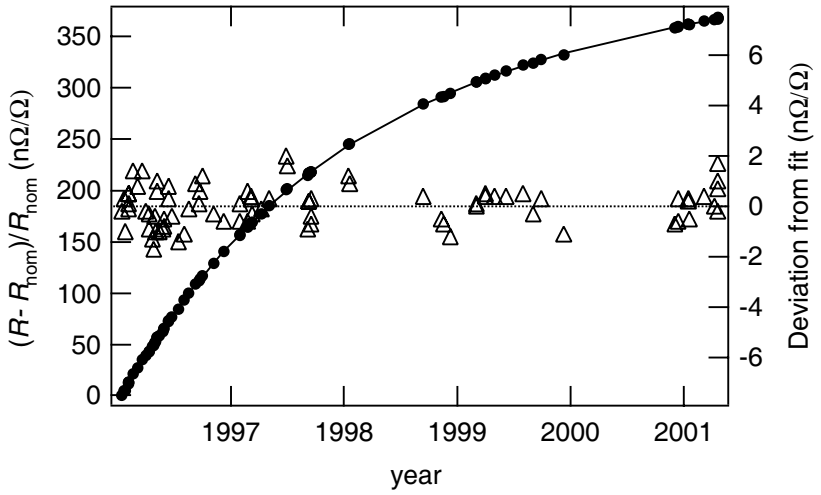

Figure 33: Tracking of a 100 Ω standard resistor measured in terms of $R_{\text{K-90}}$. The triangles (right scale) indicate the deviations of the measured data points to the fit function. Data taken at the Swiss Federal Office of Metrology and Accreditation (METAS).

To guarantee the accuracy and reproducibility of the QHR standard, the QHE device, the measurement system and the procedures have to meet an number of strict requirements. A group of experts under the auspices of the CCE has put together the "Technical Guidelines for Reliable Measurements of the Quantized Hall Resistance" [205] which, when correctly applied in practice, assure correct QHR measurements.

The resistance bridges of the type briefly introduced in section 4 are used to calibrate traditional room temperature resistance standards in terms of the QHR. As an example, figure 33 shows the measurements carried out at METAS to determine the drift behaviour of a temperature stabilized wire-wound 100 Ω resistor. The standard is kept under constant ambient conditions. As the results show, its resistance can be described with high accuracy by a smooth fitting function, which makes it usable as a transfer standard at the level of 1 nΩ/Ω.

To check the world-wide consistency of the QHR measurements at the highest accuracy level, the BIPM has started in 1993 to perform on-site comparisons of resistance ratio measurements using a transportable QHE standard and resistance bridge. The results of the bilateral comparisons (see e.g. [206]) are made public by the BIPM in a database which is accessible by internet (www.bipm.org). The comparison results obtained so far are shown in figure 34. The agreement between each laboratory and the BIPM for the $R_H(2)/100\ \Omega$ is on the order of one part in 10^9 which is well within the combined standard uncertainty of the comparisons.

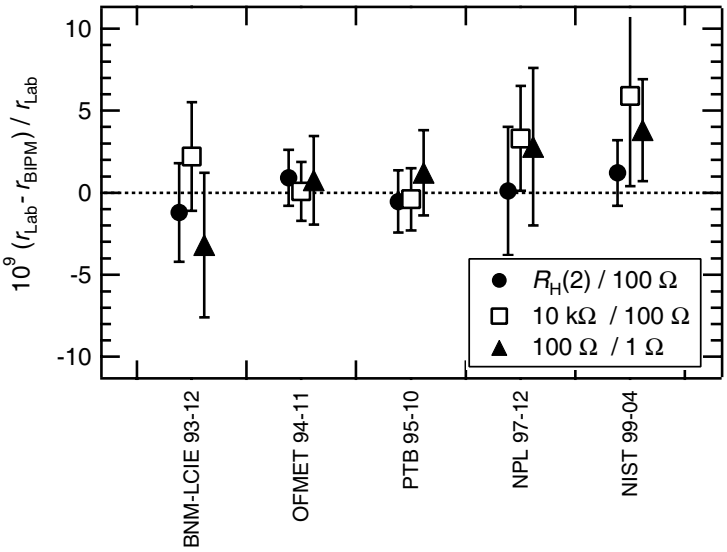

Figure 34: Results of on-site comparisons of three different resistance ratios using the BIPM transportable QHE system.

7.6 The metrological triangle

The trend in quantum metrology is to base the realization of the physical units on fundamental laws instead of physical artefacts. In the previous paragraphs, the situation for the ohm was illustrated. However, two additional quantum effects play an important role in metrology, namely the Josephson and the Single Electron Tunnelling (SET) effect.

The voltage measured across a Josephson junction irradiated by a microwave electromagnetic field of frequency f_J is

$$V_J = n\frac{h}{2e}f_J, \tag{43}$$

where n is the voltage step number. A review on voltage standards based on the Josephson effect can be found in [207, 208].

The single electron tunnelling effect was theoretically predicted in 1985 [209] and experimentally observed with appropriate interpretation in 1987 [210] (see [211, 212] for a review of SET physics). In an ultra small tunnel junction of capacitance C measured at low temperatures the charging energy $E_C = e^2/2C$ can be much larger than thermal fluctuations k_BT, leading to the observation of quantum phenomena. If such tiny tunnel junctions separate a conducting island from connecting electrodes (reservoirs), the electron number on the island can only change due to individual electrons tunnelling on or off the island, modifying the island potential by $\pm E_C$ and generating a discrete island energy spectrum. This effect,

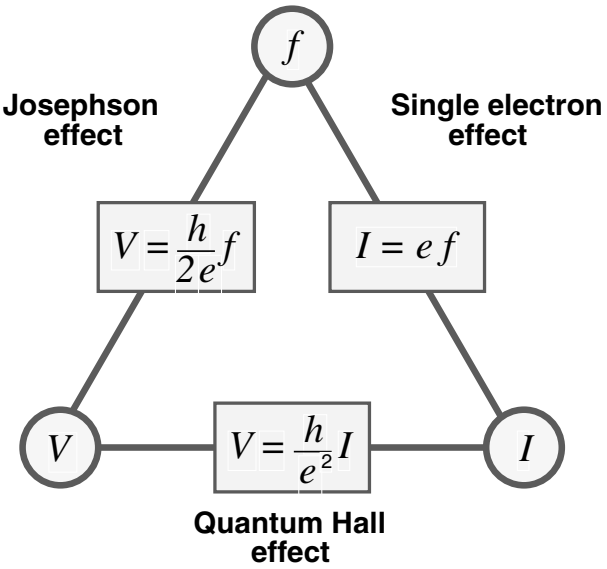

Figure 35: The metrological triangle relates the three quantum electrical effects via Ohm's law.

which prevents further electrons from tunnelling and therefore suppresses (blocks) current flow, can be compared to the classical picture of Coulomb repulsion of charge carriers and is called the 'Coulomb blockade'.

Owing to the remarkable feasibility of single electron manipulation in SET devices, an electrical current

$$I = qf \tag{44}$$

can be generated from an electron pump, where the charge q (integer multiple of the elementary charge e) is transferred through the device per cycle of an external rf drive of frequency f. The electron pump is investigated for metrological applications, with an experimentally demonstrated accuracy of 1.5×10^{-8} at a pumped current level on the order of a few pA [213].

The three quantum effects can be related by the so called metrological triangle [214] by means of Ohm's law depicted in figure 35. The closing of the metrological triangle is a very important experiment to check the consistency of the quantum electrical effects themselves.

In the practical experiment [215] shown in figure 36, an electron pump will provide a current $I = ef$, where f is the clock frequency of the pump. A quantum Hall resistance is placed in the current loop giving rise to the Hall voltage

$$V_{\mathrm{H}}(i) = \frac{R_{\mathrm{K}}}{i} \cdot ef. \tag{45}$$

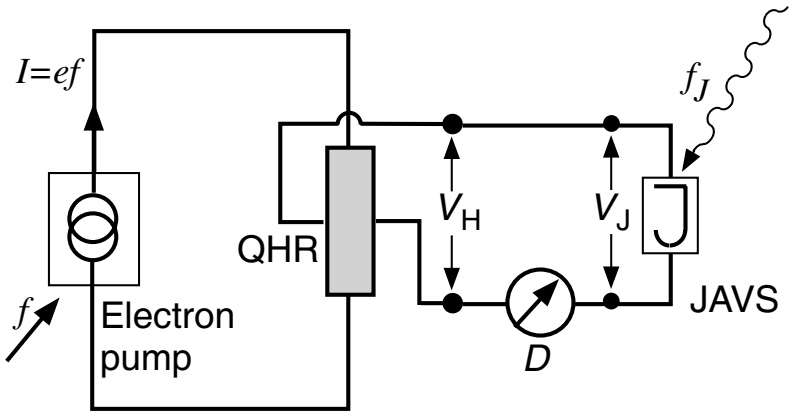

Figure 36: Experimental set-up for the verification of the metrological triangle

A Josephson voltage standard with a voltage V_{J} given by equation 43 is balanced against the Hall voltage using a null detector. The comparison of V_{H} and V_{J} gives:

$$eR_{\mathrm{K}}K_{\mathrm{J}} = in\frac{f_{\mathrm{J}}}{f}. \tag{46}$$

Since only a frequency ratio has to be measured, the frequencies do not have to be known in absolute units. In case I, R_{H} and/or V_{J} show deviations from their usual definitions, one has to introduce the following corrections: $I = ef(1+\delta_1)$, $R_{\mathrm{H}} = R_{\mathrm{K}}/i(1+\delta_2)$, $V_{\mathrm{J}} = (nf_{\mathrm{J}}/K_{\mathrm{J}})(1+\delta_3)$, and equation 46 reads now:

$$(1+\delta) = \frac{in}{2}\frac{f_{\mathrm{J}}}{f}, \tag{47}$$

where $\delta = \delta_1 + \delta_2 - \delta_3$ to the first order. Therefore, a measurement of δ provides a direct test of the consistency between the three quantum effects.

The major difficulty in the experimental realization of the metrological triangle is the very low current level of a few pA from the electron pump. In practice, the current may be amplified through a cryogenic current comparator first. Nevertheless, a further increase in the current by several orders of magnitude is needed to reach the target value for the resolution of the experiment [215].

For completeness, it should be mentioned that a different approach exists in order to close the metrological triangle [216]. Instead of being used as a current standard, the electron pump can charge a cryogenic capacitor, depositing a number N of electrons of charge e with a metrological accuracy. The voltage difference $\triangle V$ developed across the capacitor can be measured with a Josephson voltage standard. This measurement yields an absolute quantum determination of the capacitance $C = Ne/\triangle V$ with a potential relative uncertainty on the order of 10^{-8}. The cryogenic capacitor calibrated in this way can be compared with room temperature

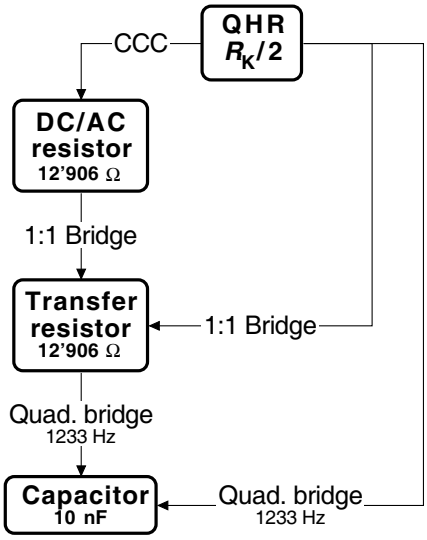

Figure 37: Schematic of the principle of the measurement chains that link the QHR to a capacitance standard. The left hand side describes the dc based method where the QHR is operated at dc, the ac/dc transfer being made using an ac/dc resistor. The right hand side shows two different methods where the QHR is used at audio frequencies. CCC stands for cryogenic current comparator.

capacitors, like the calculable capacitor. Up to now, the accuracy in the comparison of the cryogenic vacuum-gap capacitor to the laboratory capacitance standards was limited to a few parts in 10^6. However, this uncertainty will certainly be reduced by performing comparisons with high-accuracy ac bridges (see section 8.3).

8 ac Measurements of the QHR

Recently, the potential use of the QHR as an ac quantum standard has been recognized and preliminary investigations have been performed.

In low frequency electrical metrology, ac means frequencies up to 10 kHz, therefore this chapter will not review studies that describe experiments performed at higher frequencies, including the far infra red regime.

8.1 Calibration of capacitance standards based on the QHR

Since the early nineties, several national laboratories have made their representation of the farad traceable to the dc QHE. In this way, the capacitance calibrations benefit from the consistency brought in electrical metrology by the introduction

of $R_{\text{K-90}}$ and $K_{\text{J-90}}$. However, it is important to emphasize that for the absolute realization of the farad in the SI, the calculable capacitor is still required.

A measurement chain which links the QHR to a capacitance standard is depicted in the left path of figure 37. In a CCC bridge (see section 4.2), the QHR is used at dc to calibrate an ac/dc resistor with a small and well characterized ac/dc difference. Examples of such resistors are the coaxial resistor [217] or the quadrifilar resistor [218] for which the ac/dc difference can be calculated. Two ac/dc resistors are then used as secondary standards to calibrate the capacitance using a coaxial quadrature bridge. The balance condition of the bridge with $R = 12906\ \Omega$ and $C = 10$ nF imposes a measuring frequency of 1233 Hz. A different approach exists to link the capacitance standard to the QHR [219], as depicted in the right path of figure 37. In this case the QHR is operated as an ac resistance standard and directly compared with the ac/dc resistor with a coaxial 1:1 ratio bridge [220]. In a more direct approach, the QHR is directly compared to the capacitance standards. According to [219], the uncertainty obtained using the ac QHR is similar to the one from the dc method. However, the measuring time is strongly reduced by using the direct ac method making it potentially superior for calibration purpose. This measurement method relies on a good knowledge of the physics of the 2DEG at finite frequencies. This knowledge is far from being complete and will be briefly reviewed in the next section.

8.2 Characteristics of the QHR at kilohertz frequencies

The first ac measurements of the QHR took place shortly after the discovery of the QHE. In a Si-MOSFET, an increase of the measuring frequency was observed to enhance the formation of a plateau in the ρ_{xy} measurements [221]. This effect is not always observed and in some samples the frequency seems to prevent the formation of a plateau [222]. The accuracy of these early measurements was, however, limited to a few percent. On the theoretical side, a model based on the existence of semiclassical states treated in a percolation framework [223] leads to the result that the Hall conductivity should not show any deviation from its dc value, although the longitudinal conductivity should scale like $\sigma_{xx} = \omega^{-8/3} e^{(-\omega_0/\omega)}$, with ω_0 in the megahertz range. According to this model, which neglects electron-electron interactions and the influence of the temperature, the Hall resistance is less sensitive to the frequency effect than the longitudinal resistance. Later, a magnetocapacitance experiment [224] showed no frequency dependence in σ_{xx} in the range between 10 Hz and 20 kHz. This result was contradicted by a study on GaAs/AlGaAs heterostructures which showed a strong frequency dependence between 100 Hz and 20 kHz [225].

The picture emerging from the literature at the end of the eighties was far from being clear and precision measurements of the QHR were needed to understand its behaviour under ac transport conditions. The pioneering work of Melcher *et al*[226] showed that the QHR agrees with $R_{\text{K-90}}$ with an overall uncertainty of 3 $\mu\Omega/\Omega$ at 1592 Hz. This result initiated a series of experiments in several national

metrology institutes [227, 228, 229, 230, 231, 232, 233]. The main results of these precision measurements can be summarized as follows: The ac longitudinal measurements give controversial results. The minimum of R_{xx} is generally found to be around 0.3 to 0.5 mΩ, although some samples showed values up to 1 mΩ in the centre of plateau $i = 2$ at a frequency of 1 kHz. Most of the time, the range where R_{xx} keeps close to its minimum value is much narrower than that in the dc case. Experiments have been reported with no frequency [229], almost linear frequency [232] and quadratic frequency dependences [230] in the minimum of R_{xx}. Resistance plateaus have been observed in the Hall impedance for filling factor $i = 2$ and $i = 4$. The relative flatness of these plateaus is around 20 nΩ/Ω in the best cases [227, 233] and their width is much narrower then in the dc case (see figure 38 for an example). In addition, various structures appear at the edges of the plateaus which are frequency and current dependent. Such a behaviour is not yet understood.

The Hall resistance in the centre of the plateau is frequency dependent. In some cases [228], part of this dependence could be ascribed to the measurement bridge and the sample connection scheme. However, it seems that a residual linear frequency dependence on the order of 1 part in 10^7 per kilohertz comes from the sample itself [227, 233]. Lately, this linear frequency dependence could be linked to ac losses along the sample edges [234, 235]. A method was proposed to attenuate these losses by using a properly biased split back-gate. It is worth noticing that the split back-gate bias conditions, for selected devices, do not require the knowledge of the frequency behaviour of the device. A measurement of the current dependence of R_{H} at a single frequency is sufficient. Using this method, it was shown that the relative frequency dependence can be reduced to 2 parts in 10^8 per kilohertz. This improvement by one order of magnitude will certainly stimulate further work towards the application of the QHR as an ac resistance standard.

On the theoretical side, Christen *et al*[236] calculated the low-frequency admittance of a QHR using a pure edge states formalism (see section 2.5). The longitudinal Z_{xx} and Hall Z_{xy} impedances of a four terminal Hall bar can be written as

$$Z_{xx}(\omega, i) = \mathrm{j}\omega c_{\mu,13} R_{\mathrm{H}}(i)^2 \tag{48}$$

$$Z_{xy}(\omega, i) = R_{\mathrm{H}}(i) + \mathrm{j}\omega(c_{\mu,24} - c_{\mu,13}) R_{\mathrm{H}}(i)^2, \tag{49}$$

where $c_{\mu,kl}$ is the electrochemical capacitance between edge channels k and l which depends on the complex electrostatic potential distribution at the sample edges. This pure edge model predicts a linear frequency dependence for the longitudinal ac resistance as well as no intrinsic frequency dependence for the real component of the ac impedance. Such a behaviour has not yet being confirmed by experiments.

Finally, several studies analyzed the role of the sample edges in the ac behaviour of the 2DEG. A magnetocapacitance experiment [58] proved that the capacitance between a gate and the 2DEG in the quantum Hall regime scales with the device perimeter instead of the device surface, showing that the edge

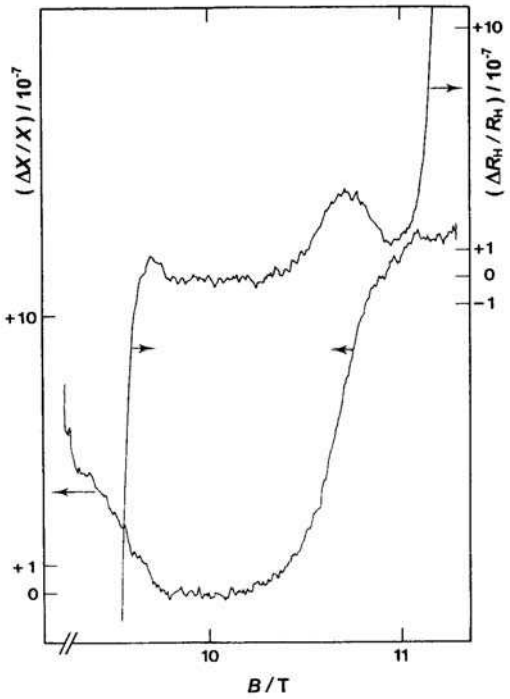

Figure 38: In-phase (R_{H}) and quadrature (X) components of the four terminal Hall impedance for the $i = 2$ plateau of a GaAs sample at 800 Hz measured with a current of 40 μA. R_{H} shows a narrow (0.3 T) flat plateau ($\Delta R_{\mathrm{H}}/R_{\mathrm{H}} \approx 2 \times 10^{-8}$) around $B = 10.1$ T (after [227]).

contribution dominates the capacitive response. In a different study [237], a fully inductive method allowed the internal capacitance of a Corbino ring to be measured in the QHE regime. A value of 1 pF/cm for a 1mm wide sample was found. This compares well with the time constant estimated from other ac measurements. In addition, a calculation [238] of the intrinsic capacitance of a Hall bar based on the current and potential distribution inside the sample gave a value for the capacitance which is two orders of magnitude smaller than the 1 pF/cm quoted above, providing further evidence of the leading role played by the edge states in the capacitance of quantum Hall devices.

8.3 Ac measurement techniques

This paragraph is not intended to cover all the coaxial bridge measurement techniques. The interested readers can find a very complete and comprehensible review

in [190]. Here we just want to emphasize a few points that are specifically related to the measurements of the QHR at low frequency.

The coaxial bridge technique requires that the impedances are defined as four terminal pair standards [239]. An important point in the measuring conditions is that no current should flow in the potential leads. This condition is easily realized in dc measurements of the QHR. In the ac case, however, the situation is more complicated. The QHR is usually located at the bottom of a cryostat and at a temperature close to 1 K. To keep the power dissipation at an acceptable level, the electrical connections are made by long resistive coaxial cables. Therefore, the series impedances and the shunt admittances of these cables cause current to flow in the potential leads inducing errors in the measurements. Another source of error is the inductive reactance produced by the bonding wires that connect the QHE device to its sample holder. As an example, a 3 mm long wire carrying a current of 40 μA in a field of 10 T vibrating with an rms amplitude of 0.13 μm corresponds to a series inductance of 100 μH [227]. A very elegant solution to these problems was introduced by Delahaye [170] with a multiple series connection scheme (see section 5.5).

One of the key elements of ac bridges is the current equalizer, commonly called a choke [190]. These chokes equalize the current flowing in the inner and outer (shield) part of the coaxial cable in any mesh of the measuring circuit making the whole bridge immune to any external perturbing electromagnetic field. The efficiency of the passive chokes usually used in ac bridges strongly depends on the resistance of the shield, which should be as small as possible. With this respect, the highly resistive coax cables used at cryogenic temperature are far from ideal. Therefore, to achieve the smallest possible measurement uncertainty, active chokes [240] have to be used.

9 Conclusion

In this review, we have summarized those aspects of the QHE which are of importance for the application of the effect as a resistance standard.

Many systematic studies have been carried out in the last two decades to assess the accuracy of the QHR. As we have shown, there is now overwhelming experimental evidence that the QHR is a universal quantity. It is independent of host material, device and plateau number at the level of a few parts in 10^{10} which is the resolution of today's measurement techniques. As a consequence, the QHR is used by all the major national metrology institutes as a dc standard for resistance. The reproducibility of this quantum standard is two orders of magnitude better than the absolute realization of the ohm in the SI. By fixing conventional values for the von Klitzing constant R_{K} and the Josephson constant K_{J}, the worldwide consistency of the electrical measurements has improved considerably during the last decade. The QHE together with the Josephson effect may also play an important role in the replacement of the last material artefact in the SI, the kilogram,

by a definition based on natural constants.

Experimental studies of the QHE with alternating current in the audio-frequency range are under way and first results show the importance of the current distribution in the device on the ac/dc difference of the Hall resistance. More theoretical and experimental work is still needed to understand and control the observed loss mechanism under ac conditions. The development of a primary ac resistance standard based on the QHE is of great importance in metrology. It will simplify the link between resistance and capacitance and, as a consequence, improve the measurement capabilities in the field of impedance measurements.

Despite the successful application of the QHE in metrology, our understanding of the effect is still incomplete. The many theoretical models explain various aspects of the QHE, at least in a qualitative way. A complete theory which conclusively explains e.g. the remarkable accuracy of the QHR is still missing. More work is also needed to understand the current distribution in Hall bar devices in the QHE regime and the relative importance of edge and bulk transport at high current. Further work should also be carried out to gain a better understanding of the processes which are responsible for the breakdown of the QHE.

Acknowledgment

The authors are grateful to Miha Furlan and Shinji Kawaji for the critical reading of the manuscript and for valuable discussions. They would also like to thank other groups for their kind permission to present figures and data.

References

[1] M. Cage, *The quantum Hall effect*, ch. Experimental aspects and metrological applications, pp. 37–67. Springer Verlag, 2nd edition, 1990.

[2] A. Hartland, "The quantum Hall effect and resistance standards," *Metrologia*, vol. 29, pp. 175–190, 1992.

[3] T. J. Witt, "Electrical resistance standards and the quantum Hall effect," *Rev. Sci. Instrum.*, vol. 69, no. 8, pp. 2823–2843, 1998.

[4] G. Landwehr, "The discovery of the quantum Hall effect," *Metrologia*, vol. 22, pp. 118–127, 1986.

[5] A. B. Fowler, F. F. Fang, W. E. Howard, and P. J. Stiles, "Magneto-oscillatory conductance in silicon surfaces," *Phys. Rev. Lett.*, vol. 16, no. 20, pp. 901–903, 1966.

[6] S. Kawaji, T. Igarashi, and J. Wakabayashi, "Quantum galvanometric effect in n-channel silicon inversion layers under strong magnetic fields," *Prog. Theor. Phys. Suppl.*, vol. 57, pp. 176–186, 1975.

[7] T. Englert and K. von Klitzing, "Analysis of ρ_{xx} minima in surface quantum oscillations on (100) n-type silicon inversion layers," *Surf. Sci.*, vol. 73, pp. 70–80, 1978.

[8] K. von Klitzing, G. Dorda, and M. Pepper, "New method for high-accuracy determination of the fine structure constant based on quantized Hall resistance," *Phys. Rev. Lett.*, vol. 45, no. 6, pp. 494–497, 1980.

[9] K. von Klitzing, "The quantized Hall effect," *Rev. Mod. Phys.*, vol. 58, no. 3, pp. 519–531, 1986.

[10] D. C. Tsui, H. L. Störmer, and A. C. Gossard, "Two-dimensional magnetotransport in the extreme quantum limit," *Phys. Rev. Lett.*, vol. 48, no. 22, pp. 1559–1562, 1982.

[11] H. L. Störmer, "Nobel lecture: the fractional quantum Hall effect," *Rev. Mod. Phys.*, vol. 71, no. 4, pp. 875–889, 1999.

[12] D. C. Tsui, "Nobel lecture: interplay of disorder and interaction in two-dimensional electron gas in intense magnetic fields," *Rev. Mod. Phys.*, vol. 71, no. 4, pp. 891–895, 1999.

[13] R. B. Laughlin, "Nobel lecture: fractional quantization," *Rev. Mod. Phys.*, vol. 71, no. 4, pp. 863–874, 1999.

[14] S. D. Sarma and A. Pinczuk, *Perspectives in quantum Hall effects.* John Wiley, Inc., 1997.

[15] R. E. Prange and S. M. Girvin, eds., *The Quantum Hall Effect, 2nd edition.* Springer-Verlag, New-York, 1990.

[16] H. Kamimura and H. Aoki, *The Physics of Interacting Electrons in Disordred Systems.* Oxford University Press, New York, 1989.

[17] M. Janssen, O. Viehweger, U. Fastenrath, and J. Hajdu, *Introduction to the Theory of the Integer Quantum Hall Effect.* VCH Verlagsgesellschaft, Weinheim, 1994.

[18] T. Chakraborty and P. Pietilainen, *The Quantum Hall Effect*, vol. 85. Springer-Verlag, New-York, 1995.

[19] T. Ando, A. B. Fowler, and F. Stern, "Electronic properties of two-dimensional systems," *Rev. Mod. Phys.*, vol. 54, no. 2, pp. 437–672, 1982.

[20] H. Aoki, "Quantised Hall effect," *Rep. Prog. Phys.*, vol. 50, pp. 655–730, 1987.

[21] D. R. Yennie, "Integral quantum Hall effect for nonspecialists," *Rev. Mod. Phys.*, vol. 59, no. 3, pp. 781–824, 1987.

[22] S. Kawaji, "Quantum transport in semiconductors surface and interface channels," *Surf. Sci.*, vol. 299/300, pp. 563–586, 1994.

[23] B. Huckestein, "Scaling theory of the integer quantum Hall effect," *Rev. Mod. Phys.*, vol. 67, no. 2, pp. 357–396, 1995.

[24] F. F. Fang and P. J. Stiles, "Effects of a tilted magnetic field on a two dimensional electron gas," *Phys. Rev.*, vol. 174, no. 3, pp. 823–828, 1968.

[25] J. F. Janak, "g factor of the two-dimensional interacting electron gas," *Phys. Rev.*, vol. 178, no. 3, pp. 1416–1418, 1969.

[26] T. Ando and Y. Uemura, "Theory of oscillatory g factor in an MOS inversion layer under strong magnetic fields," *J. Phys. Soc. Jpn.*, vol. 37, no. 4, pp. 1044–1052, 1974.

[27] T. Englert, D. C. Tsui, A. C. Gossard, and C. Uihlein, "g-factor enhancement in the 2d electron gas in GaAs/AlGaAs heterojunctions," *Surf. Sci.*, vol. 113, pp. 295–300, 1982.

[28] R. J. Nicholas, R. J. Haug, K. von Klitzing, and G. Weimann, "Exchange enhancement of the spin splitting in a GaAs-AlGaAs heterojunction," *Phys. Rev. B*, vol. 37, no. 3, pp. 1294–1303, 1988.

[29] E. H. Hall, "On a new action of the magnet on electric currents," *Am. J. Math.*, vol. 2, pp. 287–292, 1879.

[30] C. W. J. Beenakker and H. van Houten, *Solid State Physics, Ed. H. Ehrenreich and D. Turnbull*, vol. 44, ch. Quantum transport in semiconductor nanostructures, pp. 1–228. Academic Press, New York, 1991.

[31] W. van der Wel, E. G. Haanappel, J. E. Mooij, C. J. P. M. Harmans, J. P. André, G. Weimann, K. Ploog, C. T. Foxon, and J. J. Harris, "Selection criteria for AlGaAs-GaAs heterostructures in view of their use as a quantum Hall resistance standard," *J. Appl. Phys.*, vol. 65, no. 9, pp. 3487–3497, 1989.

[32] R. E. Prange, "Quantized Hall resistance and the measurement of the fine structure constant," *Phys. Rev. B*, vol. 23, no. 9, pp. 4802–4805, 1981.

[33] R. B. Laughlin, "Quantized Hall conductivity in two dimensions," *Phys. Rev. B*, vol. 23, no. 10, pp. 5632–5633, 1981.

[34] B. I. Halperin, "Quantized Hall conductance, current-carrying edge states, and the existence of extended states in a two-dimenisonal disordered potential," *Phys. Rev. B*, vol. 25, no. 4, pp. 2185–2190, 1982.

[35] P. Středa and L. Smrcka, "Thermodynamic derivation of the Hall current and the thermopower in quantising magnetic field," *J. Phys. C: Solid State Phys.*, vol. 16, pp. L895–L899, 1983.

[36] A. H. MacDonald and P. Středa, "Quantized Hall effect and edge currents," *Phys. Rev. B*, vol. 29, no. 4, pp. 1616–1619, 1984.

[37] O. Heinonen and P. L. Taylor, "Current distributions in the quantum Hall effect," *Phys. Rev. B*, vol. 32, no. 2, pp. 633–639, 1985.

[38] S. M. Apenko and Y. E. Lozovik, "The quantised Hall effect in strong magnetic fields," *J. Phys. C: Solid State Phys.*, vol. 18, pp. 1197–1203, 1985.

[39] B. E. Kane, D. C. Tsui, and G. Weimann, "Evidence for edge currents in the integral quantum Hall effect," *Phys. Rev. Lett.*, vol. 59, no. 12, pp. 1353–1356, 1987.

[40] Q. Niu and D. J. Thouless, "Quantum Hall effect with realistic boundary conditions," *Phys. Rev. B*, vol. 35, no. 5, pp. 2188–2197, 1987.

[41] R. Landauer, "Spatial variation of currents and fields due to localized scatterers in metallic conduction," *IBM J. Res. Dev.*, vol. 1, pp. 223–231, 1957.

[42] R. Landauer, "Electrical resistance of disordered one-dimensional lattices," *Philos. Mag.*, vol. 21, pp. 863–867, 1970.

[43] M. Büttiker, "Absence of backscattering in the quantum Hall effect in multiprobe conductors," *Phys. Rev. B*, vol. 38, no. 14, pp. 9375–9389, 1988.

[44] P. Středa, J. Kucera, and A. H. MacDonald, "Edge states, transmission matrices and the Hall resistances," *Phys. Rev. Lett.*, vol. 59, no. 17, pp. 1973–1975, 1987.

[45] J. K. Jain and S. A. Kivelson, "Quantum Hall effect in quasi one-dimensional systems: resistance fluctuations and breakdown," *Phys. Rev. Lett.*, vol. 60, no. 15, pp. 1542–1545, 1988.

[46] M. Büttiker, *Semiconductors and Semimetals*, vol. 35, ch. The quantum Hall effect in open conductors, pp. 191–277. Academic Press, San Diego, 1992.

[47] R. J. Haug, A. H. MacDonald, P. Středa, and K. von Klitzing, "Quantized multichannel magnetotransport through a barrier in two dimensions," *Phys. Rev. Lett.*, vol. 61, no. 24, pp. 2797–2800, 1988.

[48] S. Washburn, A. B. Fowler, H. Schmid, and D. Kern, "Quantized Hall effect in the presence of backscattering," *Phys. Rev. Lett.*, vol. 61, no. 24, pp. 2801–2804, 1988.

[49] B. J. van Wees, E. M. M. Willems, L. P. Kouwenhoven, C. J. P. M. Harmans, J. G. Williamson, C. T. Foxon, and J. J. Harris, "Suppression of Shubnikov-de-Haas resistance oscillations due to selective population or detection of Landau levels: absence of inter-Landau-level scattering on macroscopic length scales," *Phys. Rev. B*, vol. 39, no. 11, pp. 8066–8069, 1989.

[50] S. Komiyama, H. Hirai, S. Sasa, and S. Hiyamizu, "Violation of the integral quantum Hall effect: influence of backscattering and the role of voltage contacts," *Phys. Rev. B*, vol. 40, no. 18, pp. 12566–12569, 1989.

[51] B. W. Alphenaar, P. L. McEuen, R. G. Wheeler, and R. N. Sacks, "Selective equilibration among current-carrying states in the quantum Hall regime," *Phys. Rev. Lett.*, vol. 64, no. 6, pp. 677–680, 1990.

[52] P. L. McEuen, A. Szafer, C. A. Richter, B. W. Alphenaar, J. K. Jain, A. D. Stone, R. G. Wheeler, and R. N. Sacks, "New resistivity for high-mobility quantum Hall conductors," *Phys. Rev. Lett.*, vol. 64, no. 17, pp. 2062–2065, 1990.

[53] R. J. Haug, "Edge state transport and its experimental consequences in high magnetic fields," *Semicond. Sci. Techno.*, vol. 8, pp. 131–153, 1993.

[54] C. W. J. Beenakker, "Edge channels for the fractional qantum Hall effect," *Phys. Rev. Lett.*, vol. 64, no. 2, pp. 216–219, 1990.

[55] D. B. Chklovskii, B. I. Shklovskii, and L. I. Glazman, "Electrostatics of edge channels," *Phys. Rev. B*, vol. 46, no. 7, pp. 4026–4034, 1992.

[56] S. W. Hwang, D. C. Tsui, and M. Shayegan, "Experimental evidence for finite-width edge channels in the integer and fractional quantum Hall effect," *Phys. Rev. B*, vol. 48, no. 11, pp. 8161–8165, 1993.

[57] N. B. Zhitenev, R. J. Haug, K. von Klitzing, and K. Eberl, "Experimental determination of the dispersion of edge magnetoplasmons confined in edge channels," *Phys. Rev. B*, vol. 49, no. 11, pp. 7809–7812, 1994.

[58] S. Takaoka, K. Oto, H. Kurimoto, K. Murase, K. Gamo, and S. Nishi, "Magnetocapacitance and the edge state of a two-dimensional electron system in the quantum Hall regime," *Phys. Rev. Lett.*, vol. 72, no. 19, pp. 3080–3083, 1994.

[59] J. L. Vossen and W. Kern, eds., *Thin films processes II.* Academic Press, San Diego, 1991.

[60] S. M. Sze, *Physics of semiconductor devices (2nd edition).* John Wiley, New York, 1981.

[61] S. Wang, *Fundamentals of semiconductor theory and device physics.* Prentice-Hall, New Jersey, 1989.

[62] R. Dingle, H. L. Störmer, A. C. Gossard, and W. Wiegmann, "Electron mobilities in modulation-doped semiconductor heterojunction superlattices," *Appl. Phys. Lett.*, vol. 33, no. 7, pp. 665–667, 1978.

[63] D. Jucknischke, H. J. Bühlmann, R. Houdré, M. Ilegems, M. A. Py, B. Jeckelmann, and W. Schwitz, "Properties of alloyed AuGeNi-contacts on GaAs/AlGaAs heterostructures," *IEEE Trans. Instrum. Meas.*, vol. 40, no. 2, pp. 228–230, 1991.

[64] G. M. Reedtz and M. E. Cage, "An automatic potentiometric system for precision measurement of the quantized Hall resistance," *J. Res. Nat. Bur. Stand.*, vol. 92, pp. 303–310, 1987.

[65] B. Jeckelmann, W. Schwitz, H. J. Bühlmann, R. Houdré, M. Ilegems, D. Jucknischke, and M. A. Py, "Comparison of the quantized Hall resistance in different GaAs/AlGaAs heterostructures," *IEEE Trans. Instrum. Meas.*, vol. 40, no. 2, pp. 231–233, 1991.

[66] G. W. Small, "Comparison of quantized Hall resistance with 1-ohm standard," *IEEE Trans. Instrum. Meas.*, vol. 32, pp. 446–447, 1983.

[67] C. A. Hamilton, C. J. Burroughs, and K. Chieh, "Operation of NIST Josephson array voltage standard," *J. Res. Nat. Inst. Stand. Technol.*, vol. 95, no. 3, pp. 219–235, 1990.

[68] T. Endo, Y. Murayama, M. Koyanagi, J. Kinoshita, K. Inagaki, C. Yamanouchi, and K. Yoshihiro, "Measurement system for quantum Hall effect utilizing a Josephson potentiometer," *IEEE Trans. Instrum. Meas.*, vol. 34, no. 2, pp. 323–327, 1985.

[69] P. Warnecke, J. Niemeyer, F. W. Dünschede, L. Grimm, G. Weimann, and W. Schlapp, "High-precision resistance ratio measurements by means of a novel Josephson potentiometer," *IEEE Trans. Instrum. Meas.*, vol. 36, no. 2, pp. 249–251, 1987.

[70] N. L. Kusters, W. J. M. Moore, and P. N. Miljanic, "A current comparator for precision measurements of dc ratios," *IEEE Trans. Commun. Electron.*, vol. 83, pp. 22–27, 1964.

[71] M. P. MacMartin and N. L. Kusters, "A direct-current comparator ratio bridge for four-terminal resistance measurements," *IEEE Trans. Instrum. Meas.*, vol. 15, no. 4, pp. 212–220, 1966.

[72] A. D. Inglis, "A cheaper, simpler quantized Hall resistance standard," *IEEE Trans. Instrum. Meas.*, vol. 48, pp. 289–292, 1999.

[73] I. K. Harvey, "Precise low temperature dc ratio transformer," *Rev. Sci. Instrum.*, vol. 43, pp. 1626–1629, 1972.

[74] D. B. Sullivan and R. F. Dziuba, "Low temperature direct current comparators," *Rev. Sci. Instrum.*, vol. 45, no. 4, pp. 517–519, 1974.

[75] K. Grohmann, H. D. Hahlbohm, H. Lübbig, and H. Ramin, "Construction principles and properties of ironless dc and ac current comparators with superconducting shields," *PTB Mitteilungen*, vol. 5, pp. 313–318, 1973.

[76] H. Seppa, "The ratio error of the overlapped-tube cryogenic current comparator," *IEEE Trans. Instrum. Meas.*, vol. 39, no. 5, pp. 689–697, 1990.

[77] K. Grohmann, H. D. Hahlbohm, and D. Hechtfischer, "The cryo current comparator as a calculable dc ratio standard," *IEEE Trans. Instrum. Meas.*, vol. 28, pp. 205–211, 1979.

[78] P. Gutmann and V. Kose, "Optimum dc current resolution of a ferromagnetic-core flux transformer coupled SQUID instrument," *IEEE Trans. Instrum. Meas.*, vol. 36, pp. 267–270, 1987.

[79] J. Sesé, A. Camon, C. Rillo, and G. Rietveld, "Ultimate current resolution of a cryogenic current comparator," *IEEE Trans. Instrum. Meas.*, vol. 48, pp. –306, 1999.

[80] S. Q. Xue, P. Gutmann, and V. Kose, "Optimum dc current resolution for high-source resistances with a dc transformer matched rf SQUID," *Rev. Sci. Instrum.*, vol. 52, no. 12, pp. 1901–1902, 1981.

[81] J. M. Williams and A. Hartland, "An automated cryogenic current comparator resistance ratio bridge," *IEEE Trans. Instrum. Meas.*, vol. 40, no. 2, pp. 267–270, 1991.

[82] F. Delahaye and D. Bournaud, "Low-noise measurements of the quantized Hall resistance using an improved cryogenic current comparator bridge," *IEEE Trans. Instrum. Meas.*, vol. 40, no. 2, pp. 237–240, 1991.

[83] R. F. Dziuba and R. E. Elmquist, "Improvements in resistance scaling at NIST using cryogenic current comparators," *IEEE Trans. Instrum. Meas.*, vol. 42, no. 2, pp. 126–130, 1993.

[84] B. Jeckelmann, W. Fasel, and B. Jeanneret, "Improvements in the realisation of the quantized Hall resistance standard at OFMET," *IEEE Trans. Instrum. Meas.*, vol. 44, no. 2, pp. 265–268, 1995.

[85] F. Delahaye, "An ac-bridge for low-frequency measurements of the quantized Hall resistance," *IEEE Trans. Instrum. Meas.*, vol. 40, no. 6, pp. 883–888, 1991.

[86] H. Seppa and A. Satrapinski, "Ac resistance bridge based on the cryogenic current comparator," *IEEE Trans. Instrum. Meas.*, vol. 46, no. 2, pp. 463–466, 1997.

[87] M. E. Cage, B. F. Field, R. F. Dziuba, S. M. Girvin, A. C. Gossard, and D. C. Tsui, "Temperature dependence of the quantum Hall resistance," *Phys. Rev. B*, vol. 30, no. 4, pp. 2286–2288, 1984.

[88] D. C. Tsui, H. L. Störmer, and A. C. Gossard, "Zero-resistance state of two-dimensional electrons in a quantizing magnetic field," *Phys. Rev. B*, vol. 25, no. 2, pp. 1405–1407, 1982.

[89] T. Haavasoja, H. L. Störmer, D. J. Bishop, V. Narayanamurti, A. C. Gossard, and W. Wiegmann, "Magnetization measurements on a two-dimensional electron system," *Surf. Sci.*, vol. 142, pp. 294–297, 1984.

[90] D. H. Lee, S. Kivelson, and S. C. Zhang, "Quasiparticle charge and the activated conductance of a quantum Hall liquid," *Phys. Rev. Lett.*, vol. 68, no. 15, pp. 2386–2389, 1992.

[91] D. G. Polyakov and B. I. Shklovskii, "Activated conductivity in the quantum Hall effect," *Phys. Rev. Lett.*, vol. 73, no. 8, pp. 1150–1153, 1994.

[92] O. G. Balev and P. Vasilopoulos, "Drastic suppression of scattering and activated behavior in mesoscopic quantum Hall systems with smooth confinement," *Phys. Rev. B*, vol. 50, no. 12, pp. 8727–8735, 1994.

[93] M. M. Fogler, D. G. Polyakov, and B. I. Shklovskii, "Activated conductivity in the quantum Hall effect," *Surf. Sci.*, vol. 361, pp. 255–260, 1996.

[94] S. S. Mandal and V. Ravishankar, "Activated resistivities in the integer quantum Hall effect," *Phys. Rev. B*, vol. 55, no. 23, pp. 15748–15756, 1997.

[95] H. P. Wei, A. M. Chang, D. C. Tsui, and M. Razeghi, "Temperature dependence of the quantized Hall effect," *Phys. Rev. B*, vol. 32, no. 10, pp. 7016–7019, 1985.

[96] G. S. Böbinger, A. M. Chang, H. L. Störmer, and D. Tsui, "Magnetic field dependence of activation energies in the fractional quantum Hall effect," *Phys. Rev. Lett.*, vol. 55, no. 15, pp. 1606–1609, 1985.

[97] R. G. Clark, J. R. Mallett, S. R. Haynes, J. J. Harris, and C. T. Foxon, "Experimental determination of fractional charge e/q for quasiparticle excitations in the fractional quantum Hall effect," *Phys. Rev. Lett.*, vol. 60, no. 17, pp. 1747–1750, 1988.

[98] R. G. Clark, "Ground state of interacting electrons in the extreme quantum limit," *Phys. Scr.*, vol. T39, pp. 45–90, 1991.

[99] S. D. Sarma and D. Liu, "Scaling behavior of the activated conductivity in a quantum Hall liquid," *Phys. Rev. B*, vol. 48, no. 12, pp. 9166–9169, 1993.

[100] Y. Katayama, D. C. Tsui, and M. Shayegan, "Experimental study of rho-xx(t) for quasiparticle charge determination in the fractional quantum Hall effect," *Phys. Rev. B*, vol. 49, no. 11, pp. 7400–7407, 1994.

[101] S. I. Dorozhkin, M. O. Dorokhova, R. J. Haug, K. von Klitzing, and K. Ploog, "Thermally activated dissipative conductivity in the fractional quantum Hall effect," *JETP Lett.*, vol. 63, no. 1, pp. 76–82, 1996.

[102] M. Furlan, "Activated conductivities and nonuniversal behaviour in large high mobility Hall bars," *Physica B*, vol. 249, pp. 123–127, 1998.

[103] M. Furlan, "Electronic transport and the localization length in the quantum Hall effect," *Phys. Rev. B*, vol. 57, no. 23, pp. 14818–14828, 1998.

[104] D. G. Polyakov and B. I. Shklovskii, "Universal prefactor of activated conductivitiy in the quantum Hall effect," *Phys. Rev. Lett.*, vol. 74, no. 1, pp. 150–153, 1995.

[105] K. Yoshihiro, J. Kinoshita, K. Inagaki, C. Yamanouchi, J. Moriyama, and S. Kawaji, "Quantized Hall and transverse resistivities in silicon MOS n-inversion layers," *Physica B*, vol. 117, pp. 706–708, 1983.

[106] M. D'Iorio and B. M. Wood, "Temperature dependence of the quantum Hall resistance," *Surf. Sci.*, vol. 170, pp. 233–237, 1986.

[107] W. van der Wel, C. J. P. M. Harmans, and J. E. Mooij, "High-precision measurements of the temperature and current dependence of the quantized Hall resistance," *Surf. Sci.*, vol. 170, pp. 226–232, 1986.

[108] B. Tausendfreund and K. von Klitzing, "Analysis of the quantized Hall resistance at finite temperatures," *Surf. Sci.*, vol. 142, pp. 220–224, 1984.

[109] I. Ruzin and S. Feng, "Universal relation between longitudinal and transverse conductivities in the quantum Hall effect," *Phys. Rev. Lett.*, vol. 74, no. 1, pp. 154–157, 1995.

[110] W. van der Wel, C. J. P. M. Harmans, and J. E. Mooij, "A geometric explanation of the temperature dependence of the quantised Hall resistance," *J. Phys. C*, vol. 21, pp. L171–L175, 1988.

[111] B. I. Shklovskii and A. L. Efros, *Electronic properties of doped semiconductors.* Springer Verlag, Berlin, 1984.

[112] N. F. Mott, "Conduction in glasses containing transition metal ions," *J. Non-Cryst. Solids*, vol. 1, pp. 1–17, 1968.

[113] A. L. Efros and B. I. Shklovskii, "Coulomb gap and low temperature conductivity of disordered systems," *J. Phys. C*, vol. 8, pp. L49–L51, 1975.

[114] Y. Ono, "Localization of electrons under strong magnetic fields in a two-dimensional system," *J. Phys. Soc. Jpn.*, vol. 51, no. 1, pp. 237–243, 1982.

[115] K. I. Wysokinski and W. Brenig, "Absence of variable range hopping Hall conduction?," *Z. Phys. B*, vol. 54, pp. 11–15, 1983.

[116] A. Grunwald and J. Hajdu, "Some remarks on variable range hopping - in particular in the quantum Hall regime," *Z. Phys. B*, vol. 78, pp. 17–20, 1990.

[117] D. G. Polyakov and B. I. Shklovskii, "Conductivity peak broadening in the quantum Hall regime," *Phys. Rev. B*, vol. 48, no. 15, pp. 11167–11175, 1993.

[118] G. Ebert, K. von Klitzing, C. Probst, E. Schuberth, K. Ploog, and G. Weimann, "Hopping conduction on the Landau level tails in GaAs-AlGaAs heterostructures at low temperatures," *Soild State Commun.*, vol. 45, pp. 625–628, 1983.

[119] A. Briggs, Y. Guldner, J. P. Vieren, M. Voos, J. P. Hirtz, and M. Razeghi, "Low-temperature investigations of the quantum Hall effect in InGaAs-InP heterojunctions," *Phys. Rev. B*, vol. 27, no. 10, pp. 6549–6552, 1983.

[120] S. Koch, R. J. Haug, and K. von Klitzing K. Ploog, "Variable range hopping transport in the tails of the conductivity peaks between quantum Hall plateaus," *Semicond. Sci. Techno.*, vol. 10, pp. 209–212, 1995.

[121] F. W. van Keuls, X. L. Hu, H. W. Jiang, and A. J. Dahm, "Screening of the Coulomb interaction in two-dimensional variable-range hopping," *Phys. Rev. B*, vol. 56, no. 3, pp. 1161–1169, 1997.

[122] P. Svoboda, G. Nachtwei, C. Breitlow, S. Heide, and M. Cukr, "Electron conduction within Landau-level tails of medium-mobility GaAs/AlGaAs heterostructures," *Semicond. Sci. Techno.*, vol. 12, pp. 264–271, 1997.

[123] H. P. Wei, L. W. Engel, and D. C. Tsui, "Current scaling in the integer quantum Hall effect," *Phys. Rev. B*, vol. 50, no. 19, pp. 14609–14612, 1994.

[124] H. Scherer, L. Schweitzer, F. Ahlers, L. Bliek, and W. Schlapp, "Current scaling and electron heating between integer quantum Hall plateaus in GaAs/AlGaAs heterostructures," *Semicond. Sci. Technol.*, vol. 10, pp. 959–964, 1995.

[125] U. Klass, W. Dietsche, K. von Klitzing, and K. Ploog, "Imaging of the dissipation in quantum-Hall-effect experiments," *Z. Phys. B*, vol. 82, pp. 351–354, 1991.

[126] B. Jeanneret, B. D. Hall, H. J. Bühlmann, R. Houdré, M. Illegems, B. Jeckelmann, and U. Feller, "Observation of the integer quantum Hall effect by magnetic coupling to a Corbino ring," *Phys. Rev. B*, vol. 51, no. 15, pp. 9752–9756, 1995.

[127] P. C. van Son and T. M. Klapwijk, "Current contacts and current distribution in the quantum Hall effect," *Europhys. Lett.*, vol. 12, no. 5, pp. 429–434, 1990.

[128] P. C. van Son, F. W. de Vries, and T. M. Klapwijk, "Nonequilibrium distribution of edge and bulk current in a quantum Hall conductor," *Phys. Rev. B*, vol. 43, no. 8, pp. 6764–6767, 1991.

[129] D. Pfannkuche and J. Hajdu, "Potential and current distribution in an ideal Hall bar," *Phys. Rev. B*, vol. 46, no. 11, pp. 7032–7036, 1992.

[130] C. Wexler and D. J. Thouless, "Current density in a quantum Hall bar," *Phys. Rev. B*, vol. 49, no. 7, pp. 4815–4820, 1994.

[131] H. Hirai and S. Komiyama, "Local current distribution in the presence of nonequilibrium distribution of edge states," *Jpn. J. Appl. Phys.*, vol. 34, pp. 4321–4324, 1995.

[132] T. Ando, "Voltage distribution and phase-breaking scattering in the quantum Hall regime," *Surf. Sci.*, vol. 361/362, pp. 270–273, 1996.

[133] K. Tsemekhman, V. Tsemekhman, C. Wexler, and D. J. Thouless, "Quantum Hall effect: current distribution and the role of measurement," *Solid State Commun.*, vol. 101, no. 8, pp. 549–553, 1997.

[134] K. Shizuya, "Numerical study of current distribution in finite planar samples with disorder," *Phys. Rev. B*, vol. 59, no. 3, pp. 2142–2150, 1999.

[135] H. Z. Zheng, D. C. Tsui, and A. M. Chang, "Distribution of the quantized Hall potential in GaAs-AlGaAs heterostructures," *Phys. Rev. B*, vol. 32, no. 8, pp. 5506–5509, 1985.

[136] G. Ebert, K. von Klitzing, and G. Weimann, "Hall potential distribution in quantum Hall experiments," *J. Phys. C: Solid State Phys.*, vol. 18, pp. L257–L260, 1985.

[137] E. K. Sichel, H. H. Sample, and J. P. Salerno, "Equipotential distribution in the quantum Hall effect," *Phys. Rev. B*, vol. 32, no. 10, pp. 6975–6977, 1985.

[138] P. F. Fontein, P. Hendriks, F. A. P. Blom, J. H. Wolter, and L. J. Giling, "Spatial potential distribution in GaAs/AlGaAs heterostructures under quantum Hall conditions studied with the linear electro-optic effect," *Surf. Sci.*, vol. 263, pp. 91–96, 1992.

[139] R. Knott, W. Dietsche, K. von Klitzing, K. Eberl, and K. Ploog, "Electro-optic imaging of potential distributions in the quantum Hall regime," *Semicond. Sci. Techno.*, vol. 10, pp. 117–126, 1995.

[140] W. Dietsche, K. von Klitzing, and K. Ploog, "Potential drops across quantum Hall effect samples - in the bulk or near the edges?," *Surf. Sci.*, vol. 361/362, pp. 289–292, 1996.

[141] E. Yahel, A. Tsukernik, A. Palevski, and H. Shtrikman, "Evidence for bulk current in Hall bar samples and potential screening in the integer Hall effect," *Phys. Rev. Lett.*, vol. 81, no. 23, pp. 5201–5204, 1998.

[142] K. L. McCormick, M. T. Woodside, M. Huang, M. Wu, and P. L. McEuen, "Scanned potential microscopy of edge and bulk currents in the quantum Hall regime," *Phys. Rev. B*, vol. 59, no. 7, pp. 4654–4657, 1999.

[143] Y. Y. Wei, J. Weis, K. von Klitzing, and K. Eberl, "Edge strips in the quantum Hall regime imaged by a single-electron transistor," *Phys. Rev. Lett.*, vol. 81, no. 8, pp. 1674–1677, 1998.

[144] A. Yacoby, H. F. Hess, T. A. Fulton, L. N. Pfeiffer, and K. W. West, "Electrical imaging of the quantum Hall state," *Solid State Commun.*, vol. 111, pp. 1–13, 1999.

[145] B. Jeckelmann, A. Rüfenacht, B. Jeanneret, F. Overney, A. von Campenhausen, and G. Hein, "Optimization of QHE-devices for metrological applications," *IEEE Trans. Instrum. Meas.*, vol. 50, no. 2, pp. 218–222, 2001.

[146] G. Nachtwei, "Breakdown of the quantum Hall effect," *Physica E*, vol. 4, pp. 79–101, 1999.

[147] G. Ebert, K. von Klitzing, K. Ploog, and G. Weimann, "Two dimensional magneto-quantum transport on GaAs-AlGaAs heterostructures under non-ohmic conditions," *J. Phys. C: Solid State Phys.*, vol. 16, pp. 5441–5448, 1983.

[148] M. E. Cage, R. F. Dziuba, B. F. Field, E. R. Williams, S. M. Girvin, A. C. Gossard, D. C. Tsui, and R. J. Wagner, "Dissipation and dynamical nonlinear behavior in the quantum Hall regime," *Phys. Rev. Lett.*, vol. 51, no. 15, pp. 1374–1377, 1983.

[149] S. Komiyama, T. Takamasu, S. Hiyamizu, and S. Sasa, "Breakdown of the quantum Hall effect due to electron heating," *Soild State Commun.*, vol. 54, no. 6, pp. 479–484, 1985.

[150] F. Kuchar, G. Bauer, G. Weimann, and H. Burkhard, "Non-equilibrium behaviour of the two-dimensional electron gas in the quantized Hall resistance regime of GaAs/AlGaAs," *Surf. Sci.*, vol. 142, pp. 196–202, 1984.

[151] L. Bliek, E. Braun, G. Hein, V. Kose, J. Niemeyer, G. Weimann, and W. Schlapp, "Critical current density for the dissipationless quantum Hall effect," *Semicond. Sci. Technol.*, vol. 1, pp. 110–112, 1986.

[152] S. Kawaji, "Breakdown of the integer quantum Hall effect at high currents in GaAs/AlGaAs heterostructures," *Semicond. Sci. Technol.*, vol. 11, pp. 1546–1551, 1996.

[153] A. Boisen, P. Bøggild, A. Kristensen, and P. E. Lindelof, "Nonlinear current-voltage characteristics at quantum Hall resistance minima," *Phys. Rev. B*, vol. 50, no. 3, pp. 1957–1960, 1994.

[154] N. Q. Balaban, U. Meirav, and H. Shtrikman, "Crossover between different regimes of current distribution in the quantum Hall effect," *Phys. Rev. B*, vol. 52, no. 8, pp. R5503–R5506, 1995.

[155] Y. Kawano and S. Komiyama, "Breakdown of the quantized Hall effect in the vicinity of current contacts," *Phys. Rev. B*, vol. 61, no. 4, pp. 2931–2938, 2000.

[156] P. Středa and K. von Klitzing, "Critical non-dissipative current of the quantum Hall regime," *J. Phys. C: Solid State Phys.*, vol. 17, pp. L483–L486, 1984.

[157] L. Eaves and F. W. Sheard, "Size-dependent quantised breakdown of the dissipationless quantum Hall effect in narrow channels," *Semicond. Sci. Technol.*, vol. 1, pp. 346–349, 1986.

[158] S. Komiyama and Y. Kawaguchi, "Heat instability of quantum Hall conductors," *Phys. Rev. B*, vol. 61, no. 3, pp. 2014–2027, 2000.

[159] M. E. Cage, G. Marullo-Reedtz, D. Y. Yu, and C. T. van Degrift, "Quantised dissipative states at breakdown of the quantum Hall effect," *Semicond. Sci. Technol.*, vol. 5, pp. 351–354, 1990.

[160] G. Boella, L. Cordiali, G. Marullo-Reedtz, D. Allasia, G. Rinaudo, M. Truccato, and C. Villavecchia, "Analysis of time behavior in the breakdown of the integral quantum Hall effect," *Phys. Rev. B*, vol. 50, no. 11, pp. 7608–7614, 1994.

[161] F. J. Ahlers, G. Hein, H. Scherrer, L. Bliek, H. Nickel, R. Lösch, and W. Schlapp, "Bistability in the current-induced breakdown of the quantum Hall effect," *Semicond. Sci. Technol.*, vol. 8, pp. 2062–2068, 1993.

[162] S. Komiyama and H. Hirai, "Theory of contacts in a two-dimensional electron gas at high magnetic fields," *Phys. Rev. B*, vol. 40, no. 11, pp. 7767–7775, 1989.

[163] S. Komiyama, H. Hirai, S. Sasa, and T. Fujii, "Non-equilibrium population of edge states and a role of contacts in the quantum Hall regime," *Surf. Sci.*, vol. 229, pp. 224–228, 1990.

[164] G. L. J. A. Rikken, J. A. M. M. van Haaren, W. van der Wel, A. P. van Gelder, H. van Kempen, P. Wyder, J. P. André, K. Ploog, and G. Weimann, "Two terminal resistance of quantum Hall devices," *Phys. Rev. B*, vol. 37, no. 11, pp. 6181–6186, 1988.

[165] B. Jeckelmann, B. Jeanneret, and D. Inglis, "High precision measurements of the quantized Hall resistance: Experimental conditions for universality," *Phys. Rev. B*, vol. 55, no. 19, pp. 13124–13134, 1997.

[166] B. Jeanneret, B. Jeckelmann, H. J. Bühlmann, and M. Ilegems, "Influence of infrared illumination on the accuracy of the quantized Hall resistance," *IEEE Trans. Instrum. Meas.*, vol. 46, no. 2, pp. 285–288, 1997.

[167] B. Jeckelmann and B. Jeanneret, "Influence of the voltage contacts on the four-terminal quantized Hall resistance in the nonlinear regime," *IEEE Trans. Instrum. Meas.*, vol. 46, no. 2, pp. 276–280, 1997.

[168] H. Hirai and S. Komiyama, "A contact limited precision of the quantized Hall resistance," *J. Appl. Phys.*, vol. 68, no. 2, pp. 655–662, 1990.

[169] B. W. Ricketts and P. C. Kemeny, "Quantum Hall effect devices as circuits elements," *J. Phys. D: Appl. Phys.*, vol. 21, pp. 483–487, 1988.

[170] F. Delahaye, "Series and parallel connection of multiple quantum Hall-effect devices," *J. Appl. Phys.*, vol. 73, no. 11, pp. 7914–7920, 1993.

[171] F. Piquemal, J. Blanchet, G. Genevès, and J. P. André, "A first attempt to realize multiple-QHE devices series array resistance standards," *IRE Trans. Instrum.*, vol. 48, no. 2, pp. 296–300, 1999.

[172] F. F. Fang and P. J. Stiles, "Quantized magnetoresitance in multiply connected perimeters in two-dimensional systems," *Phys. Rev. B*, vol. 29, no. 6, pp. 3749–3751, 1984.

[173] A. M. Jeffery, R. E. Elmquist, and M. E. Cage, "Precision tests of a quantum Hall effect device dc equivalent circuit using double-series and triple-series connections," *J. Res. Natl. Inst. Stand. Technol.*, vol. 100, no. 6, pp. 677–685, 1995.

[174] F. Delahaye and D. Dominguez, "Precison comparison of quantized Hall resistances," *IEEE Trans. Instrum. Meas.*, vol. 36, no. 2, pp. 226–229, 1987.

[175] A. Hartland, K. Jones, J. M. Williams, B. L. Gallagher, and T. Galloway, "Direct comparison of the quantized Hall resistance in gallium arsenide and silicon," *Phys. Rev. Lett.*, vol. 66, no. 8, pp. 969–973, 1991.

[176] S. Kawaji, N. Nagashima, N. Kikuchi, J. Wakabayashi, B. W. Ricketts, K. Yoshihiro, J. Kinoshita, K. Inagaki, and C. Yamanouchi, "Quantized Hall resistance measurements," *IEEE Trans. Instrum. Meas.*, vol. 38, no. 2, pp. 270–275, 1989.

[177] C. T. van Degrift, K. Yoshihiro, M. E. Cage, D. Yu, K. Segawa, J. Kinoshita, and T. Endo, "Anomalously offset quantized Hall plateaus in high-mobility Si-MOSFETs," *Surf. Sci.*, vol. 263, pp. 116–119, 1992.

[178] K. Yoshihiro, C. T. van Degrift, M. E. Cage, and D. Yu, "Anomalous behavior of a quantized Hall plateau in a high-mobility Si metal-oxide-semiconductor field-effect transistor," *Phys. Rev. B*, vol. 45, no. 24, pp. 14204–14214, 1992.

[179] O. Heinonen and M. D. Johnson, "Failure of the integer quantum Hall effect without dissipation," *Phys. Rev. B*, vol. 49, no. 16, pp. 11230–11237, 1994.

[180] B. Shapiro, "Finite-size corrections in the quantum Hall effect," *J. Phys. C*, vol. 19, pp. 4709–4721, 1986.

[181] W. Brenig and W. Wysokinski, "Scattering approach to the von Klitzing effect," *Z. Phys. B*, vol. 63, pp. 149–154, 1986.

[182] R. Johnston and L. Schweitzer, "An alternative model for the integral quantum Hall effect," *Z. Phys. B*, vol. 72, pp. 217–224, 1988.

[183] M. Y. Azbel, "De Haas-van Alphen, quantized Hall and Meissner effects," *Soild State Commun.*, vol. 53, no. 2, pp. 147–150, 1985.

[184] J. T. Chalker, "The Hall effect in a two-dimensional electron gas," *J. Phys. C: Solid State Phys.*, vol. 16, pp. 4297–4304, 1983.

[185] K. Ishikawa, N. Maeda, K. Tadaki, and S. Uchiyama, "On the absence of finite size corrections in the quantized Hall conductance," *Phys. Lett. A*, vol. 210, pp. 321–327, 1996.

[186] A. Hartland, K. Jones, J. M. Williams, T. Galloway, B. L. Gallagher, C. R. H. White, and M. Henini, "A direct comparison of the quantized Hall resistance in high critical current gallium arsenide and silicon devices," *Surf. Sci.*, vol. 263, pp. 112–115, 1992.

[187] F. Piquemal, B. Etienne, J. P. Andre, and J. N. Patillon, "Direct comparison of quantized Hall resistances," *IEEE Trans. Instrum. Meas.*, vol. 40, no. 2, pp. 234–236, 1991.

[188] B. Jeanneret, B. Jeckelmann, H. J. Bühlmann, R. Houdré, and M. Ilegems, "Influence of the device width on the accuracy of quantization in the integer quantum Hall effect," *IEEE Trans. Instrum. Meas.*, vol. 44, no. 2, pp. 254–257, 1995.

[189] A. M. Thompson and D. G. Lampard, "A new theorem in electrostatics and its application to calculable standards of capacitance," *Nature (London)*, vol. 177, pp. –88, 1956.

[190] B. P. Kibble and G. H. Rayner, *Coaxial ac bridges*. Adam Hilger Ltd, Bristol, 1984.

[191] A. M. Jeffery, R. E. Elmquist, L. H. Lee, J. Q. Shields, and R. F. Dziuba, "NIST comparison of the quantized Hall resistance and the realization of the SI ohm through the calculable capacitor," *IEEE Trans. Instrum. Meas.*, vol. 46, no. 2, pp. 264–268, 1997.

[192] G. W. Small, B. W. Rickets, P. C. Coogan, B. J. Pritchard, and M. M. R. Sovierzoski, "A new determination of the quantized Hall resistance in terms of the NML calculable cross capacitor," *Metrologia*, vol. 34, pp. 241–243, 1997.

[193] A. Hartland, R. G. Jones, B. P. Kibble, and D. J. Legg, "The relationship between the SI ohm, the ohm at NPL, and the quantized Hall resistance," *IEEE Trans. Instrum. Meas.*, vol. 36, no. 2, pp. 208–213, 1987. Document CCE/88-9 submitted by the same authors to the 18. meeting of the Comité Consultatif d'Electricité of the CIPM (1988) gives a more recent value of the von Klitzing constant.

[194] P. J. Mohr and B. N. Taylor, "CODATA recommended values of the fundamental physical constants: 1998," *Rev. Mod. Phys.*, vol. 72, no. 2, pp. 351–495, 2000.

[195] R. S. van Dyck, P. B. Schwinberg, and H. G. Dehmelt, *The electron*, pp. 239–293. Kluwer Academic, Netherlands, 1991.

[196] T. Kinoshita, "The fine structure constant," *Rep. Prog. Phys.*, vol. 59, pp. 1459–1492, 1996.

[197] B. N. Taylor, "Basic standards and fundamental constants," *IEEE Trans. Instrum. Meas.*, vol. 38, no. 2, pp. 164–166, 1989.

[198] B. N. Taylor, "The possible role of the fundamental constants in replacing the kilogram," *IEEE Trans. Instrum. Meas.*, vol. 40, no. 2, pp. 86–91, 1991.

[199] B. P. Kibble, *Atomic Masses and Fundamental Constants 5*, pp. 545–551. New York, Plenum Press, 1976.

[200] B. P. Kibble, I. A. Robinson, and J. H. Belliss, "A realization of the SI watt by the NPL moving-coil balance," *Metrologia*, vol. 27, pp. 173–192, 1990.

[201] P. T. Olsen, W. L. Tew, E. R. Williams, R. E. Elmquist, and H. Sasaki, "Monitoring the mass standard via the comparison of mechanical to electrical power," *IEEE Trans. Instrum. Meas.*, vol. 40, no. 2, pp. 115–120, 1991.

[202] W. Beer, B. Jeanneret, B. Jeckelmann, P. Richard, A. Courteville, Y. Salvadé, and R. Dändliker, "A proposal for a new moving-coil experiment," *IEEE Trans. Instrum. Meas.*, vol. 48, no. 2, pp. 192–195, 1999.

[203] E. R. Williams, R. L. Steiner, D. B. Newell, and P. T. Olsen, "Accurate measurement of the planck constant," *Phys. Rev. Lett.*, vol. 81, no. 12, pp. 2404–2407, 1998.

[204] B. N. Taylor and P. J. Mohr, "On the redefinition of the kilogram," *Metrologia*, vol. 36, pp. 63–64, 1999.

[205] F. Delahaye, "Technical guidelines for reliable measurements of the quantized Hall resistance," *Metrologia*, vol. 26, pp. 63–68, 1989.

[206] F. Delahaye, T. J. Witt, B. Jeckelmann, and B. Jeanneret, "Comparison of quantum Hall effect resistance standards of the OFMET and the BIPM," *Metrologia*, vol. 32, pp. 385–388, 1996.

[207] C. A. Hamilton, "Josephson voltage standards," *Rev. Sci. Instrum.*, vol. 71, no. 10, pp. 3611–3623, 2000.

[208] J. Niemeyer, *Handbook of Appl. Supercond., Vol 2: Applications*, ch. Josephson voltage standards, pp. 1813–1834. IOP, Bristol, 1998.

[209] D. V. Averin and K. K. Likharev, "Coulomb blockade of single-electron tunneling, and coherent oscillations in small tunnel junctions," *J. Low Temp. Phys.*, vol. 62, no. 3/4, pp. 345–373, 1986.

[210] T. A. Fulton and G. J. Dolan, "Observation of single-electron charging effect in small tunnel junction," *Phys. Rev. Lett.*, vol. 59, pp. 109–112, 1987.

[211] H. Grabert and M. H. Devoret, eds., *Single charge tunneling, Coulomb blockade phenomena in nanostructures*, vol. 294 of *NATO ASI*. 1992.

[212] D. A. Averin and K. K. Likharev, "Single electronics: A correlated transfer of single electrons and cooper pairs in systems of small tunnel junctions," *in Mesoscopic Phenomena in Solids, edited by BL Altshuler, PA Lee, RA Webb (Elsevier)*, pp. 173–271, 1991.

[213] M. W. Keller, J. M. Martinis, N. M. Zimmerman, and A. H. Steinbach, "Metrological accuracy of the electron pump," *Appl. Phys. Lett.*, vol. 69, pp. 1804–1806, 1996.

[214] K. K. Likharev and A. B. Zorin, "Theory of the Bloch-wave oscillations in small Josephson junctions," *J. Low Temp. Phys.*, vol. 59, no. 3-4, pp. 347–382, 1985.

[215] F. Piquemal and G. Genevès, "Argument for a direct realisation of the quantum metrological triangle," *Metrologia*, vol. 37, no. 2, pp. 207–211, 2000.

[216] M. W. Keller, A. L. Eichenberger, J. M. Martinis, and N. M. Zimmerman, "A capacitance standard based on counting electrons," *Science*, vol. 285, pp. 1706–1709, 1999.

[217] R. J. Haddad, "A resistor calculable from dc to w = 10000 rad/s," *Thesis, School of Engineering and Applied Science of the Grge Washington University*, pp. –, 1969.

[218] D. L. H. Gibbings, "A design for resistors of calculable a.c./d.c. resistance ratio," *Proc. IEE*, vol. 110, no. 2, pp. 335–347, 1963.

[219] S. W. Chua, B. P. Kibble, and A. Hartland, "Comparison of capacitance with ac quantized Hall resistance," *IEEE Trans. Instrum. Meas.*, vol. 48, no. 2, pp. 342–345, 1999.

[220] J. Bohàcek, P. Svoboda, and P. Vasek, "AC QHE-based calibration of resistance standards," *IEEE Trans. Instrum. Meas.*, vol. 46, no. 2, pp. 173–275, 1997.

[221] M. Pepper and J. Wakabayashi, "Electron localisation and the 2D quantised Hall resistance," *J. Phys. C: Solid State Phys.*, vol. 15, pp. L861–L870, 1982.

[222] M. Pepper and J. Wakabayashi, "The frequency effect and the quantised Hall resistance," *J. Phys. C: Solid State Phys.*, vol. 16, pp. L113–L117, 1983.

[223] R. Joynt, "Theory of the ac breakdown of the quantum Hall effect," *J. Phys. C: Solid State Phys.*, vol. 18, pp. L331–L336, 1985.

[224] R. K. Goodall, R. J. Higgins, and J. P. Harrang, "Capacitance measurements of a quantized two-dimensional electron gas in the regime of the quantum Hall effect," *Phys. Rev. B*, vol. 31, no. 10, pp. 6597–6608, 1985.

[225] J. I. Lee, B. B. Goldberg, M. Heiblum, and P. J. Stiles, "The frequency dependence of the diagonal conductivity of a 2DEG in GaAs heterostructure in the quantum Hall regime," *Soild State Commun.*, vol. 64, no. 4, pp. 447–450, 1987.

[226] J. Melcher, P. Warnecke, and R. Hanke, "Comparison of precision ac and dc measurements of the quantized Hall resistance," *IEEE Trans. Instrum. Meas.*, vol. 42, no. 2, pp. 292–294, 1993.

[227] F. Delahaye, "Accurate ac measurements of the quantized Hall resistance from 1 Hz to 1.6 kHz," *Metrologia*, vol. 31, pp. 367–373, 1994/95.

[228] A. Hartland, B. P. Kibble, P. J. Rodgers, and J. Bohàcek, "Ac measurements of the quantized Hall resistance," *IEEE Trans. Instrum. Meas.*, vol. 44, no. 2, pp. 245–248, 1995.

[229] F. Piquemal, G. R. Trapon, and G. Genevès, "Ac measurements of the minimum longitudinal resistance of a QHE sample from 10 Hz to 10 kHz," *IEEE Trans. Instrum. Meas.*, vol. 45, no. 6, pp. 918–922, 1996.

[230] B. Wood, A. D. Inglis, and M. Côté, "Evaluation of the ac quantized Hall resistance," *IEEE Trans. Instrum. Meas.*, vol. 46, no. 2, pp. 269–272, 1997.

[231] B. M. Wood, D. A. Inglis, M. Cté, and R. B. Young, "Improved ac quantized Hall measurements," *IEEE Trans. Instrum. Meas.*, vol. 48, no. 2, pp. 305–308, 1999.

[232] F. Cabiati, L. Callegaro, C. Cassiago, V. D'Elia, and G. M. Reedtz, "Measurements of the ac longitudinal resistance of a GaAs-AlGaAs quantum Hall device," *IEEE Trans. Instrum. Meas.*, vol. 48, no. 2, pp. 314–318, 1999.

[233] S. W. Chua, A. Hartland, and B. P. Kibble, "Measurement of the ac quantized Hall resistance," *IEEE Trans. Instrum. Meas.*, vol. 48, no. 2, pp. 309–313, 1999.

[234] F. Delahaye, B. P. Kibble, and A. Zarka, "Controlling ac losses in quantum Hall effect devices," *Metrologia*, vol. 37, no. 6, pp. 659–670, 2000.

[235] J. Schurr, J. Melcher, A. von Campenhausen, K. Pierz, G. Hein, and F.-J. Ahlers, "Loss phenomena in the AC quantum Hall effect," *IEEE Trans. Instrum. Meas.*, vol. 50, no. 2, pp. 214–217, 2001.

[236] T. Christen and M. Büttiker, "Low frequency admittance of quantized Hall conductors," *Phys. Rev. B*, vol. 53, no. 4, pp. 2064–2072, 1996.

[237] B. Jeanneret, B. Jeckelmann, and B. D. Hall, "Contactless measurements of the internal capacitance of a Corbino ring in the quantum Hall regime," *IEEE Trans. Instrum. Meas.*, vol. 48, no. 2, pp. 301–304, 1999.

[238] M. E. Cage and A. Jeffery, "Intrinsic capacitances and inductances of quantum Hall effect devices," *J. Res. Natl. Inst. Stand. Technol.*, vol. 101, no. 6, pp. 733–744, 1996.

[239] R. D. Cutkosky, "Four-terminal-pair networks as precision admittance and impedance standards," *Trans. IEEE Commun. Electron.*, no. 83, pp. 19–22, 1964.

[240] D. N. Homan, "Applications of coaxial chokes to AC bridge circuits," *J. Res. NBS*, vol. 72C, no. 2, pp. 161–165, 1968.

Beat Jeckelmann and Blaise Jeanneret
Swiss Federal Office of Metrology and Accreditation
Lindenweg 50, CH-3003 Bern-Wabern, Switzerland
email: `beat.jeckelmann@metas.ch`, `blaise.jeanneret@metas.ch`

The Quantum Hall Effect, 133 – 162

Poincaré Seminar 2004

Introduction to the Fractional Quantum Hall Effect

Steven M. Girvin

1 Introduction

The quantum Hall effect (QHE) is one of the most remarkable condensed-matter phenomena discovered in the second half of the 20th century. It rivals superconductivity in its fundamental significance as a manifestation of quantum mechanics on macroscopic scales. The basic experimental observation for a two-dimensional electron gas subjected to a strong magnetic field is nearly vanishing dissipation

$$\sigma_{xx} \to 0 \tag{1}$$

and special values of the Hall conductance

$$\sigma_{xy} = \nu \frac{e^2}{h} \tag{2}$$

given by the quantum of electrical conductance (e^2/h) multiplied by a quantum number ν. This quantization is universal and independent of all microscopic details such as the type of semiconductor material, the purity of the sample, the precise value of the magnetic field, and so forth. As a result, the effect is now used to maintain (but not define) the standard of electrical resistance by metrology laboratories around the world. In addition, since the speed of light is now defined, a measurement of e^2/h is equivalent to a measurement of the fine structure constant of fundamental importance in quantum electrodynamics.

Fig. (1) shows the remarkable transport data for a real device in the quantum Hall regime. Instead of a Hall resistivity which is simply a linear function of magnetic field, we see a series of so-called *Hall plateaus* in which ρ_{xy} is a universal constant

$$\rho_{xy} = -\frac{1}{\nu}\frac{h}{e^2} \tag{3}$$

independent of all microscopic details (including the precise value of the magnetic field). Associated with each of these plateaus is a dramatic decrease in the dissipative resistivity $\rho_{xx} \longrightarrow 0$ which drops as much as 13 orders of magnitude in the plateau regions. Clearly the system is undergoing some sort of sequence of phase transitions into highly idealized dissipationless states. Just as in a superconductor, the dissipationless state supports persistent currents.

In the so-called integer quantum Hall effect (IQHE) discovered by von Klitzing in 1980, the quantum number ν is a simple integer with a precision of

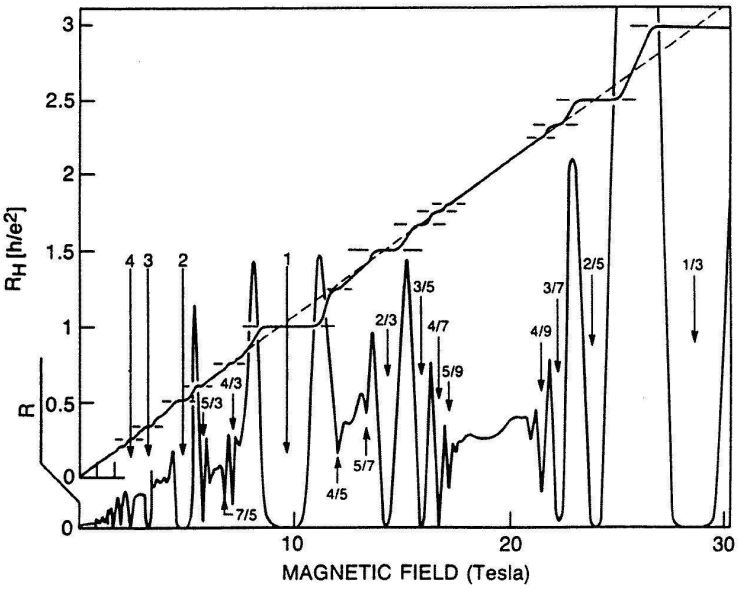

Figure 1: Integer and fractional quantum Hall transport data showing the plateau regions in the Hall resistance $R_{\rm H}$ and associated dips in the dissipative resistance R. The numbers indicate the Landau level filling factors at which various features occur. After ref. [1].

about 10^{-10} and an absolute accuracy of about 10^{-8} (both being limited by our ability to do resistance metrology).

In 1982, Tsui, Störmer and Gossard discovered that in certain devices with reduced (but still non-zero) disorder, the quantum number ν could take on rational fractional values. This so-called fractional quantum Hall effect (FQHE) is the result of quite different underlying physics involving strong Coulomb interactions and correlations among the electrons. The particles condense into special quantum states whose excitations have the bizarre property of being described by fractional quantum numbers, including fractional charge and fractional statistics that are intermediate between ordinary Bose and Fermi statistics. The FQHE has proven to be a rich and surprising arena for the testing of our understanding of strongly correlated quantum systems. With a simple twist of a dial on her apparatus, the quantum Hall experimentalist can cause the electrons to condense into a bewildering array of new 'vacua', each of which is described by a different quantum field theory. The novel order parameters describing each of these phases are completely unprecedented. A number of general reviews exist which the reader may be interested in consulting [2–10] The present lecture notes are based on the author's Les Houches Lectures. [11]

2 Fractional QHE

The free particle Hamiltonian an electron moving in a disorder-free two dimensional plane in a perpendicular magnetic field is

$$H = \frac{1}{2m}\Pi^2 \tag{4}$$

where

$$\vec{\Pi} \equiv \vec{p} + \frac{e}{c}\vec{A}(\vec{r}) \tag{5}$$

is the (mechanical) momentum. The magnetic field quenches the kinetic energy into discrete, massively degenerate Landau levels. In a sample of area $L_x L_y$, each Landau level has degeneracy equal to the number of flux quanta penetrating the sample

$$N_\Phi = L_x L_y \frac{B}{\Phi_0} = \frac{L_x L_y}{2\pi\ell^2} \tag{6}$$

where ℓ is the magnetic length defined by

$$\frac{1}{2\pi\ell^2} = \frac{B}{\Phi_0} \tag{7}$$

and $\Phi_0 = \frac{h}{e^2}$ is the quantum of flux. The quantum number ν in the quantized Hall coefficient turns out to be given by the Landau level filling factor

$$\nu = \frac{N}{N_\Phi}. \tag{8}$$

In the integer QHE the lowest ν Landau levels are completely occupied by electrons and the remainder at empty (at zero temperature). Under some circumstances of weak (but non-zero) disorder, quantized Hall plateaus appear which are characterized by simple rational fractional quantum numbers. For example, at magnetic fields three times larger than those at which the $\nu = 1$ integer filling factor plateau occurs, the lowest Landau level is only 1/3 occupied. The system ought to be below the percolation threshold (that is the electrons should be entirely localized by the weak random disorder potential) and hence be insulating. Instead a robust quantized Hall plateau is observed indicating that electrons can travel through the sample and that (since $\sigma_{xx} \longrightarrow 0$) there is an excitation gap (for all excitations except for the collective mode corresponding to uniform translation of the system which carries the current). This novel and quite unexpected physics is controlled by Coulomb repulsion between the electrons. It is best understood by first ignoring the disorder and trying to discover the nature of the special correlated many-body ground state into which the electrons condense when the filling factor is a rational fraction. Since the kinetic energy has been quenched, the Coulomb interaction has strong non-perturbative effects.

For reasons that will become clear later, it is convenient to analyze the problem in the so-called symmetric gauge

$$\vec{A} = -\frac{1}{2}\vec{r} \times \vec{B}. \tag{9}$$

Unlike the Landau gauge which preserves translation symmetry in one direction, the symmetric gauge preserves rotational symmetry about the origin. Hence we anticipate that angular momentum (rather than one component of the linear momentum) will be a good quantum number in this gauge.

For simplicity we will restrict our attention to the lowest Landau level only and (simply to avoid some awkward minus signs) change the sign of the B field: $\vec{B} = -B\hat{z}$. With these restrictions, it is not hard to show that the solutions of the free-particle Schrödinger equation having definite angular momentum are

$$\varphi_m = \frac{1}{\sqrt{2\pi\ell^2 2^m m!}} z^m e^{-\frac{1}{4}|z|^2} \tag{10}$$

where $z = (x + iy)/\ell$ is a dimensionless complex number representing the position vector $\vec{r} \equiv (x, y)$ and $m \geq 0$ is an integer.

The angular momentum of these basis states is of course $\hbar m$. If we restrict our attention to the lowest Landau level, then there exists only one state with any given angular momentum and only non-negative values of m are allowed. This 'handedness' is a result of the chirality built into the problem by the magnetic field.

It seems rather peculiar that in the Landau gauge we have a continuous one-dimensional family of basis states corresponding to one component of conserved linear momentum for this two-dimensional problem. Now we find that in a different gauge, we have a discrete one dimensional label for the basis states! Nevertheless, we still end up with the correct density of states per unit area. To see this note that the peak value of $|\varphi_m|^2$ occurs at a radius of $R_{\text{peak}} = \sqrt{2m\ell^2}$. The area $2\pi\ell^2 m$ of a circle of this radius contains m flux quanta. Hence we obtain the standard result of one state per Landau level per quantum of flux penetrating the sample.

Because all the basis states are degenerate, any linear combination of them is also an allowed solution of the Schrödinger equation. Hence any function of the form [12]

$$\Psi(x, y) = f(z) e^{-\frac{1}{4}|z|^2} \tag{11}$$

is allowed so long as f is *analytic* in its argument. In particular, arbitrary polynomials of any degree N

$$f(z) = \prod_{j=1}^{N} (z - Z_j) \tag{12}$$

are allowed (at least in the thermodynamic limit) and are conveniently defined by the locations of their N zeros $\{Z_j; j = 1, 2, \ldots, N\}$. The fact that the Hilbert

space for the lowest Landau level is the Hilbert space of analytic functions leads to some beautiful mathematics [11–13].

Another useful solution is the so-called coherent state which is a particular infinite order polynomial

$$f_\lambda(z) \equiv \frac{1}{\sqrt{2\pi\ell^2}} e^{\frac{1}{2}\lambda^* z} e^{-\frac{1}{4}\lambda^*\lambda}. \tag{13}$$

The wave function using this polynomial has the property that it is a narrow gaussian wave packet centered at the position defined by the complex number λ. Completing the square shows that the probability density is given by

$$|\Psi_\lambda|^2 = |f_\lambda|^2 e^{-\frac{1}{2}|z|^2} = \frac{1}{2\pi\ell^2} e^{-\frac{1}{2}|z-\lambda|^2}. \tag{14}$$

This is the smallest wave packet that can be constructed from states within the lowest Landau level.

Because the kinetic energy is completely degenerate, the effect of Coulomb interactions among the particles is nontrivial. To develop a feel for the problem, let us begin by solving the two-body problem. Recall that the standard procedure is to take advantage of the rotational symmetry to write down a solution with the relative angular momentum of the particles being a good quantum number and then solve the Schrödinger equation for the radial part of the wave function. Here we find that the analyticity properties of the wave functions in the lowest Landau level greatly simplifies the situation. If we know the angular behavior of a wave function, analyticity uniquely defines the radial behavior. Thus for example for a single particle, knowing that the angular part of the wave function is $e^{im\theta}$, we know that the full wave function is guaranteed to uniquely be $r^m e^{im\theta} e^{-\frac{1}{4}|z|^2} = z^m e^{-\frac{1}{4}|z|^2}$.

Consider now the two body problem for particles with relative angular momentum m and center of mass angular momentum M. The *unique* analytic wave function is (ignoring normalization factors)

$$\Psi_{mM}(z_1, z_2) = (z_1 - z_2)^m (z_1 + z_2)^M e^{-\frac{1}{4}(|z_1|^2 + |z_2|^2)}. \tag{15}$$

If m and M are non-negative integers, then the prefactor of the exponential is simply a polynomial in the two arguments and so is a state made up of linear combinations of the degenerate one-body basis states φ_m given in eq. (10) and therefore lies in the lowest Landau level. Note that if the particles are spinless fermions then m must be odd to give the correct exchange symmetry. Remarkably, this is the exact (neglecting Landau level mixing) solution for the Schrödinger equation for *any* central potential $V(|z_1 - z_2|)$ acting between the two particles.[1] We do not need to solve any radial equation because of the powerful restrictions

[1] Note that neglecting Landau level mixing is a poor approximation for strong potentials $V \gg \hbar\omega_c$ unless they are very smooth on the scale of the magnetic length.

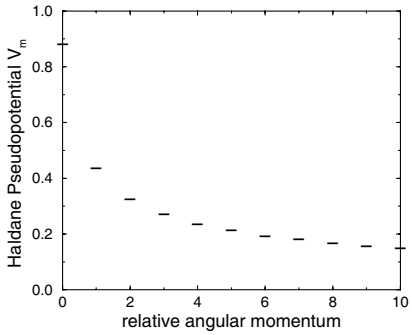

Figure 2: The Haldane pseudopotential V_m vs. relative angular momentum m for two particles interacting via the Coulomb interaction. Units are $e^2/\epsilon\ell$, where ϵ is the dielectric constant of the host semiconductor and the finite thickness of the quantum well has been neglected.

due to analyticity. There is only one state in the (lowest Landau level) Hilbert space with relative angular momentum m and center of mass angular momentum M. Hence (neglecting Landau level mixing) it is an exact eigenstate of *any* central potential. Ψ_{mM} is the exact answer independent of the Hamiltonian!

The corresponding energy eigenvalue v_m is independent of M and is referred to as the mth Haldane pseudopotential

$$v_m = \frac{\langle mM|V|mM\rangle}{\langle mM|mM\rangle}. \tag{16}$$

The Haldane pseudopotentials for the repulsive Coulomb potential are shown in Fig. (2). These discrete energy eigenstates represent bound states of the repulsive potential. If there were no magnetic field present, a repulsive potential would of course have only a continuous spectrum with no discrete bound states. However in the presence of the magnetic field, there are effectively bound states because the kinetic energy has been quenched. Ordinarily two particles that have a lot of potential energy because of their repulsive interaction can fly apart converting that potential energy into kinetic energy. Here however (neglecting Landau level mixing) the particles all have fixed kinetic energy. Hence particles that are repelling each other are stuck and can not escape from each other. One can view this semi-classically as the two particles orbiting each other under the influence of $\vec{E}\times\vec{B}$ drift with the Lorentz force preventing them from flying apart. In the presence of an attractive potential the eigenvalues change sign, but of course the eigenfunctions remain exactly the same (since they are unique)!

The fact that a repulsive potential has a discrete spectrum for a pair of particles is (as we will shortly see) the central feature of the physics underlying

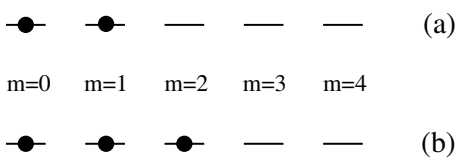

Figure 3: Orbital occupancies for the maximal density filled Landau level state with (a) two particles and (b) three particles. There are no particle labels here. In the Slater determinant wave function, the particles are labeled but a sum is taken over all possible permutations of the labels in order to antisymmetrize the wave function.

the existence of an excitation gap in the fractional quantum Hall effect. One might hope that since we have found analyticity to uniquely determine the two-body eigenstates, we might be able to determine many-particle eigenstates exactly. The situation is complicated however by the fact that for three or more particles, the various relative angular momenta L_{12}, L_{13}, L_{23}, etc. do not all commute. Thus we can not write down general exact eigenstates. We will however be able to use the analyticity to great advantage and make exact statements for certain special cases.

2.1 The $\nu = 1$ many-body state

So far we have found the one- and two-body states. Our next task is to write down the wave function for a fully filled Landau level. We need to find

$$\psi[z] = f[z]\, e^{-\frac{1}{4}\sum_j |z_j|^2} \tag{17}$$

where $[z]$ stands for $(z_1, z_2, \ldots, z_N)$ and f is a polynomial representing the Slater determinant with all states occupied. Consider the simple example of two particles. We want one particle in the orbital φ_0 and one in φ_1, as illustrated schematically in Fig. (3a). Thus (again ignoring normalization)

$$\begin{aligned} f[z] &= \begin{vmatrix} (z_1)^0 & (z_2)^0 \\ (z_1)^1 & (z_2)^1 \end{vmatrix} = (z_1)^0(z_2)^1 - (z_2)^0(z_1)^1 \\ &= (z_2 - z_1). \end{aligned} \tag{18}$$

This is the lowest possible order polynomial that is antisymmetric. For the case of three particles we have (see Fig. (3b))

$$\begin{aligned} f[z] &= \begin{vmatrix} (z_1)^0 & (z_2)^0 & (z_3)^0 \\ (z_1)^1 & (z_2)^1 & (z_3)^1 \\ (z_1)^2 & (z_2)^2 & (z_3)^2 \end{vmatrix} = z_2 z_3^2 - z_3 z_2^2 - z_1^1 z_3^2 + z_3^1 z_1^2 + z_1 z_2^2 - z_2^1 z_1^2 \\ &= -(z_1 - z_2)(z_1 - z_3)(z_2 - z_3) \\ &= -\prod_{i<j}^{3} (z_i - z_j). \end{aligned} \tag{19}$$

This form for the Slater determinant is known as the Vandermonde polynomial. The overall minus sign is unimportant and we will drop it.

The single Slater determinant to fill the first N angular momentum states is a simple generalization of eq. (19)

$$f_N[z] = \prod_{i<j}^{N}(z_i - z_j). \tag{20}$$

To prove that this is true for general N, note that the polynomial is fully antisymmetric and the highest power of any z that appears is z^{N-1}. Thus the highest angular momentum state that is occupied is $m = N-1$. But since the antisymmetry guarantees that no two particles can be in the same state, all N states from $m = 0$ to $m = N-1$ must be occupied. This proves that we have the correct Slater determinant.

One can also use induction to show that the Vandermonde polynomial is the correct Slater determinant by writing

$$f_{N+1}(z) = f_N(z) \prod_{i=1}^{N}(z_i - z_{N+1}) \tag{21}$$

which can be shown to agree with the result of expanding the determinant of the $(N+1)\times(N+1)$ matrix in terms of the minors associated with the $(N+1)$st row or column.

Note that since the Vandermonde polynomial corresponds to the filled Landau level it is the unique state having the maximum density and hence is an exact eigenstate for any form of interaction among the particles (neglecting Landau level mixing and ignoring the degeneracy in the center of mass angular momentum).

The (unnormalized) probability distribution for particles in the filled Landau level state is

$$|\Psi[z]|^2 = \prod_{i<j}^{N}|z_i - z_j|^2 \; e^{-\frac{1}{2}\sum_{j=1}^{N}|z_j|^2}. \tag{22}$$

This seems like a rather complicated object about which it is hard to make any useful statements. It is clear that the polynomial term tries to keep the particles away from each other and gets larger as the particles spread out. It is also clear that the exponential term is small if the particles spread out too much. Such simple questions as, 'Is the density uniform?', seem hard to answer however.

It turns out that there is a beautiful analogy to plasma physics developed by R. B. Laughlin which sheds a great deal of light on the nature of this many particle probability distribution. To see how this works, let us pretend that the norm of the wave function

$$Z \equiv \int d^2z_1 \ldots \int d^2z_N \; |\psi_{[z]}|^2 \tag{23}$$

is the partition function of a classical statistical mechanics problem with Boltzmann weight

$$|\Psi[z]|^2 = e^{-\beta U_{\rm class}} \tag{24}$$

where $\beta \equiv \frac{2}{m}$ and

$$U_{\rm class} \equiv m^2 \sum_{i<j} (-\ln|z_i - z_j|) + \frac{m}{4} \sum_k |z_k|^2. \tag{25}$$

(The parameter $m = 1$ in the present case but we introduce it for later convenience.) It is perhaps not obvious at first glance that we have made tremendous progress, but we have. This is because $U_{\rm class}$ turns out to be the potential energy of a fake classical one-component plasma of particles of charge m in a uniform ('jellium') neutralizing background. Hence we can bring to bear well-developed intuition about classical plasma physics to study the properties of $|\Psi|^2$. Please remember however that all the statements we make here are about a particular wave function. There are no actual long-range logarithmic interactions in the quantum Hamiltonian for which this wave function is the approximate groundstate.

To understand this, let us first review the electrostatics of charges in three dimensions. For a charge Q particle in 3D, the surface integral of the electric field on a sphere of radius R surrounding the charge obeys

$$\int d\vec{A} \cdot \vec{E} = 4\pi Q. \tag{26}$$

Since the area of the sphere is $4\pi R^2$ we deduce

$$\vec{E}(\vec{r}) = Q\frac{\hat{r}}{r^2} \tag{27}$$

$$\varphi(\vec{r}) = \frac{Q}{r} \tag{28}$$

and

$$\vec{\nabla} \cdot \vec{E} = -\nabla^2 \varphi = 4\pi Q\, \delta^3(\vec{r}) \tag{29}$$

where φ is the electrostatic potential. Now consider a two-dimensional world where all the field lines are confined to a plane (or equivalently consider the electrostatics of infinitely long charged rods in 3D). The analogous equation for the line integral of the normal electric field on a *circle* of radius R is

$$\int d\vec{s} \cdot \vec{E} = 2\pi Q \tag{30}$$

where the 2π (instead of 4π) appears because the circumference of a circle is $2\pi R$ (and is analogous to $4\pi R^2$). Thus we find

$$\vec{E}(\vec{r}) = \frac{Q\hat{r}}{r} \tag{31}$$

$$\varphi(\vec{r}) = Q\left(-\ln\frac{r}{r_0}\right) \tag{32}$$

and the 2D version of Poisson's equation is

$$\vec{\nabla} \cdot \vec{E} = -\nabla^2 \varphi = 2\pi Q \, \delta^2(\vec{r}). \tag{33}$$

Here r_0 is an arbitrary scale factor whose value is immaterial since it only shifts φ by a constant.

We now see why the potential energy of interaction among a group of objects with charge m is

$$U_0 = m^2 \sum_{i<j} \left(-\ln |z_i - z_j| \right). \tag{34}$$

(Since $z = (x+iy)/\ell$ we are using $r_0 = \ell$.) This explains the first term in eq. (25).

To understand the second term notice that

$$-\nabla^2 \, \frac{1}{4}|z|^2 = -\frac{1}{\ell^2} = 2\pi\rho_{\rm B} \tag{35}$$

where

$$\rho_{\rm B} \equiv -\frac{1}{2\pi\ell^2}. \tag{36}$$

Eq. (35) can be interpreted as Poisson's equation and tells us that $\frac{1}{4}|z|^2$ represents the electrostatic potential of a constant charge density $\rho_{\rm B}$. Thus the second term in eq. (25) is the energy of charge m objects interacting with this negative background.

Notice that $2\pi\ell^2$ is precisely the area containing one quantum of flux. Thus the background charge density is precisely B/Φ_0, the density of flux in units of the flux quantum.

The very long range forces in this fake plasma cost huge (fake) 'energy' unless the plasma is everywhere locally neutral (on length scales larger than the Debye screening length which in this case is comparable to the particle spacing). In order to be neutral, the density n of particles must obey

$$nm + \rho_{\rm B} = 0 \tag{37}$$

$$\Rightarrow \qquad n = \frac{1}{m} \, \frac{1}{2\pi\ell^2} \tag{38}$$

since each particle carries (fake) charge m. For our filled Landau level with $m = 1$, this is of course the correct answer for the density since every single-particle state is occupied and there is one state per quantum of flux.

We again emphasize that the energy of the fake plasma has nothing to do with the quantum Hamiltonian and the true energy. The plasma analogy is merely a statement about this particular choice of wave function. It says that the square of the wave function is very small (because $U_{\rm class}$ is large) for configurations in which the density deviates even a small amount from $1/(2\pi\ell^2)$. The electrons can in principle be found anywhere, but the overwhelming probability is that they are found in a configuration which is locally random (liquid-like) but with negligible

density fluctuations on long length scales. We will discuss the nature of the typical configurations again further below in connection with Fig. (4).

When the fractional quantum Hall effect was discovered, Robert Laughlin realized that one could write down a many-body variational wave function at filling factor $\nu = 1/m$ by simply taking the mth power of the polynomial that describes the filled Landau level

$$f_N^m[z] = \prod_{i<j}^{N} (z_i - z_j)^m. \tag{39}$$

In order for this to remain analytic, m must be an integer. To preserve the antisymmetry m must be restricted to the odd integers. In the plasma analogy the particles now have fake charge m (rather than unity) and the density of electrons is $n = \frac{1}{m}\,\frac{1}{2\pi\ell^2}$ so the Landau level filling factor $\nu = \frac{1}{m} = \frac{1}{3}, \frac{1}{5}, \frac{1}{7}$, etc. (Later on, other wave functions were developed to describe more general states in the hierarchy of rational fractional filling factors at which quantized Hall plateaus were observed [2, 3, 5, 7, 8].)

The Laughlin wave function naturally builds in good correlations among the electrons because each particle sees an m-fold zero at the positions of all the other particles. The wave function vanishes extremely rapidly if any two particles approach each other, and this helps minimize the expectation value of the Coulomb energy.

Since the kinetic energy is fixed we need only concern ourselves with the expectation value of the potential energy for this variational wave function. Despite the fact that there are no adjustable variational parameters (other than m which controls the density) the Laughlin wave functions have proven to be very nearly exact for almost any realistic form of repulsive interaction. To understand how this can be so, it is instructive to consider a model for which this wave function actually is the exact ground state. Notice that the form of the wave function guarantees that every pair of particles has relative angular momentum greater than or equal to m. One should not make the mistake of thinking that every pair has relative angular momentum precisely equal to m. This would require the spatial separation between particles to be very nearly the same for every pair, which is of course impossible.

Suppose that we write the Hamiltonian in terms of the Haldane pseudopotentials

$$V = \sum_{m'=0}^{\infty} \sum_{i<j} v_{m'}\, P_{m'}(ij) \tag{40}$$

where $P_m(ij)$ is the projection operator which selects out states in which particles i and j have relative angular momentum m. If $P_{m'}(ij)$ and $P_{m''}(jk)$ commuted with each other things would be simple to solve, but this is not the case. However if we consider the case of a 'hard-core potential' defined by $v_{m'} = 0$ for $m' \geq m$, then clearly the mth Laughlin state is an exact, zero energy eigenstate

$$V\psi_m[z] = 0. \tag{41}$$

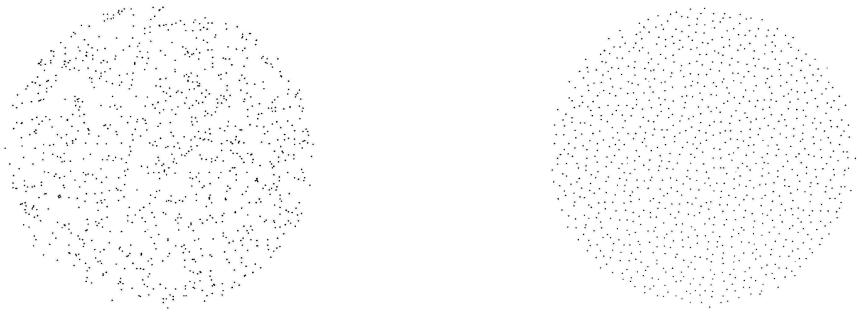

Figure 4: Comparison of typical configurations for a completely uncorrelated (Poisson) distribution of 1000 particles (left panel) to the distribution given by the Laughlin wave function for $m = 3$ (right panel). The latter is a snapshot taken during a Monte Carlo simulation of the distribution. The Monte Carlo procedure consists of proposing a random trial move of one of the particles to a new position. If this move increases the value of $|\Psi|^2$ it is always accepted. If the move decreases the value of $|\Psi|^2$ by a factor p, then the move is accepted with probability p. After equilibration of the plasma by a large number of such moves one finds that the configurations generated are distributed according to $|\Psi|^2$. (After R. B. Laughlin, Chap. 7 in [2].)

This follows from the fact that

$$P_{m'}(ij)\psi_m = 0 \tag{42}$$

for any $m' < m$ since every pair has relative angular momentum of at least m.

Because the relative angular momentum of a pair can change only in discrete (even integer) units, it turns out that this hard core model has an excitation gap. For example for $m = 3$, any excitation out of the Laughlin ground state necessarily weakens the nearly ideal correlations by forcing at least one pair of particles to have relative angular momentum 1 instead of 3 (or larger). This costs an excitation energy of order v_1.

This excitation gap is essential to the existence of dissipationless ($\sigma_{xx} = \rho_{xx} = 0$) current flow. In addition this gap means that the Laughlin state is stable against perturbations. Thus the difference between the Haldane pseudopotentials v_m for the Coulomb interaction and the pseudopotentials for the hard core model can be treated as a small perturbation (relative to the excitation gap). Numerical studies show that for realistic pseudopotentials the overlap between the true ground state and the Laughlin state is extremely good.

To get a better understanding of the correlations built into the Laughlin wave function it is useful to consider the snapshot in Fig. (4) which shows a typical configuration of particles in the Laughlin ground state (obtained from a Monte Carlo sampling of $|\psi|^2$) compared to a random (Poisson) distribution. Focussing

first on the large scale features we see that density fluctuations at long wavelengths are severely suppressed in the Laughlin state. This is easily understood in terms of the plasma analogy and the desire for local neutrality. A simple estimate for the density fluctuations $\rho_{\vec{q}}$ at wave vector $\vec{q}$ can be obtained by noting that the fake plasma potential energy can be written (ignoring a constant associated with self-interactions being included)

$$U_{\text{class}} = \frac{1}{2L^2} \sum_{\vec{q}\neq 0} \frac{2\pi m^2}{q^2} \, \rho_{\vec{q}} \rho_{-\vec{q}} \tag{43}$$

where L^2 is the area of the system and $\frac{2\pi}{q^2}$ is the Fourier transform of the logarithmic potential (easily derived from $\nabla^2 \left(-\ln\left(r\right)\right) = -2\pi \, \delta^2(\vec{r}\,)$). At long wavelengths ($q^2 \ll n$) it is legitimate to treat $\rho_{\vec{q}}$ as a collective coordinate of an elastic continuum. The distribution $e^{-\beta U_{\text{class}}}$ of these coordinates is a gaussian and so obeys (taking into account the fact that $\rho_{-\vec{q}} = (\rho_{\vec{q}})^*$)

$$\langle \rho_{\vec{q}} \rho_{-\vec{q}} \rangle = L^2 \frac{q^2}{4\pi m}. \tag{44}$$

We clearly see that the long-range (fake) forces in the (fake) plasma strongly suppress long wavelength density fluctuations. We will return more to this point later when we study collective density wave excitations above the Laughlin ground state.

The density fluctuations on short length scales are best studied in real space. The radial correlation $g(r)$ function is a convenient object to consider. $g(r)$ tells us the density at r given that there is a particle at the origin

$$g(r) = \frac{N(N-1)}{n^2 Z} \int d^2 z_3 \ldots \int d^2 z_N \;\; |\psi(0, r, z_3, \ldots, z_N)|^2 \tag{45}$$

where $Z \equiv \langle \psi | \psi \rangle$, n is the density (assumed uniform) and the remaining factors account for all the different pairs of particles that could contribute. The factors of density are included in the denominator so that $\lim_{r\to\infty} g(r) = 1$.

Because the $m = 1$ state is a single Slater determinant $g(z)$ can be computed exactly

$$g(z) = 1 - e^{-\frac{1}{2}|z|^2}. \tag{46}$$

Fig. (5) shows numerical estimates of $h(r) \equiv 1 - g(r)$ for the cases $m = 3$ and 5. Notice that for the $\nu = 1/m$ state $g(z) \sim |z|^{2m}$ for small distances. Because of the strong suppression of density fluctuations at long wavelengths, $g(z)$ converges exponentially rapidly to unity at large distances. For $m > 1$, g develops oscillations indicative of solid-like correlations and, the plasma actually freezes[2] at $m \approx 65$.

[2]That is, Monte Carlo simulation of $|\Psi|^2$ shows that the particles are most likely to be found in a crystalline configuration which breaks translation symmetry. Again we emphasize that this is a statement about the Laughlin variational wave function, not necessarily a statement about what the electrons actually do. It turns out that for $m \geq \sim 7$ the Laughlin wave function is no longer the best variational wave function. One can write down wave functions describing Wigner crystal states which have lower variational energy than the Laughlin liquid.

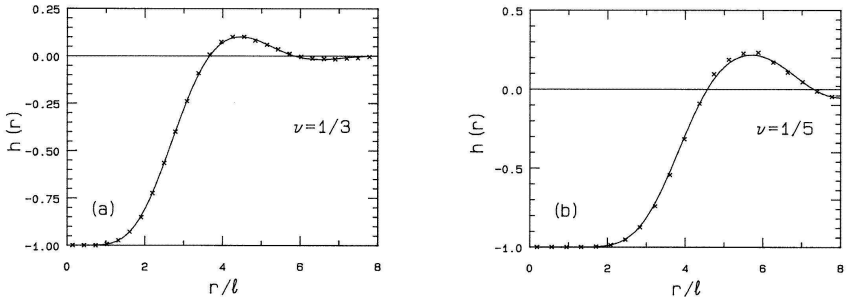

Figure 5: Plot of the two-point correlation function $h(r) \equiv 1-g(r)$ for the Laughlin plasma with $\nu^{-1} = m = 3$ (left panel) and $m = 5$ (right panel). Notice that, unlike the result for $m = 1$ given in eq. (46), $g(r)$ exhibits the oscillatory behavior characteristic of a strongly coupled plasma with short-range solid-like local order.

The Coulomb interaction energy can be expressed in terms of $g(z)$ as[3]

$$\frac{\langle\psi|V|\psi\rangle}{\langle\psi|\psi\rangle} = \frac{nN}{2}\int d^2z\,\frac{e^2}{\epsilon|z|}\,[g(z)-1] \tag{47}$$

where the (-1) term accounts for the neutralizing background and ϵ is the dielectric constant of the host semiconductor. We can interpret $g(z)-1$ as the density of the 'exchange-correlation hole' surrounding each particle.

The correlation energies per particle for $m = 3$ and 5 are [14]

$$\frac{1}{N}\,\frac{\langle\psi_3|V|\psi_3\rangle}{\langle\psi_3|\psi_3\rangle} = -0.4100 \pm 0.0001 \tag{48}$$

and

$$\frac{1}{N}\,\frac{\langle\psi_5|V|\psi_5\rangle}{\langle\psi_5|\psi_5\rangle} = -0.3277 \pm 0.0002 \tag{49}$$

in units of $e^2/\epsilon\ell$ which is ≈ 161 K for $\epsilon = 12.8$ (the value in GaAs), $B = 10$T. For the filled Landau level ($m = 1$) the exchange energy is $-\sqrt{\frac{\pi}{8}}$ as can be seen from eqs. (46) and (47).

3 Neutral Collective Excitations

So far we have studied one particular variational wave function and found that it has good correlations built into it as graphically illustrated in Fig. 4. To further bolster the case that this wave function captures the physics of the fractional Hall

[3]This expression assumes a strictly zero thickness electron gas. Otherwise one must replace $\frac{e^2}{\epsilon|z|}$ by $\frac{e^2}{\epsilon}\int_{-\infty}^{+\infty} ds \frac{|F(s)|^2}{\sqrt{|z|^2+s^2}}$ where F is the wavefunction factor describing the quantum well bound state.

effect we must now demonstrate that there is finite energy cost to produce excitations above this ground state. In this section we will study the neutral collective excitations. We will examine the charged excitations in the next section.

It turns out that the neutral excitations are phonon-like excitations similar to those in solids and in superfluid helium. We can therefore use a simple modification of Feynman's 'single mode approximation' (SMA) theory of the excitations in superfluid helium [15, 16].

By way of introduction let us start with the simple harmonic oscillator. The ground state is of the form

$$\psi_0(x) \sim e^{-\alpha x^2}. \tag{50}$$

Suppose we did not know the excited state and tried to make a variational ansatz for it. Normally we think of the variational method as applying only to ground states. However it is not hard to see that the first excited state energy is given by

$$\epsilon_1 = \min \left\{ \frac{\langle \psi | H | \psi \rangle}{\langle \psi | \psi \rangle} \right\} \tag{51}$$

provided that we do the minimization over the set of states ψ which are constrained to be orthogonal to the ground state ψ_0. One simple way to produce a variational state which is automatically orthogonal to the ground state is to change the parity by multiplying by the first power of the coordinate

$$\psi_1(x) \sim x\, e^{-\alpha x^2}. \tag{52}$$

Variation with respect to α of course leads (in this special case) to the *exact* first excited state.

With this background let us now consider the case of phonons in superfluid ^{4}He. Feynman argued that because of the Bose statistics of the particles, there are no low-lying single-particle excitations. This is in stark contrast to a fermi gas which has a high density of low-lying excitations around the fermi surface. Feynman argued that the only low-lying excitations in ^{4}He are collective density oscillations that are well-described by the following family of variational wave functions (that has no adjustable parameters) labelled by the wave vector

$$\psi_{\vec{k}} = \frac{1}{\sqrt{N}}\, \rho_{\vec{k}}\, \Phi_0 \tag{53}$$

where Φ_0 is the exact ground state and

$$\rho_{\vec{k}} \equiv \sum_{j=1}^{N} e^{-i\vec{k}\cdot\vec{r}_j} \tag{54}$$

is the Fourier transform of the density. The physical picture behind this is that at long wavelengths the fluid acts like an elastic continuum and $\rho_{\vec{k}}$ can be treated

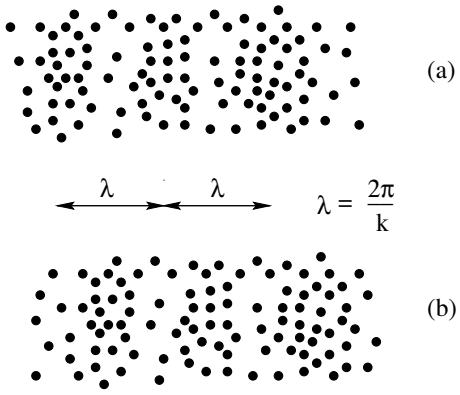

Figure 6: (a) Configuration of particles in which the Fourier transform of the density at wave vector k is non-zero. (b) The Fourier amplitude will have a similar magnitude for this configuration but a different phase.

as a generalized oscillator normal-mode coordinate. In this sense eq. (53) is then analogous to eq. (52). To see that $\psi_{\vec{k}}$ is orthogonal to the ground state we simply note that

$$\begin{aligned} \langle\Phi_0|\psi_{\vec{k}}\rangle &= \frac{1}{\sqrt{N}}\,\langle\Phi_0|\rho_{\vec{k}}|\Phi_0\rangle \\ &= \frac{1}{\sqrt{N}}\int d^3R\; e^{-i\vec{k}\cdot\vec{R}}\;\langle\Phi_0|\rho(\vec{r})|\Phi_0\rangle. \end{aligned} \tag{55}$$

where

$$\rho(\vec{r}) \equiv \sum_{j=1}^{N} \delta^3(\vec{r}_j - \vec{R}) \tag{56}$$

is the density operator. If Φ_0 describes a translationally invariant liquid ground state then the Fourier transform of the mean density vanishes for $k \neq 0$.

There are several reasons why $\psi_{\vec{k}}$ is a good variational wave function, especially for small k. First, it contains the ground state as a factor. Hence it contains all the special correlations built into the ground state to make sure that the particles avoid close approaches to each other without paying a high price in kinetic energy. Second, $\psi_{\vec{k}}$ builds in the features we expect on physical grounds for a density wave. To see this, consider evaluating $\psi_{\vec{k}}$ for a configuration of the particles like that shown in Fig. (6a) which has a density modulation at wave vector $\vec{k}$. This is not a configuration that maximizes $|\Phi_0|^2$, but as long as the density modulation is not too large and the particles avoid close approaches, $|\Phi_0|^2$ will not fall too far below its maximum value. More importantly, $|\rho_{\vec{k}}|^2$ will be much larger than it would for a more nearly uniform distribution of positions. As a result $|\psi_{\vec{k}}|^2$ will be large and this will be a likely configuration of the particles in the excited state.

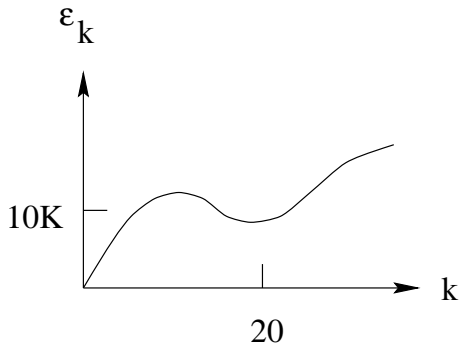

Figure 7: Schematic illustration of the phonon dispersion in superfluid liquid ^{4}He. For small wave vectors the dispersion is linear, as is expected for a gapless Goldstone mode. The roton minimum due to the peak in the static structure factor occurs at a wave vector k of approximately 20 in units of inverse Å. The roton energy is approximately 10 in units of Kelvins.

For a configuration like that in Fig. (6b), the phase of $\rho_{\vec{k}}$ will shift but $|\psi_{\vec{k}}|^2$ will have the same magnitude. This is analogous to the parity change in the harmonic oscillator example. Because all different phases of the density wave are equally likely, $\rho_{\vec{k}}$ has a mean density which is uniform (translationally invariant).

This phonon mode should not be confused with the ordinary hydrodynamic sound mode in classical fluids. The latter occurs in a collision dominated regime $\omega\tau \ll 1$ in which collision-induced pressure provides the restoring force. The phonon mode described here by $\psi_{\vec{k}}$ is a low-lying eigenstate of the quantum Hamiltonian.

At larger wave vectors there is a so-called 'roton minimum' (see Fig. (7)) in the dispersion caused by the solid-like oscillations in the radial distribution function $g(r)$ similar to those shown in Fig. 5 for the Laughlin liquid. This minimum is in some crude sense a remnant of the zone boundary phonon of the crystal.

As we mentioned previously Feynman argued that in ^{4}He the Bose symmetry of the wave functions guarantees that unlike in Fermi systems, there is only a single low-lying mode, namely the phonon density mode. The paucity of low-energy single particle excitations in boson systems is what helps make them superfluid–there are no dissipative channels for the current to decay into. Despite the fact that the quantum Hall system is made up of fermions, the behavior is also reminiscent of superfluidity since the current flow is dissipationless. Indeed, within the 'composite boson' picture, one views the FQHE ground state as a bose condensate [8, 9, 17].

It turns out that the SMA works extremely well in the FQHE as can be seen in Fig. (8). Because of the lack of density fluctuations at long wavelengths in the Laughlin ground state, the system is incompressible leading to a gap in the collective excitation spectrum at long wavelengths. This is quite different from the

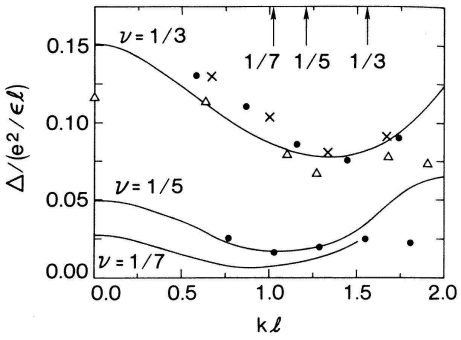

Figure 8: Comparison of the single mode approximation (SMA) prediction of the collective mode energy for filling factors $\nu = 1/3, 1/5, 1/7$ (solid lines) with small-system numerical results for N particles. Crosses indicate the $N = 7, \nu = 1/3$ spherical system, triangles indicate the $N = 6, \nu = 1/3$ hexagonal unit cell system results of Haldane and Rezayi [18]. Solid dots are for $N = 9, \nu = 1/3$ and $N = 7, \nu = 1/5$ spherical system calculations of Fano et al. [19] Arrows at the top indicate the magnitude of the reciprocal lattice vector of the Wigner crystal at the corresponding filling factor. Notice that unlike the phonon collective mode in superfluid helium shown in Fig. (7), the mode here is gapped.

case of superfluid ^{4}He in which the mode is gapless. However like the case of the superfluid, this 'magnetophonon' mode has a 'magnetoroton' minimum at finite k as illustrated in Fig. (8). The figure also shows results from numerical exact diagonalization studies which demonstrate that the single mode approximation is extremely accurate. Note that the magnetoroton minimum occurs close to the position of the smallest reciprocal lattice vector in the Wigner crystal of the same density. In the crystal the phonon frequency would go exactly to zero at this point. (Recall that in a crystal the phonon dispersion curves have the periodicity of the reciprocal lattice.)

Because the oscillator strength is almost entirely in the cyclotron mode, the dipole matrix element for coupling the collective excitations to light is very small. They have however been observed in Raman scattering [20] and found to have an energy gap in excellent quantitative agreement with the single mode approximation.

Finally we remark that these collective excitations are characterized by a well-defined wave vector $\vec{k}$ despite the presence of the strong magnetic field. This is only possible because they are charge neutral which allows one to define a gauge invariant conserved momentum [21].

4 Charged Excitations

Except for the fact that they are gapped, the neutral magnetophonon excitations are closely analogous to the phonon excitations in superfluid ^{4}He. We further pursue this analogy with a search for the analog of vortices in superfluid films. A vortex is a topological defect which is the quantum version of the familiar whirlpool. A reasonably good variational wave function for a vortex in a two-dimensional film of ^{4}He is

$$\psi^{\pm}_{\vec{R}} = \left\{ \prod_{j=1}^{N} f\left(|\vec{r}_j - \vec{R}|\right)\ e^{\pm i\theta(\vec{r}_j - \vec{R})} \right\} \Phi_0. \tag{57}$$

Here θ is the azimuthal angle that the particle's position makes relative to $\vec{R}$, the location of the vortex center. The function f vanishes as $\vec{r}$ approaches $\vec{R}$ and goes to unity far away. The choice of sign in the phase determines whether the vortex is right or left handed.

The interpretation of this wave function is the following. The vortex is a topological defect because if any particle is dragged around a closed loop surrounding $\vec{R}$, the phase of the wave function winds by $\pm 2\pi$. This phase gradient means that current is circulating around the core. Consider a large circle of radius ξ centered on $\vec{R}$. The phase change of 2π around the circle occurs in a distance $2\pi\xi$ so the local gradient seen by *every* particle is $\hat{\theta}/\xi$. We see that locally the center of mass momentum has been boosted by $\pm\frac{\hbar}{\xi}\,\hat{\theta}$ so that the current density of the whirlpool falls off inversely with distance from the core.[4] Near the core f falls to zero because of the 'centrifugal barrier' associated with this circulation. In a more accurate variational wave function the core would be treated slightly differently but the asymptotic large distance behavior would be unchanged.

What is the analog of all this for the lowest Landau level? For ψ^+ we see that every particle has its angular momentum boosted by one unit. In the lowest Landau level analyticity (in the symmetric gauge) requires us to replace $e^{i\theta}$ by $z = x + iy$. Thus we are led to the Laughlin 'quasi-hole' wave function

$$\psi^{+}_{Z}[z] = \prod_{j=1}^{N} (z_j - Z)\ \psi_m[z] \tag{58}$$

where Z is a complex number denoting the position of the vortex and ψ_m is the Laughlin wave function at filling factor $\nu = 1/m$. The corresponding antivortex

[4] This slow algebraic decay of the current density means that the total kinetic energy of a single vortex diverges logarithmically with the size of the system. This in turn leads to the Kosterlitz Thouless phase transition in which pairs of vortices bind together below a critical temperature. As we will see below there is no corresponding finite temperature transition in a quantum Hall system.

('quasi-electron' state) involves z_j^* suitably projected into the Hilbert space [11,12]:

$$\psi_Z^-[z] = \prod_{j=1}^{N} \left(2\frac{\partial}{\partial z_j} - Z^* \right) \psi_m[z] \tag{59}$$

where as usual the derivatives act only on the polynomial part of ψ_m. All these derivatives make ψ^- somewhat difficult to work with. We will therefore concentrate on the quasi-hole state ψ^+. The origin of the names quasi-hole and quasi-electron will become clear shortly.

Unlike the case of a superfluid film, the presence of the vector potential allows these vortices to cost only a finite energy to produce and hence the electrical dissipation is always finite at any non-zero temperature. There is no finite temperature transition into a superfluid state as in the Kosterlitz Thouless transition. From a field theoretic point of view, this is closely analogous to the Higg's mechanism [17].

Just as in our study of the Laughlin wave function, it is very useful to see how the plasma analogy works for the quasi-hole state

$$|\psi_Z^+|^2 = e^{-\beta U_{\rm class}}\ e^{-\beta V} \tag{60}$$

where $U_{\rm class}$ is given by eq. (25), $\beta = 2/m$ as before and

$$V \equiv m \sum_{j=1}^{N} \left(-\ln |z_j - Z| \right). \tag{61}$$

Thus we have the classical statistical mechanics of a one-component plasma of (fake) charge m objects seeing a neutralizing jellium background plus a new potential energy V representing the interaction of these objects with an 'impurity' located at Z and having unit charge.

Recall that the chief desire of the plasma is to maintain charge neutrality. Hence the plasma particles will be repelled from Z. Because the plasma particles have fake charge m, the screening cloud will have to have a net reduction of $1/m$ particles to screen the impurity. But this means that the quasi-hole has fractional fermion number! The (true) physical charge of the object is a fraction of the elementary charge

$$q^* = \frac{e}{m}. \tag{62}$$

This is very strange! How can we possibly have an elementary excitation carrying fractional charge in a system made up entirely of electrons? To understand this let us consider an example of another quantum system that seems to have fractional charge, but in reality doesn't. Imagine three protons arranged in an equilateral triangle as shown in Fig. (9). Let there be one electron in the system. In the spirit of the tight-binding model we consider only the 1S orbital on each of the three 'lattice sites'. The Bloch states are

$$\psi_k = \frac{1}{\sqrt{3}} \sum_{j=1}^{3} e^{ikj}\ |j\rangle \tag{63}$$

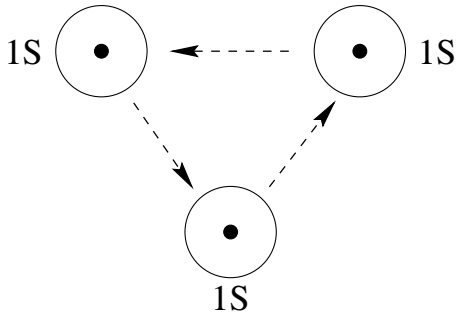

Figure 9: Illustration of an electron tunneling among the 1S orbitals of three protons. The tunneling is exponentially slow for large separations which leads to only exponentially small lifting of what would otherwise be a three-fold degenerate ground state.

where $|j\rangle$ is the 1S orbital for the jth atom. The equilateral triangle is like a linear system of length 3 with periodic boundary conditions. Hence the allowed values of the wavevector are $\left\{k_\alpha = \frac{2\pi}{3}\alpha;\ \ \alpha = -1, 0, +1\right\}$. The energy eigenvalues are

$$\epsilon_{k_\alpha} = -E_{1\mathrm{S}} - 2J\ \cos k_\alpha \tag{64}$$

where $E_{1\mathrm{S}}$ is the isolated atom energy and $-J$ is the hopping matrix element related to the orbital overlap and is exponentially small for large separations of the atoms.

The projection operator that measures whether or not the particle is on site n is

$$P_n \equiv |n\rangle\ \langle n|. \tag{65}$$

Its expectation value in any of the three eigenstates is

$$\langle\psi_{k_\alpha}|P_n|\psi_{k_\alpha}\rangle = \frac{1}{3}. \tag{66}$$

This equation simply reflects the fact that as the particle tunnels from site to site it is equally likely to be found on any site. Hence it will, on average, be found on a particular site n only 1/3 of the time. The average electron number per site is thus 1/3. This however is a trivial example because the value of the measured charge is always an integer. Two-thirds of the time we measure zero and one third of the time we measure unity. This means that the charge *fluctuates*. One measure of the fluctuations is

$$\sqrt{\langle P_n^2\rangle - \langle P_n\rangle^2} = \sqrt{\frac{1}{3} - \frac{1}{9}} = \frac{\sqrt{2}}{3}, \tag{67}$$

which shows that the fluctuations are larger than the mean value. This result is most easily obtained by noting $P_n^2 = P_n$.

A characteristic feature of this 'imposter' fractional charge $\frac{e}{m}$ that guarantees that it fluctuates is the existence in the spectrum of the Hamiltonian of a set of m nearly degenerate states. (In our toy example here, $m = 3$.) The characteristic time scale for the charge fluctuations is $\tau \sim \hbar/\Delta\epsilon$ where $\Delta\epsilon$ is the energy splitting of the quasi-degenerate manifold of states. In our tight-binding example $\tau \sim \hbar/J$ is the characteristic time it takes an electron to tunnel from the 1S orbital on one site to the next. As the separation between the sites increases this tunneling time grows exponentially large and the charge fluctuations become exponentially slow and thus easy to detect.

In a certain precise sense, the fractional charge of the Laughlin quasiparticles behaves very differently from this. An electron added at low energies to a $\nu = 1/3$ quantum Hall fluid breaks up into three charge 1/3 Laughlin quasiparticles. These quasiparticles can move arbitrarily far apart from each other[5] and yet no quasi-degenerate manifold of states appears. The excitation gap to the first excited state remains finite. The only degeneracy is that associated with the positions of the quasiparticles. If we imagine that there are three impurity potentials that pin down the positions of the three quasiparticles, then the state of the system is *uniquely* specified. Because there is no quasidegeneracy, we do not have to specify any more information other than the positions of the quasiparticles. Hence in a deep sense, they are true *elementary particles* whose fractional charge is a sharp quantum observable.

Of course, since the system is made up only of electrons, if we capture the charges in some region in a box, we will always get an integer number of electrons inside the box. However in order to close the box we have to locally destroy the Laughlin state. This will cost (at a minimum) the excitation gap. This may not seem important since the gap is small — only a few Kelvin or so. But imagine that the gap were an MeV or a GeV. Then we would have to build a particle accelerator to 'close the box' and probe the fluctuations in the charge. These fluctuations would be analogous to the ones seen in quantum electrodynamics at energies above $2m_ec^2$ where electron-positron pairs are produced during the measurement of charge form factors by means of a scattering experiment.

Put another way, the charge of the Laughlin quasiparticle fluctuates but only at high frequencies $\sim \Delta/\hbar$. If this frequency (which is $\sim$ 50GHz) is higher than the frequency response limit of our voltage probes, we will see no charge fluctuations. We can formalize this by writing a modified projection operator [22] for the charge on some site n by

$$P_n^{(\Omega)} \equiv P^{\Omega}\, P_n P^{\Omega} \tag{68}$$

where $P_n = |n\rangle\,\langle n|$ as before and

$$P^{(\Omega)} \equiv \theta(\Omega - H + E_0) \tag{69}$$

is the operator that projects onto the subset of eigenstates with excitation energies less than Ω. $P_n^{(\Omega)}$ thus represents a measurement with a high-frequency cutoff built

[5] Recall that unlike the case of vortices in superfluids, these objects are unconfined.

in to represent the finite bandwidth of the detector. Returning to our tight-binding example, consider the situation where J is large enough that the excitation gap $\Delta = \left(1 - \cos\frac{2\pi}{3}\right) J$ exceeds the cutoff Ω. Then

$$\begin{aligned} P^{(\Omega)} &= \sum_{\alpha=-1}^{+1} |\psi_{k_\alpha}\rangle\, \theta(\Omega - \epsilon_{k_\alpha} + \epsilon_{k_0})\, \langle\psi_{k_\alpha}| \\ &= |\psi_{k_0}\rangle\, \langle\psi_{k_0}| \end{aligned} \tag{70}$$

is simply a projector on the ground state. In this case

$$P_n^{(\Omega)} = |\psi_{k_0}\rangle\, \frac{1}{3}\, \langle\psi_{k_0}| \tag{71}$$

and

$$\left\langle \psi_{k_0} \middle| [P_n^{(\Omega)}]^2 \middle| \psi_{k_0} \right\rangle - \left\langle \psi_{k_0} | P_n^{(\Omega)} | \psi_{k_0} \right\rangle^2 = 0. \tag{72}$$

The charge fluctuations in the ground state are then zero (as measured by the finite bandwidth detector).

The argument for the Laughlin quasiparticles is similar. We again emphasize that one can not think of a single charge tunneling among three sites because the excitation gap remains finite no matter how far apart the quasiparticle sites are located. This is possible only because it is a correlated many-particle system.

To gain a better understanding of fractional charge it is useful to compare this situation to that in high energy physics. In that field of study one knows the physics at low energies — this is just the phenomena of our everyday world. The goal is to study the high energy (short length scale) limit to see where this low energy physics comes from. What force laws lead to our world? Probing the proton with high energy electrons we can temporarily break it up into three fractionally charged quarks, for example.

Condensed matter physics in a sense does the reverse. We know the phenomena at 'high' energies (i.e. room temperature) and we would like to see how the known dynamics (Coulomb's law and non-relativistic quantum mechanics) leads to unknown and surprising collective effects at low temperatures and long length scales. The analog of the particle accelerator is the dilution refrigerator.

To further understand Laughlin quasiparticles consider the point of view of 'flatland' physicists living in the cold, two-dimensional world of a $\nu = 1/3$ quantum Hall sample. As far as the flatlanders are concerned the 'vacuum' (the Laughlin liquid) is completely inert and featureless. They discover however that the universe is not completely empty. There are a few elementary particles around, all having the same charge q. The flatland equivalent of Benjamin Franklin chooses a unit of charge which not only makes q negative but gives it the fractional value $-1/3$. For some reason the Flatlanders go along with this.

Flatland cosmologists theorize that these objects are 'cosmic strings', topological defects left over from the 'big cool down' that followed the creation of the

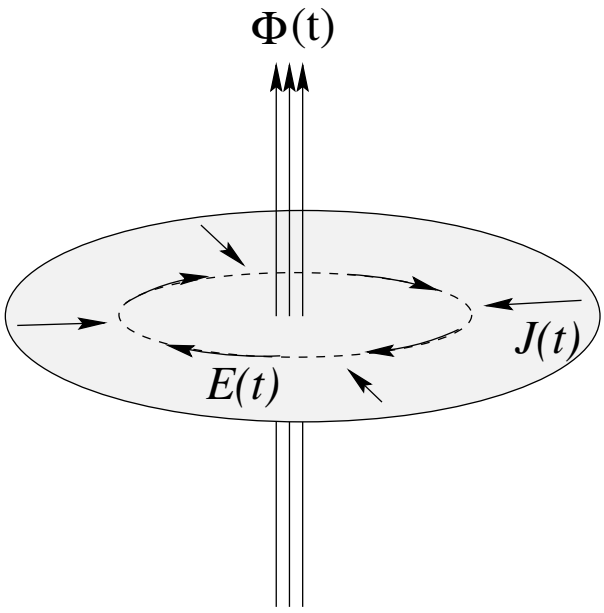

Figure 10: Construction of a Laughlin quasiparticle by adiabatically threading flux $\Phi(t)$ through a point in the sample. Faraday induction gives an azimuthal electric field $E(t)$ which in turn produces a radial current $J(t)$. For each quantum of flux added, charge νe flows into (or out of) the region due to the quantized Hall conductivity $\nu e^2/h$. A flux tube containing an integer number of flux quanta is invisible to the particles (since the Aharanov phase shift is an integer multiple of 2π) and so can be removed by a singular gauge transformation.

universe. Flatland experimentalists call for the creation of a national accelerator facility which will reach the unprecedented energy scale of 10 Kelvin. With great effort and expense this energy scale is reached and the accelerator is used to smash together three charged particles. To the astonishment of the entire world a new short-lived particle is temporarily created with the bizarre property of having integer charge!

There is another way to see that the Laughlin quasiparticles carry fractional charge which is useful to understand because it shows the deep connection between the sharp fractional charge and the sharp quantization of the Hall conductivity. Imagine piercing the sample with an infinitely thin magnetic solenoid as shown in Fig. (10) and slowly increasing the magnetic flux Φ from 0 to $\Phi_0 = \frac{hc}{e}$ the quantum of flux. Because of the existence of a finite excitation gap Δ the process is adiabatic and reversible if performed slowly on a time scale long compared to $\hbar/\Delta$.

Faraday's law tells us that the changing flux induces an electric field obeying

$$\oint_\Gamma d\vec{r}\cdot\vec{E} = -\frac{1}{c}\,\frac{\partial\Phi}{\partial t} \tag{73}$$

where Γ is any contour surrounding the flux tube. Because the electric field contains only Fourier components at frequencies ω obeying $\hbar\omega < \Delta$, there is no dissipation and $\sigma_{xx} = \sigma_{yy} = \rho_{xx} = \rho_{yy} = 0$. The electric field induces a current density obeying

$$\vec{E} = \rho_{xy}\ \vec{J}\times\hat{z} \tag{74}$$

so that

$$\rho_{xy}\oint_\Gamma \vec{J}\cdot(\hat{z}\times d\vec{r}) = -\frac{1}{c}\,\frac{d\Phi}{dt}. \tag{75}$$

The integral on the LHS represents the total current flowing into the region enclosed by the contour. Thus the charge inside this region obeys

$$\rho_{xy}\,\frac{dQ}{dt} = -\frac{1}{c}\,\frac{d\Phi}{dt}. \tag{76}$$

After one quantum of flux has been added the final charge is

$$Q = \frac{1}{c}\,\sigma_{xy}\Phi_0 = \frac{h}{e}\,\sigma_{xy}. \tag{77}$$

Thus on the quantized Hall plateau at filling factor ν where $\sigma_{xy} = \nu\,\frac{e^2}{h}$ we have the result

$$Q = \nu e. \tag{78}$$

Reversing the sign of the added flux would reverse the sign of the charge.

The final step in the argument is to note that an infinitesimal tube containing a quantum of flux is invisible to the particles. This is because the Aharonov-Bohm phase factor for traveling around the flux tube is unity.

$$\exp\left\{i\frac{e}{\hbar c}\oint_\Gamma \delta\vec{A}\cdot d\vec{r}\right\} = e^{\pm 2\pi i} = 1. \tag{79}$$

Here $\delta\vec{A}$ is the additional vector potential due to the solenoid. Assuming the flux tube is located at the origin and making the gauge choice

$$\delta\vec{A} = \Phi_0\,\frac{\hat{\theta}}{2\pi r}, \tag{80}$$

one can see by direct substitution into the Schrödinger equation that the only effect of the quantized flux tube is to change the phase of the wave function by

$$\psi \to \psi\prod_j \frac{z_j}{|z_j|} = \psi\prod_j e^{i\theta_j}. \tag{81}$$

The removal of a quantized flux tube is thus a 'singular gauge change' which has no physical effect.

Let us reiterate. Adiabatic insertion of a flux quantum changes the state of the system by pulling in (or pushing out) a (fractionally) quantized amount of charge. Once the flux tube contains a quantum of flux it effectively becomes invisible to the electrons and can be removed by means of a singular gauge transformation.

Because the excitation gap is preserved during the adiabatic addition of the flux, the state of the system is fully specified by the position of the resulting quasiparticle. As discussed before there are no low-lying quasi-degenerate states. This version of the argument highlights the essential importance of the fact that $\sigma_{xx} = 0$ and σ_{xy} is quantized. The existence of the fractionally quantized Hall transport coefficients guarantees the existence of fractionally charged elementary excitations

These fractionally charged objects have been observed directly by using an ultrasensitive electrometer made from a quantum dot [23] and by the reduced shot noise which they produce when they carry current [24].

Because the Laughlin quasiparticles are discrete objects they cost a non-zero (but finite) energy to produce. Since they are charged they can be thermally excited only in neutral pairs. The charge excitation gap is therefore

$$\Delta_c = \Delta_+ + \Delta_- \tag{82}$$

where $\Delta_\pm$ is the vortex/antivortex (quasielectron/quasihole) excitation energy. In the presence of a transport current these thermally excited charges can move under the influence of the Hall electric field and dissipate energy. The resulting resistivity has the Arrhenius form

$$\rho_{xx} \sim \gamma \frac{h}{e^2}\, e^{-\beta\Delta_c/2} \tag{83}$$

where γ is a dimensionless constant of order unity. Note that the law of mass action tells us that the activation energy is $\Delta_c/2$ not Δ_c since the charges are excited in pairs. There is a close analogy between the dissipation described here and the flux flow resistance caused by vortices in a superconducting film.

Theoretical estimates of Δ_c are in good agreement with experimental values determined from transport measurements [25]. Typical values of Δ_c are only a few percent of $e^2/\epsilon\ell$ and hence no larger than a few Kelvin. In a superfluid time-reversal symmetry guarantees that vortices and antivortices have equal energies. The lack of time reversal symmetry here means that Δ_+ and Δ_- can be quite different. Consider for example the hard-core model for which the Laughlin wave function ψ_m is an exact zero energy ground state as shown in eq. (41). Equation (58) shows that the quasihole state contains ψ_m as a factor and hence is also an exact zero energy eigenstate for the hard-core interaction. Thus the quasihole costs zero energy. On the other hand eq. (59) tells us that the derivatives reduce the degree of homogeneity of the Laughlin polynomial and therefore the energy of the quasielectron *must* be non-zero in the hard-core model. At filling factor

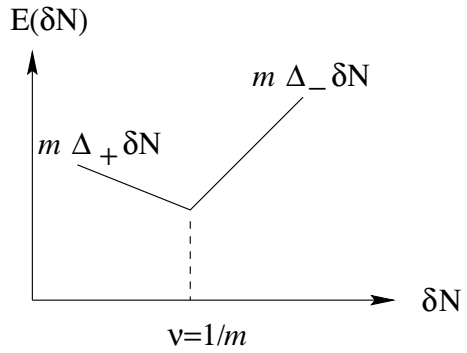

Figure 11: Energy cost for inserting δN electrons into the Laughlin state near filling factor $\nu = 1/m$. The slope of the line is the chemical potential. Its discontinuity at $\nu = 1/m$ measures the charge excitation gap.

$\nu = 1/m$ this asymmetry has no particular significance since the quasiparticles must be excited in pairs.

Consider now what happens when the magnetic field is increased slightly or the particle number is decreased slightly so that the filling factor is slightly smaller than $1/m$. The lowest energy way to accommodate this is to inject m quasiholes into the Laughlin state for each electron that is removed (or for each $m\Phi_0$ of flux that is added). The system energy (ignoring disorder and interactions in the dilute gas of quasiparticles) is

$$E_+ = E_m - \delta N \; m\Delta_+ \tag{84}$$

where E_m is the Laughlin ground state energy and $-\delta N$ is the number of added holes. Conversely for filling factors slightly greater than $1/m$ the energy is (with $+\delta N$ being the number of added electrons)

$$E_- = E_m + \delta N \; m\Delta_-. \tag{85}$$

This is illustrated in Fig. (11). The slope of the lines in the figure determines the chemical potential

$$\mu_\pm = \frac{\partial E_\pm}{\partial \delta N} = \mp m\Delta_\pm. \tag{86}$$

The chemical potential suffers a jump discontinuity of $m(\Delta_+ + \Delta_-) = m\Delta_c$ just at filling factor $\mu = 1/m$. This jump in the chemical potential is the signature of the charge excitation gap just as it is in a semiconductor or insulator. Notice that this form of the energy is very reminiscent of the energy of a type-II superconductor as a function of the applied magnetic field (which induces vortices and therefore has an energy cost $\Delta E \sim |B|$).

Recall that in order to have a quantized Hall plateau of finite width it is necessary to have disorder present. For the integer case we found that disorder

localizes the excess electrons allowing the transport coefficients to not change with the filling factor. Here it is the fractionally-charged quasiparticles that are localized by the disorder.[6] Just as in the integer case the disorder may fill in the gap in the density of states but the DC value of σ_{xx} can remain zero because of the localization. Thus the fractional plateaus can have finite width.

If the density of quasiparticles becomes too high they may delocalize and condense into a correlated Laughlin state of their own. This gives rise to a hierarchical family of Hall plateaus at rational fractional filling factors $\nu = p/q$ (generically with q odd due to the Pauli principle). There are several different but entirely equivalent ways of constructing and viewing this hierarchy which we will not delve into here [2, 3, 5].

5 Summary

In these notes I have discussed the Laughlin ground state and the basic facts of the neutral and charged collective excitations above it. These topics barely scratch the surface of the rich phenomenology of two-dimensional electron gases in the quantum Hall regime. The reader interested in further details about fractional statistics, edge states, Chern-Simons field theories, bilayer quantum Hall systems, quantum Hall ferromagnets and other more advanced topics is directed to the various reviews that are available. [2–11]

6 Acknowledgments

Much of my work on the quantum Hall effect has been in collaboration with my long time friend and collaborator Allan MacDonald. This work was supported by National Science Foundation Grant DMR-0342157.

References

[1] H. L. Störmer, *Physica* **B177**, 401 (1992).

[2] *The Quantum Hall Effect, 2nd Ed.*, edited by Richard E. Prange and Steven M. Girvin (Springer-Verlag, New York, 1990).

[3] T. Chakraborty and P. Pietiläinen, *The Fractional Quantum Hall Effect* (Springer-Verlag, Berlin, New York, 1988).

[4] Allan H. MacDonald, *Quantum Hall Effect: A Perspective* (Kluwer Academic Publishers, 1989).

[5] *Perspectives in Quantum Hall Effects*, Edited by Sankar Das Sarma and Aron Pinczuk (Wiley, New York, 1997).

[6] Note again the essential importance of the fact that the objects are 'elementary particles'. That is, there are no residual degeneracies once the positions are pinned down.

[6] *Introduction to the Theory of the Integer Quantum Hall Effect*, M. Janßen, O. Viehweger, U. Fastenrath, and J. Hajdu (VCH, Weinheim, New York, 1994).

[7] *Quantum Hall Effect*, edited by Michael Stone (World Scientific, Singapore, 1992).

[8] S. Kivelson, D.-H. Lee and S.-C. Zhang, *Scientific American*, March, 1996, p. 86.

[9] Shou Cheng Zhang, *Int. J. Mod. Phys.* B**6**, 25 (1992).

[10] A. H. MacDonald, in *Mesoscopic Quantum Physics*, Les Houches, Session LXI, eds. E. Akkermans, G. Montambaux, J.-L. Pichard and J. Zinn-Justin (North Holland, Amsterdam, 1995).

[11] S. M. Girvin, 'The Quantum Hall Effect: Novel Excitations and Broken Symmetries,' 120 pp. Les Houches Lecture Notes, in: *Topological Aspects of Low Dimensional Systems*, ed. by Alain Comtet, Thierry Jolicoeur, Stephane Ouvry and Francois David, (Springer-Verlag, Berlin and Les Editions de Physique, Les Ulis, 2000, ISBN: 3-540-66909-4), (eprint: cond-mat/9907002).

[12] S. M. Girvin and T. Jach, *Phys. Rev.* B**29**, 5617 (1984).

[13] V. Bargman, *Rev. Mod. Phys.* **34**, 829 (1962).

[14] D. Levesque, J. J. Weiss, and A. H. MacDonald, *Phys. Rev.* B**30**, 1056 (1984).

[15] R. P. Feynman, *Statistical Mechanics* (Benjamin, Reading, 1972).

[16] S. M. Girvin, A. H. MacDonald and P. M. Platzman, *Phys. Rev.* B**33**, 2481 (1986).

[17] S. M. Girvin in Chap. 10 and App. I of Ref. [2]; S. M. Girvin and A. H. MacDonald, *Phys. Rev. Lett.* **58**, 1252 (1987); S.-C. Zhang, H. Hansson, and S. Kivelson, *Phys. Rev. Lett.* **62**, 82 (1989); N. Read, *Phys. Rev. Lett.* **62**, 86 (1989); D.-H. Lee and M. P. A. Fisher, *Phys. Rev. Lett.* **63**, 903 (1989).

[18] F. D. M. Haldane and E. H. Rezayi, *Phys. Rev. Lett.* **54**, 237 (1985).

[19] G. Fano, F. Ortolani, and E. Colombo, *Phys. Rev.* B**34**, 2670 (1986).

[20] A. Pinczuk, B. S. Dennis, L. N. Pfeiffer, and K. W. West, *Phys. Rev. Lett.* **70**, 3983 (1993).

[21] C. Kallin and B. I. Halperin, *Phys. Rev.* B**30**, 5655 (1984); *Phys. Rev.* B**31**, 3635 (1985).

[22] A. Goldhaber and S. A. Kivelson, *Physics Lett.* B**255**, 445 (1991).

[23] V. Goldman and B. Su, *Science* **267**, 1010 (1995).

[24] R. de-Picciotto, M. Reznikov, M. Heiblum, V. Umansky, G. Bunin, and D. Mahalu, *Nature* **389**, 162 (1997); L. Saminadayar, D. C. Glattli, Y. Jin and B. Etienne, *Phys. Rev. Lett.* **79**, 2526 (1997).

[25] R. L. Willett, H. L. Störmer, D. C. Tsui, A. C. Gossard, and J. H. English, *Phys. Rev.* B**37**, 8476 (1988).

Steven M. Girvin
Yale University
Sloane Physics Laboratory
New Haven, CT 06520
USA
email: steven.girvin@yale.edu

The Quantum Hall Effect, 163 – 197

Poincaré Seminar 2004

Tunneling Experiments in the Fractional Quantum Hall Effect Regime

D. Christian Glattli

Abstract. The Fractional Quantum Hall effect provides a unique example of a quantum system with fractional quantum numbers. We review the tunneling experiments which have brought into evidence the fractionally charged excitations, the fractional occupation of the quantum states and the non-linear quantum transport related to the chiral Luttinger liquids properties.

1 Introduction

The quantum Hall effect is one of the most remarkable macroscopic manifestation of quantum mechanics in condensed matter after superconductivity and superfluidity. The phenomenon is observed in a two-dimensional electrons gas (2DEG) at low temperature in a high perpendicular magnetic field. Landau Levels (LL) form due to cyclotron motion quantization in 2D and are highly degenerate. However, the degeneracy can be lifted by the interactions. The system can be viewed as a flat macroscopic atom made of 10^9 electrons. As for atoms or nuclei, particular values of the filling of the electronic states lead to more stable ground states with large *energy gap* for the excitations. The equivalent of magic atomic quantum numbers are integer or fractional values of the filling factor $\nu = p/q$ of the electronic quantum states (p and q integers). The filling factor, is given by the ratio of the electron density n_s to the density $n_\phi = B/\phi_0$ of flux quantum $\phi_0 = h/e$. It can be varied either by sweeping the magnetic field or by changing the electron density. The magic values of ν are experimentally revealed by plateaus in the Hall resistance $\frac{q}{p}\frac{h}{e^2}$. The Integer Quantum Hall Effect, discovered by Klitzing [1], occurs when $\nu = p$ ($q = 1$) when there is a complete filling of the degenerate LLs. The Fractional Quantum Hall Effect [2, 3] occurs at $\nu = p/q$ ($q = 2s + 1$, s integer). The underlying physics is the Coulomb interaction which lifts the LL degeneracy to form new correlated quantum liquids with energy gap and with topological excitations having a fractional charge $e/(2s + 1)$.

The Quantum Hall effect, and in particular the Fractional Quantum Hall effect [4], have completely renewed our knowledge of quantum excitations. Topological fractionally charged excitations [3], with anyonic or exclusonic fractional quantum statistics [5], composite fermions [6] or composite bosons [7], skyrmions [8, 9], etc., ... are the natural elementary excitations required to understand the quantum Hall effect. The quantum Hall effect have made real some concepts invented

for the purpose of particle physics theories or used in mathematical physics for quantum integrable systems [10]. It is remarkable that Coulomb interaction and Fermi statistics, the simplest ingredients one can imagine, are responsible for a so rich physics. No interaction with the host material is needed as in the case of superconductivity. For macroscopic samples, however, a little amount of disorder is required to localize the topological excitations and thus to allow observation of Hall resistance quantization over a finite range of magnetic field (the Hall plateaus). It is a rare example where imperfections help to reveal a fundamental quantum effect. For narrow mesoscopic samples, disorder is to be avoid, and the QHE is revealed by the integer or fractional conductance quantization associated with the formation of chiral one dimensional edge modes. The properties of chiral edge modes are deeply related to the bulk properties of the Quantum Hall electron fluid.

I will focus here on tunneling experiments which allow for probing the fractional excitations and the fractional filling of the states. More general reviews on the quantum Hall effect can be found for example in Refs [11, 12, 9]. In these tunneling experiments, the charge transfer occurs between gapless chiral modes, called edge channels, which form at the periphery of a QHE fluid. Indeed, as the longitudinal conductance in the bulk vanishes, only these modes can generate a current in response to a potential drop. The edge channels can be easily connected to metallic contacts arranged at the periphery of the sample and then to an external circuit. In the IQHE they can be considered as good realization of 1D metals with the remarkable property that backscattering is suppressed by chirality. In the FQHE regime, they inherit from the bulk several non-trivial properties. First, they are no longer Fermi liquids. Their quantum dynamics is very similar to that of Tomonaga-Luttinger liquids predicted for 1D interacting electrons. The relevant excitations which propagate the charge information is no longer the fermionic Landau quasiparticle (the screened electron) but bosonic collective neutral modes (plasmons) instead. A remarkable consequence is the power law vanishing tunneling density of state (TDOS) at the Fermi energy. Indeed, an electron locally injected from an external contact into an FQH edge must excite many of these collective modes. If injected at the Fermi sea, no mode can be excited, and the tunneling rate vanishes (orthogonality catastrophy). A second non-trivial property inherited from the bulk is the possibility to extract from the edge a fractionally charged $e/(2s+1)$ quasiparticle for $\nu = p/(2s+1)$. Such quasiparticle tunneling between fractional edges is only observable when tunneling *through* the bulk FQHE liquid. An additional requirement due to the Luttinger liquid physics is a large bias voltage applied between the edges. Otherwise, at low voltage (and low temperature) near equilibrium, only integer charge is observed in experiments (the Luttinger liquid properties of the edges forces the quasiparticles to 'bunch' to form ordinary electrons). The detection of the fractionally charged quasiparticles have been made possible by the current noise generally associated with tunneling and called shot noise. This became recently possible thanks to the development of very sensitive current noise measurements in mesoscopic physics. For weak tunnel

current, the temporal statistics of charge transfer is Poissonian, and the current noise is a direct measure of the charge carrier. The fractional quantum Hall effect is the first, and until now unique, example of a system with fractionally charged carriers. Also using shot noise, it has been also possible to follow the cross over from fractional to integer charges when reducing the bias voltage. At equilibrium, voltage lower than k_BT the resonant tunneling of electrons between edge states can be used to probe the fraction of charge associated with the addition of a single flux quantum in the ground state using conductance measurement. The charge accumulated on a micrometer edge state ring is shown to vary by fractional increments with flux either by changing the magnetic field or by varying the size of the ring with a gate. This demonstrates that individual quantum sates participating to the formation of the collective ground state are actually filled by a fraction of electron. This is this fractional occupation which is responsible for the exact fractional quantization of the conductance.

The notes are organized as follows. Section II will describe the chiral edge one-dimensional modes which form in a finite 2D electron gas in perpendicular magnetic field. In section III, the chiral Luttinger liquid physics is presented. Tunneling experiments revealing the anomalous power law density of states will be reviewed. In section IV, non equilibrium experiments probing the charge carrier by measuring the shot noise of the current will be described. In V we will show how equilibrium resonant tunneling experiments can probe the fraction of charge which fills individual states participating to the ground state.

2 Tunneling in the Quantum Hall regime

2.1 Edge states in the integer quantum Hall regime

The kinetic energy $K = \frac{(\boldsymbol{p}-q\boldsymbol{A})^2}{2m^*}$, $q = -e$, of an electron moving freely in the plane perpendicular to a magnetic field $\mathbf{B} = B\widehat{\mathbf{z}}$ is quantized into Landau levels:

$$E_n = (n + \frac{1}{2})\hbar\omega_c \tag{1}$$

($\omega_c = eB/m^*$: cyclotron pulsation). This reflects the quantization of the cyclotron motion. As the energy depends on a single quantum number n while there are two degrees of freedom, there is a high degeneracy. The degeneracy comes from the freedom to choose the center of cyclotron orbits and is equal to the number $N_\Phi = n_\Phi S = eBS/h$ of magnetic flux quanta $\Phi_0 = h/e$ in the plane. To see this, one can replace the conjugate pairs of electron coordinates $[x, p_x]$ and $[y, p_y]$ by a new set of conjugate pairs, see Fig.1, using the cylindrical gauge $\mathbf{A} = (-By/2, Bx/2, 0)$:

$$[\xi, \eta] = [v_y/\omega_c, -v_x/\omega_c] = -i\hbar/eB \tag{2}$$

$$[X, Y] = i\hbar/eB \tag{3}$$

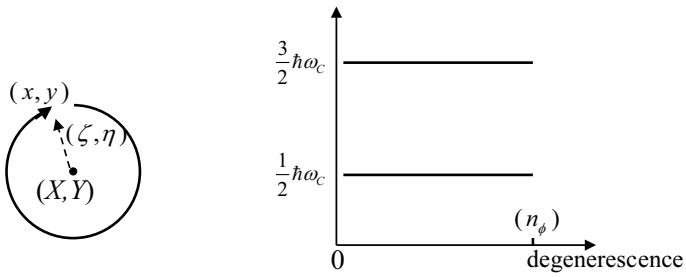

Figure 1: Left: decomposition of the electron coordinates (x, y) into cyclotron orbit coordinates (ξ, η) and the coordinates of the obit center (X, Y). Right: energy Landau levels formed by quantization of the cyclotron orbits

with

$$(x, y) = (X + \xi, Y + \eta)\,. \tag{4}$$

The Hamiltonian now writes $H = \frac{1}{2}m\omega_c^2(\xi^2 + \eta^2)$, so the first pair of conjugate coordinates represents the fast cyclotron motion. For an eigenstate $|n\rangle$ of H, the cyclotron radius is:

$$r_n = \langle n|\, \xi^2 + \eta^2\, |n\rangle^{1/2} = (n + \frac{1}{2})^{1/2} l_c. \tag{5}$$

It increases with the orbital Landau level index n. The characteristic length $l_c = (\hbar/eB)^{1/2}$ is called the magnetic length. H does not depend on the second pair of coordinates $\mathbf{R} = (X, Y)$, the center around which electrons perform cyclotron orbits. However, orbit center positions can not be chosen completely freely in the plane as announced above. The commutation relation $[X, Y] = i\hbar/eB$ put restrictions on the number of possible distinct states. There is a finite degeneracy which is easy to estimate using the following analogy. The plane is similar to the semi-classical phase space (P, Q) of a one-dimensional system for which it is known that the effective area occupied by a quantum state is h as $[Q, P] = i\hbar$. Similarly, the area occupied by a quantum Hall state is h/eB, the area of a flux quantum. The degeneracy per unit area is thus n_Φ, the density of flux quanta; it is the same for all Landau levels. The semiclassical analogy will be usefull to get intuition about the *one-dimensional* character of the dynamics of electrons in *two dimensions* contrained to stay in a given Landau Level.

2.1.1 Edge states

In real sample of finite size, the 2DEG is bounded thanks to a permanent electric field directed perpendicular and toward the perimeter. The confining electric field compensates the long range Coulomb electronic repulsion and prevents electrons to escape from the area. It can be provided by ionized donor atoms in the host

semiconductor lattice and uniformly distributed inside the region filled by electrons. Alternatively, an extra confinement can be provided by a gate negatively polarized with respect to the electrons and placed close and outside the electron area.

The Hamiltonian in presence of a potential $U(x, y)$:

$$H = \frac{(\boldsymbol{p} + e\boldsymbol{A})^2}{2m^*} + U(x, y) \tag{6}$$

can be simplified if the potential is smooth over the length l_c and $l_c |\nabla U| \ll \hbar\omega_c$. The mixing between Landau Levels can be neglected and $H \simeq \sum_n |n\rangle H_n \langle n|$. The dynamics of electrons within the n^{th} Landau level is described by the projected Hamiltonian:

$$H_n = (n + 1/2)\hbar\omega_c + U^{(n)}(X, Y) \tag{7}$$

where $U^{(n)}(X, Y) = \langle n| U(x, y) |n\rangle \simeq U(X, Y)$ is the confining potential averaged over the fast cyclotron motion. If the electric field due to confinement is along the $\widehat{y}$ direction, electrons drift along the boundary, the $\widehat{x}$ direction, with velocity $\frac{dX}{dt} = (1/eB)\partial U/\partial Y$. The Lorentz force compensates the electrostatic field, a direct consequence of the quantization of the velocity modulus ($\frac{d}{dt}(\boldsymbol{p} - (-e)\boldsymbol{A})^2 = 0$). In the bulk, $U \simeq 0$, the drift velocity is zero. Electrons do not move on average although performing fast cyclotron motion.

2.1.2 Edge channels

At zero temperature, electrons fill the Landau level up to a Fermi Energy E_F. The Fermi energy, here measured from the zero of kinetic energy, is defined by the exchange of electrons with a reservoir (practically: a contact somewhere on the edges). Here we disregard spin for simplicity and assume U translationally invariant along $\widehat{x}$ and vanishing in the bulk.

In the bulk, when $(p - \frac{1}{2})\hbar\omega_c < E_F < (p + \frac{1}{2})\hbar\omega_c$ electrons fill all the bulk states of the first p (integer) Landau Levels according to Fermi statistics. The filling factor is $\nu = p$. There is a gap $\hbar\omega_c$ for creating internal excitations which leads to vanishing longitudinal conduction in the bulk. There is also an energy cost $E_F - (n + 1/2)\hbar\omega_c$ to extract an electron from the n^{th} Landau Level to the Fermi energy.

Toward edges, Landau levels are adiabatically bend by the potential $U(Y)$ and depopulate when crossing the Fermi energy, see Fig.2(a) and (b). For the n^{th} LL this occurs at $Y = Y_{F,n}$, when the energy cost $E_F - (n + 1/2)\hbar\omega_c - U(Y_{F,n})$ vanishes. This defines p lines along the edge with gapless excitations. This lines of gapless excitations restore conduction.

The one dimensional chiral conduction modes so formed are called edge channels. They can be connected to external contacts fixing their Fermi energy. The drift of electrons along the equipotential lines generated by the confining potential gives rise to a *persistent chiral current* . When the Fermi energy rises from E_F

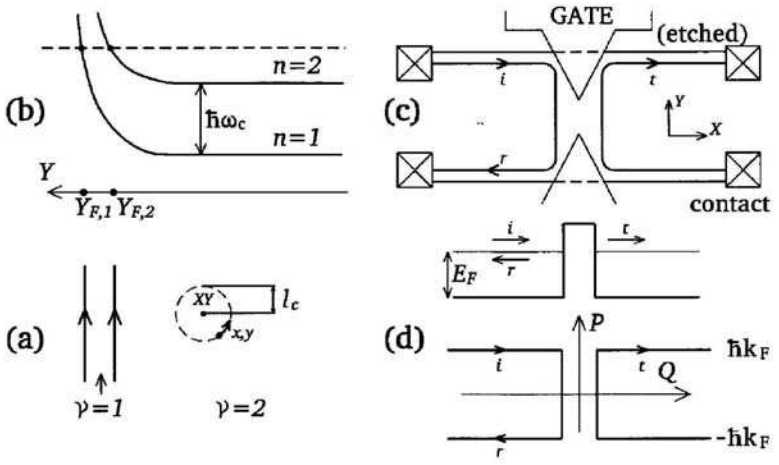

Figure 2: Left: (a) Schematic representation of edge states and of (b) the Landau level bending. (c) reflection of an edge state by a controlled artificial impurity called Quantum Point Contact. (d) analogy with 1D semiclassical trajectories in the phase space.

to $E_F + eV$, each mode contribute to increase the persistent chiral current by an equal contribution: $\Delta I = e \int_{Y_{F,n}(E_F)}^{Y_{F,n}(E_F+eV)} dy.n_\Phi(1/eB)\partial U/\partial Y = \frac{e^2}{h}V$. Thus each edge channel is associated with a conductance equal to the quantum of conductance $\frac{e^2}{h}$. This result can be equally viewed as a special case of the Landauer formula (which is valid in the more general case of quantum conductors, even in zero magnetic field) or as the quantization of Hall conductance. Landauer formula and quantized Hall conductance are direct consequence of the Pauli principle: the filling factor of quantum states is one.

2.1.3 Tunneling between edge channels

Edge channels are ideal one dimensional (chiral) conductors: the physical separation between pairs of opposite edge channels prevents backscattering and electrons propagate elastically over huge distances (∼mm at low temperature) as phonon scattering is reduced. These properties have made them a convenient tool to test the generalization of the Landauer formula: the Landauer-Büttiker relations [13, 14] derived in the context of the mesoscopic quantum transport. In order to do that it is necessary to induce intentionally elastic backscattering in a controllable way.

The tool used is a Quantum Point Contact (QPC) as shown in Fig.2(c). A negative potential applied on a metallic gate evaporated on top of the sample depletes electrons to realize a narrow constriction in the 2DEG. This allows a controllable modification of the boundaries of the sample. The separation between opposite pairs of edges channels of a given Landau level can be made so small that the overlap between wavefunctions lead to backscattering from one edge to the other. The QPC creates a saddle shape potential. When the potential at the saddle point is close but below the value $E_F - (n + \frac{1}{2})\hbar\omega_c$, electrons emitted from the upper left edge channel start to be reflected into the lower edge channel with probability $R \ll 1$ while they are still mostly transmitted with probability $T = 1 - R$. When the saddle point potential is above $U_{F,n}$ electrons are mostly reflected and rarely transmitted $T \ll 1$ and the reflection quickly reaches $R \precsim 1$.

For getting better intuition on edge channel tunneling, Fig.2(d) shows the semi classical analogy between the real space coordinates (Y, X) of the 2D Hall conductor and the (P, Q) phase space coordinate of a real 1D conductor. The physics of tunneling between opposite edge channels is clearly equivalent to that of the tunneling in a 1D system. However the chirality allows us to inject or detect electrons *at the four corners of the phase space*, something impossible with 1D systems.

Measuring the conductance is a good tool to know how many edge channels are transmitted. According to the Landauer formula, the conductance G is defined as the ratio of the current I through the QPC to the voltage difference V between the upper left and lower right contacts.

$$G = \frac{e^2}{h}(p - 1 + T) \tag{8}$$

if there are $p-1$ channels transmitted while the p^{th} channel is partially transmitted with transmission T.

Figure 3 shows the reflection of edge channels starting from $\nu = 8$ in the bulk. One starts with 8 channels transmitted and when applying negative voltage on the gate the successive reflection 6 edge channels is observed by quantized plateaux in the resistance (here, the "access" resistance $h/8e^2$ has been subtracted).

All this can be transposed to the fractional quantum Hall effect regime.

2.2 Edge states in the fractional quantum Hall regime

We will assume a spin polarized system and the first orbital Landau level partially filled: $n_s < n_\Phi$ or $\nu < 1$. Before describing fractional edge states, we will briefly present some general characteristics of the Fractional Quantum Hall effect.

Because of Landau level degeneracy, at partial filling there is a large freedom to occupy the quantum states, i.e. to fill the plane with electrons. However electrons interact and the Coulomb repulsion will reduce our freedom to distribute electrons in the plane. Let us first consider the limit of infinite magnetic field when the filling factor goes to zero. The Gaussian wavefunctions describing the

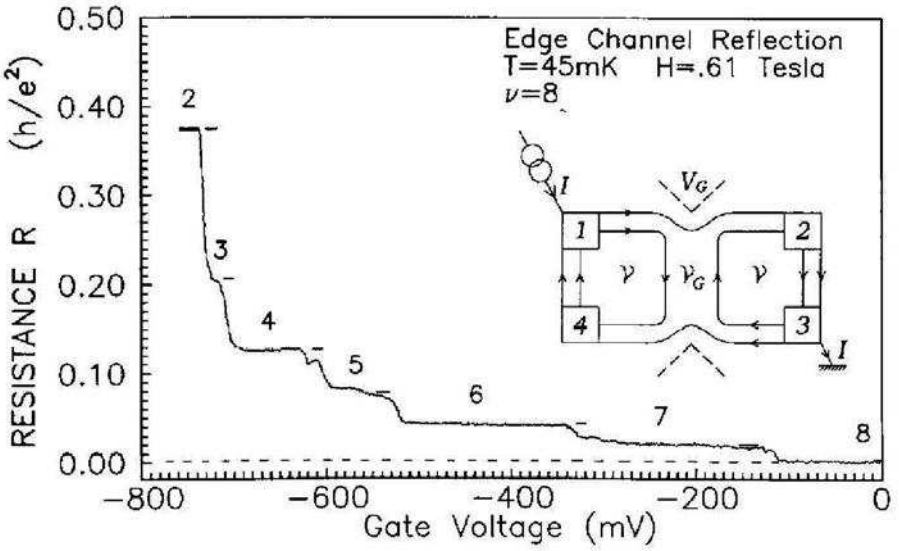

Figure 3: resistance of the QPC versus the QPC gate voltage showing the reflection of the six first edge states for $\nu = 8$, at T=45mK. The values of ν_G are indicated on the resistance plateaus. The resistance for $\nu = 8$ has been subtracted.

cyclotron motion shrink to zero. Electrons being like point charges behave classically (no overlap between quantum states) and minimize their energy to form a crystalline state (analogous to the electron crystal observed in dilute classical 2D electron systems in zero field). The Landau level degeneracy is broken and a unique ground state is formed. In the present case, weaker magnetic field, i.e. ν not too small, the wavefunctions overlap. Electrons can not be localized to a lattice but instead will form a correlated quantum liquid. For some magic filling factors, interactions will break efficiently the Landau level degeneracy to form a *unique* collective wavefunction minimizing the energy. The magic filling factors are found to be odd denominator fractions: $\nu = 1/3$,1/5, 2/3, 2/5, 3/5, 2/7, ... [15].

2.2.1 The Laughlin states

The ground state separated from a continuum of excitations by a gap Δ is described by a unique collective wavefunction. For $\nu = 1/(2s+1)$, s integer, Laughlin proposed a trial wavefunction for the ground state which was found very accurate. The wavefunction is built from single particle states in the cylindrical vector potential gauge. Using a representation of electron coordinates as $z = x + iy$ in unit of magnetic length l_c, the single particle states in the first Landau level are:

$$\varphi_m = \frac{1}{\sqrt{2\pi 2^m m!}} z^m \exp(-|z|^2). \tag{9}$$

It is instructive to look first at the Slater determinant of electrons at filling factor 1 which is a Vandermonde determinant. Its factorization gives the following wavefunction, up to a normalization constant:

$$\Psi_1 = \prod_{i<j\leq N} (z_i - z_j) \exp(-\sum_{i=1,N} |z_i|^2). \tag{10}$$

The polynomial part ensures a uniform distribution of electrons in the plane with one state, or equivalently one flux quantum, per electron on average. The zeros at $z_i = z_j$ reflects the Pauli principle and their multiplicity 1, the Fermi statistics. At filling factor $1/(2s+1)$ the polynomial for each z_i should be of degree of $(2s+1)(N-1)$ such that all electrons are also uniformly distributed on the $(2s+1)N$ states available. A uniform distribution of electrons in the plane requires a very symmetrical polynomial. Also Laughlin proposed the simple polynomial form [3]:

$$\Psi_{1/2s+1} = \prod_{i<j\leq N} (z_i - z_j)^{2s+1} \exp(-\sum_{i=1,N} |z_i|^2). \tag{11}$$

The correlation energy is efficiently minimized by the multiplicity $2s+1$ of the zeros which ensures that electrons keep away from each other. By exchanging two electrons the wavefunction is multiplied by $(-1)^{(2s+1)} = -1$. The requirement that electrons must obey Fermi statistics is satisfied. But there is more: the extra factor $(-1)^{2s}$ expresses the fact that moving two electrons around each other adds an extra phase. This phase can be viewed as the Aharanov-Bohm flux of *two* fictive flux quanta bound to each electron. This is at the origin of the composite Fermion picture mentioned below which allows to generate more complex fractions. One can also say that electrons obey a *super* exclusion principle where each particle occupies $2s+1$ quantum sates (i.e. the area of $2s+1$ flux quanta) so minimizing the interaction (there are deep connections with the concepts of exclusonic statistics and anyonic statistics [5]).

One can show that the excitations above the ground state present a gap. The meaning of the excitations is particularly clear in the case of the best known state occurring at $\nu = 1/3$. The ground state corresponds to uniform distribution of electrons, one electron per area occupied by three flux quanta. The unique wavefunction cannot be continuously deformed and the only way to decrease the density is to empty a single particle quantum state, i.e. to create a hole having the area occupied by a single flux quanta, see Fig. 4. This can be realized by multiplying the Laughlin wavefunction by $\prod_{i=1,N}(z_i - z_h)$ where z_h is the position of the hole. The so called quasi-hole carry a charge $e^* = -e/3$. The energy cost Δ_h can be obtained by estimating the energy required to create a disc of size Φ_0/B and charge $e/3$: $(4\sqrt{2}/3\pi)(e/3)^2/4\pi\varepsilon\varepsilon_0 l_c$. Similarly quasi-electron excitations with charge $e/3$ are possible and correspond to removing a flux quantum to locally increase the electronic density with an energy Δ_e. Quasi-electron or hole excitations with charge $\pm e/q$ can be generalized for other filling factor $\nu = p/q$ with q odd.

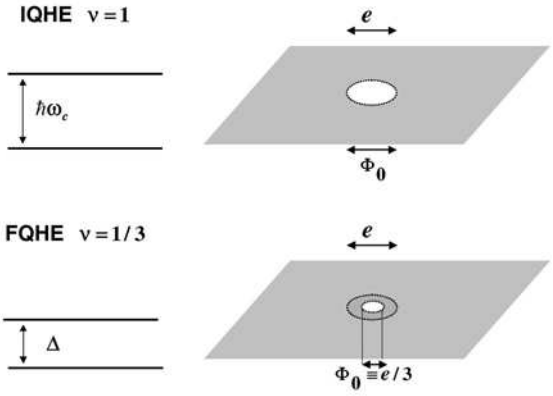

Figure 4: The introduction of an extra flux quantum in a QHE fluid leaves a hole in the collective wavefunction. In the IQHE the associated charge is e while in FQHE is it $e/3$ for $\nu = 1/3$

The excitation gap for quasi-electron quasi-hole pairs has been numerically estimated and calculations agree with a value $\Delta \simeq 0.092e^2/4\pi\varepsilon\varepsilon_0 l_c$ for $q = 3$. It does not depend on p (as far as spin polarized electrons are considered).

An interesting theoretical issue is the statistics associated with the excitations. It can be shown that when moving adiabatically two quasi-holes around each other and exchanging their positions, the collective wavefunction picks up a Berry's phase factor $\exp(i\pi/(2s+1))$. The excitations are not bosons nor fermions but obey a so-called anyonic statistics, a concept first introduced by Wilzeck in the context of particle physics.

2.2.2 Composite Fermions

Following the work of Jain [6], a hierarchy of the fractional filling factors can be made using the concept of Composite Fermions as a guide. This hierarchy followed more pioneering work made by Halperin [17] using a different approach to built higher order fractions from the basic $1/(2s+1)$ states. The concept is based on statistical transmutation of electrons in 2D (or 1D). Topological considerations show that purely 2D particles are not necessarily bosons or fermions but may have any intermediate statistics (an example is the Laughlin quasi-particles). For the same reason, it is easy to "manipulate" the statistics of 3D particles such as electrons which are Fermions provided they are forced to live in 2D (or 1D). This can be done by attaching an integer number of fictive flux quanta to each electron. The price to pay is a redefinition of the wavefunction and of the Hamiltonian. An even number of flux quanta will transform Fermions into Fermions while an odd number will transmute Fermions into Bosons. In the first case we have

Composite Fermions (CF) while in the second case Composite Bosons (CB). Both approaches have been used in the FQHE context. Both have their own merit and a bridge between them is possible. CF are believed to be appropriate for high order fractions and to describe the remarkable non Quantum Hall electronic state found at $\nu = 1/2$. CB make an interesting correspondence between the $\nu = 1/2s + 1$ states and superfluidity [7].

By attaching $2s$ flux quanta to each electron with a sign opposite to the external magnetic field flux, the resulting CF experience a reduced mean field. A mapping can then be done between FQHE states and IQHE states. As an example, for $s = 1$, the mean field attached to the "new electrons", the composite Fermions, is equivalent and opposite to the magnetic field $B_{1/2}$ at $\nu = 1/2$ [18]. The field experienced by the CF is thus $B_{CF} = B - B_{1/2}$. A filling factor $\nu = 1/3$ for electrons corresponds to a CF filling factor $\nu_{CF} = 1$. Similarly $\nu = p/(2p + 1)$ becomes $\nu_{CF} = p$. This describes a series of fractions observed between 1/2 and 1/3. For fields lower than $B_{1/2}$, $\nu = p/(2p - 1)$ also becomes $\nu_{CF} = (-)p$ and this describes fractions from 1 to 1/2. In general attaching $2s$ flux quanta to electrons describe the fractions $\nu = p/(p.2s \pm 1)$. The following table shows the correspondence for $2s = 2$:

ν	1/3	2/5	3/7	...	1/2	...	3/5	2/3	1
ν_{CF}	1	2	3	...	∞	...	3	2	1

The composite fermion picture is supported by experimental observations. The symmetric variations of the Shubnikov-de Has oscillations around $B_{1/2}$ are very similar to that observed around $B = 0$. We should emphasize that this is not a real cancellation of the external field, as the Meissner effect in superconductivity is, but the phenomenon is a pure orbital effect due to the $2s$ flux attachment. Convincing experiments have shown that the quasiparticles at $\nu \simeq 1/2$ behave very similarly to the quasiparticles at zero field ([19]; see also [20]).

The composite fermion picture can be used as a guide to understand multiple fractional edge channels.

2.2.3 Fractional edge channels

The picture of edge channels can be extended to the fractional case. Now the gap $\hbar\omega_c$ has to be replaced by the gap $\Delta_e + \Delta_h$ of the FQHE. Lets consider for example a filling factor $\nu = p/(2p + 1)$ in the bulk, i.e. p composite fermion Landau levels filled. Using this correspondence, the formation of fractional edge channels is equivalent to that described previously for the integer Quantum Hall effect. Moving from the bulk to the edge, each time a CF landau level crosses the Fermi energy a line of gapless excitation is built. These defines p chiral fractional edge channels (the last one corresponding to the 1/3 edge channel).

The CF approach for edge channels is convenient for pedagogical presentation and gives certainly a fair qualitative representation, but is certainly not complete. Including screening of the external potential in a Thomas Fermi approach is a first

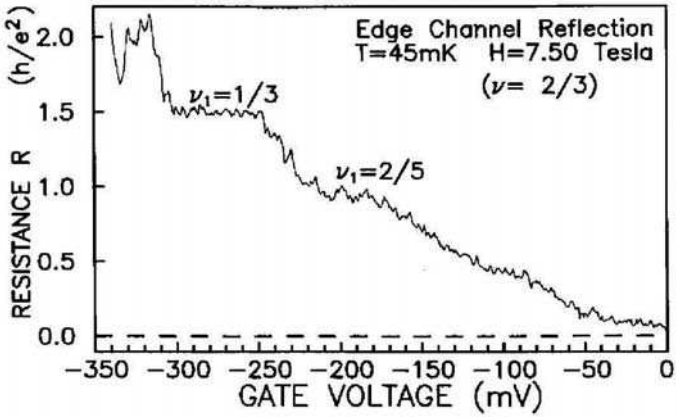

Figure 5: Fractional edge channel reflection observed for $\nu = 2/3$. The longitudinal resistance quantization indicates $\nu_G = 2/5$ and $1/3$ fractional channels. The resistance for $\nu = 2/3$ has been subtracted.

step to improve quantitatively the description [21] but this does not change qualitatively the overall picture. A important physics not included in this approach is the Luttinger liquid properties described below: it changes the transport properties. The hierarchy of fractional edge channels which can be derived in the Luttinger liquid approach coincide with that of the CF approach.

Experimentally, the existence of fractional edge channels can be probed in transport experiments using the reflection induced by a QPCs in a manner similar to the integer case. This is shown in Fig.5. Here the filling factor in the leads is $\nu = 2/3$ and the access resistance $3h/2e^2$ has been subtracted. The plateaus associated with the refection of the $2/5$ and $1/3$ edge channels are clearly observable.

The picture described here is expected to apply to smooth edges, as it is the case in ordinary samples. Another approach has been proposed for hard wall confinement in Ref.[22].

2.3 Fractional Edge Channels as Luttinger liquids

The tunnel transfer of an electron from a metallic contact to a $\nu = 1/3$ FQH liquid involves the transformation of an electron into three quasiparticles. The number of possibilities to choose 3 quasiparticles in the range eV and satisfying the energy conservation required for elastic tunneling increases rapidly with V, this immediately implies that the tunneling I-V characteristics should be non-linear. So, the fractional edge states should not behave has an ordinary Fermi liquid for which linear conduction is expected. On a different approach, a similar conclusion is obtained in the Luttinger liquid description which uses bosonic collective charge mode on the fractional edge. This is what we will describe below.

2.3.1 Hydrodynamical approach of fractional edge states

X.G. Wen [23] has first shown the deep connection between fractional edge channels and the concept of Tomonaga-Luttinger liquids[24, 25] . We will here repeat the phenomenological hydrodynamical approach of Wen in the simple case of a Laughlin state in the bulk, filling factor $\nu = 1/2s+1$. We will start with a classical approach and keep only incompressibility as a quantum ingredient.

The only possible excitations are periphery deformations of the 2D quantum Hall conductor which preserves the total area (like a 2D droplet of an ordinary liquid). This is shown schematically in Fig.6 . If we denote $y(X,t)$ the deformation of the boundary located at position $Y = Y_F$, the time varying electron density is given by:

$$n(X,Y,t) = n_s\Theta(Y - Y_F - y(X,t)) \tag{12}$$

where $n_s = \nu eB/h$ and $\Theta(x)$ is the Heaviside function. We wish to find the equations of motion for y. To do that we have to remind that, within the first Landau level, the single particle motion is given by the reduced Hamiltonian $H_1 = \frac{1}{2}\hbar\omega_c + U(Y)$ and the coordinates X and Y are conjugate with Poisson's bracket $\{X,Y\} = 1/eB$. Using the equation of motion for the 2D density: $\partial n/\partial t + \{H_1, n\} = 0$ we get the equation describing the chiral propagation of the shape deformations y at $Y = Y_F$:

$$\partial y/\partial t + v_D \partial y/\partial X = 0 \tag{13}$$

where $v_D = \frac{1}{eB}\left|\partial U/\partial Y\right]_{Y=Y_F}|$ is the drift velocity.

The potential energy associated with the deformation is

$$U = \frac{1}{2}\int dX n_s y^2 \frac{\partial U}{\partial Y} = \frac{\hbar v_D}{\nu\pi}\int dX\,(\pi n_s y)^2\,. \tag{14}$$

If we define $\widetilde{\phi}$ the charge variation integrated on the upper edge in units of π as follows:

$$\widetilde{\phi} = \pi\int_{-\infty}^{X} n_s y dX$$

and the excess charge density (per unit length) $\widetilde{\rho}$ by:

$$\widetilde{\rho} = \frac{1}{\pi}\frac{\partial\widetilde{\phi}}{\partial X} \tag{15}$$

we get the action:

$$S = -\frac{\hbar}{\pi\nu}\int dX dt \frac{\partial\widetilde{\phi}}{\partial X}\left(\frac{\partial\widetilde{\phi}}{\partial t} + v_D\frac{\partial\widetilde{\phi}}{\partial X}\right) \tag{16}$$

and the Hamiltonian is $\mathcal{H} = U$:

$$\mathcal{H} = \partial\widetilde{\phi}\partial X\Big)^2 \tag{17}$$

$$= \frac{hv_D}{2\nu}\int dX\,(\widetilde{\rho})^2\,. \tag{18}$$

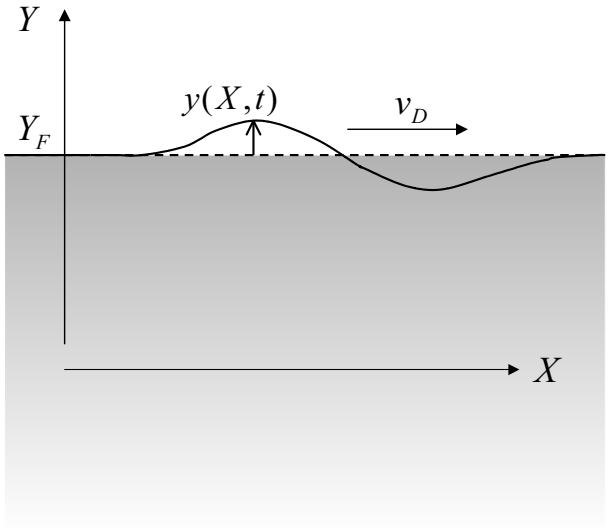

Figure 6: Wen's approach for the Chiral Luttinger liquid picture of a fractional edge channel at $\nu = 1(2s+1)$. The incompressibility of the FQHE fluid allows only periphery deformations $y(X,t)$ propagating at the drift velocity.

So far the model is purely classical. By defining the conjugate of $\widetilde{\phi}$ as $\widetilde{\pi} = -\frac{\hbar}{\pi\nu}\partial\widetilde{\phi}/\partial X$ and we can quantize the fields using:

$$\left[\widetilde{\pi}(X), \widetilde{\phi}(X')\right] = i\hbar\delta\left(X - X'\right) \tag{19}$$

At first sight, the dynamic of the bosonic modes describing the periphery deformations seems not contain more physics than that of phonons or photons. The non trivial physics arises when adding from outside an electron to the edge or removing a Laughlin quasiparticle to transfer it to the opposite edge, as it is the case in tunneling experiments. Such operation involves an infinite number of bosonic modes. This is at the origin of strong non-linearities in the transport properties, a property not shared by ordinary Fermi liquids.

By definition, the creation operator $\psi^\dagger$ for one electron on the upper edge satisfies:

$$\left[\widetilde{\rho}(X), \psi^\dagger(X')\right] = \delta(X - X')\psi^\dagger(X'). \tag{20}$$

On the other hand, the 1D excess density $\widetilde{\rho}$ is related to the conjugate of $\widetilde{\phi}$ by $\widetilde{\pi} = -\frac{\hbar}{v}\widetilde{\rho}$ and we have

$$\left[\widetilde{\rho}(X), \widetilde{\phi}(X')\right] = -i\nu\hbar\delta\left(X - X'\right) \tag{21}$$

which immediately implies

$$\psi^\dagger \propto \exp(i\widetilde{\phi}/\nu). \tag{22}$$

$\psi^\dagger$ creates a unit charge at X but it is not an electron operator unless it satisfies Fermi statistics. Exchanging two electrons at position X and X' gives $\psi^\dagger(X')\psi^\dagger(X) = \exp(-i\frac{\pi}{\nu}sgn(X-X'))\psi^\dagger(X)\psi^\dagger(X')$. The requirement that the bare particles are Fermions implies

$$\nu = 1/(2s+1). \tag{23}$$

The beauty of Wen's hydrodynamical approach is that the series Laughlin filling factors appear $1/(2s+1)$ naturally as a consequence of incompressibility and Fermi statistics.

To obtain more fractional filling factors, one must introduce additional bosonic modes at the periphery (for example: p modes for $p/(2ps+1)$ which is consistent with the composite fermion approach.

Finally, one can define similarly the quasiparticle operator which creates a charge $1/(2s+1)$ on the edge:

$$\left[\widetilde{\rho}(X), \psi^\dagger_{qp}(X')\right] = \nu\delta(X-X')\psi^\dagger_{qp}(X') \tag{24}$$

which writes as

$$\psi^\dagger_{qp} \propto \exp(i\widetilde{\phi}). \tag{25}$$

It shows *fractional* statistics $\psi^\dagger_{qp}(X')\psi^\dagger_{qp}(X) = e^{(-i\pi\nu sgn(X-X'))}\psi^\dagger_{qp}(X)\psi^\dagger_{qp}(X')$ as do a Laughlin quasiparticle.

The above set of equations for the electron operator $\psi^\dagger$ and for the bosonic modes are characteristics of those of a Luttinger liquid. Because of the direction of propagation imposed by the magnetic field (no counter propagating mode on the same edge) it is called a Chiral Luttinger Liquid. The conductance $\nu e^2/h$ correspond to the conductance ge^2/h of a Luttinger Liquid and one usually identifies $g=\nu$. As for Luttinger liquids there is an algebraic decay of the correlation functions.

We have $\left\langle \widetilde{\phi}(X,t)\widetilde{\phi}(0,0)\right\rangle = \langle 0| e^{i\mathcal{H}t}\widetilde{\phi}(X)e^{-i\mathcal{H}t}\widetilde{\phi}(0)|0\rangle = const.- \nu\ln(X - v_D t)$ and the time ordered single-particle Green's function: $\langle 0|T\left\{\psi^\dagger(X,t)\psi(0,0)\right\}|0\rangle = \exp\left(\frac{1}{\nu^2}\left\langle\widetilde{\phi}(X,t)\widetilde{\phi}(0,0)\right\rangle\right)$ decreases as $(X-v_Dt)^{-1/\nu}$. For 1/3 one see that this is the product of 3 Green's functions, reminiscent from the fact that an electron has to fill 3 states (or excite 3 quasiparticles). This gives a Tunneling Density of State (TDOS) for electrons injected at energy ε above the Fermi energy E_F which decreases as $\sim |\varepsilon - E_F|^{(1/\nu-1)}$. This implies that, for electrons tunneling between a Fermi liquid and a chiral Luttinger fractional edge channel, the finite temperature tunnel conductance $G(T)$ and the zero temperature differential conductance dI/dV show the following power laws:

$$G(T) \sim (T/T_B)^\gamma \tag{26}$$

$$\frac{dI}{dV} \sim (V/V_B)^\gamma \tag{27}$$

$$\gamma = \frac{1}{\nu} - 1 \tag{28}$$

where T_B and V_B are related to the coupling energy of the tunnel barrier. Power laws characterizing the chiral Luttinger liquid in the Fractional Quantum Hall regime have been experimentally observed (see below).

The chirality leads to some differences with ordinary Luttinger Liquids for which $1/\nu$ is to be replaced by $(g^{-1} + g)/2$. In 1D, g is related to the strength of a short range interaction which can take arbitrary values and the relation: $\gamma = (g + g^{-1} - 2)$ always holds. A *continuous variation* of the $g = \nu$ parameter is a priori not expected in the FQHE regime because the magnetic field stabilizes special fractional values of ν in the bulk (as the Jain's series). A generalization of Wen's approach for $\nu = p/(2sp + 1)$ shows that one must have p branches of bosonic modes (consistent with the CF picture). These branches interact together and give a relation between the tunneling exponent γ and ν not simply given by 28. For the simplest series of Jain's filling factor $p/(2p \pm 1)$ between 1 and 1/3 , the exponent γ is expected to be

$$\gamma = \frac{2p+1}{p} - \frac{1}{|p|} \tag{29}$$

i.e. constant ($\gamma = 2$) between filling factor 1/2 and 1/3 and decreasing linearly ($\gamma = 1/\nu \sim B$) form 2 to 1 between filling factor 1/2 and 1.

2.3.2 Experimental evidence of chiral Luttinger liquids

Tunneling electrons from a metal to the edges. The best evidence for Luttinger liquid properties is obtained by probing the tunneling density of states (TDOS). To do that, measurements have to be *non-invasive*, i.e. a weak tunnel coupling is required. Indeed, a tunneling experiment measures the TDOS only if higher order tunneling process are negligible, which means small transmission and small energy. At large energy, the current varies $\sim |\varepsilon - E_F|^{\gamma+1}$ and so the effective coupling will increase with voltage $\varepsilon \equiv eV$ or temperature $\varepsilon \equiv k_B T$.

Convincing experiments have been performed by the group of A.M. Chang [26, 27, 28]. The tunnel contact is realized using the cleaved edge overgrowth technique. By epitaxial growth on the lateral side of a 2DEG, a large tunnel barrier is first defined followed by a metallic contact realized using heavy doped semiconductor. The advantage is weak coupling and high enough barrier (to disregard change of the transparency when applying a large voltage). Also, probably important is the fact that the metallic contact close to the edge provides screening of the long range Coulomb interaction (short range is needed for having power laws).

Fig.7 shows example of I-V characteristics: a power law of the current with applied voltage $I \sim V^{\alpha}$, $\alpha = \gamma + 1$, is well defined over several current decades for $\nu = 1/3$. The exponent α found is 2.7-2.65 close to the value 3 predicted by the theory for $\gamma = \frac{1}{\nu} - 1$. For other filling factors similar algebraic variations are also observed. In the same figure, the tunneling exponent deduced from a

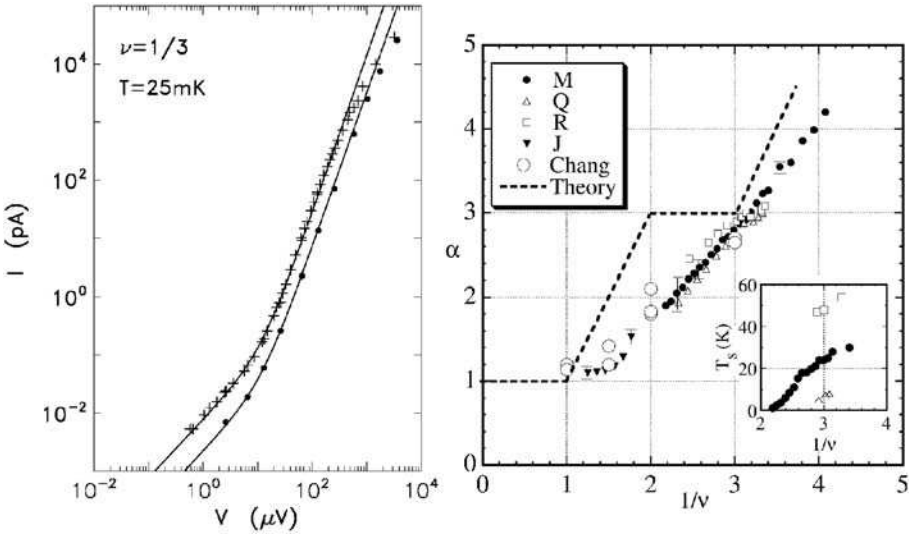

Figure 7: Left : Log-Log plot of an I-V curve at $\nu = 1/3$ clearly shows the algebraic variation of current with voltage which characterizes a Luttinger liquid. Right : the exponent α is plotted versus $1/\nu$ and compared with theoretical predictions (adapted from Ref.) .

series of I-V curves is shown as a function of the magnetic field or $1/\nu$. For filling factor $1/2 < \nu < 1/3$ the constant exponent predicted [29, 30, 31] is not observed and instead the exponent varies rather linearly with field or $1/\nu$. However, some experiments made with the cleanest samples have shown signs of a plateau in the exponent in a narrow filling factor value near 1/3.

Theoretical attempts to explain quantitatively the discrepancies have been made. Taking into account the long range Coulomb interaction slightly lowers the exponent. The modified Luttinger liquid theories can also include the finite conductivity in the bulk for non fractional filling factors. Indeed a finite conductivity modifies the dispersion relation of the bosonic chiral modes and so the exponents. With reasonable parameters these modifications are not yet able to fully reproduce the data [30, 31]. The discrepancy between experiments and predictions may be due to the reconstruction of the edge. Wen's model assume a sharp density variation at the edge of the 2D sample. In real samples, the density decreases smoothly and some additional edge states corresponding to filling factor lower than the bulk filling factor may also strongly modify the exponents. A recent work by Mandal and Jain shows that taking into account interactions between composite fermions chiral edges may lead to a continuous variation of the exponent[32]. The reader will find more in recent review made by A.M. Chang [33].

Tunneling between edges: Fractional Edge channel with an artificial impurity. Transport experiments between two fractional edges can be done using an artificial impurity, a Quantum Point Contact. Contrary to previous experiments where electrons were injected from an ordinary metal (Fermi liquid) and the coupling was weak, we can probe here the transfer of charge *through* the FQHE fluid. In particular there is no restriction on the nature of the charge (obviously e in the previous case) while they can be fractional here. For quantitative comparison to theory, this strategy however is less reliable than the previous one. For finite voltage difference V_{ds} applied across the QPC to induce a current, the shape of the scattering potential can change. This can induce a trivial variation of the transmission with V_{ds} which can make identification of power laws difficult. Measurements are thus reliable only at very low temperature (<100mK) and small voltages (<100μV) for comparison with theories.

Strong barrier. We first consider the case where barrier is high and a tunnel barrier is formed (so-called pinch-off regime). Electrons are strongly backscattered at all energies and the tunneling current is weak. The results are expected similar to that obtained in A.M. Chang's experiments. Tunneling occurring between two fractional edge (and not between a metal and a fractional edge) the dI/dV_{ds} characteristics will be proportional to the *square* of the TDOS. The exponents for the conductance is doubled. For example $\gamma = 4$, i.e. $2.(\frac{1}{\nu} - 1)$ for $\nu = 1/3$. This approach has been used by several groups. A difficulty is that sample inhomogeneities around the QPC may lead to transmission resonances difficult to control. Ref.[34] exploits the Luttinger predictions for tunneling through such a resonant state. A further difficulty is the high value of the power law for the conductance with temperature or voltage which is is expected to be measurable only at very low conductance. For $\nu = 1/3$, for example, exact finite temperature calculations of IV characteristics, see below, shows that the exponent 4, becomes the dominant term only when the conductance is smaller than $10^{-4}e^2/3h$ [35] . Otherwise an effective exponent, much smaller than 2 is observed. Up to now, no experimental group have tried to do measurements in this limit.

Weak barrier. The regime where the barrier is very weak is more interesting. Practically, the QPC gently pushes the upper edge close to the lower edge to induce a quantum transfer of particles from one edge to the other. The QPC potential is weak enough to not make appreciable change of the local filling factor. A characteristic signature of the Luttinger liquid physics is the *vanishing* transmission at low temperature or bias voltage even in the case of a so weak coupling that the transmission would be close to 1 in absence of interaction. The low energy strong backscattering limit continuously evolves toward a weak backscattering limit at large energy (large transmission). In this regime, we will see later that integer charges tunnel at low energy, while fractional charges tunnel at large energy.

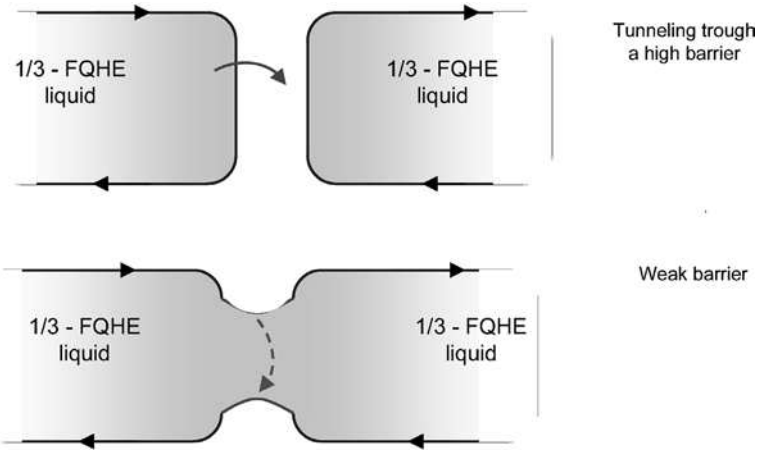

Figure 8: Schematic view of charge transfer in the case of a strong barrier (upper figure) and a weak barrier. In the later case the FQHE fluid is weakly perturbed and charge transfer occurs via the FQHE fluid.

To describe the tunneling between the upper and lower edge of Fig.8 we introduce bosonic modes $\widetilde{\rho}$ and $\widetilde{\phi}$ previously derived with the subscript $+/-$ for the upper and lower modes respectively. Without coupling by the artificial impurity, they are independent and the Hamiltonian is the sum of their Hamiltonian. The impurity of strength λ situated in $X = 0$ induces a coupling between the excitations: $\simeq \psi^{\dagger}_{qp,+}\psi_{qp,-} + \psi^{\dagger}_{qp-}\psi_{qp+}$ which gives the interaction term:

$$\mathcal{H}_{int} = \lambda \cos(\phi_+(0) - \phi_-(0)). \tag{30}$$

At low energy, the system flows to an insulating state and the conductance displays the same power law with T or V_{ds} than the one expected for a strong impurity potential (tunnel barrier)

$$G \sim \frac{e^2}{3h}\left(\frac{\varepsilon}{T_B}\right)^{2(\frac{1}{\nu}-1)} \to 0 \quad \text{for } \varepsilon \ll T_B \tag{31}$$

where T_B is an energy scale related to the impurity strength λ. At large energy, a conductance close but smaller than the quantum of conductance $\frac{e^2}{3h}$ is recovered. The Luttinger liquid theory predicts

$$G = \frac{e^2}{3h} - G_B \quad \text{with } G_B = \frac{e^2}{3h}\left(\frac{\varepsilon}{T_B}\right)^{2(\nu-1)} \to 0 \quad \text{for } \varepsilon \gg T_B. \tag{32}$$

G_B is called the backscattering conductance. If we call I the forward current, $I_0 = \frac{e^2}{3h}V_{ds}$ the current without impurity, the current associated with particles

backscattered by the impurity is $I_B = I_0 - I$ from which one can define $G_B = I_B/V$. The above formula correspond to *strong* and *weak* backscattering limits. In the first case there is a weak tunneling of particles between the left and right side, while in the second case there is a weak quantum transfer of particles between the upper edge and the lower edge. There is an interesting *duality* with $\nu \longleftrightarrow 1/\nu$.

Conformal field theories have been used to exactly solve the problem of a Luttinger liquid with one impurity providing a continuous description between both limits [36, 37]. The so-called FLS theory exploits the charge conservation when the particle are scattered by the impurity centered in $X = 0$. By defining the even and odd charge modes (and corresponding fields):

$$\widetilde{\rho^e}(X,t) = \frac{1}{\sqrt{2}}\left(\widetilde{\rho_+}(X,t) + \widetilde{\rho_-}(-X,t)\right) \tag{33}$$

$$\widetilde{\rho^o}(X,t) = \frac{-1}{\sqrt{2}}\left(\widetilde{\rho_+}(X,t) - \widetilde{\rho_-}(-X,t)\right) \tag{34}$$

for which the variable X is now limited to the semi-infinite line $X \leq 0$.

The Hamiltonian to consider reduces to:

$$\mathcal{H} = \frac{hv_D}{2\nu}\int_{-\infty}^{0} dX\left[\widetilde{\rho^o}(X,t)^2 + \lambda_1 \cos\left(\sqrt{2}\widetilde{\varphi^o}(0)\right)\right] \tag{35}$$

while the even mode is decoupled.

The equation is very similar to a Sine-Gordon equation (SG) but with the SG term only at the boundary, while $\widetilde{\rho^o}$ is solution of a free propagation equation (velocity v_D) for $X < 0$. Classically, it is easy to show that this boundary SG equation admits solutions using a combination of the natural kink and anti-kink of the ordinary SG equation. By definition, a kink (or a soliton) in the field (of the charge density) which is solution of the ordinary SG equation propagates without deformation and is also solution of the free propagation equation for $X < 0$. By linearity, superpositions of kink and anti-kinks are also solutions. The effect of the boundary term is mainly to convert kink into antikink. Physically, the effect of scattering is that a positive pulse of charge can be reflected as a negative pulse. The step from classical to quantum integrability is made using conformal field theories [36, 37]. One can show that applying a voltage bias V_{ds} between reservoirs emitting electrons in the upper and lower edges is, in the convenient basis for interacting electrons, equivalent to send a regular flow of kink which are randomly transformed into antikink. Kink and antikink respectively contribute to the forward and backscattered current. The Landauer formula adapted to this approach gives the backscattering current which expresses simply as:

$$I_B(V_{ds}, T_B) = ev_D\int_{-\infty}^{A(V_{ds})} d\alpha\rho_+(\alpha)\left|S_{+-}(\alpha - \alpha_B)\right|^2 \quad \text{and} \quad I = \nu\frac{e^2}{h}V_{ds} - I_B \tag{36}$$

were $\rho_+(\alpha)$ (not to be confused with previous notations) is the density of incoming

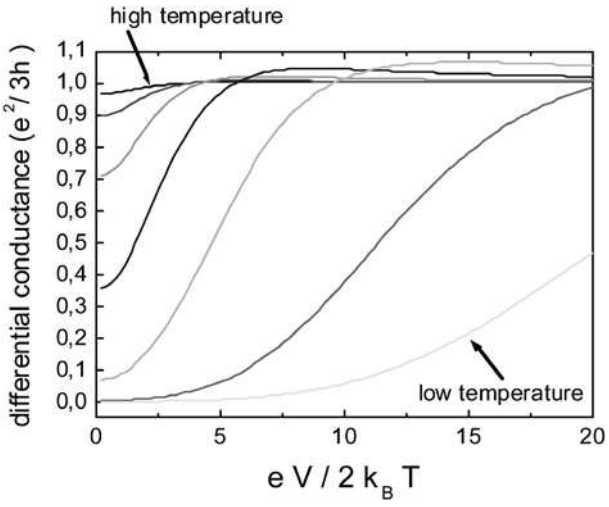

Figure 9: Theoretical curves for the differential conductance versus voltage calculated for different values of the ratio T/T_B. The numerical exact solution of Ref.[36, 37] is used. The conductance is a universal function of the variable T/T_B and $eV_{ds}/2\pi k_B T$.

kink at energy parametrized by e^{α}, and

$$|S_{+-}(\alpha - \alpha_B)|^2 = \frac{1}{1 + \exp\left[2(1-\nu)(\alpha - \alpha_B)/\nu\right]} \tag{37}$$

is the probability for kink to anti-kink conversion (the scattering probability) with α_B related to the impurity strength T_B. A series expansion in T_B/V_{ds} and V_{ds}/T_B for respectively weak and strong backscattering gives the current where all coefficients are known analytically

$$I_B = \nu \frac{e^2}{h} V_{ds} \sum_n \nu a_n(\nu) \left(\frac{V_{ds}}{T_B}\right)^{2n(\nu-1)} \quad \text{for} T_B/V_{ds} < 1 \tag{38}$$

$$I = \nu \frac{e^2}{h} V_{ds} \sum_n a_n(\frac{1}{\nu}) \left(\frac{V_{ds}}{T_B}\right)^{2n(\frac{1}{\nu}-1)} \quad \text{for} V_{ds}/T_B < 1. \tag{39}$$

The curve $I(V_{ds})$ describing the whole transition from strong to weak backscattering can be calculated. Note again the duality $\nu \longleftrightarrow 1/\nu$. For finite temperature numerical solutions are also available giving the whole information $I(V_{ds}, T)$.

For finite temperature, one can show that the conductance is a function of the reduced variable T/T_B and $eV_{ds}/2\pi k_B T$:

$$G(T, V_{ds}) = \frac{e^2}{3h} f\left(\frac{T}{T_B}, \frac{eV_{ds}}{2\pi k_B T}\right) \tag{40}$$

and measuring $G(T, 0)$ fixes the only parameter T_B. The V_{ds}/T scaling law also can be tested very accurately. Fig.9 shows theoretical calculations of the differential conductance for various values of the parameter T_B (the Bethe ansatz method for calculating the kink-antikink distribution at finite temperature has been used for the numerical calculation following the results of Ref.[36, 37]. We can see that, increasing the energy (the voltage or the temperature), leads to a progressive transition from the strong backscattering regime to the weak backscattering regime.

Fig.10 shows data obtained in our group for the conductance in the strong backscattering regime for $\nu = 1/3$. Experiments are made in the intermediate regime (i.e. $G > 10^{-4}e^2/3h$). The effective exponent deduced from a series a dI/dV_{ds} curve for different impurity strength is compared with the effective one calculated using the finite temperature exact solution. The agreement is rather good. The theoretical graph in inset of the figure shows that the asymptotic scaling exponent $2(\nu^{-1} - 1) = 4$ is not expected except for conductance lower than 10^{-4}, which is experimentally difficult to obtain. It is important to say that there are no adjustable parameters.

Indeed, there are still many open problems for a quantitative description of conductance measurements using the Luttinger liquid model. Long range interactions are one of this. One can show that the dispersion relation bosonic chiral edges modes which usually varies linearly with the wavenumber k get a contribution $k \ln(k)$. Such contribution is known from edge magneto-plasmon radiofrequency experiments realized in classical or in quantum Hall 2D electron systems where the neutral collective modes are excited and resonantly detected. When the energy is low enough such that the wavelength is larger than the width of the sample, the Coulomb interaction couple the edges. The power law of the TDOS is lost. Instead the TDOS is expected to vary with energy like $\exp(const \times (\ln \varepsilon)^{3/2})$ [38, 39, 40].

3 Fractionally charged carriers

Can an electrical current be carried by fractional charge? From quantum electrodynamics and charge conservation, it is known that the total charge of an isolated body should always be an integer number in units of e. While particles propagating freely in the vacuum are restricted to integer charge, no such absolute requirement is imposed in condensed matter to quasiparticles, the elementary excitations above the ground state which carry the current. They are the product of a complex collective motion of many particles. The topological singularities of the wave-functions may lead to many possibilities. The solitonic excitations predicted in polyacetylene or the Laughlin charges in the Quantum Hall regime are exact fractions. Fractions

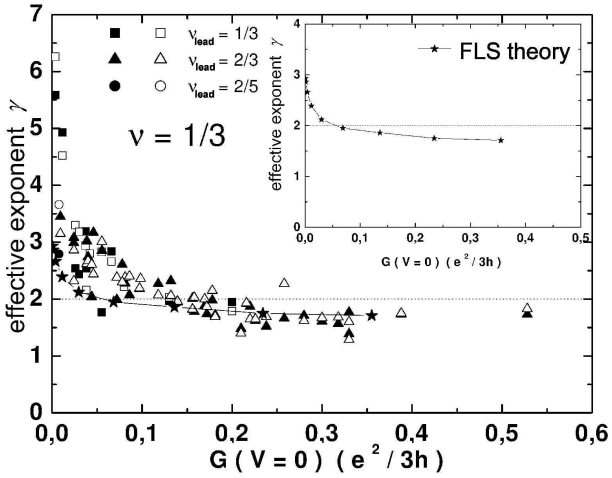

Figure 10: Exponent of the algebraic variation of the differential conductance with voltage measured in the strong backscattering regime versus the zero bias conductance normalized to $e^2/3h$. The solid line is a comparison with the FLS predictions. The scaling exponent $\alpha = 2(\nu^{-1} - 1) = 4$ is only expected in a regime of extremely low conductance (10^{-4}).

manifest particular evident or hidden symmetries. The quasiparticle charge may not be restricted to exact mathematical fraction: in Luttinger liquid theories, describing one-dimensional interacting systems, charge ge and $(1-g)e$ are expected where g is related to the interaction strength. It can take any value between 0 and 1.

Up to now the only experimentally realizable system able to display fractional charge carriers is the FQHE. But how to measure the charge carrying the current? Conductance is unable to probes directly the charge. It informs on the average rate of quasiparticles received by a contact which went through the conductor after they have been emitted by another contact. Conductance measures the quasiparticle transmission and, if interference are observed, it is sensitive to the wave nature of the quasiparticles. This is similar to optics where the average intensity of light tells about transmission but says nothing about the photon. To probe the graininess of the current one must make a further step and consider the fluctuations: the so-called shot noise. Measuring the fluctuation of light beams has given the direct evidence of the photon as the elementary grain of light. Similarly, measuring the electrical current fluctuations gives a direct information on the quanta of charge carrying the current.

According to Schottky [41], the random transfer of charge q across a conductor generates an average current $\overline{I}$ but also finite temporal fluctuations of the current ΔI around the mean value.

Consider an observation during a finite time τ. The current is related to the average number of transferred electrons $\overline{N}$ via $\overline{I} = q\overline{N}/\tau$, while the square of the current fluctuations are $\overline{(\Delta I)^2} = q\overline{I}/\tau \frac{\overline{(\Delta N)^2}}{\overline{N}}$. If the statistics of transfer events is Poissonian $\overline{(\Delta N)^2} = \overline{N}$ the well known Schottky formula is obtained:

$$\overline{(\Delta I)^2} = 2q\overline{I}\Delta f = S_I \Delta f \tag{41}$$

where we have introduce the effective frequency bandwidth of measurement $\Delta f = 2/\tau$ and the current noise power S_I. The noise power is directly proportional to the carrier charge q . This expresses that noise is a direct consequence of charge granularity. The simultaneous measure of the average current and its fluctuations gives a simple direct measurement of q, free of any geometrical or material parameters.

To measure shot-noise, one performs a non-equilibrium experiment and therefore probe excitations above the ground state: the quasiparticles. Also, the bias voltage across contacts has to be larger than k_BT otherwise the dominant noise measured is the thermal or Johnson-Nyquist noise: $S_I = 4Gk_BT$. Johnson-Nyquist noise is an equilibrium quantity which only probes conductance and not the charge of the excitations.

3.1 Shot-noise in quantum conductors

Here we discuss the origin and properties of noise in conductors. This applies immediately to the case of the Integer QHE regime. For simplicity we consider a single mode conductor or equivalently single edge channel. An artificial impurity, for example a Quantum Point Contact, is used to induce backscattering. According to the Landauer formula the left contact injects electrons at a rate eV/h where V is the voltage applied between the left and the right contact. This leads to an incoming current $I_0 = e(eV/h)$. If $\mathcal{T}$ is the transmission through the QPC, the transmitted current is:

$$I = \mathcal{T}.I_0 = \mathcal{T}\frac{e^2}{h}V \tag{42}$$

and the backscattered current:

$$I_B = I_0 - I = (1-\mathcal{T})\frac{e^2}{h}V. \tag{43}$$

One can show that the Fermi statistics is responsible of a remarkable properties: for long observation time, the incoming current appears to be noiseless (each electron arrives regularly at a frequency eV/h leading to a temporally structureless electron flow). As a result the only fluctuations arise from the binomial probability to be transmitted or reflected. The spectral density S_I of the low frequency current fluctuations is thus given by [42]:

$$S_I = 2eI_0\mathcal{T}(1-\mathcal{T}). \tag{44}$$

For multimode conductors $\mathcal{T}_n$ denoting the transmission of the n^{th} mode, the generalization is straightforward and is: $S_I = 2eI_0 \sum_n \mathcal{T}_n(1-\mathcal{T}_n)$. This prediction has been quantitatively verified in very sensitive shot noise measurement using QPC [43, 44]. A review on the remarkable low noise of quantum conductors can be found in [45]. At finite temperature, the shot noise is:

$$S_I = 2e\frac{e^2}{h}\left(\mathcal{T}^2 k_B T + \mathcal{T}(1-\mathcal{T})eV\coth\left(\frac{eV}{2k_BT}\right)\right). \tag{45}$$

At zero bias voltage the Johnson Nyquist equilibrium noise $4\left(\mathcal{T}\frac{e^2}{h}\right)k_BT$ is recovered. Above a cross-over voltage $k_BT/2e$, shot noise dominates.

Two limits are interesting to consider for the following:

- Strong backscattering regime $\mathcal{T} \ll 1$: this is the regime of Poissonian transfer from left to right of charge e.

$$S_I = 2eI \quad ; \quad I \ll I_0. \tag{46}$$

- Weak backscattering regime $1-\mathcal{T} \ll 1$: most electrons are transmitted, but there is of Poissonian transfer of "missing electrons", i.e holes, from left to right. Alternatively, in the IQHE regime, this can be viewed as Poissonian transfer of electron from the upper to the lower edge *via* the QHE fluid

$$S_I = 2eI_B \quad ; \quad I_B = I_0 - I \ll I_0. \tag{47}$$

3.2 Shot-noise in the fractional regime

In the limit of small transmission ($I \ll I_0$, strong backscattering) it is reasonable to expect transfer of charge e as correlations between left and right FQHE quantum fluids are reduced. However, for large transmission ($I_B = I_0 - I \ll I_0$, weak backscattering) the weak effect of the impurity will not affect the FQHE correlations, the Poissonian transfer of holes may correspond to Laughlin quasihole with fractional charges as shown schematically in Fig.11.

A complete understanding requires to include the Luttinger liquid dynamics of the fractional edge channels. This has been done in these two limiting cases in Ref.[46] and then by using the exact FLS Theory. For Laughlin filling factor $\nu = 1/(2s+1)$, including finite temperature, the strong and weak backscattering limiting cases give respectively:

$$S_I \simeq 2eI\coth(eV/2k_B\theta) \qquad I \ll I_0 = \frac{1}{3}\frac{e^2}{h}V \tag{48}$$

$$S_I \simeq 2\frac{e}{2s+1}I_B\coth(\frac{e}{2s+1}\frac{V}{2k_BT}) \qquad I_B = I_0 - I \ll I_0. \tag{49}$$

Here, the Johnson-Nyquist thermal noise contributions $4Gk_BT$ and $4G_Bk_BT$ have been subtracted respectively for clarity. In the first case only electrons are found

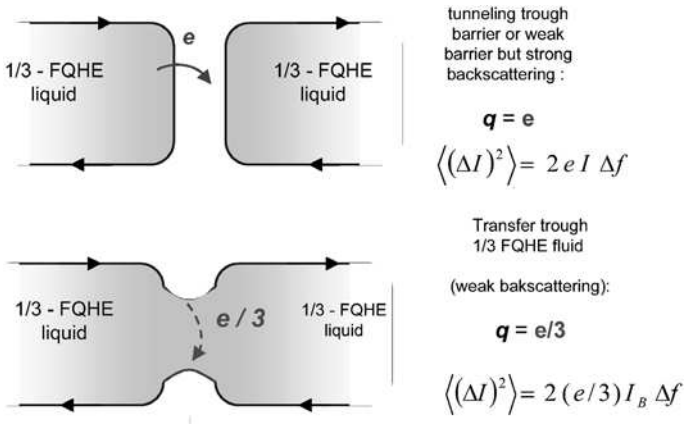

Figure 11:

to tunnel as expected. In the second case fractional charge excitations are found. In this limit, the noise provides a *direct* way to measure the fractional Laughlin charge $e/2s+1$.

A fractional $e/(2s+1)$ charge is also found in the argument of the coth function. However the meaning is different. The cross-over from thermal to shot noise corresponds to electro-chemical potential difference $\Delta\mu = eV/(2s+1)$ comparable to k_BT. However, this is not a measure of the fractional quasiparticle charge. This is a measure of the fractional filling of the quantum state at equilibrium, like the conductance $e^2/(2s+1)h$ is. This is only in the large voltage limit that $S_I \simeq 2(\frac{e}{2s+1})I_B$ really measures the quasiparticle charge. This is a non-equilibrium regime where quasiparticles excitations dominate over ground state properties. Nevertheless observation of a three times larger voltage for the thermal cross-over in noise experiments has been an important confirmation of Eq.49.

The zero temperature limit of expressions 48 and 49 have been also derived in [47] using Luttinger liquid in the perturbative limit. The exact solution of the FLS model presented in the previous section allows not only to calculate the current in all regimes but also to calculate the noise [36]. To obtain the noise, one can mimic the wavepacket approach used by T. Martin and R. Landauer for the noise of non interacting Fermions Ref.[48] . The incoming kinks of the field $\widetilde{\phi^o}$ correspond to a regular flow of solitons in $\widetilde{\rho^o}$. The regular flow is noiseless but the random scattering of kinks into anti-kinks produces noise in the outgoing current. When $|S_{+-}(\alpha-\alpha_B)|^2 \ll 1$ this a Poissonian process while if $|S_{+-}(\alpha-\alpha_B)|^2$ is not negligible, the statistics is binomial and the fluctuations are proportional to $|S_{+-}(\alpha-\alpha_B)|^2(1-|S_{+-}(\alpha-\alpha_B)|^2)$ which plays the role of the $\mathcal{T}(1-\mathcal{T})$ factor

for non-interacting electrons. The expression for the noise is thus simply

$$S_I(V) = 2e^2 v \int_{-\infty}^{A(V_{ds})} d\alpha \rho_+(\alpha) \left|S_{+-}(\alpha - \alpha_B)\right|^2 \left(1 - \left|S_{+-}(\alpha - \alpha_B)\right|^2\right). \quad (50)$$

Here $\nu = 1/(2s+1)$. Exact expressions and technical mathematical details can be found in Refs [36]. The special simple form of $|S_{+-}(\alpha - \alpha_B)|$ leads to a relation between current and noise where $S_I = \frac{v}{1-v}(V\frac{dI}{dV} - I) = \frac{v}{1-v}(I_B - V\frac{dI_B}{dV})$. From it, using the weak and strong backscattering limits of the Luttinger theory, we can easily check that $S_I \to 2(\nu e I_B)$ and $2eI$ respectively in agreement with the zero temperature limit of 48 and 49. Finite temperature predictions can also be found in Ref. [37].

3.3 Measurement of the fractional charge using noise

A difficulty of shot noise measurements in the FQH effect is that the extremely low shot noise has to be extracted from the background of relatively large amplifiers noise. Shot noise levels are extremely small both due to the smaller charge and the small available current. The latter is restricted by the fact that the FQH effect breaks down when the applied voltage is larger than the excitation gap. This excitation gap, in turn, depends crucially on the quality of the material in which the 2DEG resides. The state of the art technology currently yields samples with an excitation gap of the of the order of a few 100 μeV, leading to shot noise levels in the $10^{-29} A^2/Hz$ range.

These measurements have been performed in Saclay and in the Weizmann Institute [49][50]. A QPC is used in order to realize a local and controllable coupling between two $\nu = 1/3$ fractional edges to partially reflect the incoming current. The experiments are designed to have a best sensitivity for the weak coupling limit where Poissonian noise of the $e/3$ Laughlin quasiparticles is expected. In the experiment of Ref.[49], a cross correlation technique detects, at low frequency, the anticorrelated noise of the transmitted current I and the reflected current I_B, i.e. $S_{I,I_B} = \langle \Delta I \Delta I_B \rangle / \Delta f \simeq -2(e/3) I_B$, see Fig.12. In situ measurements of the Johnson-Nyquist noise versus temperature provide self-calibration of the current noise measured and are found consistent with independent calibration, so the shot noise is free of adjustable parameters. The magnetic field corresponds to a filling factor 2/3 in the bulk of the sample and a small region of filling factor 1/3 is created close to the QPC using the depletion effect of the gates. The size of the 1/3 region is estimated about 150 ϕ_0, sufficient to establish FQHE correlations. The advantage of doing this is that the coupling between edges occurs on a shorter scale and the controllable QPC potential is larger than the potential fluctuations inherent of sample fabrication. In the two samples measured, the combination of QPC and random potential lead to two dominant paths for backscattering. The coherent interference between paths gives rise to nearly perfect resonant tunneling peaks in the conductance. Careful measurements of the conductance resonance showed that

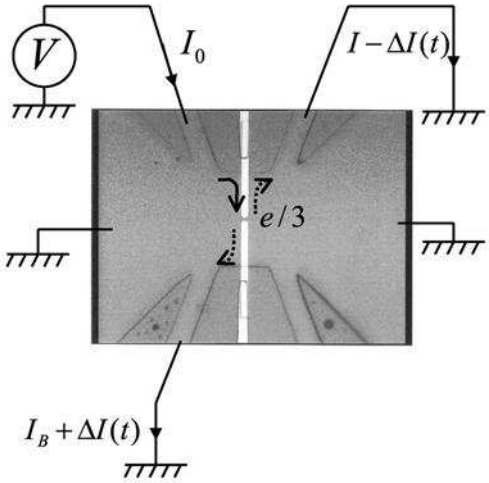

Figure 12: schematic view of the measurement. The fluctuations of the transmitted current I and of the reflected current I_B are both measured. A very fast dynamic signal analyzer calculates in real time the cross-correlation of the fluctuations. Uncorrelated noises are thus eliminated increasing the sensitivity and reliability.

tunneling was coherent. This was an important check for the quasiparticle charge measurement because this ruled out the possibility of noise suppression due to multiple uncorrelated hoping, similar to the 1/3 noise reduction factor in zero field diffusive conductors. Also the resonant conductance showed non-linear dependence on bias voltage consistent with Luttinger liquid model provided the filling factor of the bulk is used. The other group [50] used a high frequency technique in order to increase the signal bandwidth and measured the autocorrelation of the transmitted current. Here the magnetic field corresponded to a filling factor 1/3 everywhere in the sample. They found few non-linearities in the conductance, in contrast with the Luttinger liquid predictions, and this allowed them to define a bias voltage independent transmission.

In the Poissonian limit $I_B \ll I_0$, the two experiments give the same conclusion (see Fig.13) that near filling factor 1/3, shot noise is threefold suppressed. These experiments have given the most direct evidence that the current can be carried by quasiparticle with a fraction of e and that Laughlin conjecture was correct. In addition, the data showed a cross-over from thermal noise to shot noise when the applied voltage satisfies the inequality $eV/3 > 2k\theta$ (rather than $eV > 2k\theta$), indicating that the potential energy of the quasiparticles is threefold smaller as well as predicted in Eq.(11).This experiment has been now reproduced many time with different samples and measurement conditions in both laboratories.

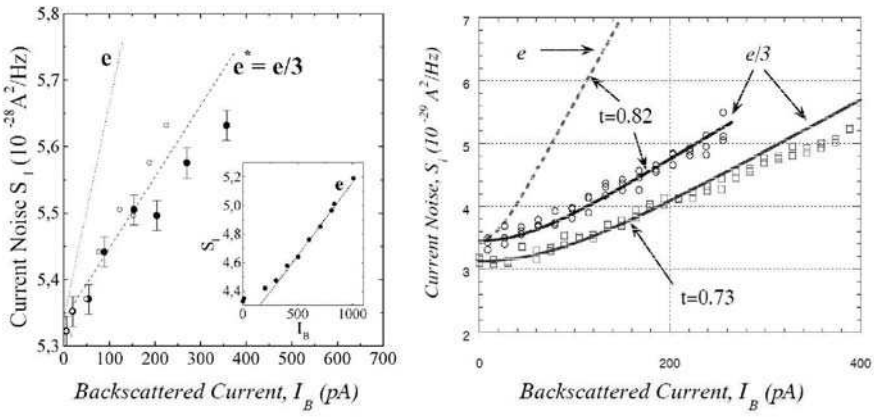

Figure 13: experimental Poissonian noise of the fractionally charged excitations in the FQHE, from Ref.[49] (left) and Ref.[50] (right).

Is it possible to go further and probe different fractional charges for less simple filling factor? Measurements close to $\nu = 2/5$ have given indications that the $e/5$ quasiparticles are the relevant excitations in this regime[51]. This last result has been analyzed in a model of non-interacting composite Fermions where Luttinger effects are neglected [52]. More recently, the same group has extended their measurement up to the filling factor 3/7 [53] and found a charge $e/7$. At very low temperature, they found an unexplained rapid increase of the effective charge. It would be useful to have a better theoretical understanding of the noise for Jain's filing factors to provide a basis for comparisons with experiments.

3.4 Cross-over from fractional to integer charge

When the strength of the artificial impurity potential is slightly increased and the energy of measurement is reduced, the strong backscattering regime sets in and one expects integer charges take over fractional charge. This has been measured in shot noise experiments [54],[55]. In ref.[54] very low temperature and pronounced Luttinger liquid effects are observed. In the same experiment it is then possible to observe both the charge $e/3$ for weak scattering and charge e at strong backscattering. Despite the strong linear I-V characteristics (due to Luttinger liquid effects), it is remarkable that the shot-noise increase linearly with current, as shown in Fig.14. In ref.[55] less non-linearities are observed as the electron temperature was higher but the strong backscattering regime was obtained by increasing the impurity strength.

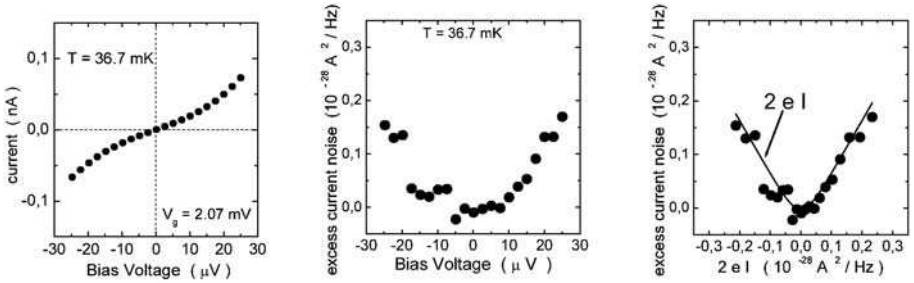

Figure 14: Although the QPC potential is very weak, at low temperature Luttinger liquid effects give rise to strong backscattering. The left figure shows the non-linear $I(V)$ curve, the center figure the shot noise versus voltage simultaneously measured, and the right figure the *linear* variation of the noise with current.

4 Fractional occupation in the ground state

In the Laughlin wave function, electrons are spread uniformly with each elementary quantum state filled by $1/(2s+1)$ electrons on average.

A fractional filling is a necessary condition for the formation of fractionally charge excitations above the ground state. Indeed, the first excited state, a Laughlin wavefunction with a quasi-hole, is obtained by emptying a quantum state, i.e. by introducing a hole in the wavefunction whose area is that of one flux quantum. In a gedanken experiment, an infinitely small solenoid piercing the plane adiabatically increases the flux from zero to ϕ_0. In place of the fractionally filled quantum state a fractional charge $e/(2s+1)$ is left.

The fractional filling is also responsible for the fractional quantization of the Hall conductance. In a Corbino geometry (a ring of radius R and finite width $W \ll R$) it is possible to generate an azimuthal solenoidal electric field E_θ by a time varying flux $\Phi(t) = \phi_0 \frac{t}{\tau}$. If G_H is the Hall conductance, the radial current density is $j_r = G_H E_\theta$. For each time slice τ, the flux variation $\Delta\Phi = \phi_0$ radially shifts all states by one unit. As they are filled by a fraction of electron, a charge $\Delta Q = e/(2s+1)$ crosses the ring from the inner to the outer perimeter. The current is $I = j_r 2\pi R = G_H \frac{\phi_0}{\tau} = \frac{\Delta Q}{\tau}$ and the Hall conductance is $\frac{1}{2s+1}\frac{e^2}{h}$.

Equilibrium conductance measurements have allowed to accurately determine the fraction of charge filling the quantum states. Resonant tunneling experiments have been used to measure the charge ΔQ in response to the flux variation $\Delta\Phi = \phi_0$ through a well defined area for filling factor 1/3 and filling factor 1 [56]. Comparison between the integer and the fractional case showed that in the later case, the charge is accurately reduced by one third.

In this experiment, a micron size disc fully depleted of electrons is realized inside a Hall bar by etching a 2D electron gas. The width of the Hall bar is locally reduced to a size larger but very close to the disc size, such that edge states running

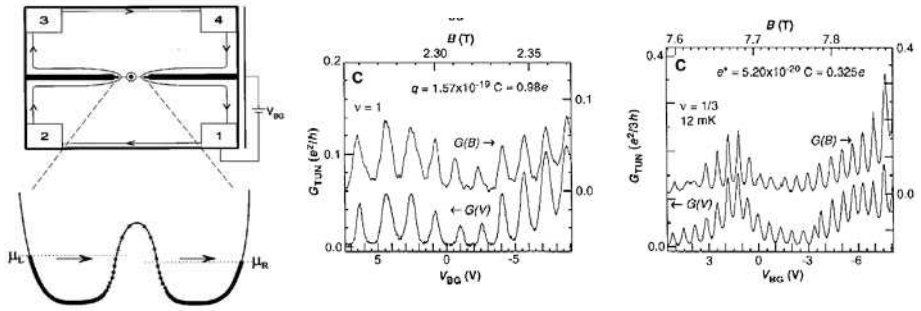

Figure 15: Resonant tunneling experiment to measure the fraction of charge associated with a quantum state at $\nu = 1/3$. Compared to the integer case, the period in gate voltage are increase by a factor 3 for 1/3 signaling a one third reduction of the charge.

along the Hall bar can pass very close to the edge states circulating around the disc, see Fig.15. Gates, placed nearby the two points where the outer and inner edge channels meet, allow to control the tunnel coupling.

The disc free of electrons embedded in the 2DEG forms a so-called anti-dot (as opposed to quantum dots which are small disc of electrons). Because of the finite size of the perimeter and of the low temperature used, the available edge states do not appear as a continuum but are quantized. In a semiclassical picture, the radius r_k of the k^{th} edge state is given by $B\pi r_k^2 = k\phi_0$ and its energy is $U(r_k)$, where $U(r)$ is the radial potential which confines the electrons (the kinetic energy has been subtracted for presentation). Edge states with $U(r_k) < E_F$ are filled by one electron in the integer regime or by one third of electrons for $\nu = 1/3$. A new state can be filled by increasing the charge by ΔQ in the disc or by reducing the magnetic flux by ϕ_0. The filling of a new state is revealed by equilibrium measurement of the tunnel conductance between the upper and lower outer edge via the anti-dot. A resonant tunneling conductance peak is observed each time the edge state energy level align with the Fermi energy. The experiment shows that the same $\Delta\Phi = \phi_0$ separates two consecutive peaks for integer and fractional cases, while the backgate voltage variation ΔV separating two peaks is found one third smaller for the fractional case. Knowing the area of the antidot and the capacitance, the absolute variation of the charge ΔQ is found consistent with e and $e/3$ (estimation of the capacitance assumes strong statements about screening in the QHE regime, but the numbers are convincing). The results are shown in Fig.15.

5 Conclusion

The Fractional Quantum Hall effect is at present, the only system in condensed matter with fractional quantum numbers. Out of equilibrium or equilibrium tunneling experiments have been able to directly or indirectly probe fractionalization.

The Luttinger liquid properties which are revealed by power law variations of the tunnel conductance can not be understood without associating carriers with non integer charge. This fractionally charged carriers has been observed directly through the current noise associated with their tunneling across opposite boundaries of FQHE fluid. The evolution of the charge from a fraction in the weak backscattering limit at large voltage to an integer in the strong backscattering limit at low voltage is consistent with the Luttinger picture and with common intuition. At the root of the fractional excitations carrying the current is the fraction of charge in the ground state which fills the individual quantum states to form Laughlin's wavefunction. This fraction of charge has been measured by equilibrium resonant tunneling conductance measurements.

To complete this picture, localized fractional charges have been observed in a recent experiment using low temperature scanning probe imaging techniques [57]. The experiment is able to map the charge distribution in a macroscopic sample. The localized charges do not participate to transport (by definition) and are responsible for the finite width of the Hall plateau and exact quantization and is a key point in the understanding of the macroscopic QHE. Localized one third charge are found both for the 2/3 and the 1/3 FQHE regime.

Fascinating properties of the FQHE excitations are still to be observe. To cite a few: the fractional statistics which could be revealed by shot noise correlations techniques, the high frequency singularity in the shot noise at frequency $eV/(2s+1)h$, the fractional excitations in the non fully polarized spin regime. The recent progresses in mastering cold atoms suggest that the QHE could be observe in different systems with different statistics and interactions. New type of measurements may also be possible and extend our range of investigation of the Quantum Hall Effect.

Acknowledgments. The author warmly thanks Patrice Roche, V. Rodriguez, Hubert Saleur, Ines Safi, Thierry Martin and Vincent Pasquier for contributions or very insightful discussions.

References

[1] K. von Klitzing, G. Dorda and M. Pepper, *Phys. Rev. Lett.* **45**, 494 (1980).

[2] D. Tsui, H.Stromer and A. Gossard, *Phys. Rev. Lett.* **48**, 1599 (1982) (FQHE).

[3] R.B. Laughlin, *Phys. Rev. Lett* **50**, 1395 (1983).

[4] See *The Quantum Hall Effect*, Richard E. Prange and Steven M. Girvin eds., Springer-Verlag, New York (1987).

[5] J.M. Leynaas and L. Myrheim, *Nuovo Cimento B* **37**, 1 (1977); S.R. Renn and D.P. Arovas, *Phys. Rev. B* **51**, 16832 (1995); S. Ouvry, *Phys. Rev. D* **50**, 5296 (1994); S. Wu *Phys. Rev. Lett.* **73**, 922 (1994).

[6] J. Jain, *Phys. Rev. Lett.* **63**, 199 (1989).

[7] S.C. Zhang, H. Hansson and S. Kivelson, *Phys. Rev. Lett.* **62**, 82 (1989); D.-H. Lee and S.-C. Zhang, *Phys. Rev. Lett.* **66**, 1220 (1991), S.C. Zhang, *Int. J. Mod. Phys.* **B6**, 25, (1992).

[8] S.L. Sondhi, A. Karlhede, S.A. Kivelson, and E.H. Rezayi, *Phys. Rev. B* **47**, 16419 (1993).

[9] S.M. Girvin, in *Topological Aspects of Low Dimensional Systems*, NATO ASI, Les Houches Summer School, A. Comtet, T. Jolicoeur, S. Ouvry and F. David Eds, Springer, p.551–570 (1999).

[10] F. Calogero, *J. Math. Phys.* **10**, 2191 (1969); B. Sutherland, *J. Math. Phys. 12*, 246 (1971); see for example D. Serban, F. Lesage and V. Pasquier, *Nucl. Phys. B* **466**, 499 (1996) and references therein.

[11] H. Störmer, *Rev. Mod. Phys.* **71**, 875 (1999).

[12] A.H. Mac Donald in *Mesoscopic Quantum Physics*, E. Akkermans, G. Montambaux, J.L. Pichard and J. Zinn-Justin eds., Elsevier Science, Amsterdam (1994); *Perspectives in Quantum Hall Effects*, Edited by Sankar Das Sarma and Aron Pinczuk (Wiley, New York, 1997).; *Topological Aspects of Low Dimensional Systems*, NATO ASI, Les Houches Summer School, A. Comtet, T. Jolicoeur, S. Ouvry and F. David Eds, Springer, p.551–570 (1999).

[13] M. Buettiker, *Phys. Rev. B* **38**, 9375 (1988).

[14] R.J. Haug et al, *Phys. Rev. Lett.* **61**, 2797 (1988).

[15] This is only true for the first orbital Landau level. For $\nu > 2$ fractions with even denominator, such as $5/2$, may occur. The quantum states are believed to be related to a non abelian permutation symetry of the electrons, a fascinating subject not treated here.

[16] R.G. Clark *et al.*, *Phys. Rev. Lett.* **60**, 1747 (1988); Y. Katayama, D.C. Tsui and M. Shayegan, *Phys. Rev. B* **49**, 7400 (1994); S.I. Dorozhkin, R.J. Haug, K. von Klitzing and H. Ploog, *Phys. Rev. B* **51**, 14729 (1995).

[17] B.I. Halperin, *Phys. Rev. Lett.* **52**, 1583 (1984).

[18] V. Pasquier and F.D.M. Haldane, *Nucl. Phys.* **516**, 719, (1998); B.I. Halperin, P.A. Lee and N. Read, *Phys. Rev. B* **47**, 7312 (1993).

[19] V.J. Goldman, B. Su, and Jain J.K., *Phys. Rev. Lett.* **72**, 2065 (1994).

[20] J.H. Smet *et al.*, *Physica B* **249–251**, 15 (1998).

[21] C.W.J. Beenakker, *Phys. Rev Lett.* **64**, 216 (1990).

[22] A.H. Mac Donald, *Phys. Rev. Lett.* **64**, 229 (1990).

[23] X.G. Wen, *Phys. Rev.* **B43**, 11025 (1991); *Phys. Rev. Lett.* **64**, 2206 (1990); *Phys. Rev* **B44**, 5708 (1991), *Int. Jour. Mod. Phys. B* **6**, 1711 (1992).

[24] J.M. Luttinger, *J. Math. Phys.* **4**, 1154 (1963); S. Tomonaga, *Prog. Theor. Phys. (Kyoto)* **5**, 544 (1950).

[25] H. Schulz *"Fermi liquids and non Fermi liquids"* in "Mesoscopic Quantum Physics",Proceedings of the Les Houches Summer School of Theoretical Physics, Session LXI, 1994, edited by E. Akkermans, G. Montambaux, J.L. Pichard and J. Zinn-Justin (Springer-Verlag).

[26] A.M. Chang, L.N. Pfeiffer, and K.W. West, *Phys. Rev. Lett.* **77**, 2538 (1996).

[27] M. Grayson, D.C. Tsui, L.N. Pfeiffer, K.W. West, and A.M. Chang, *Phys. Rev. Lett.* **80**, 1062 (1998).

[28] A.M. Chang, M.K. Wu, J.C.C. Chi, L.N. Pfeiffer, and K.W. West, *Phys. Rev. Lett.* **87**, 2538 (2001).

[29] C.L. Kane and M.P.A. Fisher, *Phys. Rev.* **B46**, 15233 (1992); *Phys. Rev. Lett.* **68**, 1220 (1992), *Phys. Rev.* **B51**, 13449 (1995).

[30] A.V. Shytov, L.S. Levitov, and B.I. Halperin, *Phys. Rev. Lett.* **80**, 141 (1998).

[31] L.S. Levitov, A.V. Shytov, B.I. Halperin, *Phys. Rev.* **B 6407 (7)**, 5322 (2001).

[32] S.S. Mandal and J.K. Jain, *Phys. Rev. Lett.* **89**, 096801 (2002).

[33] A.M. Chang, *Rev. Mod. Physics* **75**, 1449 (2003).

[34] F.P. Milliken, C.P. Umbach and R.A. Webb, *Solid State Commun.* **97**, 309 (1996).

[35] P. Roche *et al.* preprint.

[36] P. Fendley, A.W.W. Ludwig and H. Saleur, *Phys. Rev. Lett.* **74**, 3005 (1995).

[37] P. Fendley and H. Saleur, *Phys. Rev. B* **54**, 10845 (1996).

[38] K. Moon and S.M. Girvin, *Phys. Rev B* **54**, 4448 (1996).

[39] K. Imura and N. Nagaosa, *Solid State Commun.* **103**, 663 (1997).

[40] L.P. Pryadko, E. Shimshoni, and A. Auerbach, *Phys. Rev. B* **61** 10929 (2000).

[41] W. Schottky, *Ann. Phys. (Leipzig)* **57**, 541 (1918).

[42] G.B. Lesovik, *Pis'ma Zh. Eksp. Teor. Fiz.* **49**, 513 (1989); [*JETP Lett.* **49**, 592 (1989)].

[43] M. Reznikov *et al.*, *Phys. Rev. Lett.* **18**, 3340 (1995).

[44] A. Kumar *et al.*, *Phys. Rev. Lett.* **76**, 2778 (1996).

[45] Ya. M. Blanter and M. Buttiker, Shot Noise in Mesoscopic Conductors, *Phys. Rep.* **336**, 1 (2000).

[46] C.L. Kane and M.P.A. Fisher, *Phys. Rev. Lett.* **72**, 724 (1994).

[47] C. de C. Chamon, D.E. Freed and X. G. Wen, *Phys. Rev. B* **51**, 2363 (1995).

[48] Th. Martin and R. Landauer, *Phys. Rev. B* **45**, 1742 (1992); *Physica B* **175**, 167 (1991).

[49] L. Saminadayar, D.C. Glattli, Y. Jin, B. Etienne, *Phys. Rev. Let.* **79**, 2526 (1997); cond-mat/9706307.

[50] R. de-Picciotto *et al.*, *Nature* **389**, 162 (1997); cond-mat/9707289.

[51] M. Reznikov, R. de-Picciotto, T.G. Griffiths, M. Heiblum, *Nature* **399**, 238 (1999).

[52] R. de-Picciotto, cond-mat/980221.

[53] Yunchul Chung, M. Heiblum and V. Umansky, *Phys. Rev. Lett.* **91**, 216804 (2003).

[54] D.C. Glattli et al., *Physica E* **6**, 22 (2000).

[55] T.G. Griffiths et al., *Phys. Rev. Lett.* **85**, 3918 (2000).

[56] V.J. Goldman and Bo Su, *Science* **267**, 1010 (1995).

[57] J. Martin et al., *Science* **305**, 980 (2004).

D. Christian Glattli
Service de Physique de l'Etat condensé
CEA, Saclay
F-91191 Gif-sur-Yvette
&
Laboratoire Pierre Aigrain
Ecole Normale Supérieure,
24, rue Lhomond
F-75231 Paris
France
email: `cglattl@drecam.saclay.cea.fr`